HAL
open science

Comportement à étage faible des ossatures en acier à contreventement centre soumis à des actions sismiques

Daniel Balazs Merczel

To cite this version:

Daniel Balazs Merczel. Comportement à étage faible des ossatures en acier à contreventement centre soumis à des actions sismiques. Génie civil. INSA de Rennes; Budapesti műszaki és gazdaságtudományi egyetem (Budapest), 2015. Français. NNT : 2015ISAR0006 . tel-01391434

HAL Id: tel-01391434

https://theses.hal.science/tel-01391434

Submitted on 3 Nov 2016

HAL is a multi-disciplinary open access archive for the deposit and dissemination of scientific research documents, whether they are published or not. The documents may come from teaching and research institutions in France or abroad, or from public or private research centers.

L'archive ouverte pluridisciplinaire **HAL**, est destinée au dépôt et à la diffusion de documents scientifiques de niveau recherche, publiés ou non, émanant des établissements d'enseignement et de recherche français ou étrangers, des laboratoires publics ou privés.

Thèse

SPECIMEN
NON IMPRIMABLE

THESE BUTE Budapest et INSA Rennes
sous le sceau de l'Université européenne de Bretagne
pour obtenir le titre de
DOCTEUR DE L'INSA DE RENNES ET BUTE
Spécialité : Génie Civil

présentée par

Dániel Balázs Merczel

ECOLE DOCTORALE : Vásárhelyi Pál et SDLM
LABORATOIRE : LGCGM

Weak storey behaviour of concentrically braced steel frames subjected to seismic actions

György Farkas
Technical University of Budapest / *membre invite*

Thèse soutenue le 23.01.2015
devant le jury composé de :

László Dunai
Professeur, Technical University of Budapest (BUTE), Hongrie/ *président du jury*
Ahmed Elghazouli
Professeur, Imperial College London, Grande-Bretagne / *rapporteur*
Carlo Castiglioni
Professeur, Politecnico di Milano , Italie/ *rapporteur*
Herve Degée
Professeur, University of Hasselt, Belgique/ *rapporteur*
Jean-Marie Aribert
Professeur émérite INSA de Rennes / *co-encadrant*
Hugues Somja
Maître de Conférences, INSA de Rennes / Co-encadrant
János Lógó
Professeur, Technical University of Budapest (BUTE), Hongrie/ Directeur de thèse
Mohammed Hjiaj,
Professeur, INSA de Rennes / Directeur de thèse

Weak storey behaviour of concentrically braced steel frames subjected to seismic actions

Dániel Balázs Merczel

En partenariat avec

Document protégé par les droits d'auteur

WEAK STOREY BEHAVIOUR OF CONCENTRICALLY BRACED STEEL FRAMES SUBJECTED TO SEISMIC ACTIONS

by

Merczel Dániel Balázs

Dissertation

Presented to the Faculty of Civil Engineering of the

Budapest University of Technology and Economics

and

Institut Nationale des Sciences Appliquées Rennes

in partial fulfilment of the requirements for the degree of

Doctor of Philosophy

January 2015

Declaration of Authenticity

I declare that all material presented in this dissertation are either my own work or fully and specifically acknowledged wherever adapted from other sources.

03 March 2015

.....
Merczel Dániel Balázs

Acknowledgements

The research work has been completed under the support of the following projects and programs:

- Joint Supervision dissertation agreement between the Budapest University of Technology and Economics (BUTE) and INSA de Rennes University
- Campus France research grant
- Rennes Metropole scholarship
- Campus Hungary Program supported by the grant TÁMOP 4.2.4. B/1-11/1-2012-0001

I would like to express my gratitude to my supervisors, Dr. János Lógó at BUTE and Dr. Mohammed Hjiaj at INSA de Rennes for providing vital support and guidance throughout my doctoral studies. Their experience and advice helped me to develop my skills and successfully accomplish my tasks. They also provided indispensable help in managing technical issues that I have encountered regarding the organization of my work, travels and financing.

I deeply appreciated the involvement in the supervision of the research of Professor Jean-Marie Aribert. His contribution began at the definition of the topic and went up to the detailed correction of the first manuscript of the thesis, therefore his work has been determinative and indispensable. It also needs to be pointed out, that Professor Aribert repeatedly had to cover a long distance to participate at the meetings.

Special thanks to Dr. Hugues Somja, who has been practically an additional supervisor even without having been appointed as one. His daily contribution to the technical, computational and conceptual questions are duly recognised and appreciated.

I would like to thank the personnel of the Department of Structural Mechanics at BUTE and of the Department of Civil Engineering at INSA for providing a friendly environment and a helping hand to conduct my research.

I owe my humblest gratitude to my family and mostly my parents. To my mother who has shown me exceptional strength and endurance, lessons that I have benefited from and my father who encouraged me and who unfortunately could not see the end of my work.

Remerciements

Ce travail de recherche put être mené à terme grâce au support des programmes et projets suivants :

- l'accord de supervision de thèse entre Budapest University of Technology et Economics (BUTE) et l'Institut National des Sciences appliquées de Rennes (INSA)
- la subvention à la recherche de Campus France
- la bourse de Rennes Métropole
- le programme de Campus Hongrie soutenu par la subvention TÁMOP 4.2.4. B 1-11/1-2012-0001

Je souhaiterais exprimer ma gratitude envers mes directeurs de thèse, Dr. János Lógó at BUTE et Dr. Mohammed Hjiaj de l'INSA de Rennes, pour m'avoir soutenu et guidé tout au long de mon doctorat. Leur expérience et leurs conseils m'aidèrent à développer des compétences et à parvenir avec succès à accomplir ma mission. Ils furent également d'une aide précieuse pour la résolution de problèmes techniques que sont l'organisation du travail, les voyages et le financement.

J'ai profondément apprécié l'implication du Professeur Jean-Marie Aribert dans la supervision de ma recherche. Sa contribution s'appliqua de la définition du sujet jusqu'aux détails indispensables. Il m'importe aussi de souligner que le Professeur Aribert dû régulièrement couvrir une longue distance afin d'assister aux réunions.

Un remerciement particulier au Dr. Hugues Somja, dont le rôle devint presque celui d'un directeur de thèse supplémentaire sans avoir été désigné comme tel. Sa contribution quotidienne à la résolution de questions techniques, conceptuelles et de programmation furent dûment reconnues et appréciées.

J'aimerais également remercier le personnel du département de structure mécanique de BUTE et le département de génie civil de l'INSA pour m’avoir procuré un cadre agréable et favorable afin d’effectuer mon travail dans les meilleures conditions.

Je dédie mes plus humbles remerciements à ma famille et plus particulièrement à mes parents. A ma mère qui fit preuve d'une force et patience exceptionnelle, et mon père qui m'encouragea et qui, malheureusement, ne put voir l'achèvement de mon travail.

Resume

The concentric steel bracing is a commonly used way of providing lateral stiffness and resistance in both steel, composite or even concrete multi-storey framed buildings. Also it is an alternative for seismic retrofitting. The seismic performance of concentrically braced frames has been investigated by numerous authors during the past decades as several issues have been identified either related to the actual response, or the seismic design procedure implemented by standards such as the Eurocode 8. The topics are various, e.g. the cyclic dissipative behaviour of axially loaded braces, innovative bracing arrangements and members, controversial requirements imposed on the same members, localization of inelastic deformations related to the so called weak storey behaviour. The conclusion of most of the prior research conducted on the seismic performance of braced steel frames is that the actual response of a braced building differs from that of a simplified model applied by corresponding codes. Consequently, to safeguard satisfactory seismic behaviour, the Eurocode 8 standard in particular needs to be modified or amended.

In order to confine the addressed topic to a size that may be discussed sufficiently in the frame of a PhD research, in the present thesis primarily the weak storey behaviour is looked into. The questions that are attempted to be given an answer are the following:

- What are the reasons and contributing factors of the occurrence of the weak storey behaviour?
- How does the behaviour develop?
- What is the effect of the behaviour on the seismic performance and how is it related to collapse?
- What is the seismic response like of braced steel buildings designed according to Eurocode 8? Are the susceptible to exhibit weak storey behaviour?
- What are the key elements of the Eurocode 8 design procedure that do not capture adequately the behaviour and therefore need to be changed?
- What additional factors need to be introduced in Eurocode 8 that are currently not considered in any way?

Ultimately, the objective is to develop a method, which is complementary to Eurocode 8 or at least fits its framework, and which is capable of enhancing braced frame designs so that the weak storey behaviour is prevented. The method is supposed to take into consideration in some way the experiences acquired by the prior investigation into the behaviour and seismic response of braced frames. In addition, the method is intended to be easy to apply, not requiring the computer solution of large systems of equations or complicated nonlinear equations.

The dissertation is divided into five subsequent chapters. In these chapters the corresponding literature is covered, the questions above are answered via a deeper understanding of the weak storey behaviour and a new method is proposed, the performance of which is substantiated by a large number of examples. The organization of the dissertation and the contents of the chapters can be better understood via the following brief summaries:

Chapter 1

Introduction to Braced Frames, Seismic Design Principles and Analysis Methods

The objective of this chapter is to provide an overview on the seismic design of braced frames. Concepts and abbreviations are introduced, definitions are given that are referred to further on in the dissertation. Also, the necessary regulations of Eurocode 8 are introduced at the corresponding topics; however giving a comprehensive and detailed introduction to Eurocode 8 is not intended. At the end, the problem with the seismic behaviour of braced frames is discussed, which is the subject of examination in the thesis.

Chapter 2

Literature Review on the Seismic Response of Braced Frames and Brace Behaviour

The objective of this chapter is to assess the information that were gathered from articles existing prior to the dissertation and that provided an initial base to the research. In the chapter giving every available reference as a list is not intended. Rather, emphasis is put on introducing the most important features of Concentrically Braced Frames CBF-s utilizing a few selected articles. Firstly, the cyclic behaviour and failure of the braces and other members are observed. In the second part some issues regarding CBF related Eurocode 8 provisions and the unfavourable weak storey behaviour are discussed.

Chapter 3

Investigation into the seismic performance of various Eurocode 8 CBF designs

In this chapter firstly the design of various CBF-s is described. The structures are introduced, the loads and combinations are given and the method of the verification is referred to. The objective is to verify the adequacy of the buildings by advanced analysis methods such as the IDA. To this end, the nonlinear model built for the dynamic analyses is described. The performance of the buildings is examined via the IDA curves and certain regularities are identified that help to further explain the weak storey behaviour.

Chapter 4

Examination of weak storey behaviour and its reflection on the Eurocode 8 design procedure

The objective of the chapter is to identify the reasons why the Eurocode 8 CBF designs were found to have a bad performance in the previous chapter. Firstly, particular response time series are further analysed. A general response scheme is defined, characterized and proven by examined regularities. By the generalized response the gradual development mode of the weak storey behaviour is described. This understanding of the weak storey development provides a basis of critical assessment of the Eurocode 8 design criteria in the end.

Chapter 5

Robust Seismic Brace Design method: Principles, Formulation and Application

In this chapter the findings of the previous descriptive chapters are turned into requirements of new criteria imposed upon the seismic design of CBF-s. Firstly, the concepts of the new criteria are elaborated and the principles of the Robust Seismic Brace Design method are established. This is followed by a thorough investigation of the internal and external plastic work of the CBF members and loads in plastic collapse mechanisms, which are in the focus of the method. The robust performance of the new method is demonstrated by the redesign of the various CBF-s presented and found to have weak storeys in Chapter 3. In the end, simplified alternatives of the method are also given and their suitability is examined.

Table of Contents

Chapter 1. Introduction to Braced Frames, Seismic Design Principles and Analysis Methods

1.1. Introduction to the bracing of building structures 2
1.2. Earthquakes and their representation in seismic analysis and design 6
1.2.1. Strength and appearance of earthquakes 6
1.2.2. Representation of an earthquake in seismic engineering 8
1.2.3. Representation of the seismic effect in Eurocode 8 12
1.2.4. Seismic effect in practical design, the behaviour factor 14
1.2.5. Behaviour factor in Eurocode 8 16
1.3. General concepts in seismic design 19
1.3.1. Principles of capacity design 19
1.3.2. Capacity design of CBF-s in Eurocode 8 20
1.3.3. Performance-based earthquake engineering in EC8 22
1.4. Analysis methods in seismic engineering 24
1.4.1. Linear static seismic analysis methods 24
1.4.2. Nonlinear static seismic analysis 28
1.4.3. Nonlinear incremental dynamic analysis 31
1.5. Examined problem and objectives of the thesis 33

Chapter 2. Literature Review on the Seismic Response of Braced Frames and Brace Behaviour

2.1. Failure of lateral load resisting members 36
2.1.1. Braces 36
2.1.2. Columns 43
2.1.3. Connections of braces 45
2.1.4. Summary on the failure of members 46
2.2. Behavioural issues involved in the seismic design of CBF-s 47
2.2.1. Generalized seismic response of CBF-s 47
2.2.2. Solutions to the performance issues by modified design procedures 49
2.2.3. Solutions to the performance issues by innovative structural members 52

Chapter 3. Investigation into the seismic performance of various Eurocode 8 CBF designs

3.1. Design of CBF-s for numerical experiments 56
3.1.1. General introduction of buildings 56
3.1.2. Loads and effects in design 58
3.1.3. Analysis and dimensioning 60
3.1.4. Verification of ductility by pushover analysis 65
3.2. Description of model for nonlinear dynamic analysis 67
3.2.1. Geometry and discretization 67
3.2.2. Finite elements 68
3.2.3. Cyclic material model 68
3.2.4. Validation of the finite element formulation, and hysteretic dissipative model 70

3.2.5. Loading, masses and seismic excitation 70
3.2.6. Direct integration and damping 71
3.3. Evaluation of the designs, generalization of the response 73
3.3.1. Seismic response of CBF designs 73
3.3.2. Possible response alternatives 76

Chapter 4. EXAMINATION OF WEAK STOREY BEHAVIOUR AND ITS REFLECTION ON THE EUROCODE 8 DESIGN PROCEDURE

4.1. Further insight into the development of the weak storey behaviour 80
4.1.1. Deformations and displacements during seismic action 80
4.1.2. Alteration of the dynamic response due to brace deterioration 82
4.1.3. Wavelet transformation of the seismic response 85
4.1.4. Development of the weak storey behaviour 89
4.2. Causes of the non-balanced dissipation and early failure in Eurocode 8 CBF designs 90
4.2.1. Gradual qualitative change of the seismic response 90
4.2.2. Underestimated bending of the columns 91
4.2.3. Global and local slenderness limits of braces 92
4.2.4. Summary of the existing and necessary requirements on the seismic design of CBFs 93

Chapter 5. ROBUST SEISMIC BRACE DESIGN METHOD: PRINCIPLES, FORMULATION AND APPLICATION

5.1. Principles of the Robust Seismic Brace Design method 96
5.1.1. Requirements imposed to the design method 96
5.1.2. Criterion 1: preventing the weak storey collapse mechanism 98
5.1.3. Criterion 2: unifying the maximum drifts, promoting distributed dissipation 100
5.1.4. Application of the Robust Seismic Brace Design criteria 103
5.2. Formulation of the Robust Seismic Brace Design method 104
5.2.1. Geometry and material model 104
5.2.2. Internal work of the braces 105
5.2.3. Internal work of the columns 111
5.2.4. External work of the lateral loading 117
5.2.5. External work of the gravity forces 118
5.2.6. Energy equivalence, determination of load multipliers 119
5.3. Application of the Robust Seismic Brace Design method 123
5.3.1. Performance of the reinforced type 1 and type 2 CBF-s 123
5.3.2. Performance of CBF-s with only brace or column reinforcement 130
5.3.3. Performance of reinforced irregular CBF-s 132
5.3.4. Performance of CBF-s reinforced by limit analysis RSBD 135
5.3.5. Summary on the efficiency of the RSBD method 138
5.4. Simplifications of the Robust Seismic Brace Design method 141

Summary and new scientific results 146
References 150
Annex A 156
Annex B 163
Résumé en français 169
Összefoglalás és Tézisek (magyarul) 187

Chapter 1

Introduction to Braced Frames, Seismic Design Principles and Analysis Methods

The objective of this chapter is to provide an overview on the seismic design of braced frames. Concepts and abbreviations are introduced, definitions are given that are referred to further on in the dissertation. Also the necessary regulations of Eurocode 8 are introduced at the corresponding topics; however giving a comprehensive and detailed introduction to Eurocode 8 is not intended. At the end of the chapter the problem with the seismic behaviour of braced frames is discussed, which is the subject of examination in the thesis.

1.1. Introduction to the bracing of building structures

Concentrically braced frames (hereinafter referred to as CBF-s) are among the most common structural systems for resisting horizontal forces. The beam and column system of a multi-storey steel building can carry the vertical gravitational loads of the building. To provide lateral resistance, in multiple bays usually on the facade, diagonals can be placed that together with the connected beams and columns create vertical trusses, see *Figure 1.1*. The bracing is called eccentric if the diagonals are connected either to beams or columns away from the intersection of the beam-column grid. In this case the internal forces of the braces have to be transmitted by the connected member via combined axial force bending and shear. Conversely, no or a little eccentricity to the vertical grid results in concentrically braced buildings. Due to their geometry CBF-s counteract the horizontal forces by truss action that entails primarily axial forces in the members as it is depicted in *Figure 1.2*. The tensile axial forces require braces that have adequate cross-sectional area but negligible flexural stiffness. However, the reversal of the loading imposes a flexural stiffness demand on the brace to limit the slenderness and provide buckling resistance in compression. The use of stocky braces that are resistant both in tension and compression may lead to such a high structural weight premium that the application of two braces with opposite tilt is often more efficient. In this arrangement the slender diagonals in compression are expected to buckle and to exhibit a negligible axial force, while the tensile braces provide the whole resistance. Consequently, even if two bays are braced, like in the arrangement in the *Figure 1.2*, only one participates in counteracting the lateral loading in a given direction. With the reversal of the loading the roles of the opposite braces change of course.

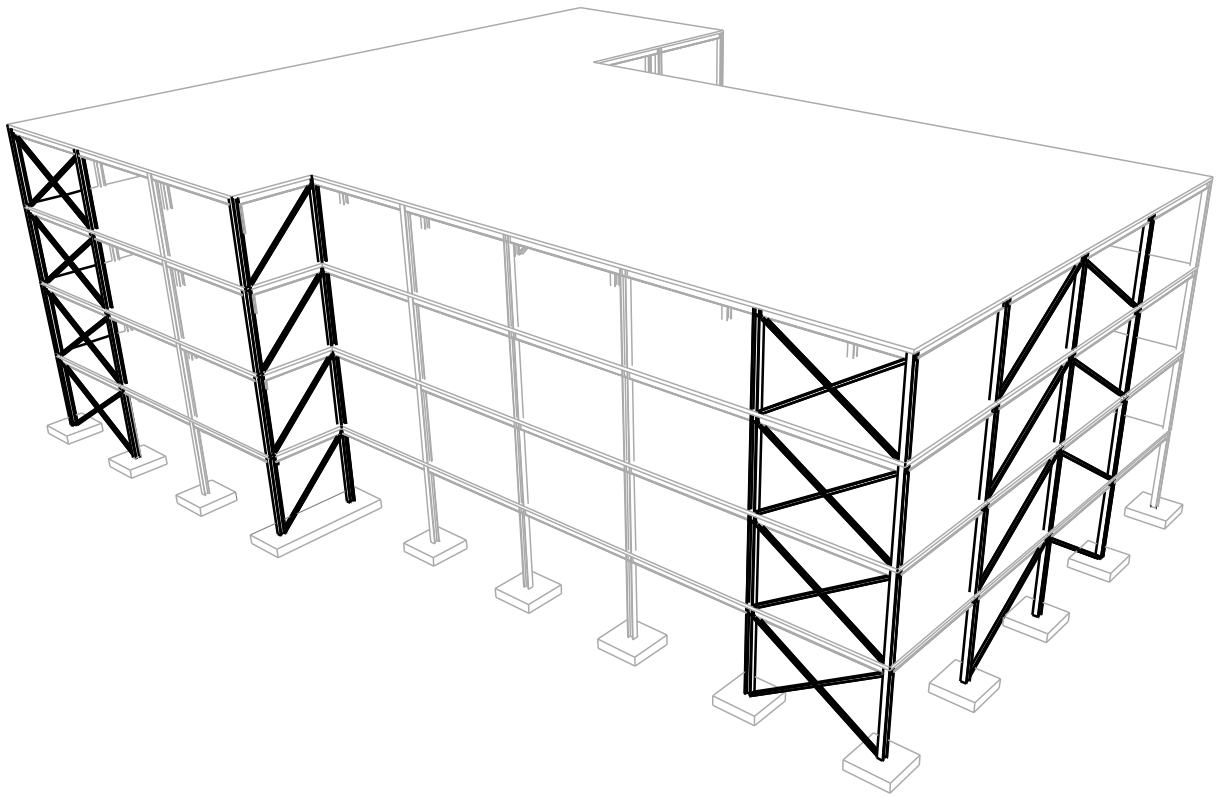

Figure 1.1; *Building with braced bays on the facade*

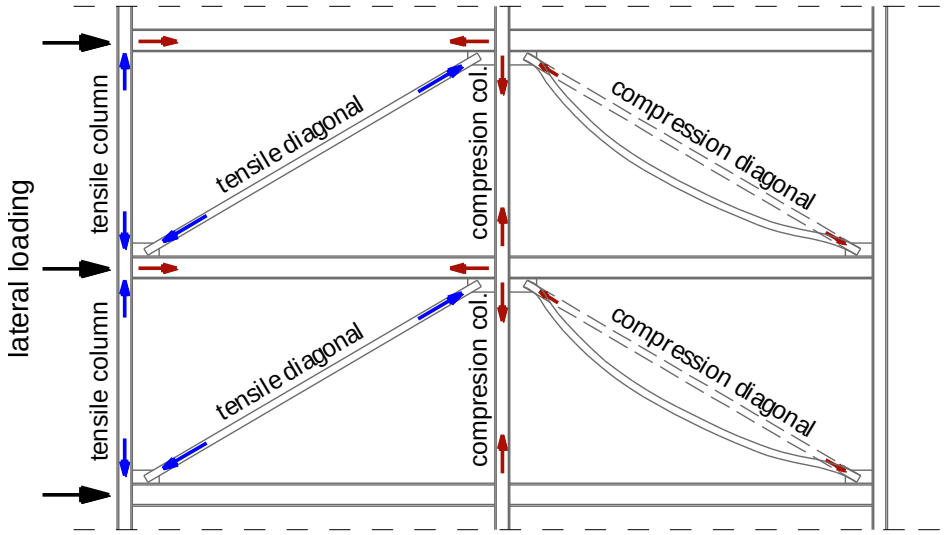

Figure 1.2*; Truss action in braced frame*

Concentric bracing exists in various arrangements. Some basic forms are depicted in *Figure 1.3*. The basic characteristics that affect the choice between the arrangements are introduced below.

- In **Regular diagonal bracing** the diagonals are straight links between the nodes of the structural grid; therefore the lateral loading is resisted solely by axial forces in the members of the vertical truss. The position of the brace is closer to being parallel with the horizontal loading than in most other arrangements. Therefore, the normal force that develops in the less inclined diagonal brace is smaller than in another with a steeper geometry. One main concern about the location of the diagonals is that the bracing mostly prevents door or window openings. Therefore, X or V arrangements may be favoured over regular diagonal bracing as the formers only require one bay for the braces in both directions.
- The **X-bracing** arrangement is also favourable because the tensile brace supports the compression brace in the middle. By this, both the slenderness and the out-of-plane deformations of the buckled diagonal are greatly reduced without having to use cross sections different from what are necessary in a regular diagonal arrangement. Yet, the intersection may require additional costly connections and is often a probable location of failure.
- **V or inverted V bracing** is concentric and therefore can counteract the lateral loading by truss action but only if the compression bar does not buckle. The buckling resistance of the compression bar is reached usually at a substantially smaller loading than the tensile ultimate resistance of the tension brace. If the buckled diagonal does not carry any further loading the growing axial force of the tensile diagonal has to be carried by the connected beam. The component that is perpendicular to the beam results in bending of the beam, so the resistance is not provided solely by truss action. This behaviour is not necessarily better or worse, but inevitably different from the strictly truss behaviour of diagonal bracings. Consequently, the topic of the seismic behaviour of V-braced CBF-s is beyond the scope of the present investigation.
- **Two-storey X-bracing** combines the advantages of the former arrangements. It gives the possibility of placing openings in the middle of the bays and

safeguards truss action. The behaviour is roughly the same as of regular diagonal bracing apart from local effects at the beam intersection. However, the larger angle with the horizontal loading implies larger axial demand in the braces.

– **K-bracing** may result in the bending of the columns due to similar reasons to what has been introduced for V-bracing. The bending of the columns and the huge gravity forces may cause second order and stability problems, that greatly increases collapse hazard. Therefore, K-bracing is not recommended and in seismic resistant buildings it is generally prohibited by codes.

The unnecessary bending resistance of the members in the lateral load resisting favours the use of pinned connections. Not only the diagonal ends, but also the column splices and the beam-column connections can be perfect hinges without harming structural stability. Moreover, the large stiffness of the vertical truss limits the lateral drifts and vibrations of low frequencies in the braced buildings, therefore provides occupancy comfort and impedes damages in the non-structural parts. Consequently, there is no need to use moment resisting connections in braced frames, so CBF-s are conventionally built as ordinary trusses with hinges.

The only detrimental effect of the great number of hinges is that the level of statical indeterminacy is low. The loss of any bar results in a mechanism and the collapse of the building. This practically means that the smallest ultimate resistance of the individual members is also the resistance of the whole structure. Ordinary trusses generally are considered not to have postcritical resistance, they are meant to remain elastic in service.

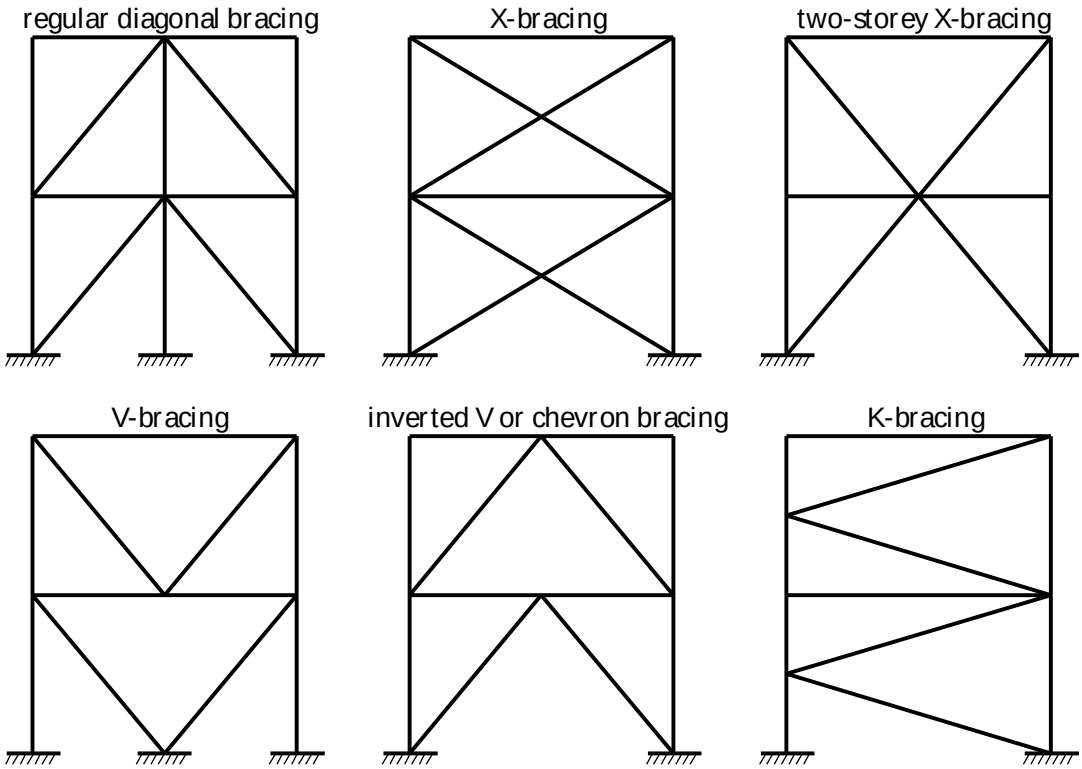

Figure 1.3*; Various bracing configurations*

In the assessment of the lateral displacement of braced frames two contributing factors can be distinguished, see *Figure 1.4*. The lateral shear force results in the elongation of the braces and by it the horizontal drift of the slabs without tilt. Furthermore, the axial deformation of the columns in tension and compression yields rotations and displacements

alike a restrained vertical cantilever. In CBF-s the braces are usually long and have a smaller cross section, so their contribution to the displacements is substantial. Conversely, the columns must have large cross sections to resist the gravity forces without the loss of stability. The displacements coming from bending therefore may be negligible compared to the shear displacements up to a certain point. In tall buildings however the bending effect may become significant or even superior to the shear effect. In engineering practice according to an empirical rule of thumb if the ratio of the building height, H_{tot}, and the span of the braced bay, B, is under 5, shear deformations may dominate. At and above 5 bending becomes more relevant, so that it cannot be neglected.

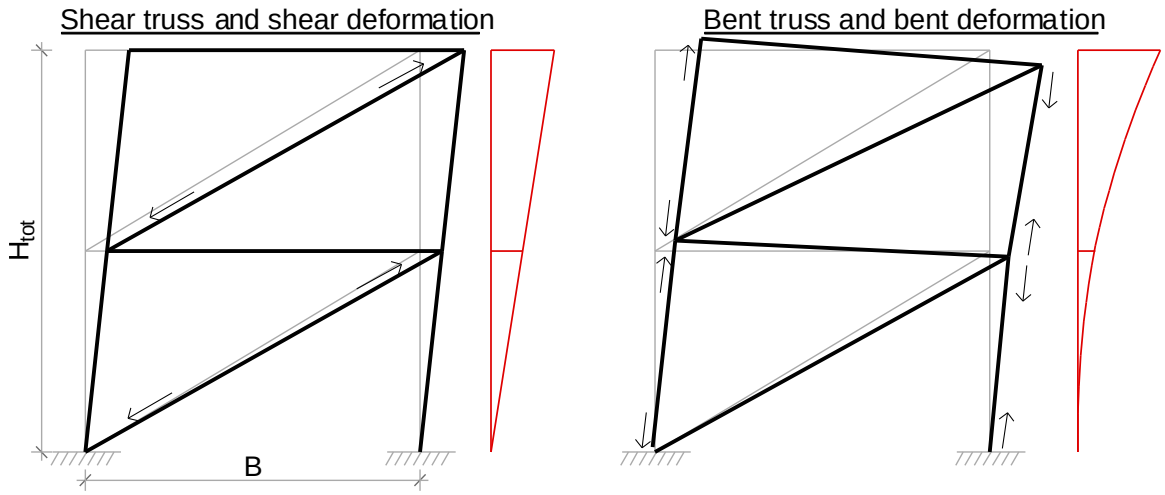

Figure 1.4; *Sources of lateral drift in braced buildings*

1.2. Earthquakes and their representation in seismic analysis and design

1.2.1. Strength and appearance of earthquakes

An earthquake is a result of a sudden release of energy in the Earth's crust that creates seismic waves. The source of the energy is the movement of the tectonic plates that forces the edges of the plates to deform and store mechanical energy via the deformation. Earthquakes can also be experienced away from tectonic fault lines as a result of volcanic activity for example. The origin of the quake is the so called hypocentre, this is the source from where the waves propagate. The perpendicular projection of the hypocentre on the surface is the epicentre where the destruction is usually the largest. Earthquakes have been recorded for centuries and since the mid 19th century they are even measured by seismometers. To quantify the strength of an earthquake various scales have been developed. Some, like the Mercalli-Cancani-Sieberg (MCS) or the Medvediev-Sponhauer-Karnik (MSK) scale distinguish the earthquakes based upon their effect mostly in the built environment. As these are strongly dependent on the epicentral distance and the density of habitation, they are not appropriate to compare seismicity on different sites. For the sake of site independent comparison numerous magnitude scales are in use and still being developed. The magnitude is a dimensionless number that grades the size of earthquakes upon the measured amplitudes of the waves. The most commonly known scale was developed by Charles Richter. The Richter magnitude depends on the largest registered amplitude and can be computed from:

$$M_L = \log_{10}\left(\frac{A}{A_0}\right) \tag{1.1}$$

where M_L is the Richter magnitude, A is the maximum excursion of the seismograph and A_0 is a parameter that depends on the epicentral distance. In practice earthquakes that have a magnitude smaller than 3.0 are usually not perceivable. The Richter scale is usually wrongly referred to in reports as present day the moment magnitude scale is preferably used. This scale measures earthquakes in terms of the released energy and is mostly formulated to overlap with the predecessor Richter scale but correct it in the strong earthquake region. The moment magnitude is calculated as:

$$M_w = \frac{2}{3}\log_{10}\left(M_0\right) - 6.0 \tag{1.2}$$

In the equation above the released energy is given by the M_0 [MJ] seismic moment. One step on this logarithmic scale corresponds to a $10^{1.5}$~32 times increase of the seismic energy and two steps is about a 10^3=1000 increase. Though energy is not limited, the amount of energy that can be stored in the solid crust before it is released is limited, therefore earthquakes that have a magnitude higher than 9.0 are rare. The largest recorded earthquake happened in Chile in 1960 and its magnitude was 9.5.

The magnitude is also useful to estimate the potential number of earthquakes of that magnitude on a certain area. In the exponential relation below a and b are parameters specific to the considered location.

$$\log N = a + b \cdot M \tag{1.3}$$

Globally the annual anticipated number and magnitude of earthquakes is illustrated by the following table [1]:

Table 1.1; *Annual number and intensity of earthquakes globally*

Magnitude	*Size*	*Number*
8 -	Great	1
7 - 7.9	Major	18
6 - 6.9	Strong	120
5 - 5.9	Moderate	800
4 - 4.9	Light	6200

In a seismologist's point of view the magnitude scales are suitable to measure the size of earthquakes but in terms of structural engineering this information about a certain event is far from adequate. Building structures are directly subjected to the displacements, velocities and accelerations caused by the mechanical wave propagation. These largely depend on several additional factors like the epicentral distance and the various mechanical parameters of the underlying soil. Consequently, the seismic hazard of structures is always site specific. Instead of the magnitude, what is necessary in structural engineering are the actual recorded displacement, velocity and acceleration time series (hereinafter accelerogram) during past earthquakes, see *Figure 1.5*.

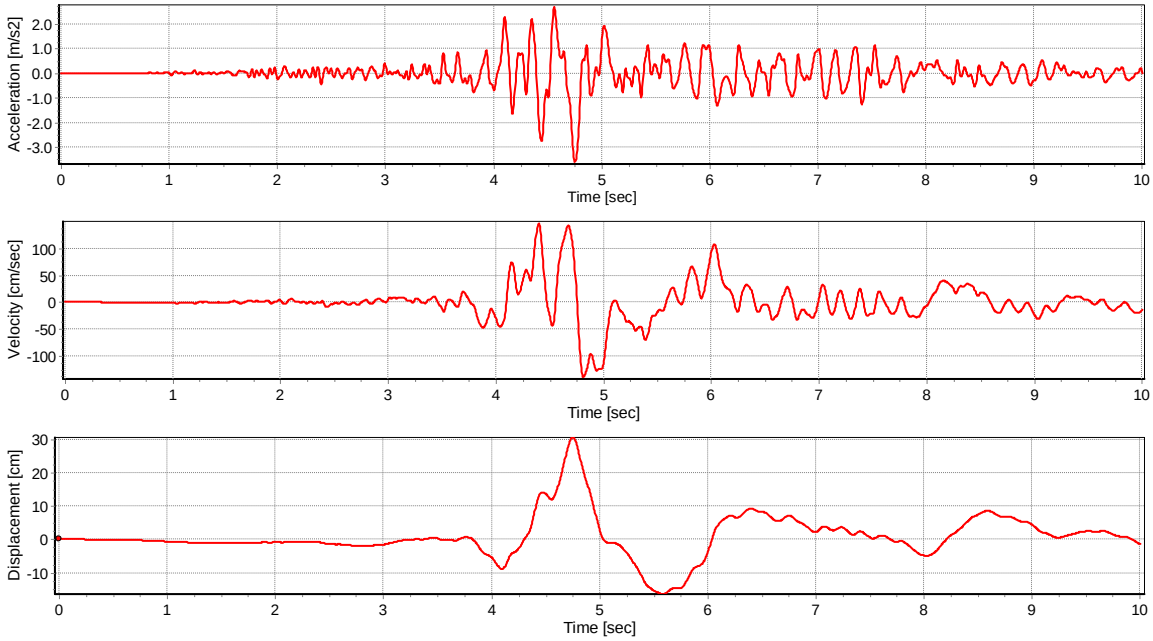

Figure 1.5; *Acceleration, velocity and displacement records*

The most vital information that can be derived from the records are the duration and the maximum peaks. The maximum displacements can be important for instance in the design of utility lines, however for building structures the Peak Ground Acceleration (PGA) is more useful as, according to Newton's second law, the inertia forces are resulted by the accelerations. In *Table 1.2* past earthquakes and their maximum effects are presented [2].

Table 1.2; *Recorded maximum effects of past earthquakes*

Earthquake	*Epi. distance [km]*	*Magnitude*	*Acceleration [a_g/g]*	*Velocity [cm/s]*	*Displacement [cm]*
San Fernando 1971	30	6.4	0.32	27	9.4
San Fernando 1971	7	6.4	1.17	112	37
El Centro 1940	11.5	6.7	0.35	36	20
San Francisco 1957	11.5	5.3	0.11	4.9	2.2

1.2.2. Representation of an earthquake in seismic engineering

The analysis of buildings is possible by means of applying acceleration records on the supported nodes of finite element models of the structures that are nonlinear both in material and geometry. This is called Nonlinear Time History Analysis (NTHA). Conducting such type of analysis requires a lot of work in the model building, post processing of the huge amount of data, computational capacity and time. Moreover, the analysis of one particular earthquake does not even mean much as seismic actions can be very versatile. But strictly speaking we do not need to consider the whole loading history; it is satisfactory to know the maximum seismic action effects. For this purpose the response spectrum analysis is in common practice, the basis of which will be introduced in the following.

Let us consider the dynamic equilibrium equation of a multiple degree of freedom (MDOF) system.

$$\mathbf{M}\ddot{\mathbf{y}}(t)+\mathbf{C}\dot{\mathbf{y}}(t)+\mathbf{K}\mathbf{y}(t)=0 \tag{1.4}$$

The vector of absolute displacements is denoted by **y**(t) and **M** and **K** are the mass and stiffness matrices. The structure is loaded by the z(t) imposed displacement record. Though this displacement is physically realized at the foundations, in the equations it is considered at every node in the horizontal direction. In order to assign the displacements to every node in the appropriate direction, z(t) is multiplied by the $\mathbf{J_a}$ pointer vector that has the value 1 in the positions corresponding to the horizontal direction and 0 elsewhere. The absolute displacement vector now can be expressed as the sum of the ground displacement and the relative displacement vector, **x**(t).

$$\mathbf{y}(t)=\mathbf{x}(t)+\mathbf{J_a}z(t)=\mathbf{x}(t)+\begin{bmatrix}1\\0\\0\\1\\\vdots\\0\end{bmatrix}z(t) \tag{1.5}$$

The matrix differential equation can be rewritten using **x**(t) and z(t) instead of **y**(t):

$$\begin{gathered}\mathbf{M}\left(\ddot{\mathbf{x}}(t)+\mathbf{J_a}\ddot{z}(t)\right)+\mathbf{C}\left(\dot{\mathbf{x}}(t)+\mathbf{J_a}\dot{z}(t)\right)+\mathbf{K}\left(\mathbf{x}(t)+\mathbf{J_a}z(t)\right)=0\\ \mathbf{M}\ddot{\mathbf{x}}(t)+\mathbf{M}\mathbf{J_a}\ddot{z}(t)+\mathbf{C}\dot{\mathbf{x}}(t)+\mathbf{C}\mathbf{J_a}\dot{z}(t)+\mathbf{K}\mathbf{x}(t)+\mathbf{K}\mathbf{J_a}z(t)=0\end{gathered} \tag{1.6}$$

Regarding that internal forces only develop from relative displacements:

$$\mathbf{K}\mathbf{J}_{\mathbf{a}} z(t) = 0 \text{ and } \mathbf{C}\mathbf{J}_{\mathbf{a}} \dot{z}(t) = 0 \tag{1.7}$$

Consequently the matrix differential equation is:

$$\mathbf{M}\ddot{\mathbf{x}}(t) + \mathbf{C}\dot{\mathbf{x}}(t) + \mathbf{K}\mathbf{x}(t) = -\mathbf{M}\mathbf{J}_{\mathbf{a}} \ddot{z}(t) \tag{1.8}$$

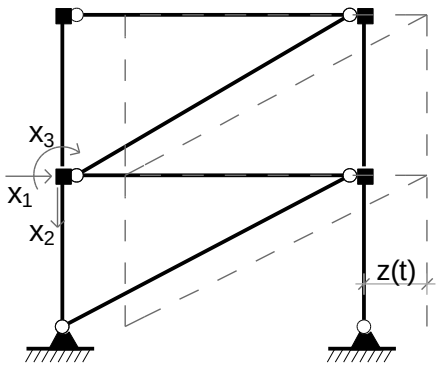

Figure 1.6; *Structural model for seismic analysis*

The original base displacement problem is thereby rewritten into a general force excitation problem where on the right side the function of the force excitation is given by the product of masses and the earthquake acceleration record. If the natural frequencies, $\boldsymbol{\omega}_0$, and the corresponding orthogonal modes are known, Eq.(1.8) can be rewritten in a more favourable form. Supposing that the matrix $\boldsymbol{\Phi}$ contains the modal vectors and that it is normalized to the mass matrix we can introduce a new unknown vector instead of $\mathbf{x}$(t) and substitute it into Eq.(1.8).

$$\mathbf{x}(t) = \boldsymbol{\Phi}\mathbf{f}(t) \tag{1.9}$$

$$\boldsymbol{\Phi}^T\mathbf{M}\boldsymbol{\Phi}\ddot{\mathbf{f}}(t) + \boldsymbol{\Phi}^T\mathbf{C}\boldsymbol{\Phi}\dot{\mathbf{f}}(t) + \boldsymbol{\Phi}^T\mathbf{K}\boldsymbol{\Phi}\mathbf{f}(t) = -\boldsymbol{\Phi}^T\mathbf{M}\mathbf{J}_{\mathbf{a}} z(t) = \mathbf{q}(t) \tag{1.10}$$

Considering that in the equation above the matrix products are

$$\boldsymbol{\Phi}^T\mathbf{M}\boldsymbol{\Phi} = \mathbf{I} \tag{1.11}$$

$$\boldsymbol{\Phi}^T\mathbf{C}\boldsymbol{\Phi} = \left\langle 2\boldsymbol{\xi}_r\boldsymbol{\omega}_r \right\rangle \tag{1.12}$$

$$\boldsymbol{\Phi}^T\mathbf{K}\boldsymbol{\Phi} = \left\langle \boldsymbol{\omega}_0^2 \right\rangle \tag{1.13}$$

where ξ_r is the vector of the damping ratios of each mode. The matrix differential equation can be decoupled into n independent differential equations.

$$\begin{bmatrix} 1 & & 0 \\ & \ddots & \\ 0 & & 1 \end{bmatrix} \ddot{\mathbf{f}}(t) + 2\begin{bmatrix} \xi_1\omega_1 & & 0 \\ & \ddots & \\ 0 & & \xi_n\omega_n \end{bmatrix} \dot{\mathbf{f}}(t) + \begin{bmatrix} \omega_1^2 & & 0 \\ & \ddots & \\ 0 & & \omega_n^2 \end{bmatrix} \mathbf{f}(t) = \mathbf{q}(t) \tag{1.14}$$

The solution to this problem can be found in the form of summing the elementary contributions of the modes. The expression for the relative displacement vector is:

$$\mathbf{x}(t) = -\sum_{r=1}^{n} \frac{1}{\omega_{0r}^*} \boldsymbol{\Phi}_r \boldsymbol{\Phi}_r^T \mathbf{M}\mathbf{J}_{\mathbf{a}} \int_0^t \ddot{z}(t) e^{-\frac{\gamma}{2}\omega_{0r}^*(t-\tau)} \sin \omega_{0r}^*(t-\tau) d\tau \tag{1.15}$$

where $\mathbf{\Phi}_r$ is the rth mode of vibration, the star in the upper index of ω indicates damped natural frequency and γ characterizes the damping (of an equivalent single degree of freedom system). The later is in relation with the ratio of the equivalent damping and the critical damping which is commonly used in engineering practice:

$$\gamma = \frac{\xi[\%]}{50}$$
$$\xi = \frac{c_{equiv}}{c_{crit}} = \frac{c_{equiv}}{2\sqrt{km}} \tag{1.16}$$

In Eq.(1.14) the integral gives a scalar which is a function of time and also depends on the damping. Let R be defined as follows:

$$R(\gamma, \omega_{0r}, t) = \frac{1}{\omega_{0r}^*} \int_0^t \ddot{z}(t) e^{-\frac{\gamma}{2}\omega_{0r}^*(t-\tau)} \sin \omega_{0r}^*(t-\tau) d\tau \tag{1.17}$$

If we compute the *R* factors in advance, the summation in Eq.(1.15) is fast and easy. However, it is exactly the computation of the integral that causes difficulties and in engineering practice it may not even be possible if appropriate accelerograms are not available. Yet, as it has been mentioned before, it is adequate to know only the maximum of *R* during the seismic excitation. $S_d(\gamma,\omega_{0r})$ is called the displacement spectrum of the earthquake and it gives the maximum responses as a function of the damping and the natural frequency of the considered mode. To determine the maximum velocity and acceleration we can define $S_v(\gamma,\omega_{0r})$ velocity spectrum and $S_a(\gamma,\omega_{0r})$ acceleration spectrum likewise. The three spectra are with good approximation related in the following way:

$$S_a(\gamma, \omega_{0r}) = \omega_{0r} S_v(\gamma, \omega_{0r}) = \omega_{0r}^2 S_d(\gamma, \omega_{0r}) \tag{1.18}$$

Velocity and acceleration spectra that are computed in the above presented way are called pseudo-spectra. The earthquake spectra are advantageous representations of the anticipated seismic action in an engineering point of view as they give information on the maximum effect. The most common representation of spectra is plotting the response against the period, *T*, of the structure. In *Figure 1.7* the acceleration and the displacement spectra of the earthquake, depicted before in *Figure 1.5*, are presented. As it can be seen, the curves are given for various values of the ξ damping ratio. The structural damping in general is the result of the appearance of inelastic deformations that cause energy dissipation in the structure. Such deformations can be minor cracks, slip or localized plastic deformation of connections etc. Some damping is always present in every structure, but the actual value depends on the structural material and system and also the secondary members and their connection. An average value of the damping ratio that shall be used if no better estimate is made for a structure is 5%. In *Table 1.3* some recommendations are listed for the value of the damping ratio for various structural systems [3].

The use of an acceleration spectrum such as the one presented before in *Figure 1.7/a* is practical, but still certain issues have to be taken into account. Firstly, the curve of the spectrum is very uneven, thus even small changes of the period i.e. small changes of the structural system can entail significant changes in the buildings response. Furthermore, as it has been mentioned before, conducting the seismic analysis for one particular earthquake is not very prudent since earthquakes can be very versatile.

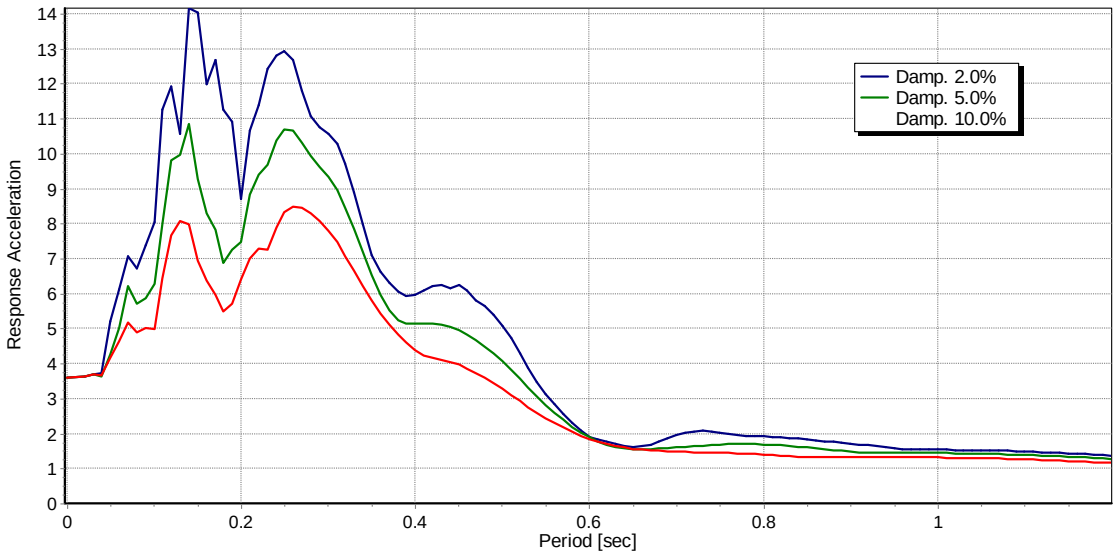

Figure 1.7/a; *Acceleration spectra for different viscous damping*

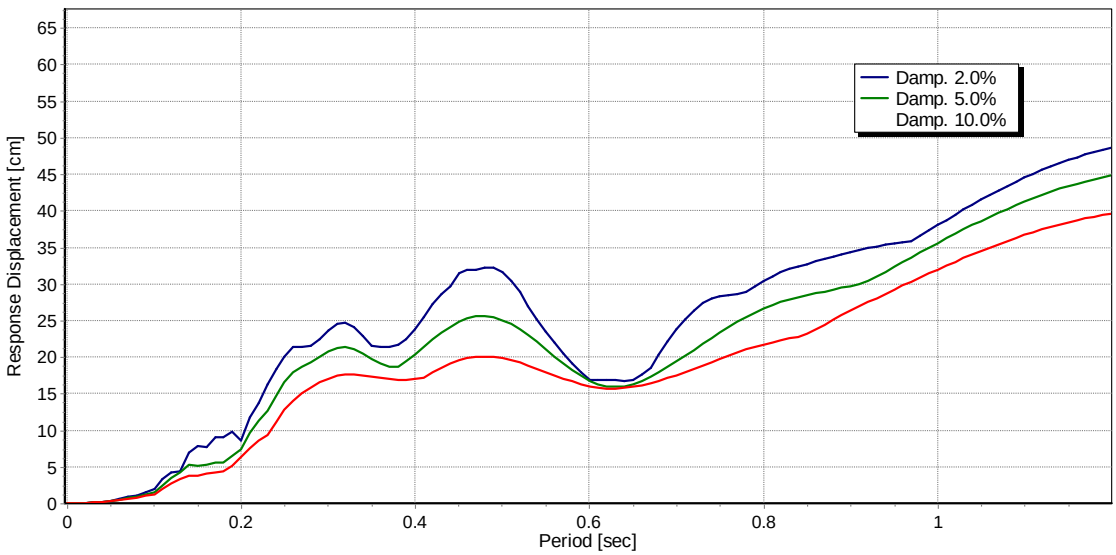

Figure 1.7/b; *Displacement spectra for different viscous damping*

Table 1.3; *Recommended values of the damping ratio*

Structural type	*ξ [%]*
welded steel frame with flexible secondary members	2-3
welded steel frame with traditional secondary members	4-5
steel structure with bolted assemblies	5-6
reinforced concrete frame	5-7
masonry wall structure	7-10
timber structure with dowel type connections	6-8

In seismic design standards such as the Eurocode 8 [4][5] this is treated by defining design response spectra that are smooth and flattened upper envelopes of several individual spectra that correspond to past earthquake records. In seismic standards the effect of the soil conditions on the response is also accounted for and the importance of the designed building modifies the seismic hazard as well.

1.2.3. Representation of the seismic effect in Eurocode 8

In the Eurocode 8 seismic design standard the following elastic response spectra are defined:

- Horizontal, type 1 acceleration response spectra, $S_e(T)$, for "stronger" ground motions
- Horizontal, type 2 acceleration response spectra, $S_e(T)$, for "weaker" ground motions, the magnitude of which is M<5.5
- Displacement response spectra, $S_{De}(T)$
- Vertical acceleration response spectra, $S_{ve}(T)$

The acceleration response spectra are formulated in four subsequent period intervals. The equations, presented below in the table are valid for both type 1 and type 2 earthquakes.

Table 1.4; *Definition of Eurocode 8 elastic horizontal acceleration spectrum*

Interval	$S_e(T)$
$0 \le T \le T_B$	$\gamma_I a_{gR} S\left[1+\frac{T}{T_B}\left(2.5\eta-1\right)\right]$
$T_B \le T \le T_C$	$\gamma_I a_{gR} S \cdot 2.5\eta$
$T_C \le T \le T_D$	$\gamma_I a_{gR} S \cdot 2.5\eta \frac{T_C}{T}$
$T_B \le T \le 4s$	$\gamma_I a_{gR} S \cdot 2.5\eta \frac{T_C T_D}{T^2}$

In the equations the importance class of the designed building is denoted by γ_I. The code distinguishes four importance classes. The values of the importance factor can be selected individually by the countries applying the code in a national annex, but recommended values are given. For buildings having minor importance e.g. sheds or barns the importance factor is 0.8. For buildings of regular importance the factor is 1.0. For more important buildings such as schools and for vital structures like hospitals or power plants the recommended values are 1.2 and 1.4 respectively.

The reference value of the PGA on rock, a_{gR}, is site specific. It can be chosen using seismic hazard maps usually provided in the national annexes. If the value is below 0.08g or 0.04g the considered area is qualified as low or very low seismicity area and in these cases simplified or no seismic analysis is required.

The design spectra in Eurocode 8 are determined for 5% viscous damping. Any difference of the damping ratio from this value is accounted for via the damping correction factor, η. The value of the factor is therefore 1 in case of 5% damping and may be determined by the expression:

$$\eta = \sqrt{10/\left(5+\xi\right)} \ge 0.55 \tag{1.19}$$

The remaining parameters of the equations in *Table 1.4* depend on the soil conditions. There are five main soil classes from A to E A being solid rock and E being soft alluvial layers. The soils may be identified by wave propagation velocity, cohesion or penetration test results. In special cases that do not match the requirements of the classes A to E, studies for

the definition of the seismic action are required. The parameters belonging to the various soil classes and the different types of earthquakes are presented below:

Table 1.5; *Parameters of Type 1 spectra*

Soil class	*S*	T_B	T_C	T_D
A	1.00	0.15	0.4	
B	1.20	0.15	0.5	
C	1.15	0.20	0.6	2.0
D	1.35	0.20	0.8	
E	1.40	0.15	0.5	

Table 1.6; *Parameters of Type 2 spectra*

Soil class	*S*	T_B	T_C	T_D
A	1.00	0.05	0.25	
B	1.35	0.05	0.25	
C	1.50	0.10	0.25	1.2
D	1.80	0.10	0.30	
E	1.60	0.05	0.25	

Substituting these parameters into the expressions in *Table 1.4*, the type 1 and 2 spectra for 5% damping are depicted in *Figure 1.8*.

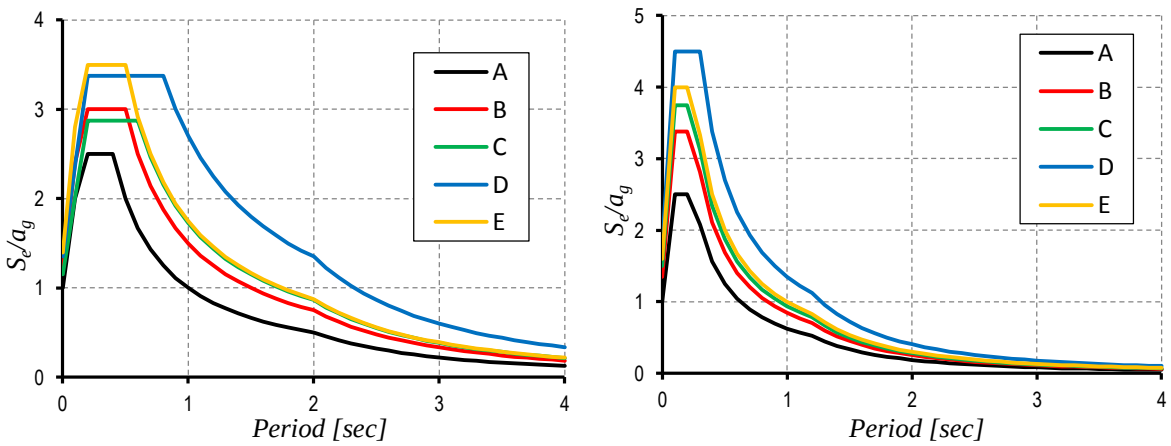

a) Type 1 spectra *b) Type 2 spectra*

Figure 1.8*; Eurocode 8 earthquake spectra*

The elastic displacement spectrum of Eurocode 8 can be calculated from the acceleration spectrum with an expression similar to the one presented in Eq.(1.18):

$$S_{De}(T) = S_e(T)\left[\frac{T}{2\pi}\right]^2 \tag{1.20}$$

However, if the stiffness of the structure is very small and the period is high, the displacements given by the formula above are not attained as the ground can move under the structure. Consequently, the displacement spectrum is extended to periods over 4 seconds and in this range the displacement response decreases down to the maximum ground

displacement defined by Eq.(1.21). As structures with so small stiffness are practically unusual the detailing of this extension is hereby omitted.

$$d_g = 0.025\gamma_I a_{gR} S T_C T_D \tag{1.21}$$

A schematic (and enlarged) diagram of the acceleration, velocity and displacement spectra is presented in *Figure 1.9*. If the period is zero or very small ($T<T_B$) i.e. the building is rigid, the motion of the structure follows the motion of the ground. These structures practically have to be designed to withstand the maximum acceleration of the ground. If the period is between T_B and T_C the acceleration is the largest and is independent of the stiffness. Structures, the period of which is in this interval, are called acceleration sensitive. If the structure is flexible and the period exceeds T_D, then the displacements are independent of the period and they are substantially larger than the displacements of the ground. These buildings are displacement sensitive and they need to be designed to have sufficient displacement capacity. Buildings belonging to the intermediate interval ($T_C < T < T_D$) are velocity sensitive because in this case the velocities are the largest.

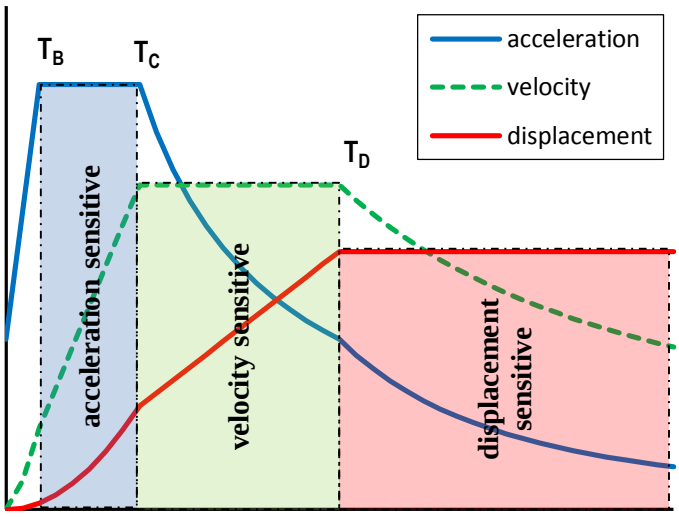

Figure 1.9; *Acceleration, velocity and displacement spectra*

The vertical elastic response spectrum is defined with the same parameters as the horizontal spectra. The vertical design acceleration, a_{vg}, can be calculated from the horizontal by multiplying it with 0.9 for type 1 and 0.45 for type 2 earthquakes. The vertical component shall only be considered if the design acceleration exceeds 0.25g~2.5 m/s^2, and only for large span beams and cantilevers and other special cases in buildings. Such special cases and also a sufficiently high seismicity will not be considered in the present work, so hereafter the vertical seismic effect will be neglected.

1.2.4. Seismic effect in practical design, the behaviour factor

The lateral forces calculated with an elastic acceleration response spectrum can be enormous as the PGA amplified by the appropriate value from the spectrum may be comparable or even larger than the acceleration of gravity. If in design we require the lateral resisting members to remain elastic i.e. counteract the large seismic actions without any damage, the dimensions have to be huge. In the meantime the design seismic action usually

has a long return period, therefore it is likely that the large structural weight premium that elastic design imposes will not be utilized during the service life of the building. This is economically hardly acceptable. A resolution to this problem has been proposed by Newmark et al. [6] who observed that the elastic displacements of one building (with a period $T>T_C$) and the inelastic displacements of another with the same period but substantially smaller resistance are roughly equal when subjected to the same ground motion. In other words, a stronger and a significantly weaker building may have the same seismic resistance given that the weak building is capable of exhibiting adequately large inelastic deformations. Consequently, it is enough to design a building to sustain reduced seismic forces and then extrapolate the displacement effects to the desired strength. This idea has been incorporated in seismic design codes via a reduction or behaviour factor.

An explanation of the concept of designing structures taking into consideration the reduction of the design seismic effect is given by Ballio and Setti [7][8][9]. Let us consider a structure and subject it to an earthquake multiple times with different levels of the PGA. Also let us suppose that the response is characterised by the maximum displacements of the top and depict these against the ground acceleration, see *Figure 1.10*. When the acceleration is small the building remains elastic so the response is represented by a straight line from the origin to point B. Beyond point B the inelastic displacements, depicted by the curve are inferior to the extrapolated displacements depicted by the dashed line. This is a direct consequence of the dissipation detailed later in section 1.3.1. At certain acceleration however, the curve of the inelastic displacements intersects in point C the dashed line. Beyond this point second order effects may strongly amplify the displacements so that the structure attains collapse by dynamic instability, i.e. the displacements rapidly grow without notable change of the loading. The behaviour factor in Eurocode 8 may be defined as the ratio of the ultimate seismic effect corresponding to collapse, α_u, and the one corresponding to the elastic limit, α_{el}. In other words, the ratio of the accelerations in point C and B:

$$q = \frac{a_u}{a_{el}} \tag{1.22}$$

If we design a structure the elastic resistance of which is at point B to a reduced seismic action defined by point A, we may expect that the inelastic displacement response of the structure to the real ground motion, point E, will necessarily be smaller than the extrapolated elastic response, point D in the figure. The design with an appropriately chosen behaviour factor permits to conduct elastic analysis and gives an estimation of the effects to the benefit of safety.

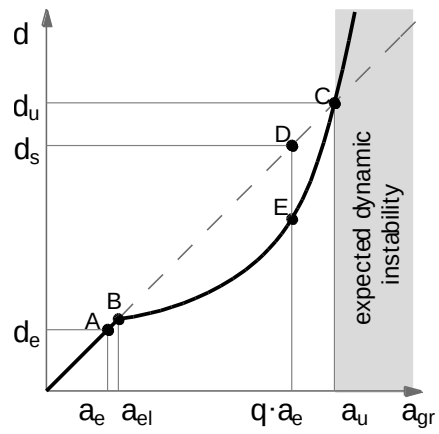

Figure 1.10; *Theoretical inelastic ground acceleration – displacement response [7]*

1.2.5. Behaviour factor in Eurocode 8

As it has been presented before, Eurocode 8 permits the use of the q behaviour factor in design. The method of application is that the elastic acceleration spectrum can be reduced by the behaviour factor, see *Figure 1.11*. The obtained reduced spectrum is the design spectrum to the effects of which elastic design can be conducted. The definition of the design spectrum is the following:

Table 1.7; *Definition of Eurocode 8 design horizontal acceleration spectrum*

Interval	$S_e(T)$
$0 \le T \le T_B$	$\gamma_I a_{gR} S\left[\frac{2}{3}+\frac{T}{T_B}\left(\frac{2.5}{q}-\frac{2}{3}\right)\right]$
$T_B \le T \le T_C$	$\gamma_I a_{gR} S \cdot \frac{2.5}{q}$
$T_C \le T \le T_D$	$\max\left\{\gamma_I a_{gR} S \cdot \frac{2.5}{q}\frac{T_C}{T}; \beta\gamma_I a_{gR}\right\}$
$T_B \le T \le 4s$	$\max\left\{\gamma_I a_{gR} S \cdot \frac{2.5}{q}\frac{T_C T_D}{T^2}; \beta\gamma_I a_{gR}\right\}$

As it can be seen, a lower bound acceleration is defined in the $T>T_c$ period range. The recommended value of the β factor is 0.2.

From the results of the elastic analysis the inelastic displacements are (in theory overestimated by extrapolating the acquired elastic displacements linearly with the q_d displacement behaviour factor.

$$d_s = q_d d_e \quad \text{where} \quad q_d = q \tag{1.23}$$

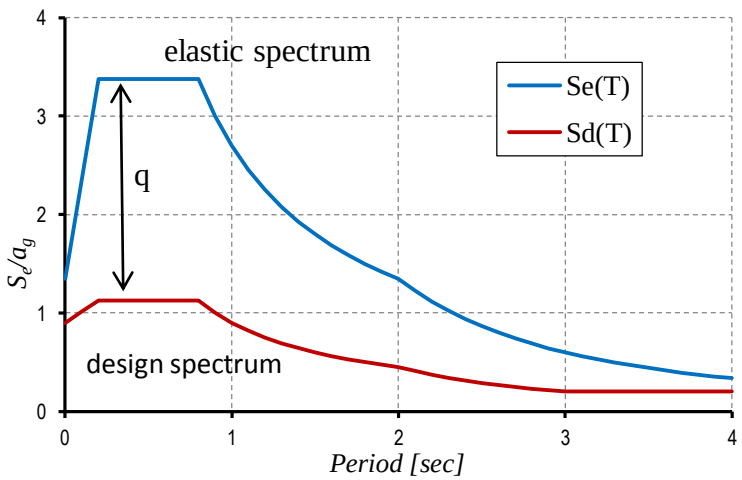

Figure 1.11; *Elastic and design Eurocode 8 acceleration spectra*

It has to be noted though, that the two behaviour factors, q and q_d can only be deemed equal if the period is sufficiently large ($T>T_C$). Short period buildings are very stiff therefore they are designed to the largest accelerations and they exhibit moderate displacements. The occurrence of inelastic deformations is usually in conjunction with the loss of stiffness and the increase of displacements, so the displacement response of structures belonging to the

short period range is larger than the linear approximation. In this case q_d is larger than q; the details of the calculation are omitted here.

As it has been mentioned before, the design to reduced seismic actions is only valid if the structure is indeed capable of sustaining the inelastic deformations without collapse. The inelastic displacement capacity is well described by the ductility which is similar in definition to the behaviour factor, but expresses the ratio of the ultimate, d_u, and elastic limit, d_e, displacements instead of the action effect:

$$\mu = \frac{d_u}{d_e} \tag{1.24}$$

Obviously the ductility capacity of a structure has to be equal or greater than the behaviour factor considered in the design. Various structural types possess various achievable ductility capacity and therefore the behaviour factor has upper bound limits that changes with the structural type. In the meantime, q also has a practically recommended lower limit being 1.5, due to various factors such as friction of connection, minor irreversible deformations, etc. Fundamentally, structures are classified into three ductility classes; low (DCL), medium (DCM) and high (DCH). These classes primarily differ in the allowed cross-sectional class, according to Eurocode 3 [10], of the inelastic members and of course the allowed behaviour factor. In the table below the classification and the behaviour factors of some typical steel structural types are presented:

Table 1.8; *Behaviour factors for various steel structures*

Structural type	*DCL*	*DCM*	*DCH*
allowed cross-sectional class (EN 1993-1-1)	*1, 2, 3*	*1, 2*	*1*
Moment resisting frames	1,5 - 2	4	$5\alpha_u/\alpha_1$
Diagonally braced frame		4	4
V-braced frame		2	2.5
Eccentrically braced frame		4	$5\alpha_u/\alpha_1$

As it can be seen, the allowed behaviour factor of diagonally braced frames is 4 in both DCM and DCH classes. This is due to the basis of the classification. The ductility of braced frames primarily comes from the tensile ductility of the diagonals and the tensile ductility does not depend on the cross-sectional classification, therefore there shall be no difference between DCM and DCH classes. It is also important to note that according to the table there are clear differences between the behaviour of various braced frame arrangements. The reason to this distinction has been explained in the beginning of the chapter in 1.1.

The definition of the q factor considers the seismic action level that corresponds to first yield. For a single degree of freedom (SDOF) structure this is equal to the ultimate load corresponding to the development of a plastic mechanism, see *Figure 1.12*. In this case only one plastic hinge is needed to form a plastic collapse mechanism. In a MDOF system however, multiple plastic hinges are needed that do not develop at the same seismic action level. The level of the first yield, α_1 differs from the ultimate level, α_u. This difference allows the behaviour factor to be dependent on the α_u/α_1 multiplier. In case of concentrically braced frames this effect shall not be considered because in CBF-s it assumed that there is no difference between the two load levels.

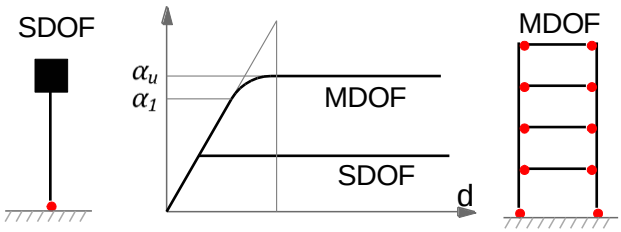

Figure 1.12; *Inelastic reserve of MDOF systems*

Furthermore, it is apparent, that between the low ductility class and the medium and high ductility classes there is a major qualitative difference. This will be further explained in the following.

1.3. General concepts in seismic design

1.3.1. Principles of capacity design

As it has been explained before, in order to conduct seismic analysis applying a reduction of the seismic action via the behaviour factor, it has to be ensured that the structure has adequate ductility capacity. On one hand, the behaviour factor has to be appropriately chosen for the designed structural type, it cannot be arbitrarily large. On the other hand, the structure has to be made capable of exhibiting inelastic deformations. These concerns are incorporated in the capacity design philosophy.

The principles of the capacity design were elaborated by Thomas Paulay [11]. The three main steps describing the method of design are:

- An appropriate behaviour factor has to be determined that is in correlation with the expected ductility of the structural type.
- The inelastic zones of the structure have to be designated and these need to be detailed so that they can undergo repeated cycles of plastic deformations without failure.
- Structural members that participate in the seismic resistance but are not expected to exhibit inelastic deformations have to be provided with an overstrength that safeguards that they remain elastic indeed during the earthquake.

The number of the zones or cross-sections where we permit inelastic deformations depends on the level of statical indeterminacy of the structure. If it is n, then maximum n+1 zones has to be plastic in order to create a plastic yield mechanism which corresponds to the ultimate resistance of the structure. Out of the two examples below the one on the left is statically determinate (n=0), therefore only the brace have plastic deformations. In the second case the moment resisting beam-column connections increase n by 2, so for the plastic yield mechanism two plastic hinges are also required.

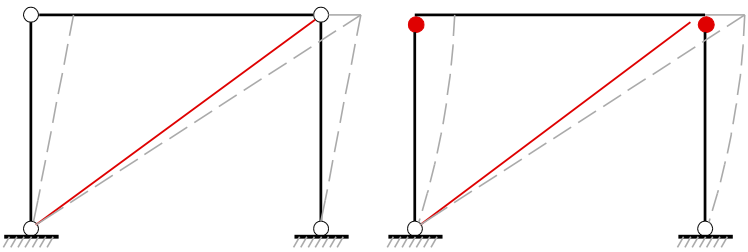

Figure 1.13; *Plastic collapse mechanisms*

In the selection of the plastic zones we have a limited freedom. In the first example even the beam could be plastic under the compressive forces of the lateral load or in the second case the plastic hinges could be located on the beam. In general the plastic zones develop in cross sections where the internal forces are high. Out of these locations by adjusting the resistances to the effects, the desired ones can be selected. The selection of course has to be in favour of promoting the largest possible decrease of the seismic actions in design. If we considered the ductility as the measure of the mechanisms then unlimited displacements would be desirable. Yet, displacements are limited in practice by the deformation capacity of the material. Therefore, a plastic mechanisms utility in providing a better seismic behaviour shall be expressed rather in terms of energy as it is described hereafter.

Through the ground displacements seismic input energy is transmitted into the structure that is transformed into various forms of mechanical energy. The components of the energy balance are depicted in the following "equation":

$$\{seismic\ input\ energy\} = \left\{ \begin{array}{c} elastic\ deformation \\ + \\ kinetic\ energy \\ + \\ dissipation\ via\ damping \\ + \\ dissipation\ via\ plasticity \\ + \\ soil\ deformation \end{array} \right\}$$

Structures belonging to the low ductility class are not expected to dissipate energy by dissipation via large plastic deformations. These structures are therefore also categorized as low dissipative. Conversely, buildings belonging to the DCM and DCH ductility class dissipate energy by the plastic deformation of the so called dissipative members and they are considered as dissipative structures. The dissipation in general is directly accountable for the decrease of seismic forces because the more the seismic input energy is decreased by dissipation, the less energy is stored as elastic deformations and velocity (representing the kinematic energy).

It is obvious that for low dissipative structures the capacity design procedure is not applicable as the second two main steps cannot be interpreted as the absence of large plastic dissipation means the absence of a plastic mechanism. For dissipative structures however, a plastic mechanism has to be defined with the aim of maximizing the dissipation (coming from unitary displacement), the dissipative members need to able to dissipate energy and the non-dissipative members have to respect additional rules in order to remain elastic. As a consequence, seismic codes to penalize the seismic effects of non-dissipative members by various sources of overstrength and the members need to be designed to withstand these amplified actions. The enlarged effects have the form of:

$$E_{Ed} = \gamma \Omega \gamma_{ov} \cdot E_{Ed,E} \tag{1.25}$$

where:

$E_{Ed,E}$	is the design effect of the seismic action
γ_{ov}	is the overstrength coming from the difference between the nominal and real yield stress of the material
Ω	the ratio of the effect and the resistance of the dissipative member
γ	additional safety factor to take into consideration strain hardening

1.3.2. Capacity design of CBF-s in Eurocode 8

In Eurocode 8 the promoted mechanism and the structure-specific regulations of capacity design are as follows. In CBF-s the large majority of the connections and splices may be considered as pinned as the structure is stiff and stable without moment resisting

connections. Consequently, the level of statical indeterminacy is low and only a limited number of members, mostly the braces, can be dissipative members. In classical design CBF-s are supposed to develop a global plastic mechanism when subjected to seismic actions, see *Figure 1.14*. Depending on the direction of the loading all the braces in tension get equally elongated and the ones in compression buckle. This mechanism allows the largest possible dissipation in the structure as every brace participates in the dissipation of the seismic input energy and therefore the global mechanism provides the largest reduction of the internal forces in the structure. Also, by the uniform distribution of the drifts on every floor a significant ductility capacity can be achieved.

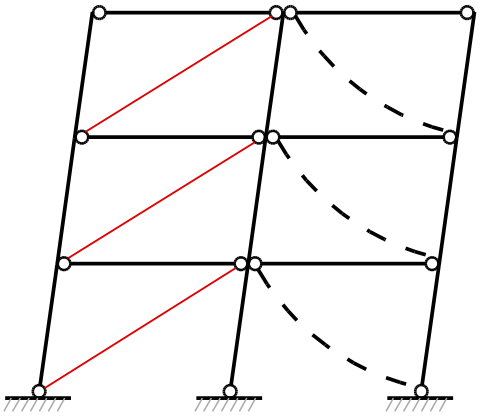

Figure 1.14; *Global plastic mechanism of CBF-s*

Due to the buckling of the compression braces the small residual axial forces can be neglected and it is allowed to conduct the linear analysis considering the (tensile) braces of one bay only. Concerning the requirements imposed to the members, the braces have to be designed to the axial forces occurring in the design seismic combination of actions:

$$N_{br,Ed} \leq N_{pl,Rd} \tag{1.26}$$

where N_{Ed} is the design axial force and $N_{pl,Rd}$ is the plastic tensile resistance of the brace cross section. In addition, Eurocode 8 defines limitations to the relative global slenderness also:

$$\bar{\lambda} \leq 2.0 \tag{1.27}$$

and especially for X-braced configurations:

$$1.3 \leq \bar{\lambda} \tag{1.28}$$

The relative global slenderness is the ratio between the slenderness and the elastic limit slenderness:

$$\bar{\lambda} = \frac{\lambda}{\lambda_1} \text{ with } \lambda_1 = \pi\sqrt{\frac{E}{f_y}} \tag{1.29}$$

The upper bound defined in Eq.(1.27) is imposed to prevent the rapid degradation of the resistance of the braces. Furthermore this limits the plastic out-of-plane deformation [12] of gusset plates which are prone to low-cycle fatigue failure. The lower bound assures the sufficient flexibility of the diagonals and avoids the occurrence of normal forces in the columns that significantly differ from the results obtained with the one-brace model. Also the

lower bound slenderness ensures buckling of the compressive diagonal before the yield of the tensile diagonal.

For the sake of homogeneous dissipative behaviour the simultaneous yield of the braces on every floor has to be ensured. Eurocode 8 aims to promote this by a condition given for the overstrength factors, Ω_i, realized on the different floors, making them closely uniform. It needs to be verified that the maximum storey overstrength for the seismic combination of actions does not differ from the minimum by more than 25%:

$$\frac{\Omega_{\max}}{\Omega} \leq 1.25 \tag{1.30}$$

where the global overstrength factor, Ω, is defined as the minimum storey overstrength:

$$\Omega = \min \Omega_i \tag{1.31}$$

and,

$$\Omega_i = \frac{N_{pl,Rd,i}}{N_{br,Ed,i}} \tag{1.32}$$

where $N_{pl,Rd}$ is te axial resitance and $N_{br,Ed}$ is the axial effect. For the design of the non-dissipative columns and beams Eurocode 8 requires the fulfilment of the following condition:

$$N_{Rd}\left(M_{Ed}\right) \geq N_{Ed,G} + 1.1 \cdot \gamma_{ov} \cdot \Omega \cdot N_{Ed,E} \tag{1.33}$$

where $N_{Rd}(M_{Ed})$ is the axial resistance in accordance with Eurocode 3, taking into consideration the interaction with the design bending effect M_{Ed}. $N_{Ed,G}$ and $N_{Ed,E}$ are the axial forces due to the non-seismic and the seismic actions respectively. The material overstrength factor, γ_{ov}, accounts for the random variability of the yield stress. Its recommended value is 1.25, but it may be varied in corresponding National Annexes. The amplification coefficient 1.1 represents the increase of the yield stress of the dissipative members due to strain-hardening. The total overstrength, $1.1\gamma_{ov}\,\Omega$ is a way to account for the resistance reserve of the non-dissipative members. In principle, it ensures that the resistance of the non-dissipative members is adequate until the plastic yield of all the diagonals.

1.3.3. Performance-based earthquake engineering in EC8

The seismic design concepts and the specific requirements of Eurocode 8 that have been introduced so far primarily intend to prevent structural collapse. However, failure prevention and the preservation of life shall not be the only concerns especially if the earthquake is weaker than the one considered in design. On one hand maintaining the operation of some building types is more important than of others e.g. hospitals, utility stations, schools. On the other hand, in case of more frequent quakes, the damages of non-structural members should be prevented making the continuous occupancy possible.

The Structural Engineers Association of California (SEAOC) proposed the performance requirements [13][14] depicted by *Figure 1.15*. In the concept of Performance-Based Earthquake Engineering (PBEE) four performance requirements are proposed to four seismic action levels defined by their return period in years.

In Eurocode 8 both the requirements and the action levels are less detailed but the concept in principal correlates with the presented figure. The differences of the importance of

the buildings are considered at the definition of the seismic action as the PGA is scaled by the γ_I importance factor. For buildings of extraordinary or critical importance 20% or 40% increase of the seismic effect is recommended. In order to reasonably couple the seismic hazard and the performance target, Eurocode 8 imposes two fundamental requirements that are approximately indicated by the red dots in the figure.

- **No-collapse requirement**: the primary structural members have to be verified that they have adequate strength and ductility so that structural integrity is retained after the seismic action. The reference earthquake associated with this state has a return period $T_{NCR}=475$ years.
- **The damage limitation requirement**: the structure shall withstand earthquakes of smaller return period without extensive damage that may limit the use or the cost-of-which shall be disproportionally high. The reference earthquake associated with this state has a return period $T_{NCR}=95$ years.

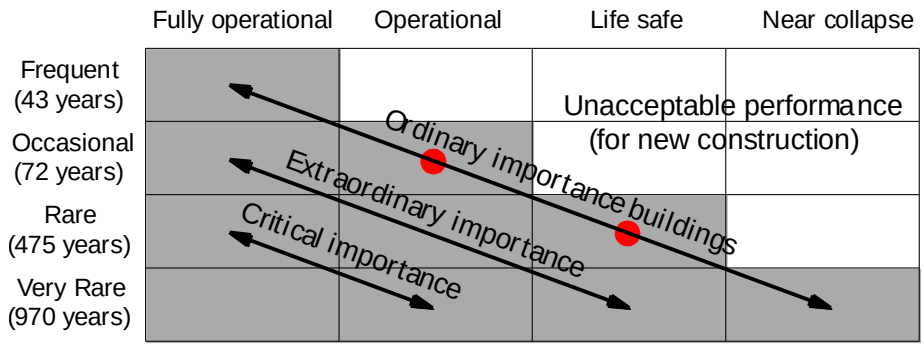

Figure 1.15; *Performance requirements for buildings of various importance*

In the damage limitation design state performance targets are imposed upon the inelastic relative drifts of adjacent floors, i.e. the interstorey drifts. The main difference between the different requirement levels is whether or not the non-structural elements, the damage of which is intended to be limited, are brittle, ductile or flexibly connected to the primary members. Considering a building with not particularly sensitive non-structural elements, the not rigorous, but for steel buildings commonly used limitation of the maximum inelsatic interstorey drift, d_r is:

$$d_r \nu \leq 0,010h \tag{1.34}$$

where h is the storey height and ν is the reduction factor taking into account the lower return period of the seismic effect as d_r is to be computed with the seismic action associated with the no-collapse state. The recommended value of the reduction factor for buildings of ordinary importance is ν=0.5, though national annexes may give even less rigorous values. In other words, according to Eq.(1.35), the requirement for damage limitation can be interpreted as the maximum allowed interstorey drift is 2% of the storey height regarding the seismic action considered in no-collapse design state since:

$$d_r \leq 0,010h/\nu = 0.020h \tag{1.35}$$

1.4. Analysis methods in seismic engineering

1.4.1. Linear static seismic analysis methods

Previously we have defined the practical form of the seismic action that needs to be applied in seismic analysis and also presented the basic principles of seismic design and performance requirements. Hereby the most common methods of linear static seismic analysis will be presented in with the seismic action is defined by the acceleration spectra.

Given a single degree of freedom (SDOF) structure with predefined damping, importance class and behaviour factor, the maximum structural response can be directly derived using the appropriate response spectra and the structure's one and only period. Conversely, the response of an *n*-storey multi degree of freedom (MDOF) structure is defined by multiple parameters such as the n masses, stiffness and damping on the different storeys. In order to obtain equivalent lateral seismic forces to which elastic static analysis can be computed, two methods may be used. The simpler lateral force method and the mostly computerized modal response spectrum analysis are both included in the Eurocode 8 design code. Their use is summarized in the following.

In the lateral force method of analysis it is assumed that the response is characterized by a representative parameter e.g. the top lateral displacement and the shape of the deformed structure follows a predefined function. This function is conventionally linear, see *Figure 1.16/a*. This way the MDOF system is substituted by an equivalent SDOF. The sum of the equivalent loading is calculated using the SDOF approximation but for the analysis it is redistributed along the height following the assumed shape.

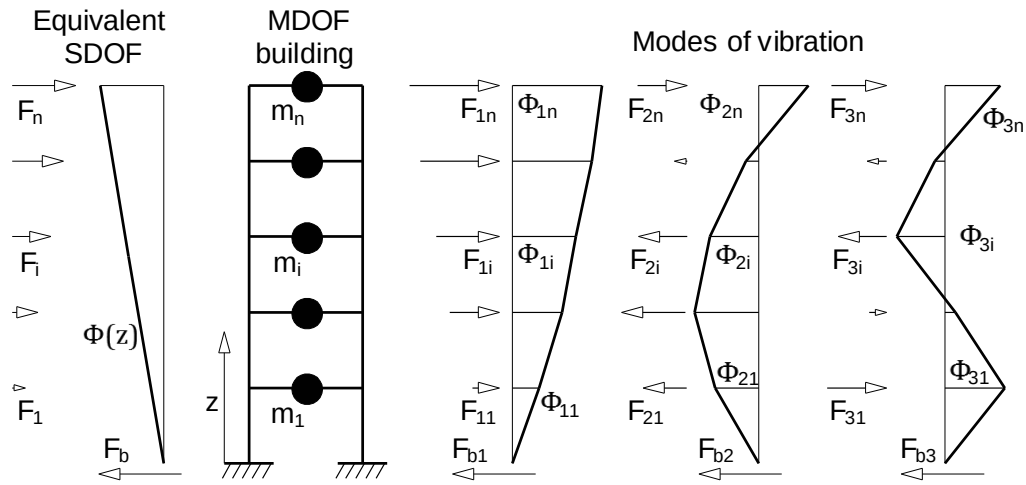

a) lateral force method *b) modal response spectrum method*

Figure 1.16; *Equivalent lateral loading in linear seismic analysis methods*

First of all, the fundamental period, T_1, of the building has to be determined in order to define the maximum acceleration from the elastic response spectrum. In hand calculation, which is what the lateral force method is developed for, the period can only be estimated by various empirical formulas given in the standard or by other simple methods such as the method of Rayleigh. Having determined the acceleration response, the seismic base shear force is calculated by Newton's second law as follows:

$$F_b = S_d\left(T_1\right)\cdot m\cdot\lambda \tag{1.36}$$

where m is the mass of the whole building and λ is a correction factor to take into account that actually it is not the whole mass that exhibits rigid-bodily movement. In most multistorey buildings the recommended value of this factor is 0.85. The redistribution of the total base shear is proportional to the masses of the slabs, m_i, and the lateral displacements, s_i, determined by the approximate shape function:

$$F_i = F_b \frac{s_i m_i}{\sum s_j m_j} \tag{1.37}$$

If the shape function is indeed considered to be simply linear, the lateral displacements can be replaced by the height of the storeys above the basement, z_i.

$$F_i = F_b \frac{z_i m_i}{\sum z_j m_j} \tag{1.38}$$

The equivalent lateral forces can be used in combination with other effects in regular static analysis and the dimensioning can be carried out respecting also the specific requirements of capacity design.

As it has been shown, one advantage of the modal response spectrum analysis is that it decouples the dynamic equilibrium equation into a series of SDOF problems. For each, a mode of vibration and the corresponding period can be computed and the response of the MDOF structure can be expressed as a combination of the different modes. The modal combination does not only apply for the displacements of course, see Eq.(1.15), but also for the equivalent lateral loading. The base shear of the mode i can be calculated with an expression similar to Eq.(1.36).

$$F_{bi} = S_d\left(T_i\right) \cdot m_i^* \tag{1.39}$$

where m_i^* is the modal mass participation, previously approximated for the fundamental mode by m and λ, and computed as:

$$m_i^* = \frac{\left(\mathbf{\Phi}_i^T \mathbf{M} \boldsymbol{\iota}\right)^2}{\mathbf{\Phi}_i^T \mathbf{M} \mathbf{\Phi}_i} \tag{1.40}$$

where $\mathbf{\Phi}_i$ is the modal vector, $\mathbf{M}$ is the mass matrix and $\boldsymbol{\iota}$ is a pointer vector indicating the components in the considered direction. The modal lateral load vector for the mode i is once again proportional to the mode shape and the masses:

$$\mathbf{p}_i = \mathbf{\Phi}_i \frac{\mathbf{M}}{\mathbf{\Phi}_i^T \mathbf{M} \boldsymbol{\iota}} \frac{\left(\mathbf{\Phi}_i^T \mathbf{M} \boldsymbol{\iota}\right)^2}{\mathbf{\Phi}_i^T \mathbf{M} \mathbf{\Phi}_i} S_d\left(T_i\right) = \mathbf{\Phi}_i \mathbf{M} \frac{\mathbf{\Phi}_i^T \mathbf{M} \boldsymbol{\iota}}{\mathbf{\Phi}_i^T \mathbf{M} \mathbf{\Phi}_i} S_d\left(T_i\right) \tag{1.41}$$

The application of both static methods has further requirements and limits. First of all, the lateral force method shall only be used if the fundamental period is not too elevated (T_1<2.0; $4T_C$), because in such a case it is likely that the upper modes with shorter period may not be negligible any more, which is what is assumed in the method. The upper modes may also be relevant if the building is irregular in elevation, i.e. abrupt, at least 20% changes of stiffness or mass from one storey to the other are present in the structure. For such building the use of the lateral force method is not allowed. Eurocode 8 gives a more detailed definition for the regularity in elevation and also for the regularity in plan which is deemed to

determine whether the use of independent planar models in both lateral directions is appropriate or spatial model has to be built. Hereby these details are omitted.

If we consider every mode of a certain structure using the modal response spectrum analysis, the sum of the modal participations is 1.0, so all the mass is considered. Unfortunately for a multistorey building, especially when using spatial finite element models, the number of the modes can be enormous, requiring long computation time. It is therefore adequate to consider only a number of modes that add up to 90% modal mass participation altogether, insofar as every mode having a participation of 5% or more is accounted for. Usually considering the first few modes is enough to satisfy these conditions.

If all the relevant modes and the equivalent lateral loads are computed, the combination of the modes may be done by simply summing the effects of the different modes. It has to be noted though, that the response spectrum method by definition gives the maxima in each mode. These maxima are not attained in the same time instant during the earthquake; therefore the summing is a very conservative approximation. Consequently, two other methods are commonly used instead in practice. The Square Root of the Sum of Squares (SRSS) gives a better approximation of the maximum earthquake effect, E_E, to be considered:

$$E_E = \sqrt{\sum_i \left(E_{Ei}\right)^2} \tag{1.42}$$

The SRSS method supposes that the response of the different modes is independent, therefore it tends to give results very different from NTHA results if the periods of some modes are close. If the periods of any two modes do not satisfy the condition below, they cannot be considered independent and instead of the SRSS the Complete Quadratic Combination (CQC) has to be utilized.

$$T_j \leq 0.9 T_i \tag{1.43}$$

The CQC method determines the combination of the modal effects with regard to the correlation coefficient, ρ_{ij}, of every two modes.

$$E_E = \sqrt{\sum_i \sum_j \left(E_{Ei} \rho_{ij} E_{Ej}\right)} \tag{1.44}$$

The correlation coefficients can be collected into a symmetric correlation matrix. The elements in this matrix on the main diagonal are 1.0 and apart from the diagonal the larger the difference of the periods is, the smaller the correlation gets. The coefficients are computed as follows:

$$\rho_{ij} = \frac{8\xi^2 \left(1+\alpha_{ij}\right)\alpha_{ij}^{3/2}}{\left(1-\alpha_{ij}^2\right)^2 + 4\xi^2 \alpha_{ij}\left(1+\alpha_{ij}\right)^2} \text{ where } \alpha_{ij} = \frac{T_j}{T_i} \tag{1.45}$$

It is also necessary to combine the response in the two separately analysed orthogonal directions. In Eurocode 8 the so called 30% rule is implemented, so the effects in the two planar directions (still neglecting the vertical) need to be combined as:

$$\begin{aligned} &E_{Edx} \text{"+"} 0.03 E_{Edy} \\ &0.30 E_{Edx} \text{"+"} E_{Edy} \end{aligned} \tag{1.46}$$

The introduced elastic static analysis methods that are conducted on perfect models of the building are inherently not capable of incorporating effects such as the accidental eccentricity of the masses or the second order effects. Consequently, in Eurocode 8 it is required to penalize the seismic action effects by factors that represent these phenomena.

The eccentricity of the centre of mass (CoM) of the slabs and the centre of stiffness (CoS) already implies the torsion of the building. This eccentricity can be further amplified by the uncertainty of the distribution of the mass on the floor slab. This effect can either be approximately taken into account by multiplying the seismic action effects of the lateral resisting members by δ, defined below, or by estimating the accidental eccentricity, e_{ai}, and applying a concentrated torsional moment on every floor in both senses.

$$\delta = 1 + 0.6\frac{x}{L_e} \tag{1.47}$$

$$M_{ai} = e_{ai}F_i \text{ where } e_{ai} = \pm 0.05L_i \tag{1.48}$$

where x is the eccentricity of a lateral resisting member to the centre of mass, L_e is the distance between the outermost resisting members and L_i is the floor dimension. All these distances are perpendicular to the direction of the seismic loading, F_i, and are depicted in *Figure 1.17*. If the lateral resisting system non-symmetric the coefficients in Eqs. (1.47) and (1.48) are 0.12 and 0.10.

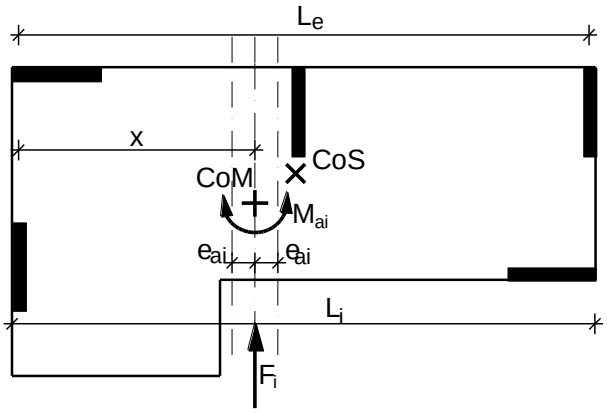

Figure 1.17; *Eccentricity of seismic loading and accidental torsion*

The lateral displacements and the vertical gravity forces together result in an additional overturning moment, see *Figure 1.18*. The larger the lateral displacement is, the more significant this moment becomes and the more it gradually decreases the structure's resistance to lateral loading. This effect is often referred to as the P – Δ effect. The P - Δ cannot be computed with the initial geometry as in that case the gravity force is not eccentric to the vertical members. In order to consider in the analysis the eccentric gravity forces either second order computations need to be conducted, or the first order analysis result need to be altered by approximate formulas.

In order to account for second order effects in Eurocode 8 the interstorey drift sensitivity coefficient needs to be calculated. This coefficient is the ratio of the destabilizing and stabilizing moment and is expressed as follows:

$$\theta = \frac{P_{tot} \cdot d_r}{V_{tot} \cdot H} \tag{1.49}$$

where P_{tot} is the gravity load considered on and above a storey in the seismic design situation, V_{tot} is the total seismic storey shear, H is the storey height and d_r is the design inelastic interstorey drift computed according to Eq.(1.23). The value of the coefficient shall not exceed 0.3. If the coefficient is smaller than 0.1 then second order effects can be neglected, otherwise the effects of the seismic action need to be amplified multiplying by:

$$\frac{1}{1-\theta} \tag{1.50}$$

The two presented formulas concerning the second order effects in Eurocode 8 were found to be rigorous and impose significant but rather unnecessary resistance need on steel structures [15]. The authors propose to consider the elastic displacements instead of the plastic, but enlarging the sensitivity factor on the basis of the considered ductility:

$$\theta_e = \frac{P_{tot} \cdot d_e}{V_{tot} \cdot H} \leq 0.1\omega \tag{1.51}$$

where ω is 1.0 for q=1.0, 0.65 for q=1.5 and 0.5 in every other case. If $\theta_e > 0.1\omega$, the amplification of the effects shall be done by:

$$\frac{1}{1-q\left(\theta_e - 0.10\omega\right)} \tag{1.52}$$

The above expressions have been recently (2014) approved by the French Standardisation Committee in the form of:

$$\theta = \frac{P_{tot} \cdot d_e}{\Omega_u \cdot V_{tot} \cdot H} \leq 0.1 \text{ where } \Omega_u = 0.5q \tag{1.53}$$

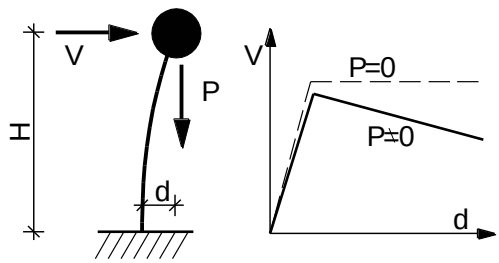

Figure 1.18; *P – Δ effect of SDOF system*

1.4.2. Nonlinear static seismic analysis

For the purposes of linear elastic static analysis the seismic loading is always defined by the design spectrum which is obtained from the elastic spectrum via transformation depending on the behaviour factor. In this transformation a rough estimation of the inelastic behaviour is incorporated. In order to resolve the uncertainty related to the inelastic behaviour and to verify if the assumed plastic mechanism is developed, in accordance with the principles of capacity design, inelastic calculations may be conducted. The most common non-linear static procedure for the seismic analysis of structures is the Pushover Analysis (PA) that will be essentially introduced in the following.

The pushover analysis is performed for monotonically increased increments of equivalent horizontal seismic loads (representing the inertia forces) with simultaneous and

invariant, mostly gravity forces. This procedure uses a series of sequential elastic analyses, superimposed to approximate a force-displacement capacity diagram of the overall structure. The mathematical model of the structure is modified to account for reduced resistance and stiffness due to the yielding components. The lateral distribution is increased until the structure reaches its ultimate resistance or until a prescribed displacement of a control node.

In practice the model of the building, where all necessary material nonlinearities are accounted for, is loaded by the simultaneous gravity forces and a lateral load pattern, see *Figure 1.19*. According to Eurocode 8 provisions the pattern is either constant or modal, mostly corresponding to the fundamental mode which is usually approximately linear as it is depicted in the figure. In subsequent load steps the lateral loading is increased by multiplying with a load parameter, λ, but as the lateral loading is usually normalized, the parameter is equal to the base shear that characterizes the seismic effect. The computations are controlled by the lateral displacement of a control node i.e. the centre of mass of the top floor. The diagram depicting the base shear, F_b, plotted against the control displacement, d, is called the capacity curve, presented also in the figure below.

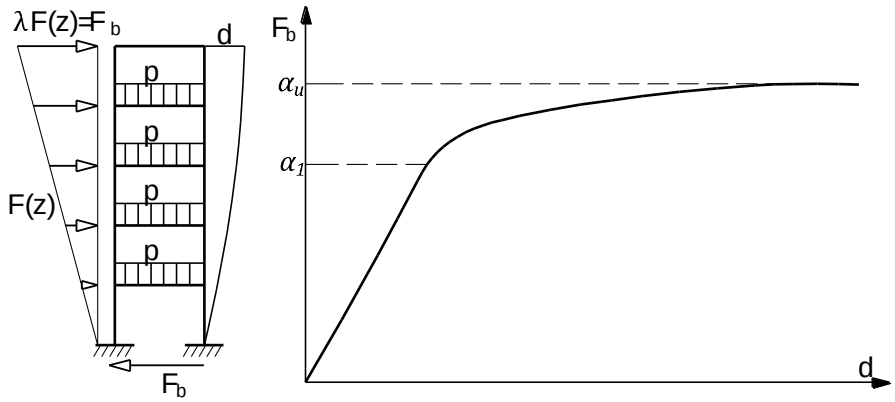

Figure 1.19; *Pushover analysis loading and capacity curve*

The pushover analysis has multiple purposes. On one hand the development of the plastic collapse mechanism can be investigated which can substantiate the judicious choice of the q factor for elastic design. Also, the ratio of the ultimate resistance, α_u, and first yield, α_1, can be determined, which may be used to further enlarge the behaviour factor, see 1.2.5. In addition the pushover analysis can be used to verify if the structure has adequate displacement capacity as from the definition of the seismic action a target displacement can be calculated.

In order to cross-refer the MDOF capacity curve with the earthquake spectrum it has to be substituted by an equivalent SDOF systems curve as the spectra refer to such systems. The mass of the equivalent SDOF system is defined as:

$$m^* = \sum m_i \Phi_i \tag{1.54}$$

where m_i is the mass on the ith floor and Φ_i is the corresponding displacement (Φ_n=1.0). The transformation factor between the MDOF and SDOF systems is obtained by:

$$\Gamma = \frac{m^*}{\sum m_i \Phi_i^2} \tag{1.55}$$

Both the displacement and the base shear need to be divided by the transformation factor to get the capacity curve of the SDOF system, see *Figure 1.20/a*.

$$F^* = \frac{F_b}{\Gamma} \text{ and } d^* = \frac{d_n}{\Gamma} \tag{1.56}$$

Further explanation is more spectacular if the capacity curve and also the response spectrum is represented in Acceleration Displacement Response Spectrum (ADRS) format. This representation is related to the capacity spectrum method [16]. For the capacity curve the base shear needs to be transformed into acceleration with the following formula:

$$S_a = \frac{F^*}{m^*} \tag{1.57}$$

For the response spectrum the expression of the transformation acceleration - period is the same as already introduced before:

$$S_d = \frac{S_a}{\omega^2} = S_a \left[\frac{T}{2\pi} \right]^2 \tag{1.58}$$

In *Figure 1.20/b* the green curve and the dark blue representing the elastic demand and the inelastic capacity cannot be compared. First, the elastic demand has to be transformed into inelastic. This is usually carried out by computing an equivalent viscous damping factor from the hysteresis damping and by this factor the elastic demand curve is reduced [17]. The details of this procedure are hereby omitted. The inelastic demand is depicted by the orange line and the intersection of the inelastic capacity and demand curves gives the so called performance point of the SDOF structure. To this performance point a bilinear, light blue, idealised capacity curve can be fitted. It is required that the areas under the actual and the idealized curves, i.e. the deformation energy, E_m^*, have to be equal. Thus, the yield displacement of the SDOF system is:

$$d_y = 2\left(d_m^* - \frac{E_m^*}{F_y^*} \right) \tag{1.59}$$

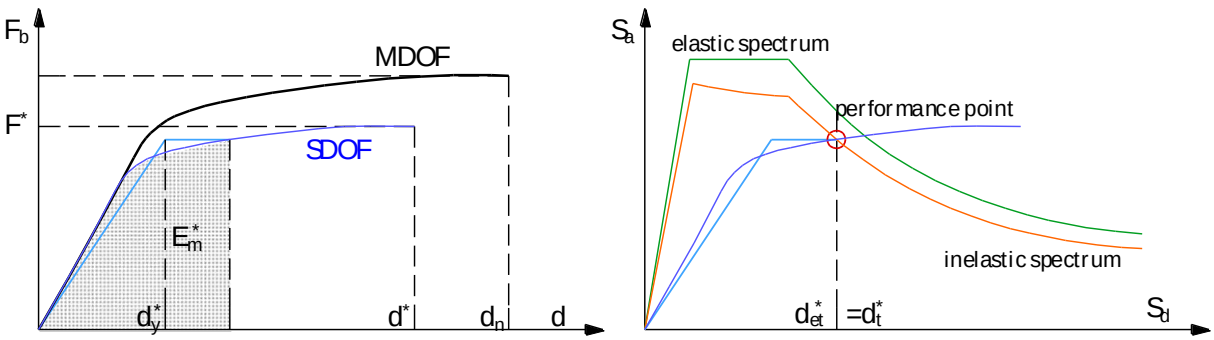

a) transformation of capacity curve *b) ADRS format of demand and capacity*

Figure 1.20; *Transformation of capacity curve and determination of target displacement*

The elastic segment of the idealized curve determines the stiffness of the equivalent SDOF system from which the period and the elastic target displacement can be computed.

$$T^* = 2\pi \sqrt{\frac{m^* d_y^*}{F_y^*}} \tag{1.60}$$

$$d_{et}^{*} = S_e\left(T^{*}\right)\left[\frac{T^{*}}{2\pi}\right]^2 \tag{1.61}$$

The inelastic and the elastic target displacement of not acceleration-sensitive SDOF systems are equal, as depicted in the figure. The target displacement of the original MDOF system is simply obtained by using the transformation factor again:

$$d_t = \Gamma d_t^{*} \tag{1.62}$$

The target displacement is an objective that the capacity curve of the MDOF system has to exceed monotonically increasing to be considered adequate. Otherwise, the structure does not possess the ductility needed to withstand a design-strength earthquake.

As it has been explained, in pushover analysis the response of the MDOF system is related to the response of a SDOF system, implying that the response is controlled by a single mode shape that remains unchanged. However, in reality the invariant distribution may not properly represent the distribution of forces during an earthquake in a MDOF system. Moreover, the invariant force distributions cannot account for the contributions of higher modes to the response or changes of the modal behaviour, which may not be negligible in multi-storey buildings.

1.4.3. Nonlinear incremental dynamic analysis

In the already introduced static seismic analysis methods the structures have been subjected to necessarily time-independent forces. It is possible however to conduct real dynamic analysis by applying accelerations records to the supported nodes of structural models, as it has been mentioned in 1.2.2. Time history analysis is essentially solving the differential equations of motion for the displacements, velocities and accelerations in very short time steps. This is necessary on one hand for the sake of accuracy and on the other hand because the acceleration records of earthquakes change also very rapidly. Though it is possible to conduct linear dynamic analysis, it is not particularly common, since in the numerical simulation of earthquake responses, what dynamic analysis practically is, inelastic material behaviour can hardly be avoided.

The acceleration records used for nonlinear time history analysis can be actual earthquakes recorded in the past. The problem with such is that they may not be available in sufficiently large numbers for any area of interest. Nevertheless, it is also possible to generate artificial records of prescribed length and guiding spectrum. Eurocode 8 for instance requires artificial acceleration records to be at least 10 seconds long and their spectrum shall not be less than 90% of the desired 5% damped spectrum for any period. In addition to these parameters it has to be noted that the “severeness” of records can be measured by a spectral intensity [18] and the intensity of artificial records are usually higher than of natural ones implying larger demands in general.

In practice a structure can be verified for being able to withstand a chosen earthquake, but a more comprehensive understanding of the resistance can be acquired if the structure is subjected to the same earthquake with various intensities. The idea of monotonically increasing the strength of the seismic loading is somewhat parallel to the concept of the introduced nonlinear static analysis methods, therefore it is sometimes referred to as dynamic pushover. The definitions related to the dynamic pushover and a more commonly used name,

Incremental Dynamic Analysis (hereinafter IDA), have been published by Vamvatsikos et al [19][20].

In IDA the intensity of the earthquake is characterised by an appropriately chose intensity measure e.g. the PGA or the spectral acceleration corresponding to the period of the first mode, $S_a(T_1)$. The scaling of the record is done by multiplying the intensity measure by a scale factor, a number ranging from zero up to a selected maximum. The damage measure is another observable quantity in the nonlinear response that is suitable to characterize the damage state of the structure. Alternatives of the damage measure are the base shear, ductility or the maximum Interstorey Drift Ratio (IDR), which is the difference of the lateral drift of two adjacent stories divided by the storey height in percent.

$$IDR = \frac{X_{i+1} - X_i}{H}[\%] \tag{1.63}$$

In later chapters of the present work on IDA diagrams the IDR will be plotted against the scale factor of the PGA as it is presented in *Figure 1.21*. The performance of a building is either limited by the IDA curve converging to a vertical asymptote, meaning the attainment of dynamic instability, or by a predefined maximum damage measure, beyond which material failure is assumed.

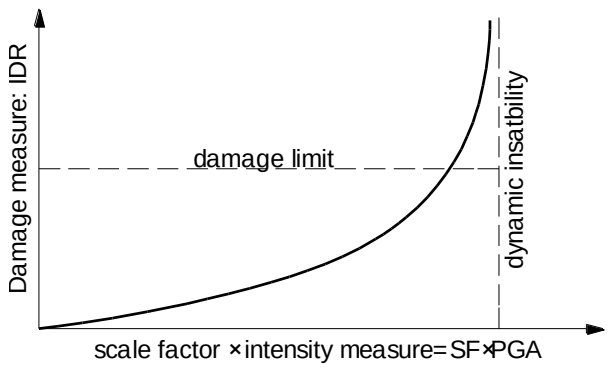

Figure 1.21; *Theoretical IDA diagram*

Attention has previously been drawn that the analysis of the response to one earthquake may not be representative as quakes can be very versatile. It is not surprising therefore, that in Eurocode 8 a minimum of three artificial accelerograms are to be used. If at least seven are used that correspond to the same design spectrum, it is allowed to consider the mean of the seven independent results. The availability of an even larger number of independent computations provides the possibility of evaluating the structural performance on a probabilistic basis. In this approach from the large number of IDA curves cumulative distribution functions, so called fragility curves, can be derived that provide information on the probability of exceeding given intensities without failure. From the fragility curve and from site-specific hazard curves the probability of failure for a given reference period can be computed. The process of this analysis type is discussed in the previously referenced articles, but further details are hereby omitted as in the present work probabilistic analysis is not conducted.

1.5. Examined problem and objectives of the thesis

As it has been discussed before, in classical design CBF-s are supposed to develop a global plastic mechanism when subjected to seismic actions, see *Figure 1.22/a*. Depending on the direction of the loading all the braces in tension get equally elongated and the ones in compression buckle. This mechanism allows the largest possible dissipation in the structure as every brace participates in the dissipation of the seismic input energy and therefore the global mechanism provides the largest reduction of the internal forces in the structure. Also, by the uniform distribution of the drifts on every floor a significant drift capacity can be achieved. In order to utilize the maximum available plastic deformation capacity it has to be ensured that all the braces undergo plastic deformations on every floor. In the meantime the non-dissipative members i.e. the columns and beams have to remain elastic. In design the occurrence of plasticity in the braces only has to be safeguarded by a notable overstrength demand imposed on the columns and beams, in compliance with the principles of capacity design.

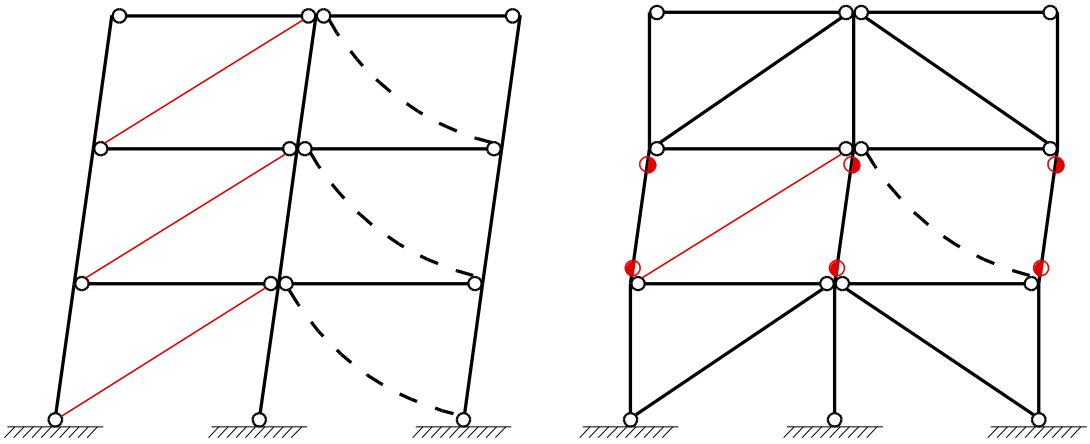

a) global mechanism *b) local mechanism*

Figure 1.22; *Global and local storey plastic collapse mechanism of CBF*

Although the global plastic mechanism is the one that simplified design procedures assume, it is well known that another collapse mechanism is very likely to develop. The mechanism is often referred to as the weak storey or soft storey mechanism, see *Figure 1.22/b*, and it has been observed in recent earthquakes [21]. In a weak storey mechanism the plastic deformations are localized on one or a very limited number of floors. When the brace in tension reaches its axial resistance limit, the compression diagonal is already buckled, so the columns have to carry all the additional horizontal inertia forces. While in the case of the global plastic mechanism the columns remain straight, a weak storey mechanism causes the double curvature of the columns as they counteract the horizontal forces by flexure. If the lateral seismic action is large enough plastic hinges form on the top and the bottom of the bent columns above or under the floor slabs and a storey mechanism develops. In the case of this local mechanism the lateral displacement of the top is approximately equal to the storey drift of the weak storey only. Furthermore, all the plastic dissipation of the building is realized only on the weak storey and the rest remain unexploited. Consequently, the dissipation of a local mechanism is by far smaller than of the global mechanism. Moreover, in a local mechanism columns are subjected to significant bending which is what they are not designed to resist originally, supposing a truss action. Because of the bending of the columns

the weak storey behaviour incorporates the possibility of an early collapse which should be prevented.

This thesis focuses on the likelihood of the weak storey behaviour and the weak storey collapse of diagonally concentrically braced frames designed according to Eurocode 8 provisions. The performance of CBF-s will be evaluated by means of IDA. In the evaluation the emphasis will primarily be put on the occurrence of the weak storey behaviour and not on the resistance of the designs. The NTHA results will be further analysed to understand the nature and development of the weak storey behaviour. Ultimately, the objective is to develop supplementary conditions to Eurocode 8 that can enhance the designs by preventing the occurrence of weak storeys.

Chapter 2

Literature Review on the Seismic Response of Braced Frames and Brace Behaviour

The objective of this chapter is to assess the information that were gathered from articles existing prior to the thesis and that provided an initial base to the research. In the chapter giving every available reference as a list is not intended. Rather, emphasis is put on introducing the most important features of CBF-s utilizing a few selected articles. Firstly, the cyclic behaviour and failure of the braces and other members are observed. In the second part some issues regarding CBF related Eurocode 8 provisions and the unfavourable weak storey behaviour are discussed.

2.1. Failure of lateral load resisting members

As discussed before, in incremental dynamic analysis the performance of a building is usually evaluated by means of plotting an appropriately chosen damage measure against the seismic intensity measure. When the IDA curve converges to an asymptote, see *Figure 1.21*, the lateral displacements increase without notable change of the scale factor. In this case a plastic collapse mechanism is formed and failure of the building is attained. Though IDA results usually exhibit such convergence, in reality the limited deformability of the building materials may cause the local failure of certain members. Prior to the full development of the theoretical collapse mechanism, excessive local cyclic and plastic deformations may cause ruptures and eventually the fracture of joints or the dissipative members i.e. the braces. As the level of statical indeterminacy is low in CBF-s, such a loss of one member participating in the lateral resistance can be directly related to the collapse of the building. The allowable damage measure or, in future discussions, the IDR therefore has to be given an upper bound beyond which collapse is assumed.

In the following paragraphs the different possibilities of failure of the lateral load resisting members of a CBF are presented and assessed. This study relies primarily on the available literature. The objective is to give estimation to the interstorey drift range at which the excessive damage of the braces, gusset plates or the columns causes failure. The beams are not considered in this assessment as they are generally assisted by floor slabs in transmitting the horizontal forces.

2.1.1. Braces

The use of rectangular or circular hollow sections for the diagonal braces is in common practice as the catalogues of these sections are versatile. Therefore, the actual cross-sectional area can be well adjusted to the imposed need. The other advantage of using hollow sections for bracing is that these sections have equal or at least significant flexural stiffness in both two principal cross-sectional directions, so requirements imposed to the slenderness of the brace can be cost-effectively satisfied. To understand the fracture life of such axially loaded diagonals, their cyclic behaviour has to be characterised by an idealised force - deformation model [22][23][24].

Assuming that the brace is initially subjected to compression, the first stage of the behaviour is described by the 0 - A branch in *Figure 2.1*. In this elastic state the axial deformation is small and the out-of-plane deformation of the bar is primarily given by the amplification of the initial imperfection. In point A the buckling load is reached. Along the A – B branch the plastic deformation of the mid section implies the formation of a plastic hinge and extensive axial and lateral displacement. The B – C and C – D branches correspond to elastic unloading and tensile loading. In point D the eccentric tension causes plasticity in the mid section again but in the other sense. Along the D – E branch the stiffness grows in conjunction with the straightening of the bar. In point E the tensile yield is attained. Between E and F plastic elongation is realized which results the 0 - G residual elongation after the F – G branch of unloading.

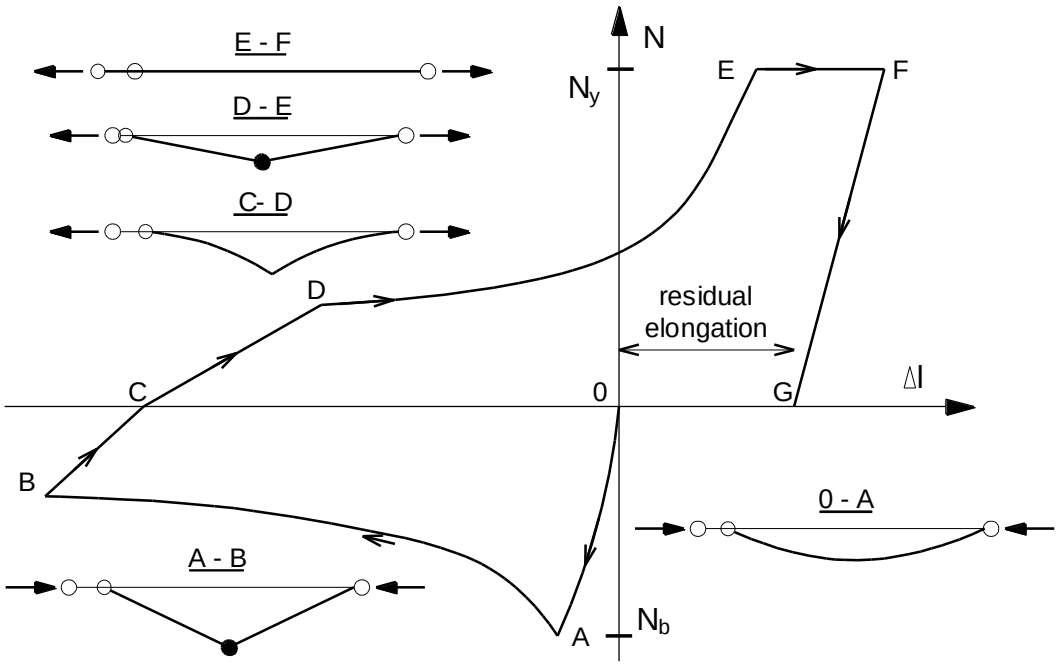

Figure 2.1; *Theoretical elasto-plastic behaviour of axially loaded brace*

When a CBF is subjected to seismic action the braces may exhibit several cycles of the introduced force-displacement diagram, however the tensile yield is not reached in every cycle. *Figure 2.2* depicts the normalized axial force – axial displacement diagram of a brace in a 20 second cyclic excitation by an artificial acceleration record. In this diagram most of the tensile peaks do not cause yield, however in three cycles considerable plastic elongation is realized. As the deformed length of the brace becomes larger than the original length, buckling occurs even in the positive displacement range, where otherwise tensile behaviour would be expected. In the meantime the buckling load decreases. Consequently, the bar buckles in every cycle and plastic deformations cumulate primarily at the midspan of the bar in a plastic hinge. Also due to the increased length, for the full development of the tensile resistance of the brace larger axial displacements are needed. Therefore, in the case of small tensile displacements the counteracting force in the brace is diminished significantly i.e. the initial stiffness decreases. Moreover, the lateral displacements in buckling and the rotation of the plastic hinge become larger. Also the residual deformations in the plastic hinge facilitate the buckling and decrease the force corresponding to the buckling.

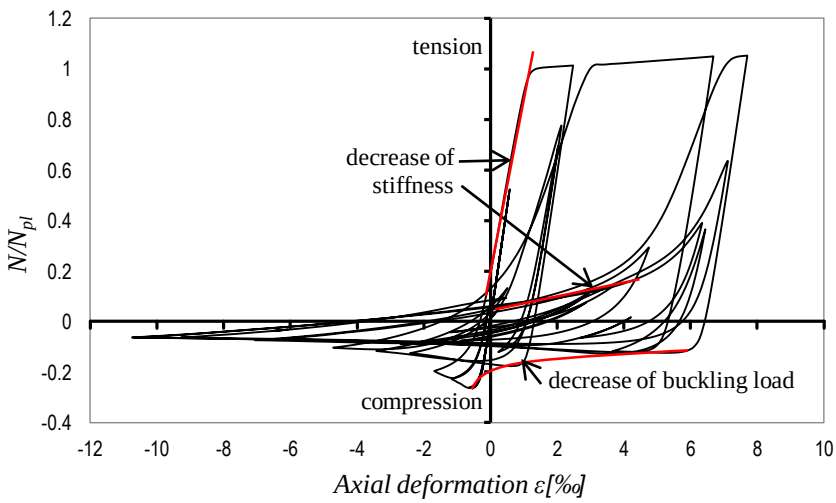

Figure 2.2; *Characteristic normalized axial force – deformation diagram of brace*

The plastic hinge in the mid section generally appears associated with local plate buckling. In the repeated cycles the buckled pattern folds and unfolds over and over again and the edges in the buckled zone undergo repeated alternating plastic deformations. The accumulation of plastic deformations may lead to a local low-cycle fatigue rupture, see *Figure 2.3*. The yield in alternating directions in subsequent load cycles causes cracks to appear and those gradually propagate in the otherwise ductile steel material. Therefore, the net cross-sectional area of the brace and with it its resistance decrease abruptly. Consequently, it is important to know the level of the displacement range where the cyclic loading inflicted failure of the diagonals can be expected and also what parameters affect the resistance to cyclic loading.

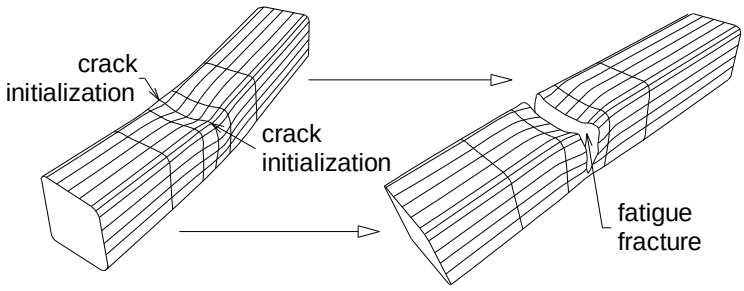

Figure 2.3; *Fatigue fracture of hollow brace subjected to cyclic axial loading*

In order to examine the fracture life of rectangular and square hollow section braces several authors conducted comprehensive experimental surveys [22][23][25][26][27][28][29][30]. Upon the assessment of the cyclic test results various methods and formulas were established that aim to predict the fracture life [31][32][33][34][35]. Although the formulas may differ, the different authors agree that the most important factors influencing the rupture of hollow braces are the global and the local slenderness and the material grade. Taking into consideration some or all of these factors the great majority of the formulas express the displacement ductility capacity, μ_Δ, of the braces which is defined as the ratio of the realized axial deformation and the one corresponding to the first yield ε_y.

$$\mu_\Delta = \frac{\Delta L}{L \cdot \varepsilon_y} \tag{2.1}$$

The displacement ductility in the referenced articles is mostly determined by experimental testing. In the test setups the loading is imposed axial displacement with the same monotonically growing amplitude in tension and compression. The ductility result of the tests is given by the maximum attained amplitude before failure, therefore it does not correspond specifically to tension or compression; it is rather an absolute value. Some authors attempted to consider not only the maximum deformation, but the whole loading history. Shaback and Brown [31] present a cumulative measure of ductility that takes into account the characteristics of the loading history prior to failure. The accumulated fracture ductility, $\mu_{\Delta,f}$, is defined as the weighted sum of the $\mu_{\Delta,1}$ and $\mu_{\Delta,2}$ ductility in the subsequent cycles, see *Figure 2.4*.

$$\mu_{\Delta,f} = \sum\left(0.1\mu_{\Delta,1} + \mu_{\Delta,2}\right) \tag{2.2}$$

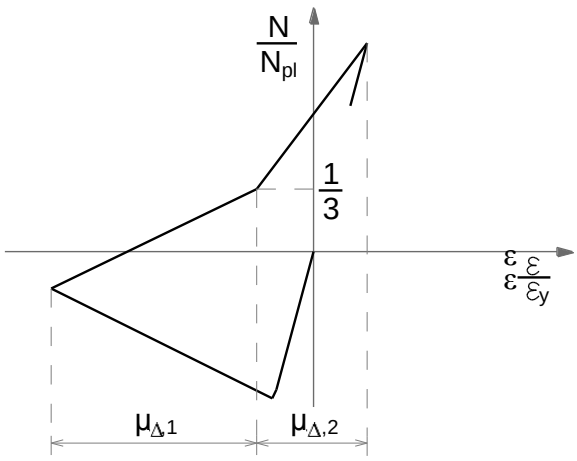

Figure 2.4; *Compressive and tensile ductility according to Shaback et al. [31]*

Also predictive equations are given that have been calibrated by tests on cold-formed carbon steel square hollow section bracing members. The maximum attainable ductility is:

$$\mu_{\Delta,f}^{\max} = C_s \frac{\left(350/f_y\right)^{-3.5}}{\left[\left(b-2t\right)/t\right]^{1.2}} \left(\frac{4\left(b/d\right)-0.5}{5}\right)^{0.55} \left(70\right)^2 \quad \text{if: } \frac{KL}{r} < 70 \tag{2.3a}$$

$$\mu_{\Delta,f}^{\max} = C_s \frac{\left(350/f_y\right)^{-3.5}}{\left[\left(b-2t\right)/t\right]^{1.2}} \left(\frac{4\left(b/d\right)-0.5}{5}\right)^{0.55} \left(\frac{KL}{r}\right)^2 \quad \text{if: } \frac{KL}{r} \geq 70 \tag{2.3b}$$

where C_s is an empirical constant (equal to 0.065), KL is the buckling length, b is the longer and d is the shorter face of the rectangular section, t is the thickness, r is the radius of gyration and f_y is the yield strength in N/mm^2. This method requires the detailed knowledge of the force – displacement response but this may not be available in most cases. With this method we cannot provide a preliminary estimate for the ultimate storey drift corresponding to the local failure of the braces. Nevertheless, other available methods for the estimation of the displacement ductility capacity are independent of the history of the hysteretic loops. Such relationships were given by Tremblay et al. [32], Goggins et al. [33] and Nip et al. [34][35] for example.

Goggins et al. observed three properties influencing the capacity of their test specimens i.e. the yield strength, the global and the local slenderness. For each parameter the authors provide independent formulas that have been calibrated by the test data:

$$\mu_\Delta = 22.4 - 14\left(f_y - f_{y,nom}\right)/f_{y,nom} \tag{2.4}$$

$$\mu_\Delta = 26.2\bar{\lambda} - 0.7 \tag{2.5}$$

$$\mu_\Delta = 29.1 - 1.07\left(\frac{b}{t}\right) \tag{2.6}$$

Tremblay et al. proposed a simple linear relationship between the sum of the maximum ductility, μ_f, reached in both tension, μ_t, and compression, μ_c, before fracture, and the relative global slenderness:

$$\mu_f = 2.4 + 8.3\bar{\lambda} = \mu_t + \mu_c \tag{2.7}$$

For the sake of comparison with other formulas expressing the ductility as the largest deformation either in compression or tension, we shall assume that the reached ductility in

tension and compression are equal. Hence, Eq. (2.7) can be divided by two to express the displacement ductility:

$$\mu_\Delta = 1.2 + 4.15\bar{\lambda} \tag{2.8}$$

Tremblay et al. observed in their test procedures that the choice between diagonal bracing in different bays or the X-braced arrangement of the bracing members may affect the fracture life as well. Therefore they have chosen the rotation at the bar end as a suitable indicator of the brace damage. The ultimate rotation θ_f is calculated as:

$$\theta_f = 0.091\left(\frac{b_0}{t}\frac{d_0}{t}\right)^{-0.1}\left(\frac{KL}{r}\right)^{0.3} \tag{2.9}$$

where b_0 and d_0 are the inner widths of the two faces of the rectangular section and KL/r is the global slenderness. For the conversion of the rotation to out-of-plane and axial displacements the following equations can also be found in [32]:

$$\theta = 2\sqrt{\frac{\delta_c}{2L}} \text{ with } \delta_c = \left(\mu_c + \mu_t - 1\right)\delta_y \tag{2.10}$$

where L is the bar length for pinned-end diagonal braces and δ_y is the elongation corresponding to tensile yield. Assuming again that the ductility in tension and compression are equal and expressing the tensile yield as:

$$\delta_y = \frac{f_y}{E}L \tag{2.11}$$

where f_y is the yield stress and E is the modulus of elasticity of the material, we can express the displacement ductility from Eq. (2.9) with the ultimate rotation:

$$\delta_c = \left(\frac{\theta}{2}\right)^2 2L = \left(\mu_c + \mu_t - 1\right)\delta_y = \left(2\mu - 1\right)\frac{f_y}{E}L \tag{2.12}$$

$$\mu_\Delta = \frac{\theta_f^{\,2}}{4}\frac{E}{f_y} + 0.5 \tag{2.13}$$

Nip et al. conducted tests on specimens with various cross-sections, slenderness parameters and material types. In their experimental program the differences between the behaviour of hot-rolled, cold-formed carbon steel and stainless steel sections are emphasized. The authors established a predictive expression for the displacement ductility that takes into consideration the co-existing influence of both the global and the local slenderness and the material grade. Furthermore different sets of parameters are given for the different material types.

<u>Hot-rolled carbon steel (HR):</u>

$$\mu_\Delta = 3.69 + 6.97\bar{\lambda} - 0.05\left(b/t\varepsilon\right) - 0.19\bar{\lambda}\left(b/t\varepsilon\right) \tag{2.14}$$

<u>Cold-formed carbon steel (CF-CS):</u>

$$\mu_\Delta = 6.45 + 2.28\bar{\lambda} - 0.11\left(b/t\varepsilon\right) - 0.06\bar{\lambda}\left(b/t\varepsilon\right) \tag{2.15}$$

<u>Cold-formed stainless steel (CF-SS):</u>

$$\mu_\Delta = -3.42 + 19.86\bar{\lambda} + 0.21\left(b/t\varepsilon\right) - 0.64\bar{\lambda}\left(b/t\varepsilon\right) \tag{2.16}$$

where:

$$\varepsilon = \sqrt{\frac{235}{f_y}} \tag{2.17}$$

The displacement ductility results, which can be obtained by the application of the formulas presented above, differ significantly. For the sake of comparison the ductility calculated with Eq. (2.6, 2.8, 2.13, 2.14, 2.15, 2.16) are depicted in *Figure 2.5* and *Figure 2.6*. The results obtained by Eq. (2.5) show such a large discrepancy from the rest that it has been neglected. On both figures either the local or the global slenderness is constant while the other is variable in a practically feasible range. In *Figure 2.5* the local slenderness, *b/t*, is taken to be 20 while in *Figure 2.6* the relative global slenderness is 1.80. In the diagrams the condition of Tremblay is the one expressed by Eq. (2.8) and Tremblay rotation is obtained by Eq. (2.13). The dotted curve of Goggins depicts Eq. (2.6). The solid lines designated as Nip HR, CF-CS, CF-SS depict Eq. (2.14,2.15,2.16) respectively.

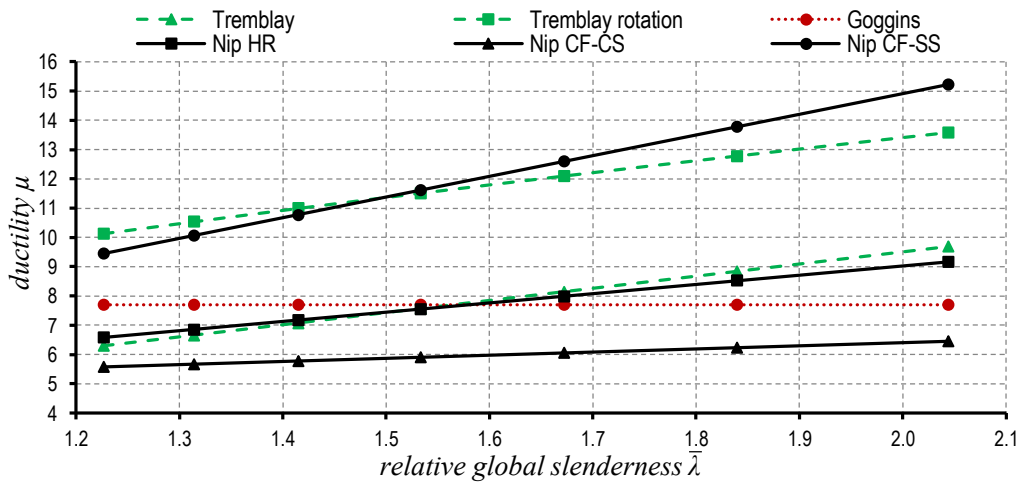

Figure 2.5; *Comparison of ductility results with the variation of the global slenderness*

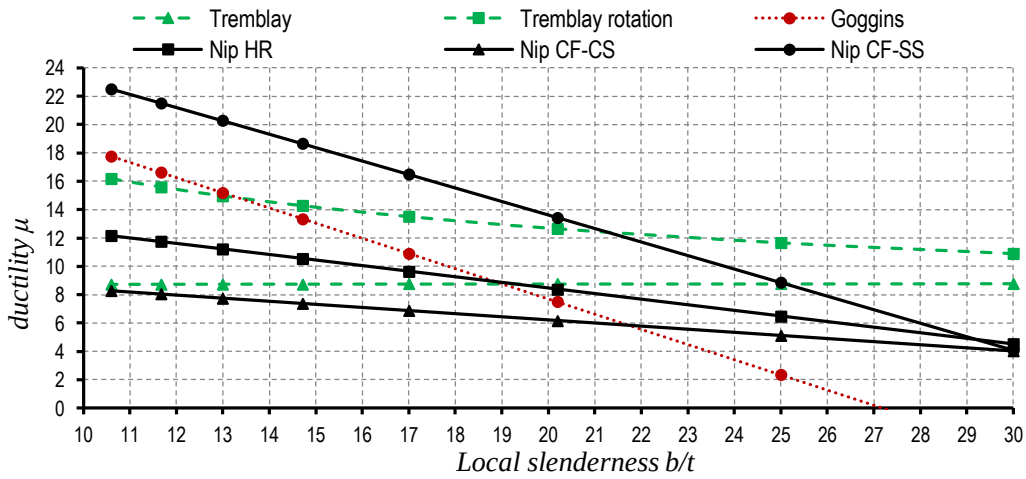

Figure 2.6; *Comparison of ductility results with the variation of the local slenderness*

The curves presented in the two diagrams define a wide interval of the ductility, however the solid lines represent different material types or manufacturing process. The criteria of Tremblay and Goggins are not dependent on either the local or the global slenderness though both are seemingly decisive factors. The ductility obtained by Tremblay's rotation criterion tends to overestimate the rest and according to [34] also the experimental results. The formulas given by Nip et al. take into consideration all the relevant factors

affecting the ductility capacity of rectangular hollow sections. Moreover, these formulas provide the best fit with numerous experiments, see [34][35]. Consequently, in the following we consider only these for regular carbon steel members.

The upper boundary of the studied interval of the relative global slenderness in *Figure 2.5* corresponds to the limitations defined in Eurocode 8, therefore it is not only feasible, but necessary. The lower bound of the local slenderness depicted in *Figure 2.6* is the range where most catalogued rectangular hollow sections can be found and the upper bound, 30, is closely the limit of the highly ductile cross-sectional class 1, as defined in Eurocode 3 [10]. With respect to these two intervals an anticipated range for the displacement ductility can be defined. If we neglect in terms of practice unlikely and extreme cross sections, Eq. (2.14) gives the interval of approximately 4 to 13 for the displacement ductility of hot rolled sections, while Eq. (2.15) results 4 to 8 for cold formed sections.

The loading history of a brace subjected to seismic action differs significantly from the imposed displacement loadings that the presented formulas were calibrated with. Nevertheless, an estimation of the anticipated maximum interstorey drift range that corresponds to the failure of the diagonals can be calculated as demonstrated hereafter, considering the dimensions of the CBF structures that will be presented later on in chapter 3. In these buildings the span *B* and the storey height *H* are 6 and 3 metres respectively and the unloaded length of the diagonals *L* is 6.708 metres, see *Figure 2.7*. From the definition of the ductility presented in Eq. (2.1), the elongation of the brace that corresponds to failure can be expressed with the anticipated ductility capacity and the bar length:

$$\Delta L = L \cdot \varepsilon_y \cdot \mu_\Delta = L \cdot \frac{f_y}{E} \cdot \mu_\Delta \tag{2.18}$$

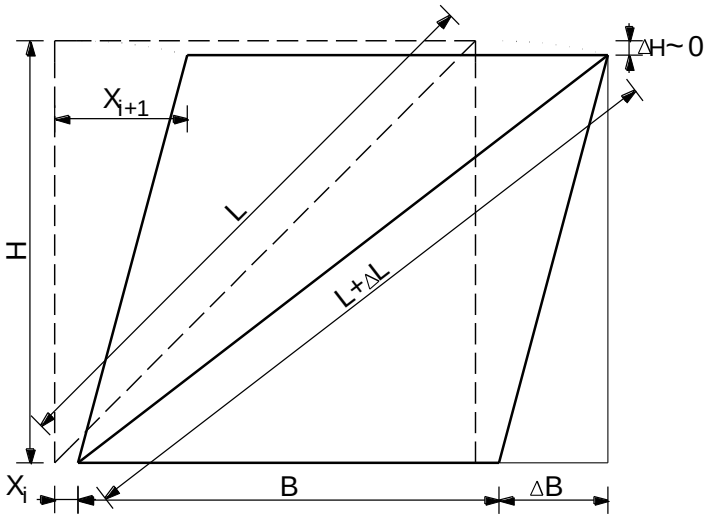

Figure 2.7; *Deformed shape of braced bay*

If we neglect the vertical shortening, from the elongation of the brace we can express the interstorey drift, which is the difference of the lateral displacements, X_i, of adjacent floors:

$$\begin{aligned} (L+\Delta L)^2 &= \left(B + \left(X_{i+1} - X_i\right)\right)^2 + H^2 \\ X_{i+1} - X_i &= \sqrt{(L+\Delta L)^2 - H^2} - B \end{aligned} \tag{2.19}$$

Substituting this and Eq. (2.18) into Eq. (1.63) given for the interstorey drift ratio:

$$IDR = \frac{X_{i+1} - X_i}{H} = \frac{\sqrt{\left(L + L \cdot \frac{f_y}{E} \cdot \mu_\Delta\right)^2 - H^2} - B}{H} \tag{2.20}$$

By taking into consideration the practically realizable range of the ductility capacity of hot-rolled sections, as defined before, we can determine the IDR range where the failure of the braces can be expected. For the studied structural arrangement this range is between 1.1 and 3.6% if the considered steel grade is S235 and it would be 1.7 to 5.5% for S355.

2.1.2. Columns

As it has been discussed before, the brace deterioration gradually devolves the horizontal loading on the columns. Supposing that the lateral drift is realized mainly on one floor so that a weak storey develops, the columns of this floor become double-curved and notable bending occurs in the members that, in the hypotheses of classical design, should only be subjected to axial loading. The columns may be restrained at both ends or only at one, but in both cases the peak of the moment diagram is located at the floor slabs. Therefore, in the case of large lateral drifts, plastic hinges may occur at the ends of the columns. Ultimately, the rotation of the plastic hinges may lead to the failure of the columns, therefore the rotation capacity has to be examined. The rotation capacity of the columns, without adequate restraints, is not limited by the ultimate deformation of the sections but by the local buckling of the plates on the compression side [36], see *Figure 2.8*. The rotation capacity can be defined as the rotation θ_{max} corresponding to the maximum value M_{max} (monotonic loading) of the bending moment or the ultimate rotation θ_{ult} given by the intersection of the descending post-buckling curve with the theoretical full plastic moment M_p. Accordingly, two distinct regions must be considered: the pre-buckling branch and the post-buckling region. The determination of the moment-rotation curve can be achieved using finite elements. However, it requires very dense meshes in the local buckling zone which increases significantly the computing cost. The pre-buckling part is monotonically increasing and can be determined for steel section by integrating the moment curvature curve. The post-buckling branch has been determined using the plastic mechanism theory proposed by Gioncu which was implemented in a software program called DUCTROT M (DUCTility of ROTation for Members) [37][38].

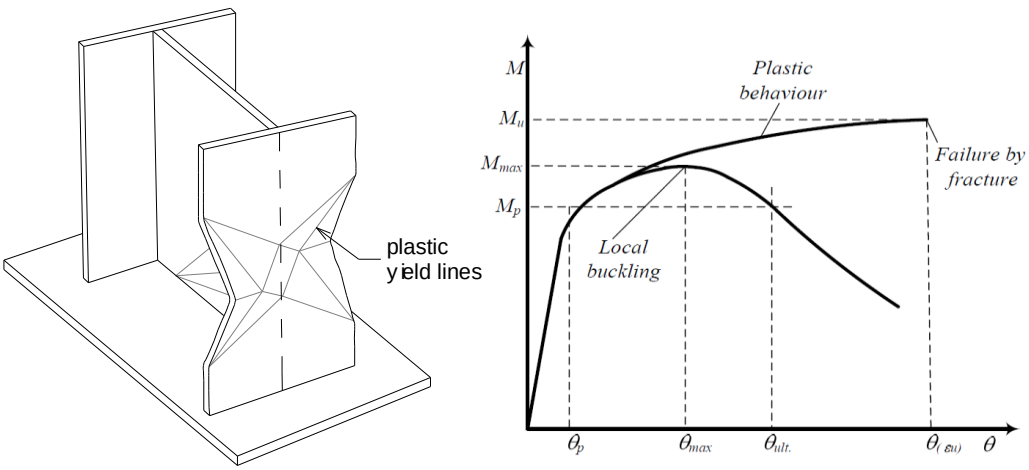

Figure 2.8; *Local buckling and plastic behaviour of column section*

The domain of plastic rotation capacity of steel sections covers a vast literature. Unfortunately, in the case of bent and simultaneously compressed members, the available sources are less numerous. In the available articles, to the authors' knowledge, the case, where the ratio of the design axial force and the plastic resistance exceeds 0.5 is not covered. As the columns of a CBF tend to be, with few exceptions, in this upper region, a reliable estimation of the rotational capacity of the columns cannot be given. Nevertheless, in *Table 2.1*, a few examples calculated with DUCTROT are presented. As it can be seen, the rotation capacity of every example is rather elevated, even if the axial loading is significant. However, it has to be noted, that repeated cyclic plastic deformations may rapidly decrease the rotation capacity [37].

Table 2.1; *Annual number and strength of earthquakes globally*

section name	N/N_{pl}	θ_b
HEA 160	0,335	49 mrad
HEA 180	0,564	54 mrad
HEB 200	0,507	58 mrad
HEB 240	0,679	50 mrad
HEM 240	0,647	59 mrad
HD 320×198	0,695	53 mrad

On the other hand, some building codes impose limitation to the relative global slenderness, $\bar{\lambda}$, of the columns to allow plastic hinges to form while avoiding their occurrence away from the ends at unrestrained interior points. Japanese regulations [39] define the following equation for columns with restrained connections at both ends:

$$\frac{N}{N_{pl}} + 0.78\bar{\lambda} \le 1.0 \text{, or for } \frac{N}{N_{pl}} \le 0.15 \;\; \bar{\lambda} \le 1.6 \tag{2.21}$$

and for columns with an ordinary hinge on one end:

$$\frac{N}{N_{pl}} + 1.32\bar{\lambda} \le 1.0 \text{, or for } \frac{N}{N_{pl}} \le 0.15 \;\; \bar{\lambda} \le 1.07 \tag{2.22}$$

where N is the axial load and N_{pl} is the plastic axial resistance. In New Zealand [40] a limitation for columns with limited ductility is defined in the form of:

$$\frac{N}{N_{pl}} < \begin{cases} 0.7 \\ \dfrac{1+\beta-\bar{\lambda}}{1+\beta+\bar{\lambda}} \end{cases} \tag{2.23}$$

where β is the so-called moment ratio that shortly is 1.0 for columns with clamped ends and 0 for columns with one hinged end. In *Figure 2.9* the two limitations are compared. The dashed curves depict the New Zealand limit and the solid lines stand for the Japanese criteria of Eq. (2.21) and Eq. (2.22). The diagram shows a rather good correlation of the two regulations.

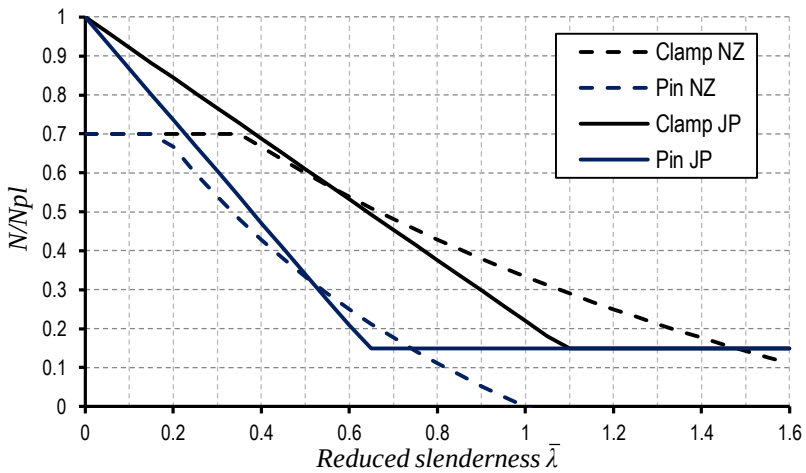

Figure 2.9; *Slenderness limits of columns to prevent the development of internal plastic hinges*

Other building standards also impose additional requirements on columns and braced frames in general. In the USA both ordinary and the so called special CBF-s (SCBF) [44] are limited in building height [41]. Such limitations are also imposed in Canada [42] and New Zealand [43]. In the design of SCBF-s flexure is expected in braced bay columns so splices have to be located in the middle third of the storey height. The splice has to be able to carry 50% of the moment and 100% of the shear capacity of the smaller column. According to the Canadian standard the columns have to be continuous on every second floor at least and they are to be designed to resist 20% of their plastic moment resistance along with the maximum axial effect. These selected examples demonstrate that several building codes pay special attention to the design of columns (of braced bays).

2.1.3. Connections of braces

Besides the braces and the columns there are specific performance requirements imposed to the connections of the braces also. The lateral buckling of the diagonals forces end rotations on the bar ends and the out-of-plane bending of the gusset plates. The deformation of the gusset causes stress peaks at the re-entrant welded corner of the gusset plate and this leads to crack initiation and ultimately fracture. On the behaviour and design of ductile gusset plates several articles can be found in the literature [45][46][47]. Most of these present studies of experiments conducted on various gusset plate arrangements, but a fracture condition related to geometry and material properties, like in the case of hollow braces, is not available unfortunately. Instead, in [45] for example Yoo et al. introduce a detailed procedure to the design of higher performance gusset plates. According to corresponding standards and related articles the gusset plates are adequately designed, if a linear clearance of $2t_p$, where t_p is the thickness of the plate, or an elliptical clearance of $8t_p$ is provided for a rectangular or tapered gusset plate, see *Figure 2.10*. The numerous cyclic tests revealed that without the application of advanced gusset plate design methods but respecting the minimal requirements for clearance, crack initiation in the welds of the connections can be expected at about 2% to 3% storey drift ratio.

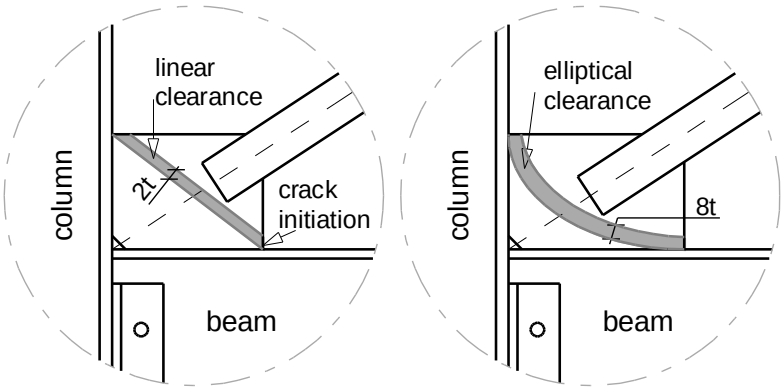

Figure 2.10; *Linear and elliptical clearance of gusset plates*

2.1.4. Summary on the failure of members

The objective of this section was to give a description of the different failure modes and criteria of the lateral load resisting members of CBF-s. As it could have been expected, the definition is not clear and also not easy because of the complex nature of the cyclic, cumulating damage-caused failure. Nevertheless, by the use of experimental results and simplified criteria an interstorey drift ratio range, where the failure of certain members is anticipated, can be defined. As it has been presented the failure of rectangular hollow sections may occur at very low lateral displacements, even at 1.1 % IDR. However, the capacity of the same section type may exceed even 3% IDR. A similar threshold was found for gusset plates as well. The failure of the gusset can be expected approximately between 2% and 3% IDR. For the columns an ultimate drift range has not been specified due to the lack of sources, yet the estimated rotation capacities in the few examined cases in *Table 2.1* were found to be elevated. It also has to be noted, that in a CBF under seismic effect, primarily the braces are subjected to repeated plastic excursions. In the bent columns, that are a lot more flexible in terms of lateral displacement, plastic deformations are realized at significantly higher drifts than in the braces. The flexibility of the columns and the anticipated significant rotation capacity of the stocky cross sections may provide a ductility capacity that is superior to the one of the braces.

In our future analyses the chosen damage measure will be the interstorey drift ratio. The failure will be anticipated in the interval from 2% up to 3% in order to take into consideration the uncertainties of the collapse criteria, but supposing that a careful detailing of the gusset plates and a judicious choice of columns and braces has been made. It is important to note, that by this 2-3% we suppose the use of S235 steel grade. Higher strength structural steels would provide larger ductility capacity.

2.2. Behavioural issues involved in the seismic design of CBF-s

2.2.1. Generalized seismic response of CBF-s

The cyclic behaviour and fracture life of the bracing members introduced before have certain implications on the global seismic response of a braced frame. Observations and detailed description on these effects are given by Elghazouli [12] and Tremblay [48].

In the referenced articles both authors ascertain that CBFs typically exhibit large variations in story drift and inelastic demand over their height when subjected to strong ground motions [49]. This behaviour is mainly due to the degradation in brace resistance that results from large inelastic excursions and/or successive compression load cycles beyond buckling. The low post-yield tangent stiffness of the braces can lead to a concentration of inelasticity in one level over the height of a multi-storey frame. This behaviour would take place even when buckling was delayed or prevented. It could also occur even when brace capacities were relatively well balanced with demands over the height, as required in recent revisions of EC8. The severity of this phenomenon depends on several factors including brace properties, bracing configuration, number of stories, type of ground motions, etc. Moreover, the cumulating damage of the braces limits the attainable maximum interstorey drift, according to Elghazouli, at about 2 – 3%, which is consistent with the assumptions made previously.

One important characteristic influencing the response and contributing to the localization of the demand on a weak storey is the overstrength neglected in design. There are several sources of overstrength such as material overstrength or non-structural members. Most notably, overstrength is often a direct consequence of the simplification of the design approach, particularly in terms of the redistribution of internal forces in the structure. In European practice the compression diagonals can be neglected as the design is based on the tensile resistance of the braces, whereas in several codes, such as US guidelines [50], the design base is the buckling capacity in compression. In the former approach the residual force in the compression diagonal, while in the later the reserve of the tensile brace yields overstrength. The magnitude of the overstrength depends on the slenderness of the braces, see *Figure 2.11/a*, and therefore it is usually not equal on every floor. On floors closer to the base of a building the slenderness and consequently the neglected overstrength in EC8 design are usually larger than on storeys on the top. Elghazouli also draws attention that the overstrength may notably influence the ductility demand. Taking a look at *Figure 2/11/b* one may see that for a CBF, designed with behaviour factor q=4 according to EC8, the ductility demand may be higher than the assumed ductility capacity (equal to q). The demand increases with the slenderness, that yet again indicates that the upper floors are more prone to exhibiting weak storey behaviour.

In the inelastic response of a building the plastic deformations are mainly caused by seismic forces corresponding to the fundamental mode and the higher modes usually result in elastic deformations only [51]. Therefore, in an alternative approach it can be assumed that the spectral response of the higher modes shall not be decreased by a behaviour factor that is used for the first mode. Instead, smaller behaviour factors should be considered which amplifies the relevance of the higher modes in the inelastic response, thus increasing the likelihood of localization.

The concentration of demand on a weak storey may also be resulted by the specific signature of the earthquake [48]. According to Tremblay, a near field earthquake is by far the

most critical as it imposes one (or very few) large impulse on the structure. Such an impulse is likely to amplify the first plastic deformations that occur [52].

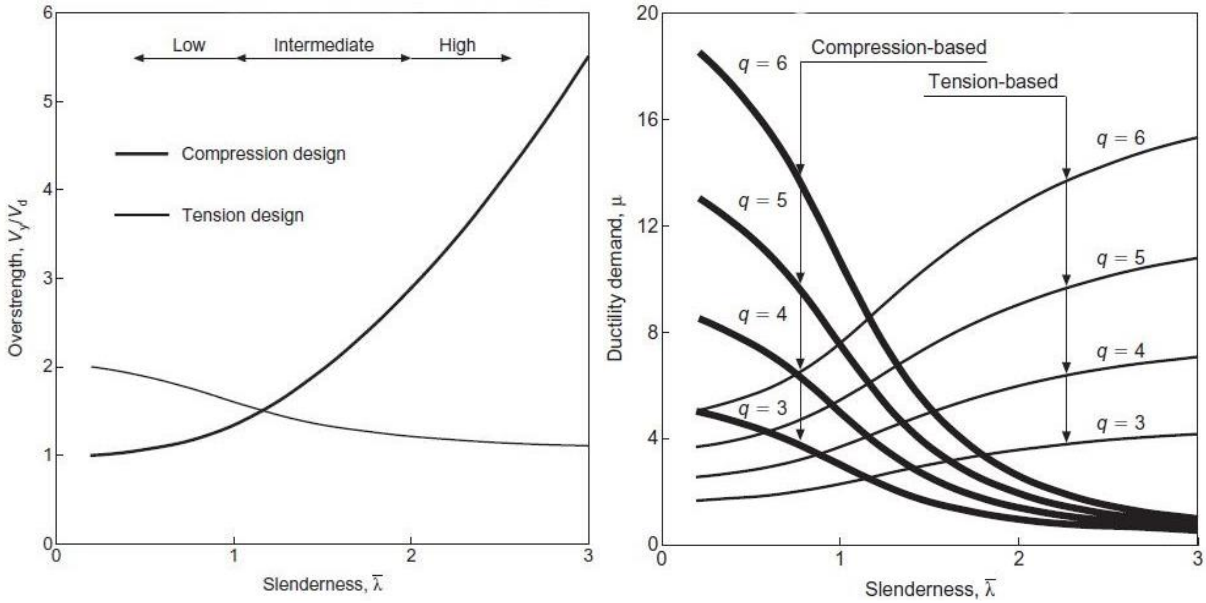

a) change of overstrength *b) change of ductility demand*

Figure 2.11*; Change of overstrength and ductility demand with brace slenderness [12]*

Following Tremblay [48] another factor involved in the localization of deformation is the P-Δ effect. When subjected to several cycles of inelastic deformations, a structure tends to drift towards one direction, generally after a large inelastic excursion has taken place towards that direction. This “crawling” or “ratcheting” response is due to the gravity loads supported by the deformed structure. These gravity loads are producing additional lateral loads pushing the structure further away from its initial position. With the lateral sway of the building the storey height slightly diminishes and the huge gravity forces loose potential energy. This loss is difficult to restore because it would require the lifting of the gravity loads, so structures naturally tend to migrate towards the direction that is associated with the shortening.

According to Tremblay, the above-mentioned parameters affect the response of a multi-storey CBF in a way that the larger differences between the estimated and the actual seismic demand are located in the upper (one third) or in the lower storeys. Furthermore, the severity of the localization increases with the number of storeys. To mitigate the detrimental effects of the localization both authors propose that the columns should be designed with continuous splices. This can provide supplementary resistance to the gradually decreasing brace resistance insofar as the columns have adequate reserve. Elghazouli presents an example where the same CBF is designed with a) constant brace cross section and pinned column splices, b) demand-proportional diagonals and pinned splices, c) constant brace cross section and continuous column splices, d) demand-proportional diagonals and continuous splices. The responses to the same excitation obtained with NTHA are depicted in *Figure 2.12*. The favourable effect of the columns and the proportional braces is clear, given that the responses of the storeys show the smallest discrepancy in the d) case. The flexural resistance of the columns is therefore indispensable even if in linear analysis such demand may not seem necessary. The need of the columns additional resistance is accounted for in various redesign attempts and also building codes that are to be introduced in the following.

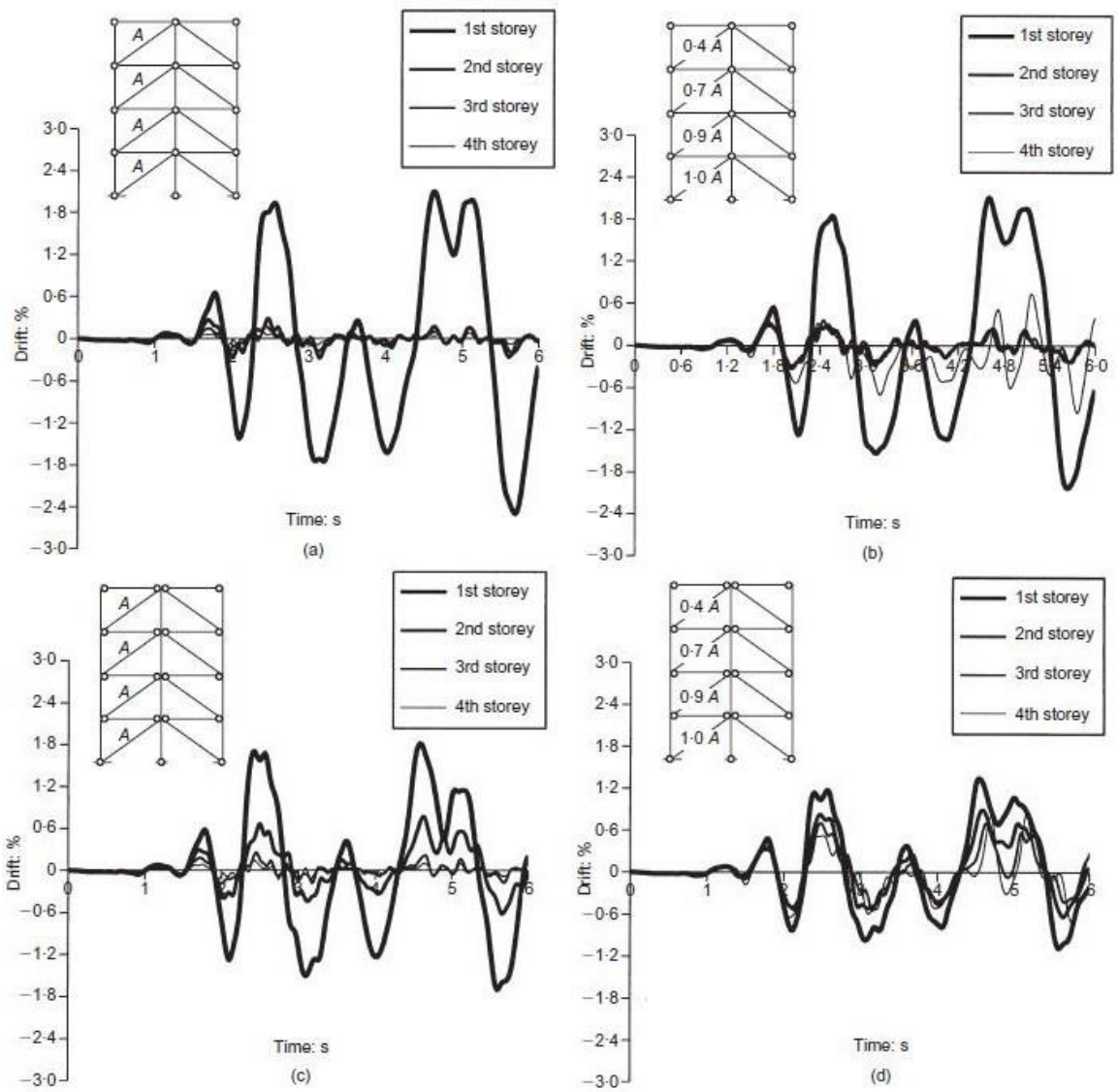

Figure 2.12; *Distribution of interstorey drift over height [12]*

2.2.2. Solutions to the performance issues by modified design procedures

Apart from the performance problems resulted by the above discussed factors a practicing engineer may encounter difficulties when elaborating a design with the provisions of Eurocode 8 for CBF-s, presented in 1.3.2. To resolve such problems and enhance the seismic performance several authors developed additional requirements or modifications to the Eurocode 8 design criteria.

Having observed the relevance of the resistance reserve provided by the columns Elghazouli [53] proposed a formula that expresses the ratio of the sum of the horizontal stiffness provided by the continuous columns and the axial stiffness of every brace. The stiffness ratio is calculated as:

$$\beta_k = \frac{L_d \sum I_c}{h_c^3 \cos\alpha \sum A_d} \tag{2.24}$$

where L_d and A_d are the length and cross-sectional area of the diagonal, h_c and I_c are the height and the second moment of area of the columns and α is the angle of the brace and the

horizontal plane. Depending on the uniformity of the storey overstrength factors calculated by Eq. (1.32), by setting a requirement to the stiffness ratio (value on the horizontal axis), the normalized ductility demand on the involved storeys can be expected to be as given by the corresponding value on the vertical axis of *Figure 2.13*.

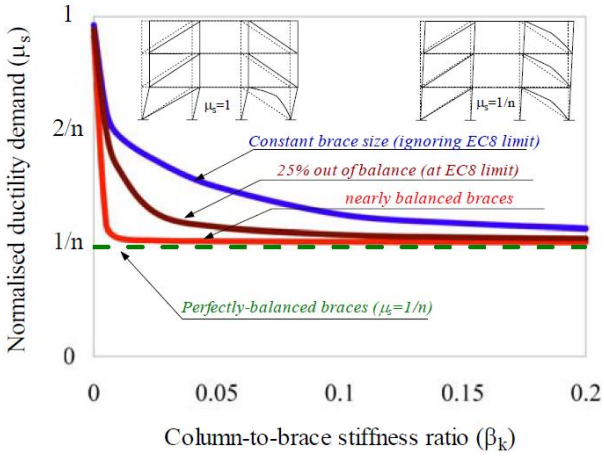

Figure 2.12*; Demand distribution in braced frames [53]*

In their articles Longo et al [54][55] and Brandonisio et al [56] have a different approach to the seismic design of CBF-s. They highlight certain drawbacks of the Eurocode 8 design procedure and propose modifications. In the referenced articles it is pointed out that defining the overstrength factor as the minimum of the storey overstrength, Eq. (1.30), and penalizing the seismic internal forces of non-dissipative members with it, Eq. (1.32), does not comply with the principles of capacity design as it only ensures the structural integrity up to first yield and not the complete development of a global collapse mechanism. Also, it is emphasized that the non-dimensional slenderness of the braces and the storey overstrength factors are closely interrelated. If the choice of cross section is governed by slenderness limitations rather than by axial strength demand unfeasible or at least vastly oversized designs may occur. On the upper floors of a CBF the axial resistance demand in the braces is rather small in comparison with lower floors. If multiple braced bays are implemented in the building for the sake of providing torsional stiffness the axial resistance need may be even less. The low axial force requires small cross section that entails large slenderness. As the slenderness has an upper limit, Eq. (1.26), larger cross sections must be applied which gives rise to the overstrength on the upper floors. Because of the uniformity condition, Eq. (1.29), the resistance has to be increased on all the other floors as well and consequently the global overstrength rises to a value significantly greater than 1.0. The high overstrength penalizes the non-dissipative members with a substantial steel weight premium. Such a design is cost-ineffective and imposes a significant overdesign need on the connections and foundations also. In the meantime in taller buildings or when the plan layout consists only a limited number of braced bays the axial demand of the braces can be so large that the cross-sectional area requirement and the minimum limit of the slenderness for X-braced configurations, Eq. (1.27), together result an unfeasible solution in the utilized range of cross sections.

The authors in the referenced articles agree that capacity design principles necessitate the use of internal forces corresponding to the complete development of the global collapse mechanism. Alternatively, the use of the maximum storey overstrength as overstrength factor.

$$\Omega = \max \Omega_i \tag{2.25}$$

In addition Brandonisio et al. propose to obliterate the minimum slenderness limit and instead take into account that stocky braces in compression may substantially contribute to the resistance and enlarge the overstrength. The overstrength coefficient, ξ_i, is calculated as the ratio of the lateral resistance corresponding to the buckling of the compression member, $N_{b,Rd,i}$, and the equivalent seismic loading above the examined storey.

$$\xi_i = \frac{2N_{b,Rd,i} \cdot \cos\alpha}{\sum_{j=i}^{n} F_{h,j}} \tag{2.26}$$

This coefficient can only be relevant if the slenderness is below the neglected limit of 1.3, but in that case it may indicate that the considered storey has larger resistance with the compression brace and smaller axial forces than solely considering the plastic axial resistance of the tensile diagonal. Therefore, it is recommended to define the overstrength factor as follows:

$$\Omega^* = \max\left(\Omega_i; \xi_i\right) \tag{2.26}$$

The contradiction between adjusting the brace resistances to the demands to respect the uniformity condition imposed on the storey overstrength and in the meantime having to provide adequately large cross sections not to let the slenderness rise above 2.0 is resolved by Longo et al in [55]. The authors introduce the concept of the reduced section solution, the concept of which is fundamentally reducing the brace section at the ends in order to calibrate the resistance to the demand but without considerably enlarging the slenderness, see *Figure 2.13*.

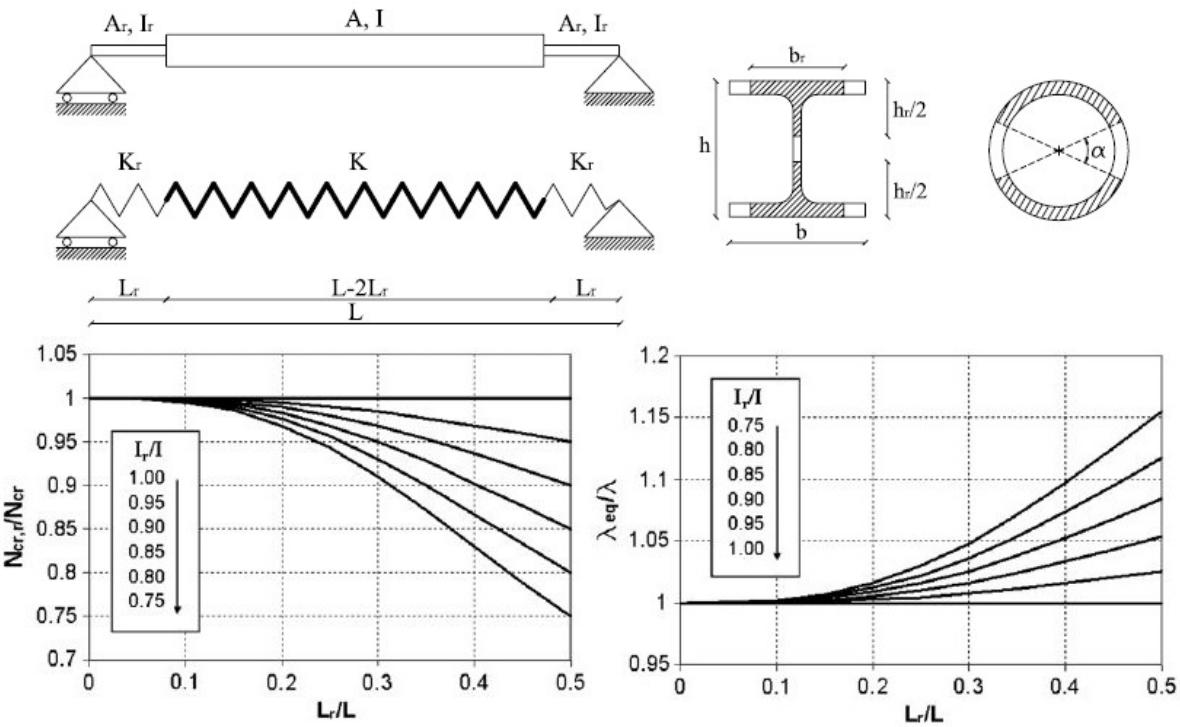

Figure 2.13*; Concept of the reduced section solution [55]*

The length of the reduction, L_r, has a lower bound in order to safeguard the undisturbed tensile plastic deformation of the reduced section. The minimum length commonly adopted for coupon tensile tests is:

$$L_{r,\min} = 5.65\sqrt{A_r} \tag{2.27}$$

where A_r is the reduced section area. In the diagrams presented also in *Figure 2.13* one can see that by reducing the inertia by 25% on a length of 0.3 times the bar length, the axial buckling resistance only decreases by 10% while the slenderness increases by 5%. Consequently the section reduction is effective in adjusting the net cross-sectional area but maintaining the stability features of the brace.

The presented redesign methods are mostly successful in resolving the problems encountered in design such as unfeasible designs, contradictory requirements or unnecessarily large weight premium. In order to assess the performance of the method of Longo et al, the IDA response of a 4-storey CBF designed for PGA=0.35g is depicted in *Figure 2.14*. In the diagrams the ductility demand over the ductility limit of the braces is plotted against the PGA. The acceleration where failure is attained (by any of multiple conditions not detailed here) is indicated by a vertical line. The first diagram corresponds to an initial EC8 design, yet it has to be noted, that the design violates the uniformity condition on the top floor due to the maximum slenderness limit. The second diagram shows a solution where the columns are designed taking into account the largest and prominent storey overstrength. For the third diagram the reduced section solution is implemented in design, so that every storey overstrength is equal to 1.0. The utility of the methods is obvious as they provide feasible designs that have a resistance superior to the demand considered in design. These redesigns however are not appropriate to promote the global plastic mechanism, as flagrant discrepancies exhibited by the third or fourth floor even below the design strength of the seismic action clearly indicate the presence of the weak storey behaviour.

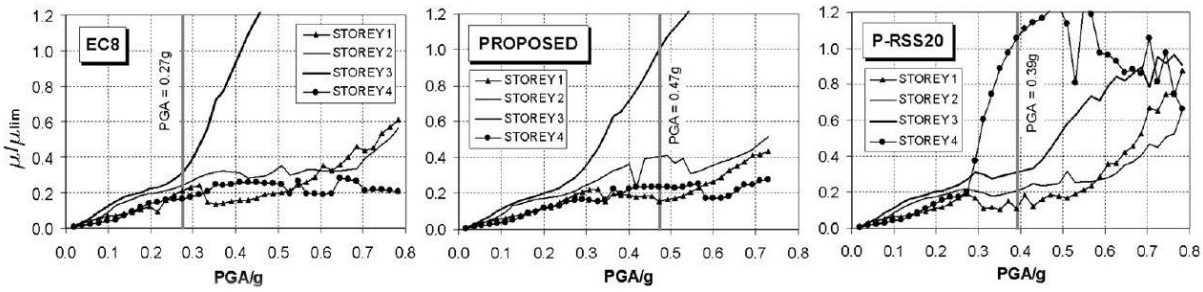

Figure 2.14*; Performance of enhanced design method [55]*

2.2.3. Solutions to the performance issues by innovative structural members

Understanding that the brace buckling and deterioration, both in terms of resistance and dissipation, are accountable for the development of the weak storey behaviour led to the appearance of alternative solutions, involving bracing configurations that exhibit superior response and/or bracing configurations that encourage the more uniform distribution of the inelastic demand. These, otherwise state-of-the-art solutions are not subjects of the dissertation therefore they are just basically introduced in the following paragraphs.

One innovative bracing member that has dynamically spread throughout the world in building practice and also studied by many researchers [57][58][59] is the buckling restrained brace or commonly BRB. Buckling restrained braces are special diagonals that consist of a ductile steel core that actually participates in the resistance and concrete/steel mantle in which the steel core is encased. As there is no bond between the core and the mantle due to a very thin air gap in between and since the mantle is not firmly attached to

both brace ends, the mantle does not resist any bit of the axial loading. Instead, it ensures that in compression the steel core does not buckle, but undergoes plastic deformations just like in tension. Conceptual sections of a BRB showing the main parts are presented in *Figure 2.15*.

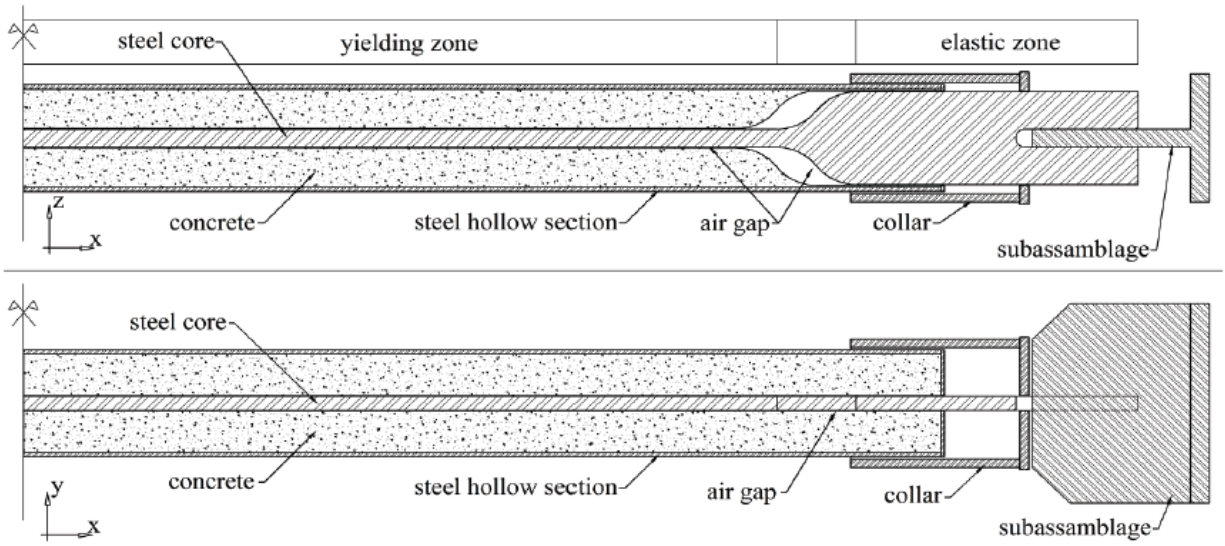

Figure 2.15*; Sections of a buckling restrained brace [59]*

The advantage of utilizing BRB bars instead of conventional steel section is that in compression the axial force – displacement diagram is not pinched, as it is presented in *Figure 2.16*, and by the broader hysteretic loops of a BRB substantially more energy is dissipated. Moreover, BRB-s do not even deteriorate rapidly due to local buckling as conventional braces do. This favourable behaviour allows for behaviour factors in buckling restrained braced frames by far larger (q=7 [59]) than of usual CBF-s. The trade-off for the high performance is the elevated cost and additional practical demands in detailing.

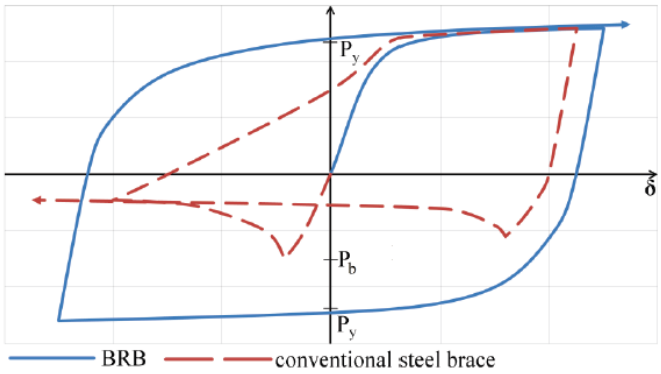

Figure 2.16*; Axial force – displacement cycle of buckling restrained and conventional brace [59]*

Buckling restrained braces may have a strongly enhanced performance, but they do not necessarily solve the problem of weak storey development. To this end Tremblay [48] proposes brace arrangements that are meant to safeguard that the lateral motion of the building follows strictly a conventional first mode in which the drift and thus the deformations are uniform, see *Figure 2.17*. The concept is providing a highly reinforced, rigid vertical truss which is pinned in one point at the base. This truss therefore does not resist lateral seismic forces directly as it can simply rotate about its support. The purpose of this truss is to remain elastic and consequently closely straight throughout the seismic event and to bring all the dissipative members on every floor equally into bear. The dissipative members may be BRB-s or conventional, bi-directional braces as well. In his corresponding

article Tremblay found these solutions very effective and well performing. It has to be pointed out though that such arrangements necessitate special structural and even architectural solutions.

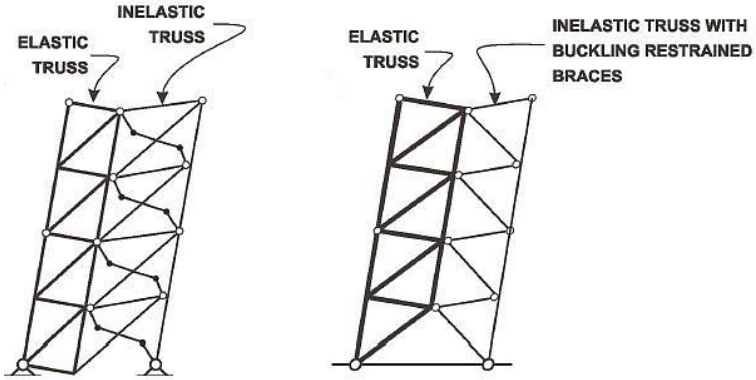

Figure 2.17*; Innovative concentric brace arrangements [48]*

The idea of the elastic truss is implemented in self-centering braced frames also [60]. These braced frames are fixed to the base by post-tensioning cables that enable the uplift of the column base beyond a predefined overturning moment. After the uplift the braced frame rotates about the compression support and does not carry additional seismic loading, but provide a vertical restoring force, see *Figure 2.18*. Due to the uplift the frame remains elastic and is capable to compel uniform deformation on every storey. These braced frames are operational in not seismic situations without the need of an attached secondary bracing, unlike the solutions presented before. The disadvantage is that since these trusses are meant to remain elastic, they do not dissipate significant energy. Only the vertical stressing cables or the fuses may be dissipative members. These systems are therefore usually coupled with another system capable of dissipation, but prone to localized collapse i.e. a typical situation in the seismic retrofit of existing buildings. Latest research focuses on adding dissipative fuses to these systems [61].

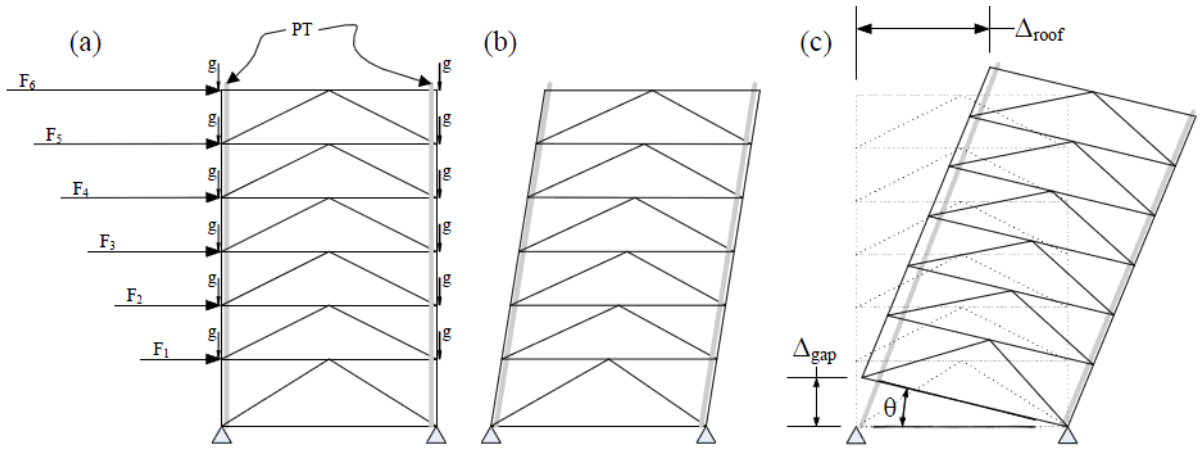

Figure 2.18*; Self-centering braced frame [60]*

Chapter 3

Investigation into the seismic performance of various Eurocode 8 CBF designs

In this chapter firstly the design of various CBF-s is described. The structures are introduced, the loads and combinations are given and the method of the verification is referred to. The objective is to verify the adequacy of the buildings by advanced analysis methods such as the IDA. To this end, the nonlinear model built for the dynamic analyses is described. The performance of the buildings is examined via the IDA curves and certain regularities are identified that help to further explain the weak storey behaviour.

3.1. Design of CBF-s for numerical experiments

In the previous chapters the weak storey phenomenon has been introduced. The digest of some articles published on the seismic behaviour of CBF-s indicated that CBF-s are particularly susceptible to exhibit this adverse behaviour. Some authors investigated the discovered weaknesses of the corresponding parts of Eurocode 8 and proposed supplementary criteria. It has also been briefly referred to that several other seismic building codes have more stringent regulations than Eurocode. All this suggests that Eurocode 8 CBF designs may not have a satisfactory seismic performance in all respects. In order to verify this assumption various buildings have to be designed for later numerical experimental purposes. In the following the design process of these CBF-s is presented.

3.1.1. General introduction of buildings

The numerous buildings primarily differ in the number of storeys, but there are also two structural systems and irregular cases. There are 4, 6, 8 and 10 storey-high buildings denoted by CBF4, CBF6, CBF8 and CBF10, respectively. The buildings are identical in plan. They are built on an orthogonal raster grid that consists of the same four bays in both plan directions. A 3 dimensional view of a 4-storey CBF is presented in *Figure 3.1*. The span of the bays is 6 metres each, that gives a 24×24 metre overall plan layout. The storey height is 3 metres in every building and on every floor.

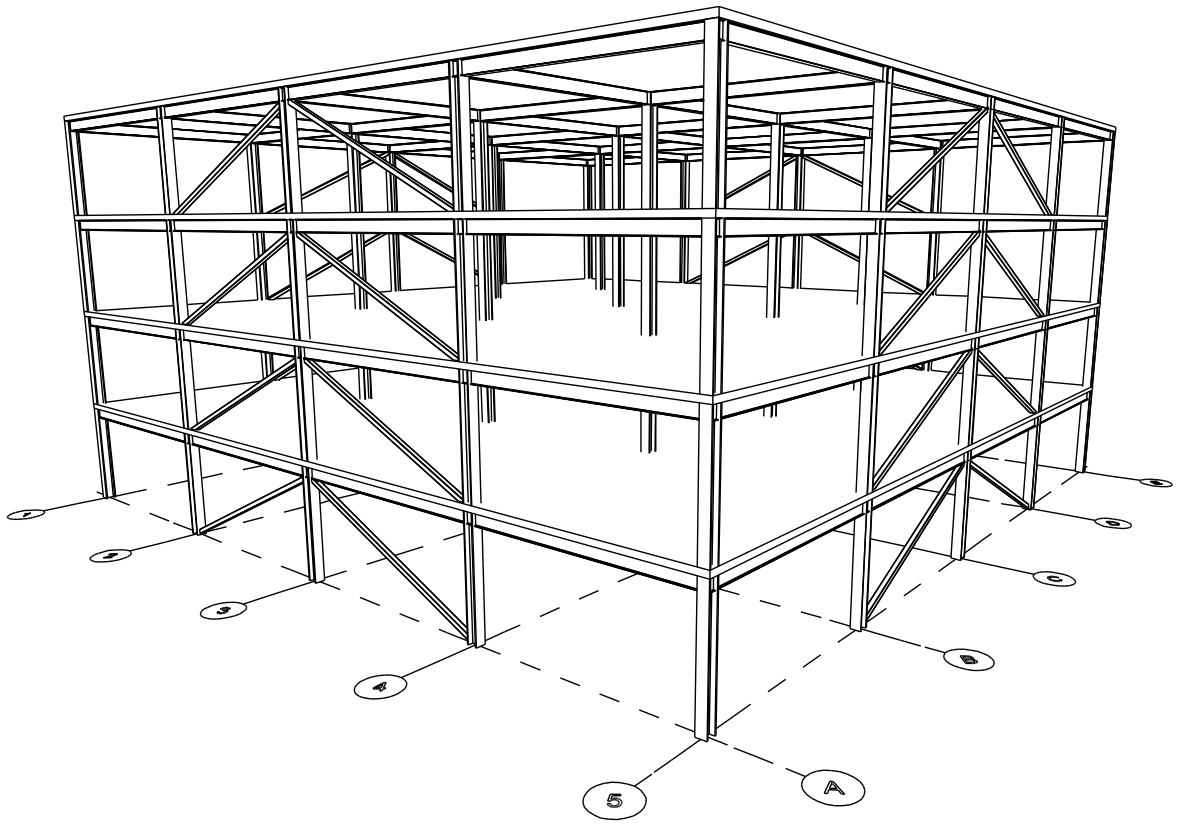

Figure 3.1*; Perspective view of 4-storey CBF*

In the buildings where the lateral resistance in both directions is provided by braces on the four outermost grids, see *Figure 3.2/a*, only the columns that are connected to the diagonals i.e. the ones that are participating in the lateral resistance are continuous throughout the whole height of the building, but pinned at the base. All the other column

splices are hinged and located at the slab levels. The continuous, H-section columns are positioned in a way that their strong principal axis, i.e. I_y second moment of area, participates in the lateral resistance. These structural types are denoted in the results later on by the number 1 following the storey number e.g. CBF41 (4-storey CBF with bracing in both directions). In the buildings where the lateral resistance is provided by moment resisting frames (hereinafter MRF) in one direction and by bracing in the other, see *Figure 3.2/b*, all the columns are continuous and positioned in a way that their strong principal axis works in the plane of the MRF and the weak in the direction of the bracing. In these buildings every column is considered in the lateral resistance as they are interconnected by the slabs. These buildings are denoted by the number 2 after the storey number e.g. CBF42.

Both the gravity and the lateral loadings are distributed on the steel frame members by a concrete slab. However the steel I section beams are placed under the slab as ribs, in the design it has been assumed that there is no composite behaviour. The slabs merely distribute the loads and provide horizontal diaphragms and the steel frame carries the loads independently.

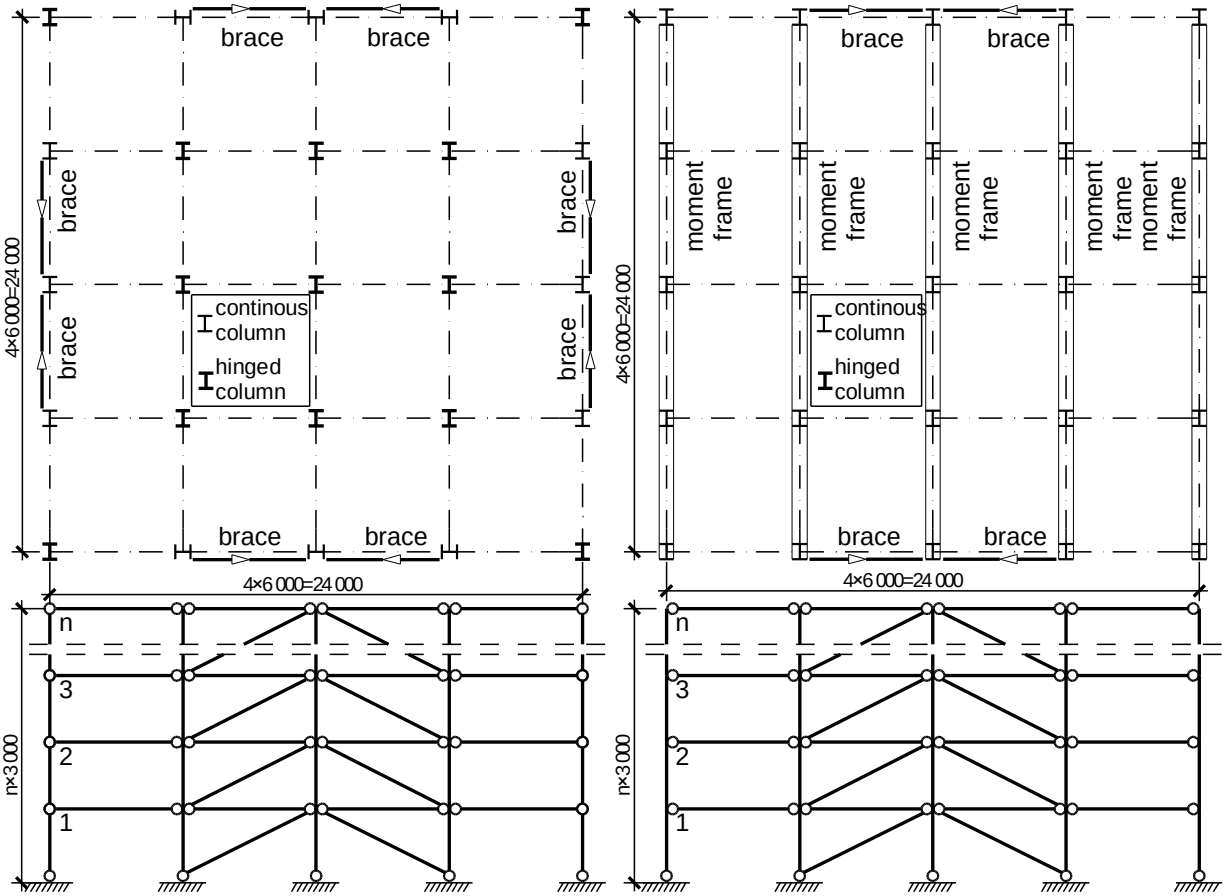

a) CBF in both directions (Type 1) *b) MRF – CBF buildings (Type 2)*

Figure 3.2*; Plan view and structural model of CBF-s*

The first irregularity in design is based upon the idea that an appropriate seismic behaviour shall permit the use of a behaviour factor higher than the currently permitted in Eurocode 8, similarly to the regulations corresponding to SCBF-s [44]. To examine the viability of this idea, CBF41 and 61 are designed according to Eurocode 8 rules, but considering q=5. These alternatives are indicated by the acronym Q5 in the designation of the building. It has to be noted, that the fundamental periods of the taller buildings are so high, that the difference between the designs with behaviour factor 4 or 5 is negligible. Another

special case that has been considered is the change of the mass on some floors. In CBF81 on the upper 4 floors a 20%, and in CBF61 on the upper 3 floors a 50% weight premium is assumed. For the sake of comparability in the second case the behaviour factor is not decreased, though the building does not satisfy the requirement of the regularity in elevation [4]. In the designation of these buildings the letter M is indicated. The following table summarizes all the different CBF-s and emphasizes their particularities and also gives the period of the first mode of vibration. In the designation the acronym EC8 refers to the method of the seismic design i.e. Eurocode 8.

Table 3.1; *List and specifications of CBF-s*

Building	*Features*	*Period (T_1 sec)*
CBF41-EC8	4-storey CBF in both directions	1.13
CBF42-EC8	4-storey MRF – CBF	1.19
CBF61-EC8	6-storey CBF in both directions	1.65
CBF62-EC8	6-storey MRF – CBF	1.61
CBF81-EC8	8-storey CBF in both directions	2.10
CBF82-EC8	8-storey MRF – CBF	2.04
CBF101-EC8	10-storey CBF in both directions	2.54
CBF102-EC8	10-storey MRF – CBF	2.41
CBF41Q5-EC8	4-storey CBF, design with behaviour factor q=5	1.21
CBF61Q5-EC8	6-storey CBF, design with behaviour factor q=5	1.68
CBF61M-EC8	6-storey CBF, 50% mass irregularity, upper half	1.78
CBF81M-EC8	8-storey CBF, 20% mass irregularity, upper half	2.17

3.1.2. Loads and effects in design

The dead loads consisting of the structural self weight and regular layers on the floor slabs are considered as an evenly distributed load on the floor slabs. The load itself and the safety factor are:

$$g = 6.77\frac{kN}{m^2} \quad \gamma_g = 1.35 \tag{3.1}$$

The live load is considered to be a B category (office occupation) evenly distributed load according to Eurocode 1 [62]. The load itself and the related partial factors are:

$$q = 3\frac{kN}{m^2} \quad \gamma_q = 1.5 \quad \psi_{0,q} = 0.7 \quad \psi_{2,q} = 0.3 \tag{3.2}$$

Snow load has been considered to be negligible in the present study as it has no significant effect on the lateral load bearing structure and it has no contribution to the mass that has to be taken into consideration in seismic analysis. From Table 4.2 of Eurocode 8 the value ϕ=1.0 has been considered for the benefit of safety.

In order to obtain a realistic design regarding every structural member wind effect has been considered. The definition of the loading complies with EN 1991-1-4 [63].
The fundamental value of the wind velocity is:

$$v_{b0} = 23.6\frac{m}{s} \tag{3.3}$$

The season factor, directional factor and the air density are:

$$c_{season} = 1.0 \quad c_{dir} = 1.0 \quad \rho = 1.25\frac{kg}{m^3} \tag{3.4}$$

The basic wind velocity and velocity pressure are:

$$\begin{gathered} v_b = v_{b0} \cdot c_{dir} \cdot c_{season} = 23.6\frac{m}{s} \\ q_b = \frac{1}{2} \cdot \rho \cdot v_b^2 = 0.348\frac{kN}{m^2} \end{gathered} \tag{3.5}$$

The terrain category is assumed to be III. The turbulence, orography and terrain factors are:

$$\begin{gathered} k_i = 1.0 \quad C_0 = 1.0 \\ k_r = 0.19\left(\frac{z_0}{z_{0.II}}\right)^{0.07} = 0.215 \\ \text{with:} \quad z_0 = 0.3m \quad z_{0.II} = 0.05m \end{gathered} \tag{3.6}$$

The pressure coefficients on the wind and leeward sides of the buildings:

$$C_{pe,D} = 0.8 \;\; C_{pe,E} = -0.5 \tag{3.7}$$

where the D surface is the windward and the E is the leeward. The height of the buildings differ therefore the roughness and exposure factors are different for each. Also for the taller buildings (CBF8 and CBF10) two reference heights are considered. The mentioned two factors are calculated with the formulas below:

$$\begin{gathered} C_r = k_r \cdot \ln\left(\frac{z_e}{z_0}\right) \\ C_e = C_r^2 \cdot C_0^2 \cdot \left(1 + \frac{7 \cdot k_r \cdot k_i}{C_r \cdot C_0}\right) \end{gathered} \tag{3.8}$$

The characteristic wind load of the buildings is calculated as follows and the results are listed below:

$$w = q_b \cdot C_e \cdot C_{pe} \tag{3.9}$$

Table 3.2; *Distributed windload on wind and leeward sides [kN/m²]*

surface	**CBF4**	**CBF6**	**CBF8**		**CBF10**	
	$z_e=h$	$z_e=h$	$z_e=b$	$z_e=h$	$z_e=b$	$z_e=h$
D	0.509	0.644	0.644	0.729	0-644	0.792
E	-0.318	-0.403	-0.403	-0.456	-0.403	-0.495

The safety and combination factors of the wind load are:

$$\gamma_w = 1.5 \quad \psi_{0,w} = 0.6 \quad \psi_{2,w} = 0.0 \tag{3.10}$$

The earthquake acceleration response spectrum has been considered to be the type 1 in EC8 assuming B type soil conditions, see *Figure 3.3*. The design ground acceleration is taken to be 0.25*g=2.453 m/s*^{2}, where *g* is the acceleration of gravity. The behaviour factor, *q*, is 4 in agreement with the structure-specific regulations of the standard.

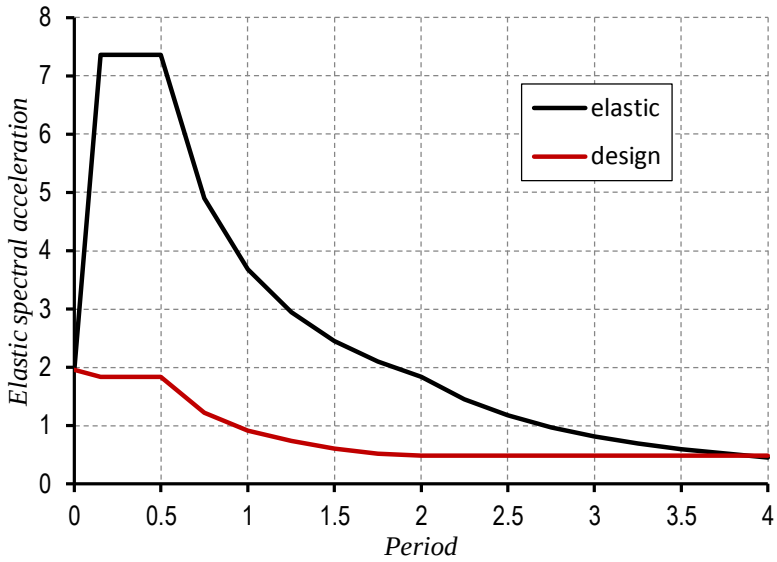

Figure 3.3*; Elastic and design spectra used in the design of the CBF-s*

For the above introduced loading the structural members have been verified not only in seismic, but also in ultimate and serviceability design states. The corresponding load combinations are:

$$p_{ULS1} = \gamma_g \cdot g + \gamma_q \cdot q + \gamma_w \cdot \psi_{0,w} \cdot w$$
$$p_{ULS2} = \gamma_g \cdot g + \gamma_q \cdot \psi_{0,q} \cdot q + \gamma_w \cdot w \tag{3.11}$$

in ultimate limit state,

$$p_{SLS1} = g + q + \psi_{0,w} \cdot w$$
$$p_{SLS2} = g + \psi_{0,q} \cdot q + w \tag{3.12}$$

in serviceability limit state with characteristic combinations and

$$p_{EQ} = g + E_{Ed} + \psi_{2,q} \cdot q \tag{3.13}$$

in seismic limit states, where E_{Ed} denotes the seismic effect.

3.1.3. Analysis and dimensioning

The analysis and design has been carried out using a 3 dimensional model of the buildings in which the braces of one bay on each side were neglected. In the seismic analysis the modal response spectrum analysis method has been implemented considering a sufficient number of modes to exceed 90% mass participation in the lateral directions. For the combination of the modal responses the complete quadratic combination method has been used. Both horizontal components of the earthquake have been considered, therefore for buildings belonging to the structural model type 2 i.e. MRF-s in one direction, bracing in the other, the specific sections of Eurocode 8 for MRF-s have been applied also. The q factor has been 4 for both structural systems so that building types 1 and 2 can be compared. To

account for accidental torsional effects the accidental eccentricity has been considered according to Eq. (1.47). All the members were designed to respect the corresponding parts of both Eurocode 3 [10] and 8 [4].

In the dimensioning of the diagonals it has been assumed that the braces do not carry the gravity loads and also that there are no drilled holes that decrease the gross cross sections. In the design of the braces the following requirements have been verified:

- The slenderness is less than 2.0; also a lower boundary of 1.3 was applied to avoid twitching of the slender bars (though the buildings are not X-braced), Eqs. (1.26)(1.27)
- The plastic ultimate axial resistance of the tensile brace is higher than the effect, Eq. (1.25)
- The uniformity condition is respected, i.e. the maximum overstrength does not exceed the minimum by more than 25%, Eq. (1.29)

The columns and beams have been verified according to the provisions of EN 1993.1.1 clause 6.3.3. The evaluated formulas are:

$$\frac{N_{Ed}}{\frac{\chi_y N_{Rk}}{\gamma_{M1}}} + k_{yy}\frac{M_{y,Ed}+\Delta M_{y,Ed}}{\chi_{LT}\frac{M_{y,Rk}}{\gamma_{M1}}} + k_{yz}\frac{M_{z,Ed}+\Delta M_{z,Ed}}{\frac{M_{z,Rk}}{\gamma_{M1}}} \le 1 \tag{3.14}$$

$$\frac{N_{Ed}}{\frac{\chi_z N_{Rk}}{\gamma_{M1}}} + k_{zy}\frac{M_{y,Ed}+\Delta M_{y,Ed}}{\chi_{LT}\frac{M_{y,Rk}}{\gamma_{M1}}} + k_{zz}\frac{M_{z,Ed}+\Delta M_{z,Ed}}{\frac{M_{z,Rk}}{\gamma_{M1}}} \le 1 \tag{3.15}$$

where:

$N_{Ed}, M_{y,Ed}, M_{z,Ed}$	design values of internal forces
$\Delta M_{y,Ed}, \Delta M_{z,Ed}$	excess moments for class 4 sections (=0)
$N_{Rk}, M_{y,Rk}, M_{z,Rk}$	plastic resistances
χ_y, χ_z	buckling reduction factors
$k_{yy}, k_{yz}, k_{zy}, k_{zz}$	interaction factors
$\gamma_{M1} = 1.0$	

In seismic design states the internal effects have been amplified in accordance with Eq. (1.32), that is:

$$N_{Ed,E} = N_{Ed,g} + 1{,}1 \cdot \gamma_{ov} \cdot \Omega \cdot N_{Ed,E} \tag{3.16}$$

The interaction factors were calculated as follows (Annex B of EN 1993-1-1):

$$k_{yy} = C_{my}\left(1 + \left(\bar{\lambda}_y - 0.2\right)\frac{N_{Ed}}{\chi_y N_{Rk}/\gamma_{M1}}\right) \tag{3.17}$$

$$k_{zz} = C_{mz}\left(1 + \left(2\bar{\lambda}_z - 0.6\right)\frac{N_{Ed}}{\chi_z N_{Rk}/\gamma_{M1}}\right) \tag{3.18}$$

$$k_{yz} = 0.6k_{zz} \quad k_{zy} = 0.6k_{yy} \tag{3.19}$$

$$C_{my}, C_{mz} = 0.6 + 0.4\psi \ge 0.4 \tag{3.20}$$

The buckling reduction factors were calculated as follows:

$$\chi_y = \frac{1}{\phi_y + \sqrt{\phi_y^2 - \bar{\lambda}_y^2}} \quad \chi_z = \frac{1}{\phi_z + \sqrt{\phi_z^2 - \bar{\lambda}_z^2}} \tag{3.21}$$

$$\phi_y = \frac{1 + \alpha_y\left(\bar{\lambda}_y - 0.2\right) + \bar{\lambda}_y^2}{2} \quad \phi_z = \frac{1 + \alpha_z\left(\bar{\lambda}_z - 0.2\right) + \bar{\lambda}_z^2}{2} \tag{3.22}$$

where α imperfection factor is 0.34 for bending about the y and 0.49 for bending about the z principal axis. The lateral torsional buckling reduction factor χ_{LT} is assumed to be 1.0. In the verification of the beams it has been assumed that concrete slab prevents the lateral torsional buckling and also the buckling about the weak axis, but there is no composite action. Therefore, the beams were verified with a simplified form of Eq. (3.14):

$$\frac{N_{Ed}}{\frac{\chi_y N_{Rk}}{\gamma_{M1}}} + k_{yy} \frac{M_{y,Ed} + \Delta M_{y,Ed}}{\chi_{LT} \frac{M_{y,Rk}}{\gamma_{M1}}} \leq 1.0 \tag{3.23}$$

where:

$$k_{yy} = C_{my}\left(1 + \left(\bar{\lambda}_y - 0.2\right)\frac{N_{Ed}}{\chi_y N_{Rk}/\gamma_{M1}}\right) \quad \text{and} \quad C_{my} = 0.95 \tag{3.24}$$

In serviceability limit state limits l/200 for vertical and H/500 for horizontal deflection has been considered. In Annex B detailed results are provided on the dimensioning of each member. In the following tables the cross sections of the internal and external (facade) columns, beams of the braced bays, braces, and also the slenderness of the braces and the storey overstrength factors are depicted as the later two are relevant in terms of the seismic design. Below the tables the ratio of the maximum and the minimum storey overstrength is indicated. As it can be seen the storey overstrengths are rather uniform in every building. In certain cases on some floors the overstrength is slightly below 1.0 or the slenderness is a little beyond the allowed limit. Nevertheless, despite these small deficiencies the designs are considered adequate.

Table 3.3a; *CBF41-EC8*

storey	*int.col.*	*ext.col.*	*beam*	*brace*	$\bar{\lambda}$	*Ω*
4	HEA 160	HEA 140	IPE 300	100×4	1.83	1.05
3	HEB 180	HEA 200	IPE 300	100×6.3	1.87	0.99
2	HEB 220	HEB 200	IPE 360	100×8	1.91	0.97
1	HEB 260	HEB 240	IPE 360	100×10	1.95	0.99
						$\Omega_{max}/\Omega_{min}$=1.08

Table 3.3b; *CBF42-EC8*

storey	*int.col.*	*ext.col.*	*beam*	*brace*	$\bar{\lambda}$	*Ω*
4	HEA 180	HEA 200	IPE 300	100×4	1.83	1.09
3	HEB 180	HEB 200	IPE 300	100×6	1.87	0.97
2	HEB 220	HEB 220	IPE 360	100×8	1.91	1.00
1	HEB 260	HEB 280	IPE 360	100×10	1.95	1.04
						$\Omega_{max}/\Omega_{min}$=1.12

Table 3.4a; *CBF61-EC8*

storey	*int.col.*	*ext.col.*	*beam*	*brace*	$\bar{\lambda}$	Ω
6	HEA 160	HEA 160	IPE 300	90×5	2.08	1.00
5	HEB 180	HEA 180	IPE 300	100×6	1.89	0.98
4	HEB 220	HEB 200	IPE 300	100×8	1.95	1.04
3	HEB 240	HEB 220	IPE 300	100×10	1.95	1.04
2	HEB 280	HEB 240	IPE 360	100×10	1.95	1.01
1	HEB 300	HEB 280	IPE 360	120×10	1.63	1.00
						$\Omega_{max}/\Omega_{min}$=1.06

Table 3.4b; *CBF62-EC8*

storey	*int.col.*	*ext.col.*	*beam*	*brace*	$\bar{\lambda}$	Ω
6	HEA 180	HEA 180	IPE 300	90×5	2.08	1.00
5	HEB 180	HEB 180	IPE 300	100×6	1.89	0.98
4	HEB 240	HEB 200	IPE 300	100×8	1.95	1.01
3	HEB 260	HEB 240	IPE 300	100×10	1.95	1.04
2	HEB 280	HEB 260	IPE 360	100×10	1.95	0.99
1	HEB 320	HEB 320	IPE 360	120×10	1.63	1.00
						$\Omega_{max}/\Omega_{min}$=1.06

Table 3.5a; *CBF81-EC8*

storey	*int.col.*	*ext.col.*	*beam*	*brace*	$\bar{\lambda}$	Ω
8	HEA 160	HEA 160	IPE 300	90×5	2.06	0.99
7	HEB 180	HEA 180	IPE 300	100×6.3	1.87	1.05
6	HEB 220	HEB 200	IPE 300	100×8	1.95	1.01
5	HEB 240	HEB 220	IPE 300	100×10	2.01	1.10
4	HEB 280	HEB 240	IPE 360	120×10	1.63	1.01
3	HEB 300	HEB 280	IPE 360	120×10	1.63	0.98
2	HEM 240	HEB 320	IPE 360	140×10	1.38	0.98
1	HEM 240	HEM 240	IPE 360	140×10	1.38	1.00
						$\Omega_{max}/\Omega_{min}$=1.12

Table 3.5b; *CBF82-EC8*

storey	*int.col.*	*ext.col.*	*beam*	*brace*	$\bar{\lambda}$	Ω
8	HEA 180	HEA 200	IPE 300	90×5	2.06	1.02
7	HEB 180	HEB 180	IPE 300	100×6.3	1.87	0.99
6	HEB 220	HEB 200	IPE 300	100×8	1.95	0.99
5	HEB 260	HEB 240	IPE 300	100×10	2.01	1.03
4	HEB 280	HEB 260	IPE 360	120×10	1.63	1.13
3	HEB 300	HEB 300	IPE 360	120×10	1.63	1.03
2	HD320×158	HD320×158	IPE 360	140×10	1.38	1.08
1	HD360×179	HD320×158	IPE 360	140×10	1.38	1.01
						$\Omega_{max}/\Omega_{min}$=1.14

Table 3.6a; *CBF101-EC8*

storey	*int.col.*	*ext.col.*	*beam*	*brace*	$\bar{\lambda}$	Ω
10	HEA 160	HEA 160	IPE 300	100×5	1.86	0.98
9	HEB 180	HEA 180	IPE 300	100×8	1.95	1.00
8	HEB 220	HEB 200	IPE 300	100×10	2.01	1.00
7	HEB 240	HEB 220	IPE 300	120×10	1.60	1.11
6	HEB 280	HEB 260	IPE 360	120×10	1.60	1.02
5	HEB 300	HEB 280	IPE 360	140×10	1.36	1.07
4	HEM 240	HEB 320	IPE 360	140×10	1.36	1.01
3	HEM 240	HEM 240	IPE 360	140×12.5	1.39	1.09
2	HEM 260	HEM 260	IPE 360	140×12.5	1.39	1.03
1	HEM 280	HD320×198	IPE 360	140×12.5	1.39	0.98
					$\Omega_{max}/\Omega_{min}$=1.11	

Table 3.6b; *CBF102-EC8*

storey	*int.col.*	*ext.col.*	*beam*	*brace*	$\bar{\lambda}$	Ω
10	HEA 180	HEB 180	IPE 300	100×5	1.86	1.02
9	HEB 180	HEB 180	IPE 300	100×8	1.95	1.02
8	HEB 220	HEB 220	IPE 300	100×10	2.01	1.02
7	HEB 260	HEB 240	IPE 300	120×10	1.63	1.10
6	HEB 280	HEB 280	IPE 360	120×10	1.63	1.01
5	HEB 300	HEB 320	IPE 360	140×10	1.38	1.07
4	HD320×158	HD320×158	IPE 360	140×10	1.38	1.00
3	HD320×158	HD360×179	IPE 360	150×10	1.27	0.99
2	HD360×179	HD360×196	IPE 360	140×12.5	1.39	1.06
1	HD360×196	HD400×237	IPE 360	140×12.5	1.39	1.00
					$\Omega_{max}/\Omega_{min}$=1.11	

Table 3.7a; *CBF41Q5-EC8*

storey	*int.col.*	*ext.col.*	*beam*	*brace*	$\bar{\lambda}$	Ω
4	HEA 160	HEA 140	IPE 300	90×4	2.05	1.06
3	HEB 180	HEA 180	IPE 300	90×6	2.09	1.05
2	HEB 220	HEB 180	IPE 300	90×8	2.14	1.04
1	HEB 260	HEB 220	IPE 360	100×8	1.91	0.99
					$\Omega_{max}/\Omega_{min}$=1.07	

Table 3.7b; *CBF61Q5-EC8*

storey	*int.col.*	*ext.col.*	*beam*	*brace*	$\bar{\lambda}$	Ω
6	HEA 160	HEA 140	IPE 300	100×4	1.83	1.05
5	HEB 180	HEA 180	IPE 300	100×6	1.88	1.04
4	HEB 220	HEB 180	IPE 300	110×6.3	1.71	1.00
3	HEB 240	HEB 220	IPE 300	100×8	1.91	1.01
2	HEB 280	HEB 240	IPE 360	100×10	1.95	1.06
1	HEB 300	HEB 280	IPE 360	110×10	1.76	1.05
					$\Omega_{max}/\Omega_{min}$=1.06	

Table 3.8a; *CBF61M-EC8*

storey	*int.col.*	*ext.col.*	*beam*	*brace*	$\bar{\lambda}$	Ω
6	HEA 180	HEA 160	IPE 300	100×6	1.87	1.00
5	HEB 220	HEA 200	IPE 300	100×8	1.91	0.98
4	HEB 260	HEB 220	IPE 360	100×10	1.95	0.99
3	HEB 280	HEB 240	IPE 360	120×10	1.63	1.00
2	HEB 320	HEB 280	IPE 360	120×10	1.60	0.98
1	HEM 240	HEB 300	IPE 360	140×10	1.36	1.01
					$\Omega_{max}/\Omega_{min}$=1.02	

Table 3.8b; *CBF81M-EC8*

storey	*int.col.*	*ext.col.*	*beam*	*brace*	$\bar{\lambda}$	Ω
8	HEA 180	HEA 160	IPE 300	100×5	1.85	1.00
7	HEB 200	HEA 200	IPE 300	100×8	1.91	1.08
6	HEB 240	HEB 200	IPE 360	100×10	2.01	1.03
5	HEB 260	HEB 240	IPE 360	140×7.1	1.32	1.02
4	HEB 300	HEB 280	IPE 360	120×10	1.63	1.02
3	HEB 320	HEB 320	IPE 360	140×10	1.38	1.09
2	HEM 240	HEM 240	IPE 360	140×10	1.38	1.00
1	HEM 260	HEM 260	IPE 360	150×10	1.27	1.00
					$\Omega_{max}/\Omega_{min}$=1.09	

3.1.4. Verification of ductility by pushover analysis

In order to verify whether or not the designed CBF-s have adequate ductility that matches the considered behaviour factor pushover analysis has been conducted for most buildings presented above. As all the results demonstrated the same behaviour regardless of storey number, load pattern or structural model (2-way CBF or MRF-CBF) herein only a brief description is given.

In every case plastic deformations in the mid sections of the compression braces are realized on most if not all the floors. Tensile plastic deformation however occurs only on one, or in case of the larger buildings, two storeys. The storey of yield is always located at the bottom third of the building, mostly first or second floor. One representative example is depicted in *Figure 3.*4. The pushover analysis has been carried out for both a constant and an

inverted triangular load pattern, according to Eurocode 8 provisions, and these capacity curves are depicted by red and green. The increasing branch of the capacity curves is slightly curved as the resistance of the buckled braces decreases as the out-of-plane deformation grows. The appearance of tensile yield on any floor practically means the end of the increasing branch. As the first yield occurs at relatively small lateral displacements the target displacement is never reached with the increasing branch by far. Such adversities incorporated in the use of the pushover analysis itself have been identified before [19].

Attempts were made to enhance the behaviour of the structures but these led to excessive reinforcement of the diagonals and adequate capacity curves were not acquired. The standardized pushover analysis did not provide feasible designs in any case. This can be mainly due to the fact that in structures of low level of statical indeterminacy the appearance of plastic members changes the modal behaviour significantly. Consequently the lateral load pattern of the pushover analysis should be updated which is not negligible as the result of the pushover analysis is inherently very sensitive to the shape of the load pattern. One alternative solution to the successful application of pushover analysis on CBF structures may be the Adaptive Modal Combination Procedure of Kalkan and Kunnath [64] [65].

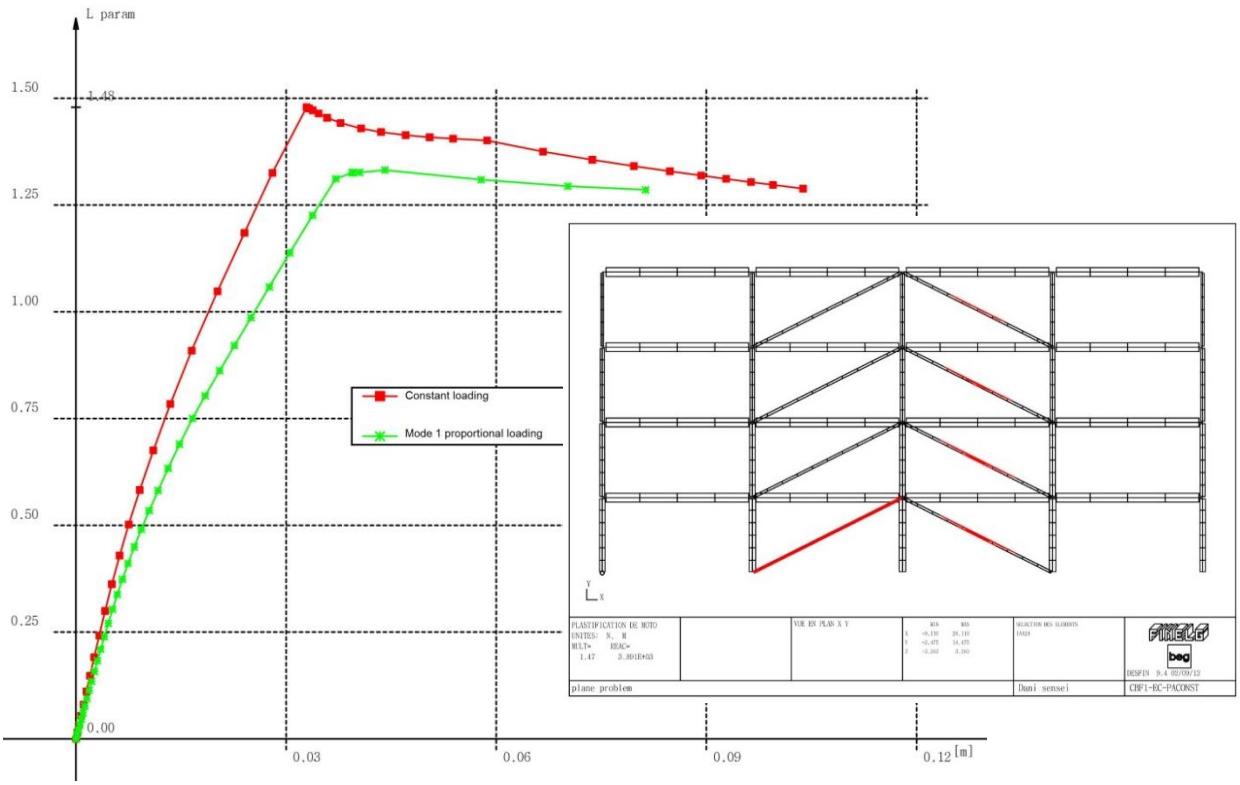

Figure 3.4*; Representative results of pushover analysis of CBF-s*

3.2. Description of model for nonlinear dynamic analysis

In order to determine the seismic performance of the various CBF buildings an incremental dynamic analysis program has been carried out. The nonlinear time history analysis computations have been executed with the use of FinelG finite element analysis software [66]. In the following paragraphs the features of the numerical models and the numerical experimental protocol for the evaluation of the designs will be introduced.

3.2.1. Geometry and discretization

For the nonlinear computations 2D models have been built, equivalent to the original 3D designs. Within the framework of this research all considered CBF-s are symmetrical to at least one vertical plane, which is parallel to the outermost braced frames. This plane of symmetry permits to consider only one half of the building, consisting of one external braced frame and two internal unbraced frames. The columns of the unbraced frames are projected on the plane of the main facade frame in order to reduce the problem to two-dimensional, see *Figure 3.5*. The diaphragm effect of the floor slabs is modelled by horizontal constraints between the nodes of the main frame and the projected leaning columns at the height of the slabs. As the second row of the interior columns is cut by the plane of symmetry, half of their mechanical properties belong to the neglected part of the building and only the other half shall be considered. For this reason the modulus of elasticity and the ultimate stress of the steel material for these columns is divided by two. The connections of the members to the nodes are either pinned or perfectly rigid. In case of the columns the connection type is determined by the building type that has been described in detail previously.

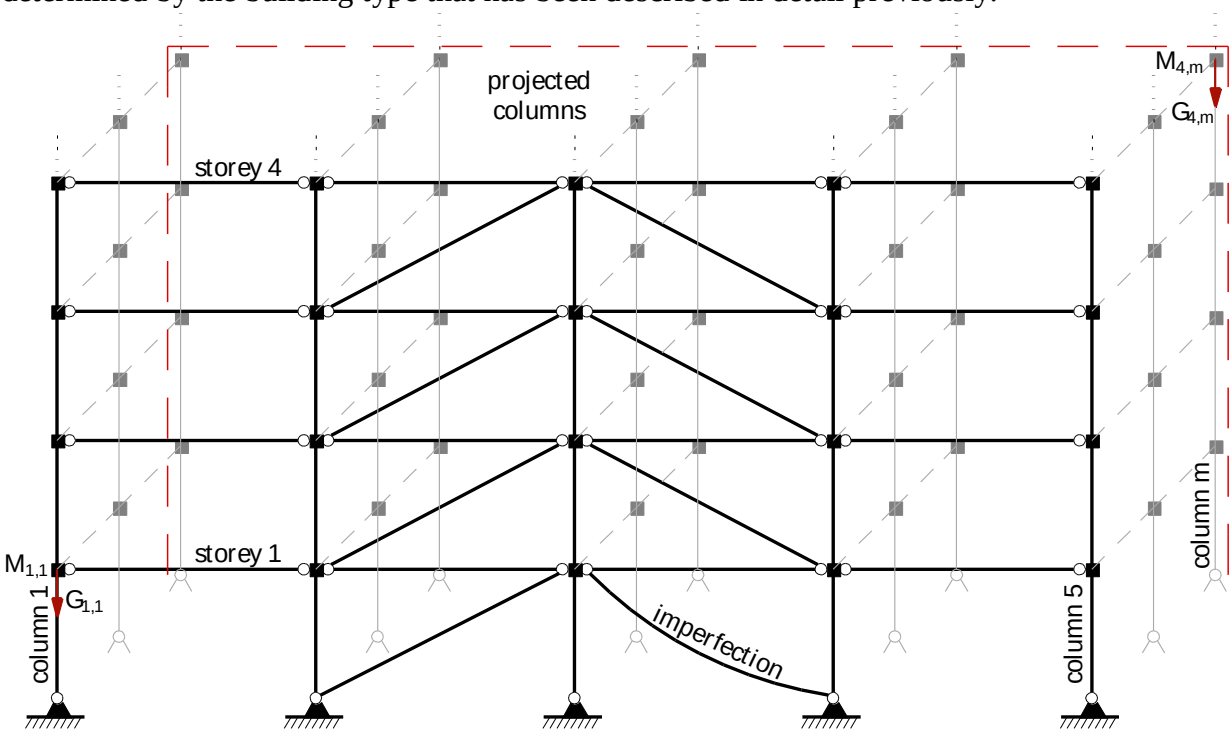

Figure 3.5*; 3D – 2D projection of CBF structure*

The co-rotational formulation applied in the computation software effectively handles large displacements, but in order to account for the expected large deformations also the members have to be divided into multiple finite elements. The braces are divided into ten

elements to have reliable convergence. For columns that are pinned at both ends and beams not participating in the horizontal resistance such refinement of the discretization is not needed.

3.2.2. Finite elements

Every member of the model is built up using the type 35, 2 dimensional beam element of FinelG. The beam elements have 3 nodes and 7 degrees of freedom. The total number of DOF corresponds to two rotational at end nodes and 5 translational, see *Figure 3.6*. A relative translational DOF in the middle is necessary to represent the strong variations of the centroid position when the behaviour of the section is not symmetric. As usual for fibre element, the section forces at the element nodes are computed using both a longitudinal and transversal integration scheme. The integration along the beam length is performed using 3 integration points. For each longitudinal integration point, a transversal integration scheme is performed. On the webs of the thin-walled sections 5 integration points are located and the flanges are divided by 7 points along the plate length and 3 along the thickness. In the fillets additional integration points are considered.

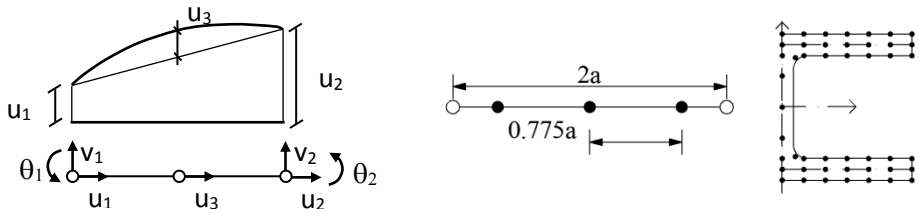

Figure 3.6*; DOF and integrations points of finite element*

The displacement constraints are modelled by nonlinear constraint elements using lagrangian multipliers. This fictitious element is used to define additional optionally nonlinear conditions to the system of equations. In the considered case the element expresses that the displacements of the nodes that the element is assigned to are equal.

3.2.3. Cyclic material model

For the appropriate description of the real behaviour of a brace, a constitutive model that accurately represents the cyclic dissipation shall be used. For steel members in a one-dimensional stress - strain state the use of the Giuffré – Menegotto – Pinto law [67] is in common practice. This model provides a smooth, curved transition between the elastic and plastic branches. Furthermore kinematic hardening and the Bauschinger effect are taken into consideration. The relationship between the stress and the deformation is written as follows:

$$\bar{\sigma} = b\bar{\varepsilon} + \frac{(1-b)\bar{\varepsilon}}{\left(1+\bar{\varepsilon}^{R}\right)^{1/R}} \tag{3.25}$$

$$\bar{\varepsilon} = \frac{\varepsilon - \varepsilon_r}{\varepsilon_0 - \varepsilon_r} \tag{3.26}$$

$$\bar{\sigma} = \frac{\sigma - \sigma_r}{\sigma_0 - \sigma_r} \tag{3.27}$$

ε_0 and σ_0 define the point which is the intersection of the tangent of the initial elastic branch and the tangent of the asymptotic branch describing the yield, see *Figure 3.7*. ε_r and σ_r define the point of the last load reversal. The inclination of the hardening branch is defined by the ratio of the initial (E_0) and the hardening (E_h) modulus of elasticity:

$$b = \frac{E_h}{E_0} \tag{3.28}$$

The curved transition between the two branches is defined by R in Eq. (3.25). In case of cyclic response, after each reversal the curvature reduces with the previous plastic excursion ξ, according to the following expressions:

$$R_n = R_0 - \frac{A_1 \xi_n}{A_2 + \xi_n} \tag{3.29}$$

$$\xi_n = \frac{\varepsilon_{r,n} - \varepsilon_{r,n-1} - \dfrac{\sigma_{r,n} - \sigma_{r,n-1}}{E_0}}{\varepsilon_{0,n} - \varepsilon_{r,n}} \tag{3.30}$$

where R_0 is the value of the curvature in the first loading, A_1 and A_2 are material dependent parameters. The applied set of material parameters is [67]:

$$\begin{aligned} E_0 &= 210GPa \\ E_h &= 2.1GPa \\ f_y &= 235MPa \\ \nu &= 0.3 \\ R_1 &= 20 \\ A_1 &= 18.5 \\ A_2 &= 0.15 \end{aligned} \tag{3.31}$$

where f_y and ν denote the yield stress and the Poisson's ratio respectively.

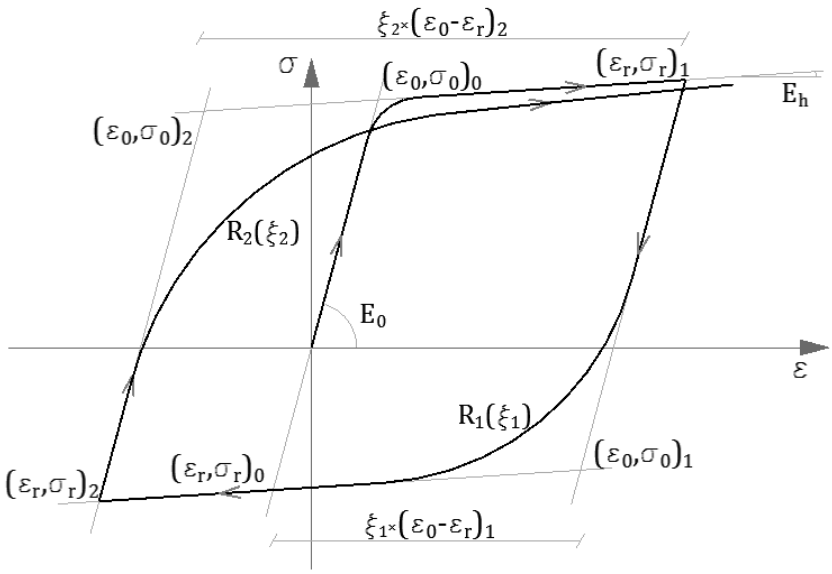

Figure 3.7*; Giuffré – Menegotto – Pinto constitutive law*

3.2.4. Validation of the finite element formulation, and hysteretic dissipative model

In order to validate the accuracy of the nonlinear finite element models the results of an experimental test, carried out by Black et al [22], has been adopted and modelled with FinelG. A bar with a 4 in × 4 in × 0.25 in square hollow section and 10 feet length is loaded with an alternating and monotonically growing-amplitude imposed displacement sequence. During the loading inter alia the axial displacements and the axial forces were measured. In *Figure 3.8* the measured and the computed behaviour of the brace is presented. As it can be seen, the curves are mostly overlapping one another. The figure shows that the performance of the hysteretic model is good as the stiffness, the ultimate strength and the degradation phenomenon are simulated successfully. Some differences can be seen in the compression behaviour as the buckling of plates at the mid section that decreases the compressive resistance, is not represented by the beam element model applied in the analysis.

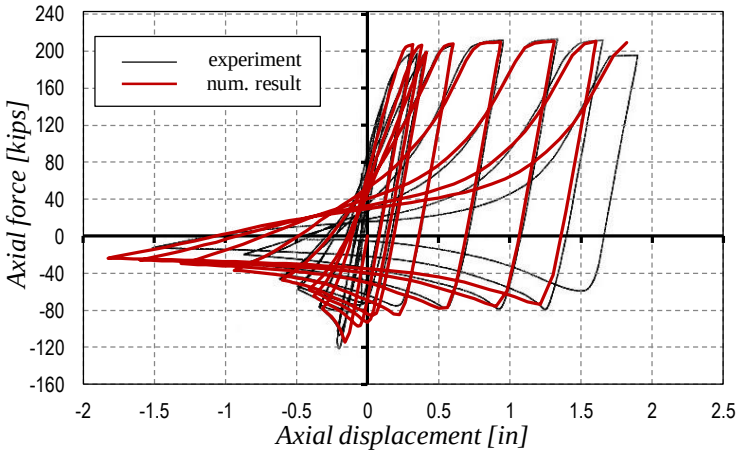

Figure 3.8*; Experimental and numerical brace response [22]*

3.2.5. Loading, masses and seismic excitation

In the NTHA computations apart from the seismic excitation the simultaneous gravity loading and the corresponding masses are considered. The gravity forces and the masses are reduced into the nodes of the adjacent columns. Given that the simultaneous gravity loading is 7.67 kN/m^2 the vertical force and mass that one internal column is loaded by at every slab intersection is:

$$G = 7.67\, {}^{kN}\!/_{m^2} \cdot 6m \cdot 6m = 276.12kN \quad M = \frac{G}{9.81 m/s^2} = 28.147 tons \tag{3.32}$$

The external and the corner columns are of course loaded with the half or one quarter of the values above.

To accurately account for the buckling of the braces in compression the perfect straight geometry of the diagonals are altered. An initial sinusoidal imperfection with an amplitude of L/250 (in accordance with EN1993-1-1 5.3.2.) is considered. In addition, the self weight of the braces is also applied as distributed load.

For the seismic loading seven artificial acceleration records have been selected. The figures of the accelerograms can be found in Annex A. The length of each excitation is 20 seconds and the spectra of the ground motions have been fitted to the design spectrum, see *Figure 3.9*. The used accelerograms are benchmarks in the RFCS OPUS research program [68]. This selection of artificial records complies with the corresponding parts of Eurocode 8

(EN1998-1 4.3.3.4.3) and so it is permitted to consider the mean of the obtained seven results later in the evaluation. For IDA purposes the acceleration records are applied with various intensities. The acceleration records are scaled by multiplying the peak ground acceleration by a scale factor ranging from 0.1 up to 2.0.

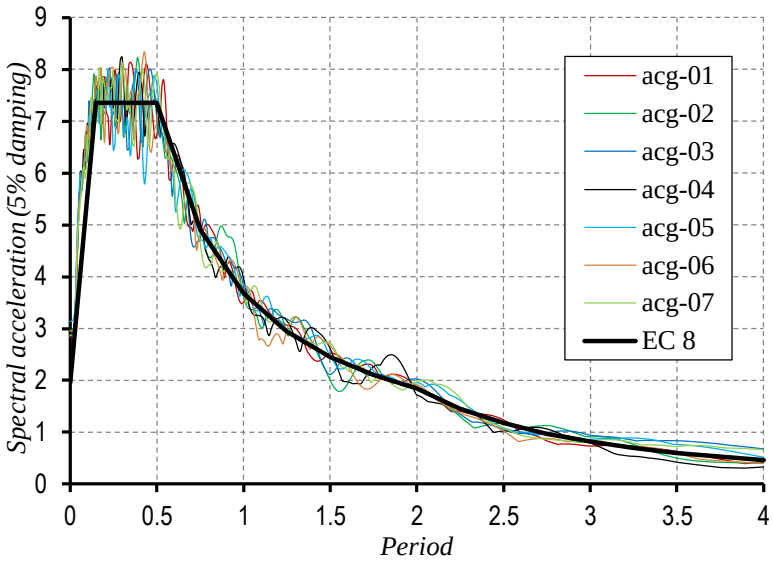

Figure 3.9; *Design and artificial spectra*

3.2.6. Direct integration and damping

In the numerical model mass and stiffness proportional damping has been applied. The damping matrix is given by:

$$\mathbf{C} = \eta\mathbf{M} + \delta\mathbf{K} \tag{3.33}$$

This type of damping is normally referred to as Rayleigh damping. In mode superposition analysis, the damping matrix must have the following properties in order for the modal equations to be uncoupled:

$$\begin{aligned} 2\omega_n\xi_n &= \mathbf{v}_n^T\mathbf{C}\mathbf{v}_n = \eta\mathbf{v}_n^T\mathbf{M}\mathbf{v}_n + \delta\mathbf{v}_n^T\mathbf{K}\mathbf{v}_n \\ 0 &= \mathbf{v}_n^T\mathbf{C}\mathbf{v}_m \quad n \neq m \end{aligned} \tag{3.34}$$

where ω_n and ξ_n are the natural frequency and the damping ratio of the mode *n* and *v* denotes the modal vector. Because of the orthogonality properties of the mass and stiffness matrices this can be rewritten as:

$$2\omega_n\xi_n = \eta + \delta\omega_n^2 \quad \text{or} \quad \xi_n = \frac{1}{2\omega_n}\eta + \frac{\omega_n}{2}\delta \tag{3.35}$$

Apparently, the modal damping can be specified for two modes exactly. In the numerical analysis the first and second modes were selected.

$$\begin{bmatrix} \xi_1 \\ \xi_2 \end{bmatrix} = \frac{1}{2}\begin{bmatrix} \frac{1}{\omega_1} & \omega_1 \\ \frac{1}{\omega_2} & \omega_2 \end{bmatrix}\begin{bmatrix} \eta \\ \delta \end{bmatrix} \tag{3.35}$$

As the primary lateral resisting members in a CBF are mostly connected by welding to gusset plates the two damping ratios were set to be equally 4%. Solving for the two parameters of damping we get:

$$\begin{aligned} &\xi_1 = \xi_2 = \xi \\ &\delta = \frac{2\xi}{\omega_1 + \omega_2} \\ &\eta = \omega_1 \omega_2 \delta \end{aligned} \tag{3.36}$$

The dynamic equilibrium equation is solved for the seismic response of the structures using the Newmark direct integration method. This step-by-step method determines the displacements, velocities and accelerations at time *t* from the solution found at time *t-Δt*. For good convergence the time step has been 0.01 second in the analysis. The method has two parameters, α and β, that are used in the theory of the method to truncate the Taylor's series of the displacement and velocity:

$$\mathbf{u}_t = \mathbf{u}_{t-\Delta t} + \Delta t \dot{\mathbf{u}}_{t-\Delta t} + \frac{\Delta t^2}{2} \ddot{\mathbf{u}}_{t-\Delta t} + \ldots \approx \mathbf{u}_{t-\Delta t} + \Delta t \dot{\mathbf{u}}_{t-\Delta t} + \frac{\Delta t^2}{2} \ddot{\mathbf{u}}_{t-\Delta t} + \alpha \Delta t^3 \dddot{\mathbf{u}}_{t-\Delta t} \tag{3.36a}$$

$$\dot{\mathbf{u}}_t = \dot{\mathbf{u}}_{t-\Delta t} + \Delta t \ddot{\mathbf{u}}_{t-\Delta t} + \frac{\Delta t^2}{2} \dddot{\mathbf{u}}_{t-\Delta t} + \ldots \approx \dot{\mathbf{u}}_{t-\Delta t} + \Delta t \ddot{\mathbf{u}}_{t-\Delta t} + \beta \Delta t^2 \dddot{\mathbf{u}}_{t-\Delta t} \tag{3.36b}$$

If the acceleration is assumed to be linear within the time step, the following equation can be written:

$$\dddot{\mathbf{u}} = \frac{\left(\ddot{\mathbf{u}}_t - \ddot{\mathbf{u}}_{t-\Delta t}\right)}{\Delta t} \tag{3.37}$$

Substituting this into Eq. (3.36a) and (3.36b) produces Newmark's equations in standard form:

$$\mathbf{u}_t = \mathbf{u}_{t-\Delta t} + \Delta t \dot{\mathbf{u}}_{t-\Delta t} + \left(\frac{1}{2} - \alpha\right) \Delta t^2 \ddot{\mathbf{u}}_{t-\Delta t} + \alpha \Delta t^2 \ddot{\mathbf{u}}_t \tag{3.38a}$$

$$\dot{\mathbf{u}}_t = \dot{\mathbf{u}}_{t-\Delta t} + \left(1 - \beta\right) \Delta t \ddot{\mathbf{u}}_{t-\Delta t} + \beta \Delta t \ddot{\mathbf{u}}_t \tag{3.38b}$$

The equations above can be solved by iteration for each time step or by Wilson's direct solution [69]. For the sake of stability[69], the two parameters of the method were chosen to be α=0.25 and β=0.5.

3.3. Evaluation of the designs, generalization of the response

3.3.1. Seismic response of CBF designs

The main objective of the numerical testing program is to see whether the designs are prone to weak storey behaviour or not and if so, can early member failure be anticipated. In order to observe these phenomena, IDA diagrams depicting the evolution of the maximum interstorey drift ratio of each floor with respect to the scale factor of the peak ground acceleration have been derived from the computation data. From the lateral displacement data series of the floor slabs the instantaneous interstorey drift ratios have been calculated and for each acceleration record and storey the maxima have been adopted. To assign one diagram to one building the mean of the seven result sets has been considered. In every diagram the floors are represented separately so that prominent differences between the storey responses can easily be visualized. In *Figures 3.10 – 3.15* the IDA curves of each building are presented. In the diagrams the anticipated range of the member failure (2-3%) and the design PGA (Scale factor = 1.0) are indicated.

Looking at the diagrams it can be observed, that the families of the curves are rather broad. The upper floors deviate from the rest at a small scale factor, approximately 0.25, where the occurrence of first yield is anticipated, as the behaviour factor is 4. After 0.25 on the scale factor axis, in the nonlinear response range, the largest and the smallest maximum IDR results show great differences.

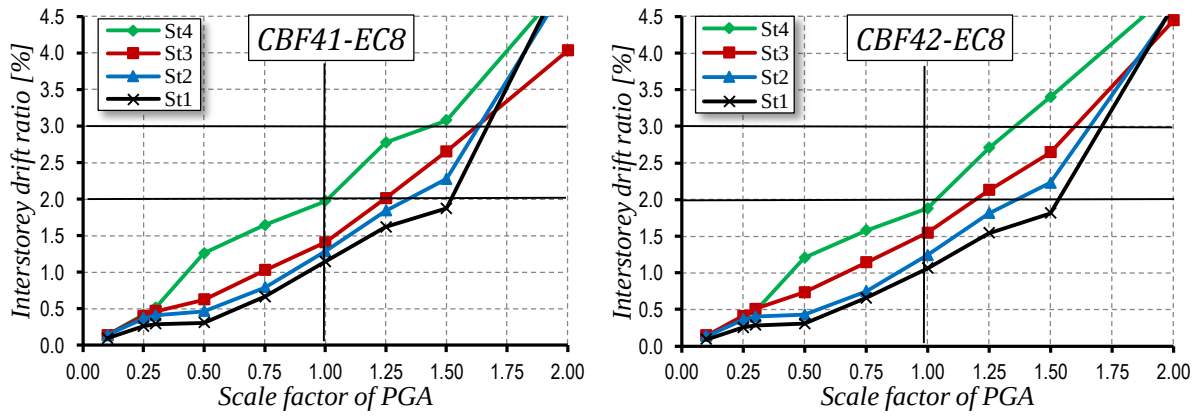

a) IDA diagram CBF41-EC8 *b) IDA diagram CBF42-EC8*

Figure 3.10; *IDA diagrams of 4-storey CBF-s (averages of 7 records)*

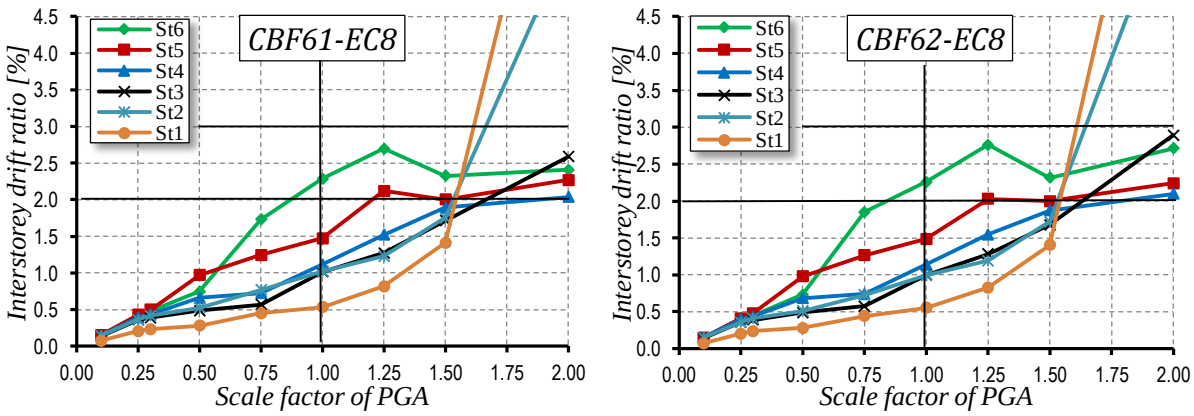

a) IDA diagram CBF61-EC8 *b) IDA diagram CBF62-EC8*

Figure 3.11; *IDA diagrams of 6-storey CBF-s (averages of 7 records)*

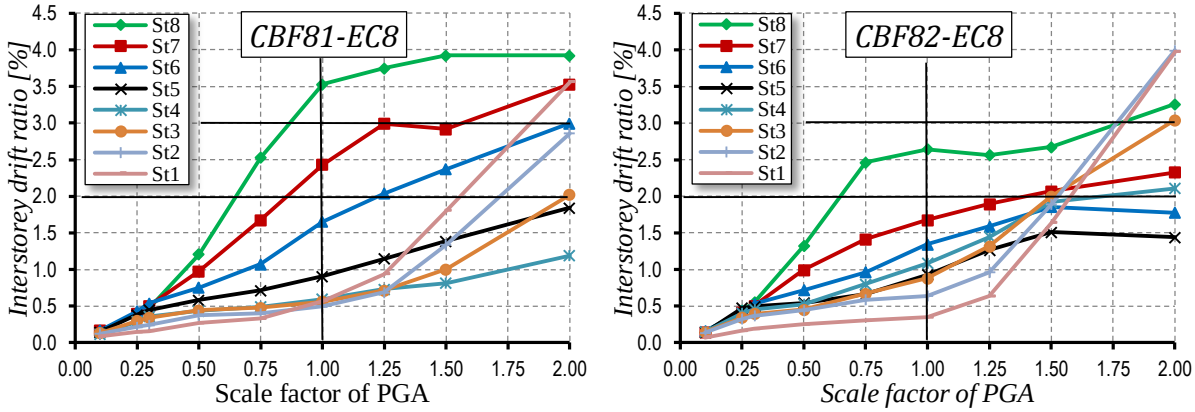

a) IDA diagram CBF81-EC8 *b) IDA diagram CBF82-EC8*

Figure 3.12; *IDA diagrams of 8-storey CBF-s (averages of 7 records)*

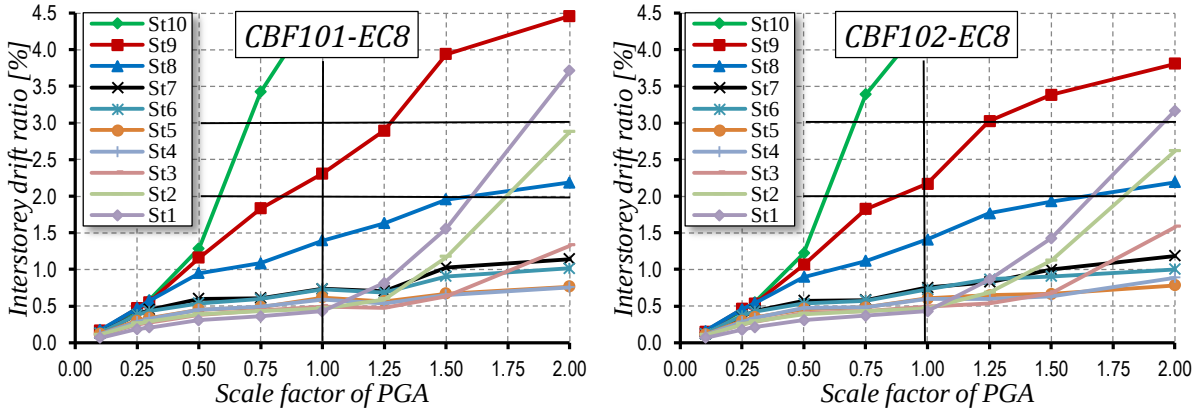

a) IDA diagram CBF101-EC8 *b) IDA diagram CBF102-EC8*

Figure 3.13; *IDA diagrams of 10-storey CBF-s (averages of 7 records)*

The differences are large even at a scale factor below the design level and especially in the higher buildings the discrepancy escalates. It can be observed that the maximum interstorey drift is tendentiously multiple times larger than the minimum. The buildings therefore do not exhibit a well distributed dissipation; there are storeys that undergo lot larger plastic excursions than others. It is also important to note that the rise of the outlier drifts on the upper floors decreases and at higher scale factors other floors may even catch up. In other words, high ductility demands are realized but asymptotic curve is not as the drifts are not growing exponentially beyond measure. Steep increase of the curves that corresponds to the development of a collapse mechanism is rather observed on the first and second floors in some cases at high scale factors. This structural response corresponds more to the development of a localized plastic collapse mechanism. In most diagrams the 2% drift ratio is exceeded at a scale factor smaller than one, that otherwise corresponds to the design action. So, the CBF-s also tend to exhibit early failure either because of the damage of the secondary members (damage limitation state) or because of the failure of the primary members of the lateral resistance in the 2-3% estimated range. Comparing the response of the different structural solutions (CBF or MRF-CBF) we can see that the elevated flexural resistance of all the continuous columns in building type 2 may lightly moderate the discrepancy in the interstorey drifts, but it is clear that significant changes are not achieved.

Regarding the buildings designed initially with behaviour factor q=5, in *Figure 3.14*, it can be seen that the designs are not necessarily, in every aspect worse than the originals with q=4, see *Figure 3.10/a* and *3.11/a*. The increase of the drifts is slightly steeper and

asymptotic curves are attained at smaller scale factors. However, the family of the curves of CBF61Q5-EC8 is slimmer than the one of the original, CBF61-EC8, and also the interstorey drift corresponding to failure is reached at a higher scale factor. It has to be noted though that the differences between the designs with behaviour factor 4 or 5 are minor in terms of cross-sectional sizes, see *Tables 3.3/a, 3.4/a* and 3.*7/a, 3.7/b*.

The results obtained for the cases where mass irregularities were considered are presented in *Table 8/a* and *b* and in *Figure 3.15*. In these cases the discrepancy between the upper floors, where the additional masses are located, and the lower floors is more flagrant then for the regular buildings, see *Figure 11/a* and *12/a*.

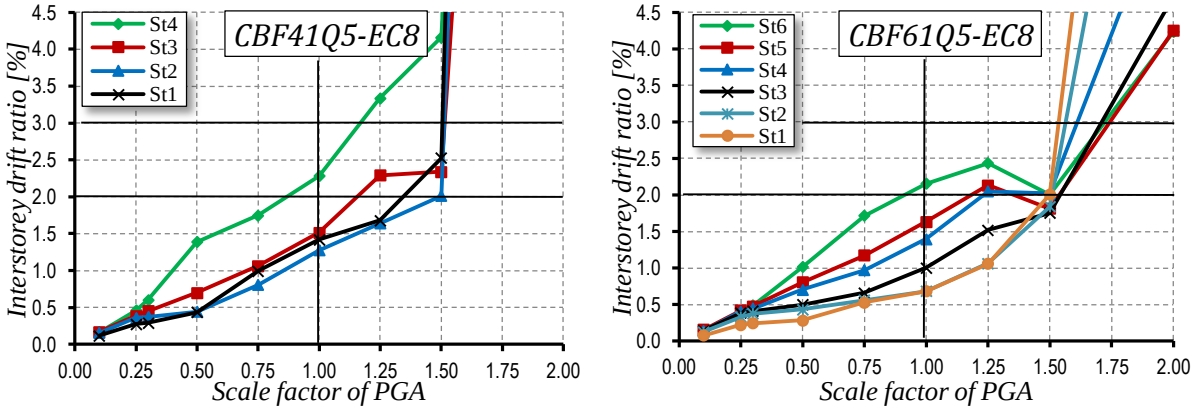

a) IDA diagram CBF41Q5-EC8 *b) IDA diagram CBF61Q5-EC8*

Figure 3.14*; IDA diagrams of CBF-s designed with q=5 (averages of 7 records)*

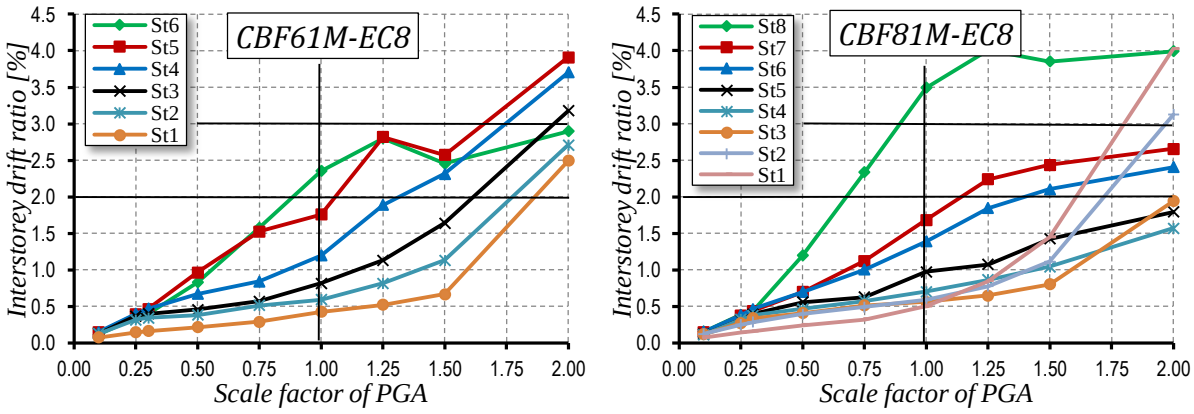

a) IDA diagram CBF61M-EC8 *b) IDA diagram CBF81M-EC8*

Figure 3.15*; IDA diagrams of CBF-s with mass irregularity (averages of 7 records)*

As the results indicate a unanimous adverse behaviour in every building we can conclude that the CBF-s designed according to Eurocode 8 are susceptible to develop weak storeys even when subjected to seismic actions that are significantly smaller than the design level. Moreover, in the great majority of the analysed CBF-s the 2% IDR is already exceeded at scale factor 1.0, and in some, the results are even larger than 3% therefore the designs are not only susceptible to exhibit weak storey behaviour, but also to an early collapse.

3.3.2. Possible response alternatives

In the diagrams of *Figure 3.16* and *Figure 3.17* idealized IDA curves are presented. Each diagram corresponds to an imaginary four-storey CBF therefore four curves are depicted denoting the floors separately. In these hypothetical examples the 2% interstorey drift is considered to be a sharp collapse criterion. In the case of the global mechanism the interstorey drifts are equal on every storey and the IDA curves of the different floors have to be the same. Hence *Figure 3.16/a* depicts the ideal behaviour of a CBF assuming the development of the global plastic yield mechanism in all circumstances. Though this behaviour is expected, or at least targeted in design, in reality it can barely be realized. In the cluttered dynamic response of a building to an earthquake excitation plasticity does not occur in the same time on all the storeys. Consequently, there is no uniform plasticity and there is no uniform interstorey drift either. The real curves obtained by IDA calculations are more alike the ones presented in *Figure 3.16/b*. Here one may find inevitable differences between the responses of the floors. Due to these differences, the collapse of a CBF can be realized in various ways. This is depicted in *Figure 3.17*.

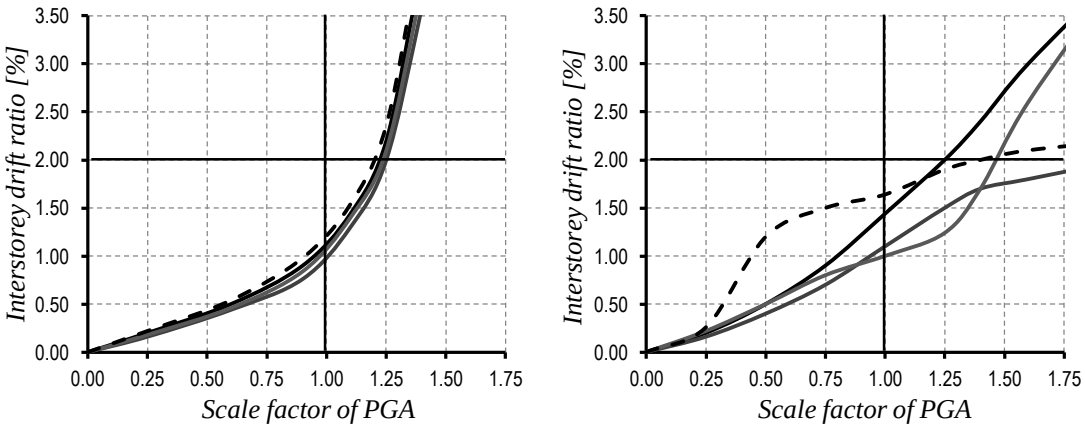

a) global mechanism *b) realistic response*

Figure 3.16*; Global mechanism and realistic IDA curves of CBF-s*

In the diagram of *Figure 3.17/a* the dashed curve deviates from the cluster of the other three. Though there is a significant rise of the drift at a low scale factor, early collapse is not realized. Either because that particular floor is just more flexible than the others but has adequate resistance, or because the appearing yield at higher intensities on the other three floors decreases the requisitions of the one under consideration. The collapse limit is attained at a scale factor higher than the design level, therefore the building is considered adequate. Conversely, the behaviour of the building is not optimal as below the design level the lateral displacements are concentrated on one floor. The significant drifts may cause damages in the non-structural members, while the other floors are not efficient. Although this building exhibits the soft storey phenomenon, there is no weak storey collapse whatsoever. Collapse is reached when the first line intersects the failure limit before the curves of the other floors. Though failure is attained on one floor only, this is not a weak storey failure since the collapse is not related to the preceding weak storey phenomenon. CBF41 is one example of a moderately developing weak storey that does not cause early failure. Furthermore, if we impose a bit less stringent demands for the lateral drifts and we assume a judicious choice of structural members that provides larger ductility capacities, we may say that the roughly 2.3 – 2.6% attained maximum interstorey drift ratio in CBF61, 62 and 82 shall not be considered

failure. Thus, in these buildings the evidently realized weak storey phenomenon does not cause early collapse either.

The diagram in *Figure 3.17/b* depicts a soft storey phenomenon-induced early collapse. In this case the concentration of the large lateral displacements lead to the failure of one or several members, therefore the building collapses at a scale factor smaller than the design level. Moreover, the large relative drifts may cause severe early damages to the non-structural members, which also indicates the inadequacy of the response. Although the building may have been designed to have adequate lateral resistance, so that the failure is reached beyond the design level, still the disproportional plastic deformations lead to an early collapse. CBF81, 101 and 102 exhibit such inadequate response.

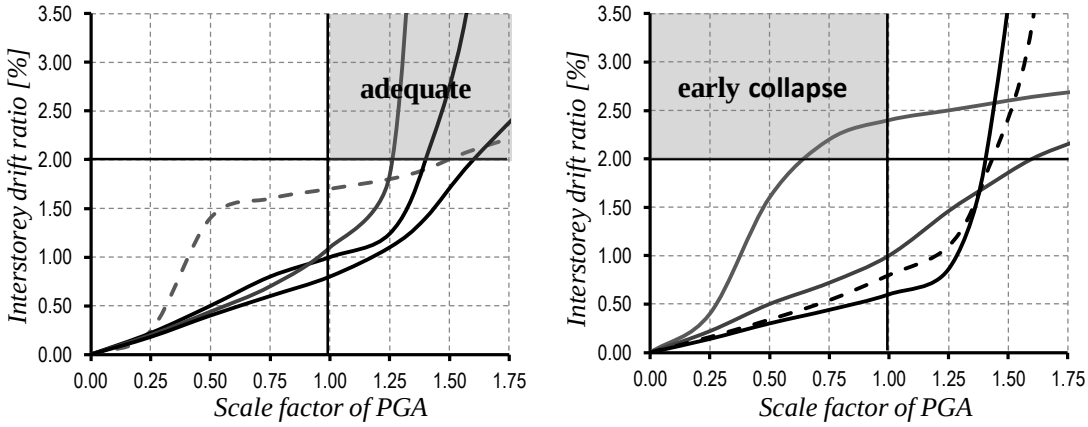

a) weak storey without early failure *b) storey with early failure*

Figure 3.17*; Characteristic IDA curves of CBF-s*

It is clear that the soft storey phenomenon has to be avoided as it facilitates collapse or just entails an adverse plastic behaviour. In order to obtain the optimal global plastic or more precisely, a distributed dissipative behaviour, the differences between the storey drifts have to be reduced as much as possible. This practically means that the upper and lower envelopes of the IDA curves are to be close to each other. However, even a building with a weak storey likelihood can be adequate as it can be seen in *Figure 3.17/a*. Therefore, the development of a weak storey and the actual collapse can be uncoupled as one does not necessarily mean the other. The weak storey phenomenon does facilitate and therefore may result in collapse due to extensive localized plastic deformations, but it may also result only uneven dissipation.

In the various IDA diagrams in 3.3.1 one can observe weak storey behaviour at scale factors below and over the design strength also, but the magnitude of the unwanted behaviour is not necessarily proportional to the growing effect. In CBF61, 62 and 82 for example the deviation of the weak storeys decreases at larger seismic load levels. The fact that the weak storey behaviour may occur at low seismic excitation but may also get strongly mitigated as the loading increases shows that the likelihood of the weak storey behaviour is not related solely to the magnitude of the loading. So, the weak storey phenomenon is not simply due to inadequacy to the imposed loading as one may think, but the weakness of one floor, in terms of lateral drift, in comparison with the other floors. The soft storey behaviour is an inherent susceptibility of the structure coming from the structural arrangement, the cross-sectional properties and connections. If so, the possibility of the occurrence of a weak storey might be controlled taking into consideration only the characteristics of the structure, without the exact definition of the magnitude of the seismic action it has to withstand [70].

The assumption that the occurrence of a weak storey depends more on the structural proportions than on the provided resistance can be proved indirectly. Considering CBF41 and 61 it can be seen that there are moderately developed weak storeys on the top floors in both cases. Let us make an attempt to enhance the behaviour of the two buildings by providing additional resistance on these floors. Replacing the braces obtained by the Eurocode 8 design on the top floors by SHS 100×6 diagonals we get the IDA curves presented in *Figure 3.18*. Firstly, we can see that the top floors became overreinforced. This is not surprising as the selection of the new cross sections is not based on a refined design analysis. Comparing to the originals in *Figure 10/a* and *11/a*, it can also be noticed that the storeys below (3rd and 5th) exhibit a worse behaviour after reinforcement. In CBF61 the presence of the weak storey behaviour can clearly be seen on the 5th floor. The additional resistance does not enhance the performance of the buildings just modifies the storey of the localization. The reinforcing of the storeys that were found to be inadequate does not necessarily yield satisfactory designs and the disappearance of the weak storey phenomenon. Therefore, it is clear that strengthening the structure on the basis of the experienced effects may not provide better designs and that the likelihood of the weak storey behaviour is indeed not simply a storey resistance issue.

The observations so far show that the weak storey phenomenon is present in CBF-s and that it can not be prevented by simple reinforcing. In order to understand the underlying reasons of the behaviour and to determine what effects need to be introduced to an effective design procedure, the

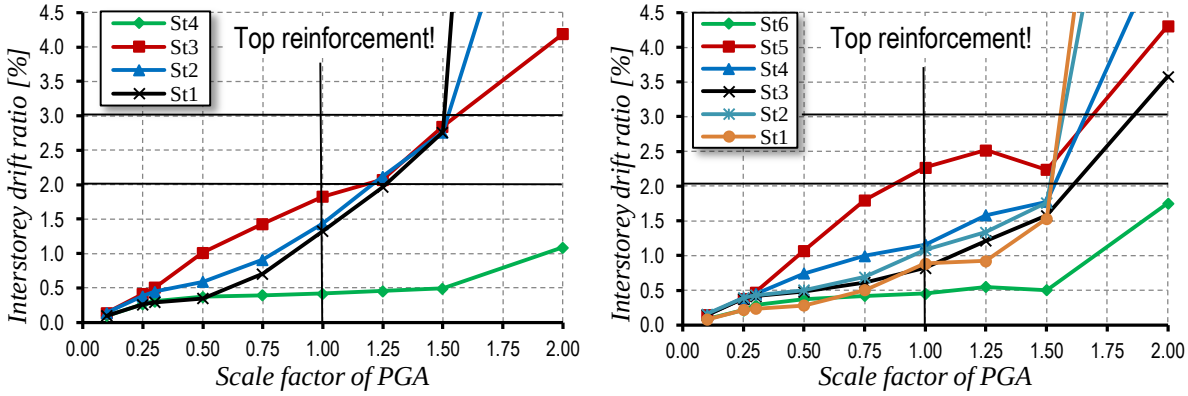

a) CBF-41 *b) CBF-61*

Figure 3.18*; IDA diagrams of reinforced CBF-s (averages of 7 records)*

Chapter 4

Examination of the weak storey behaviour and its reflection on the Eurocode 8 design procedure

The objective of the chapter is to identify the reasons why the Eurocode 8 CBF designs were found to have a bad performance in the previous chapter. Firstly, particular response time series are further analysed. A general response scheme is defined, characterized and proven by examined regularities. By the generalized response the gradual development mode of the weak storey behaviour is described. This understanding of the weak storey development provides a basis of critical assessment of the Eurocode 8 design criteria in the end.

4.1. Further insight into the development of the weak storey behaviour

4.1.1. Deformations and displacements during seismic action

The analyses of the buildings presented before yielded such adverse results and experiences that necessitate the understanding and the qualitative description of the seismic response of CBF-s exhibiting weak storey behaviour. With the thorough examination of the displacement data series of the whole building and the deformations of members, certain regularities can be discovered in the behaviour regardless of storey number or the actual applied acceleration record. These regularities are amplified and therefore rather conclusive in cases where the weak storey behaviour is clearly realized. Such a case is given by accelerogram 2 at 0.75 scale factor in the 4-storey CBF41, see *Figure 4.1*. In the following, important observations will be presented on this example.

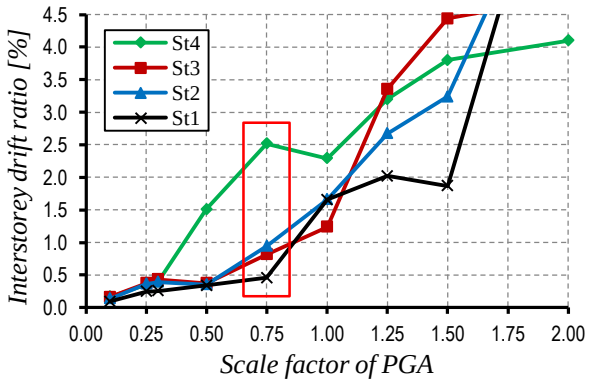

Figure 4.1; *IDA diagram of CBF41, accelerogram 2*

Taking a look at the deformed shape of the model in *Figure 4.2* after a seismic action we can see that all the braces have a triangular buckled shape. At the mid section of the bracing bars plastic hinges form. In repeated cycles the cumulating plastic deformations gradually facilitate the buckling by rotation of the plastic hinge. Eventually this leads to the angular buckled shape. In the meantime plastic elongations increase the length of the bars; consequently the diagonals have to be already in compression after the seismic excitation when the building is laterally unloaded. Plastic elongations therefore further amplify the triangularity of the braces.

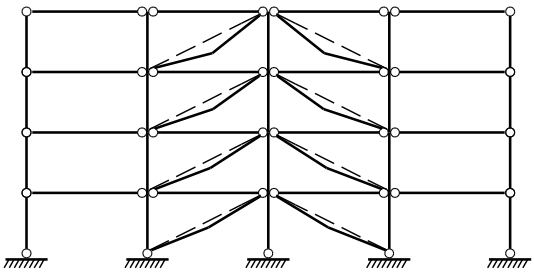

Figure 4.2; *Deformed shape of CBF after seismic effect*

Also we can notice in the figure that the magnitude of the triangular imperfection introduced to the system by the plastic strains may vary on the different floors. The larger triangular-like imperfection implies larger relative lateral drifts on the particular storey which also indicates the occurrence of a weak storey. The weak storey behaviour is therefore interrelated with large interstorey drifts, cumulating plastic elongations and the consequential triangular brace deformation.

The lateral displacements of the floor slabs during the selected 20-second excitation are depicted in *Figure 4.3*. It can be seen that the top floor exhibits disproportionally large displacements compared to the other three storeys. The development of the attained maximum interstorey drift ratios on the different floors, presented in *Figure 4.4*, is even more convincing that on the top a weak storey developed. While the motion of the first three floors is seemingly synchronized and proportional during the 20-second record, the top floor shows differences. The curve of this floor does not exactly follow the same reversals as the other three, the maxima are disproportionally large and also slightly protracted. There is a clear discrepancy between the motions of the weak storey and the other floors.

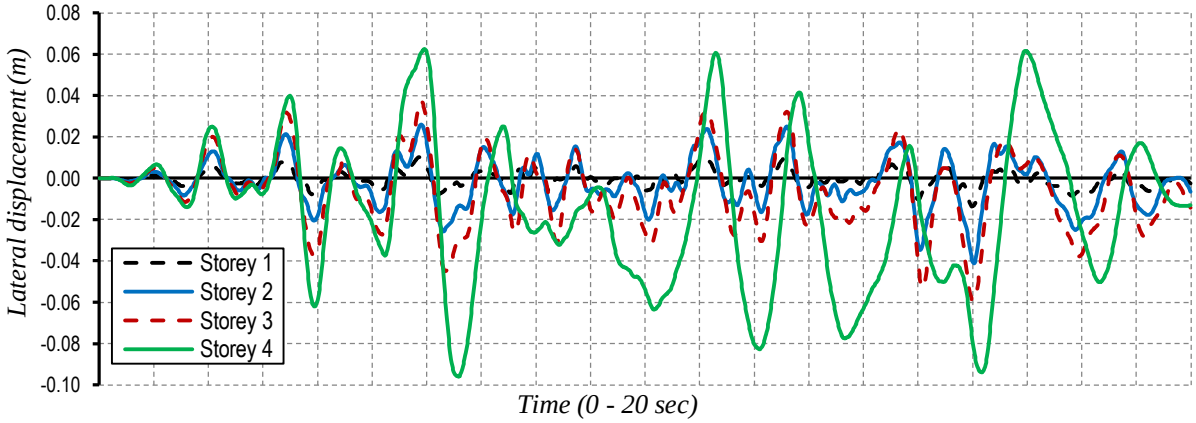

Figure 4.3*; Lateral displacements of slabs in CBF-41, scale factor 0.75 (accelerogram 2)*

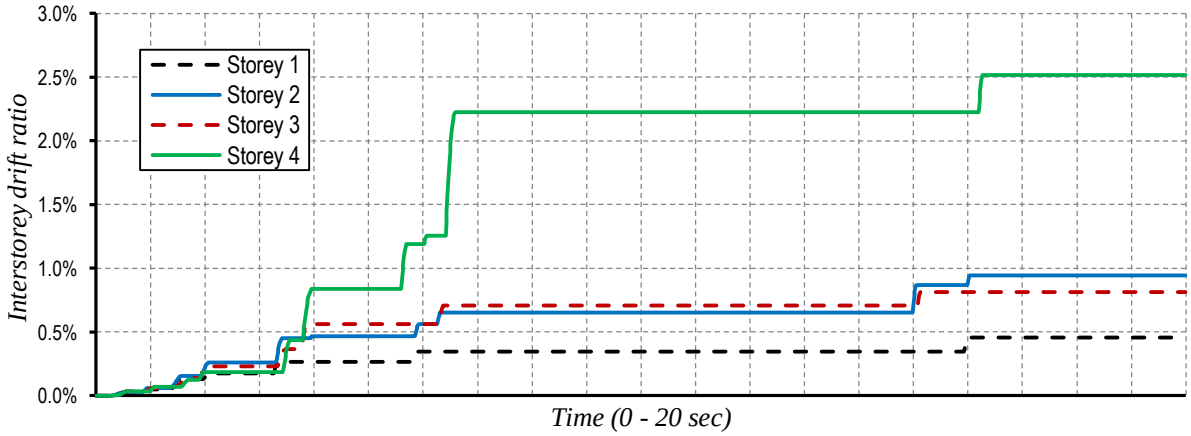

Figure 4.4*; Maximum interstorey drift ratios in CBF-41, scale factor 0.75 (accelerogram 2)*

As it can be seen, the occurrence of a weak storey results qualitative differences in the motion of the weak storey and the rest. Furthermore the prominent triangular deterioration of the braces is also found to be juxtaposed with the weak storey development. In the following an interrelation of this brace imperfection and the discrepancy of the motion are set in evidence.

4.1.2. Alteration of the dynamic response due to brace deterioration

As the braces are the main horizontal load bearing elements, mainly their axial stiffness determines the lateral stiffness of a storey. So, the developing triangular imperfection of these bars has to cause a significant alteration of the dynamic behaviour of the structure. To verify this assumption a series of natural frequency analyses have been conducted on the elastic model of the four-storey braced frame. The perfect model with two straight bracing bars has been altered. At the midpoints of the diagonals perpendicular offsetting by 10 centimetres at each step up to 50 centimetres has been introduced. This has resulted triangular shape braces.

The 50 cm out-of-plane deformation of the mid section can be expressed in terms of realised displacement ductility of the braces using Tremblay's formula [32]:

$$v = 0.7\sqrt{\delta_c \cdot L_H} \text{ with } \delta_c = \left(\mu_c + \mu_t - 1\right)\delta_y \tag{4.1}$$

where v is the displacement perpendicular to the axis of the bar, L_H is the buckling length, μ_c and μ_t are the realized tensile and compressive displacement ductility and δ_y is the elongation corresponding to yield. Supposing that the tensile and compressive realized ductility are the same, the 50 cm out-of-plane deformation is reached when both are equal to 5.5. By the use of Eq. (1.63) one may find that 1.54% IDR corresponds to this ductility, so the assumed imperfection is practically realizable without the risk of failure.

The triangular alteration of the diagonals has been done at every floor separately to analyse the effect of developed weak storeys. Also the same imperfections have been applied on every floor simultaneously which corresponds to the development of the global yield mechanism. Furthermore, the natural frequencies of the perfect model with one diagonal on every floor have been computed, neglecting the buckled bar in compression, accordingly to Eurocode 8 provisions. In *Table 4.1* the frequencies of the modes of vibration for the more relevant first and second modes are listed. The rows of the table correspond to the different levels of the introduced imperfection while the columns differ in the storey of the imperfection. For the sake of comparison, the modal frequencies of the perfect model with one brace are 0.84 Hz and 2.26 Hz respectively. One can see in the results of the table that with the concurrent increase of the imperfection of all the braces the decrease of the frequencies in the two modes is roughly proportional. However this is not the case when the triangular modification is done to the braces of one floor only. For example the growing imperfection on the first floor halves the frequency of the first mode but barely changes the second. Consequently it is not only the frequency of the modes that changes.

Table 4.1; *Natural frequencies of imperfect 4-storey CBF-s*

imperfection magnitude [cm]	**Natural frequency of mode 1 [Hz]**					**Natural frequency of mode 2 [Hz]**				
	storey of imperfection					*storey of imperfection*				
	1	*2*	*3*	*4*	*all*	*1*	*2*	*3*	*4*	*all*
10	0.95	0.99	1.03	1.09	0.69	2.75	3.12	2.95	2.36	1.90
20	0.67	0.87	0.78	0.82	0.41	2.52	3.07	2.71	1.90	1.13
30	0.54	0.76	0.65	0.64	0.29	2.46	3.03	2.62	1.79	0.82
40	0.47	0.59	0.58	0.53	0.22	2.43	2.99	2.58	1.75	0.65
50	0.43	0.57	0.54	0.46	0.18	2.42	2.98	2.56	1.73	0.56

The introduced imperfection of the braces modifies the stiffness matrix of the structure. It decreases the stiffness values corresponding to the end nodes of the altered braces only. Therefore the new stiffness matrix of the structure is not proportional to the original, while the mass matrix remains the same. So, the mode shapes have to change also. In *Figure 4.5* the modal frequencies and shapes and the modal mass participation (MMP) are indicated. These results are presented for the perfect four-storey building and two imperfect ones. *Figure 4.5/b* corresponds to a concurrent 40 cm imperfection on every floor while *Figure 4.5/c* depicts the case where the same imperfection is introduced only on the 4th storey. The mode shapes of *Figures 4.5/a* and *4.5/b* are seemingly similar. The modal analysis of the perfect model well describes the response of a CBF where every floor participates in the dissipation. In *Figure 4.5/c* the mode shapes of the building with a developed weak storey show that the first mode is approximately the movement of the floor above the weak one. Conversely, the second mode primarily consists of the vibration of the stories below the weak storey; the slab above is closely still. Visibly, the existence of a floor with a low lateral stiffness decouples the relevant modes of the building to modes that describe the motion of the floors above or below the weak storey and these modes substantially differ from the originals of the perfect model.

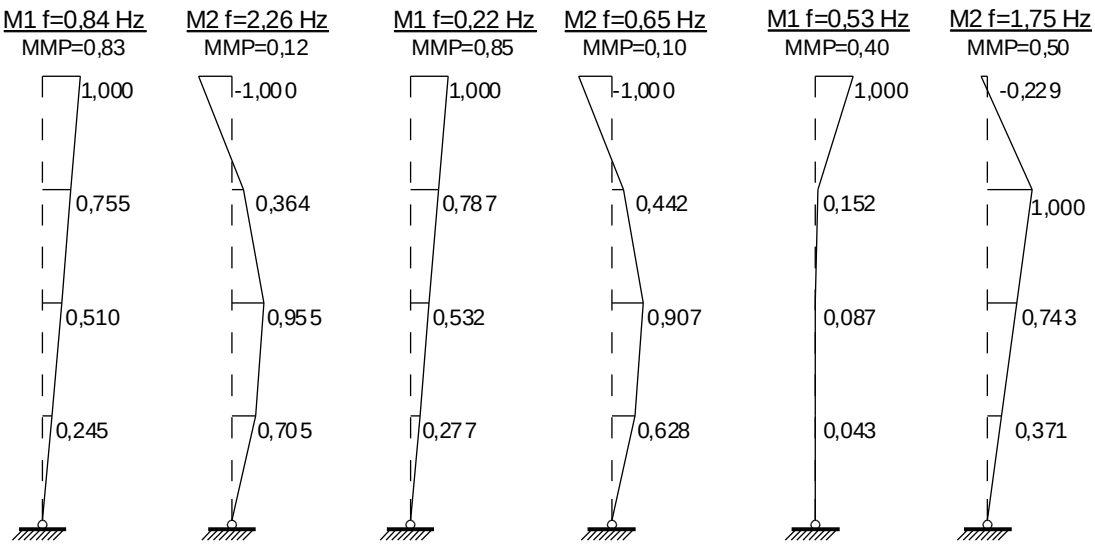

a) perfect model *b) concurrent 40 cm imperfection* *c) 40 cm imperfection on 4th floor*

Figure 4.5*; Mode shapes of perfect and imperfect 4-storey models*

The introduced modelling of the brace deterioration by triangle-shaped diagonals is a rough analogy that has to be verified. One possibility is to analyse the involvement of the modes in the description of the displacements. In order to recreate the actual displacement time series presented in *Figure 4.3* by the mode shapes, Schmidt decomposition can be used. The time dependent displacement vector, $\underline{d}(t)$, can be recreated by the elementary contributions of the orthogonal modal vectors, v_i, multiplied by time dependent coefficients.

$$\underline{d}(t) = \alpha_1(t) \cdot \underline{v}_1 + \alpha_2(t) \cdot \underline{v}_2 + \ldots \tag{4.2}$$

In the equation above the coefficients are computed in every time instant as:

$$\alpha_i(t) = \frac{\underline{d}(t) \cdot \underline{v}_i}{\underline{v}_i \cdot \underline{v}_i} \tag{4.3}$$

Our objective is to see how accurately the displacements of a certain storey can be recreated by the use of the perfect or the imperfect fundamental mode. By this, we aim to

examine which model can describe the actual motion of the building better, the original perfect or the analogous imperfect one. Therefore Eqs. (4.2) and (4.3) are evaluated for only one modal vector in the following cases. In the case of the perfect model the considered mode is the first in *Figure 4.5/a*. In the imperfect case, because of the decoupling mentioned before, the first mode of *Figure 4.5/c* has to be used to recreate the top floors motion and the second mode of the same figure is needed to recreate the motion of the third floor. The displacements of the 1st and 2nd floors are featureless small therefore hereby they are neglected. The real displacements of the 4th and 3rd floors and their recreation with the involvement of the designated modes are depicted in *Figure 4.6*. It can be observed in both diagrams that after the first 4 seconds, i.e. the occurrence of plastic deformation, the curve recreated with the perfect mode gradually deviates from the real displacements. Not all the reversals are accounted for and values become notably different also. Conversely, with the imperfect mode shapes the displacements of both storeys are accurately or at least better represented. These results indicate that the imperfect modes better describe the motions of the deteriorating structure. Therefore, the previously introduced changes of the modal behaviour of a CBF are seemingly realized in the response during a seismic action and this may be effectively analysed by the triangular brace analogy.

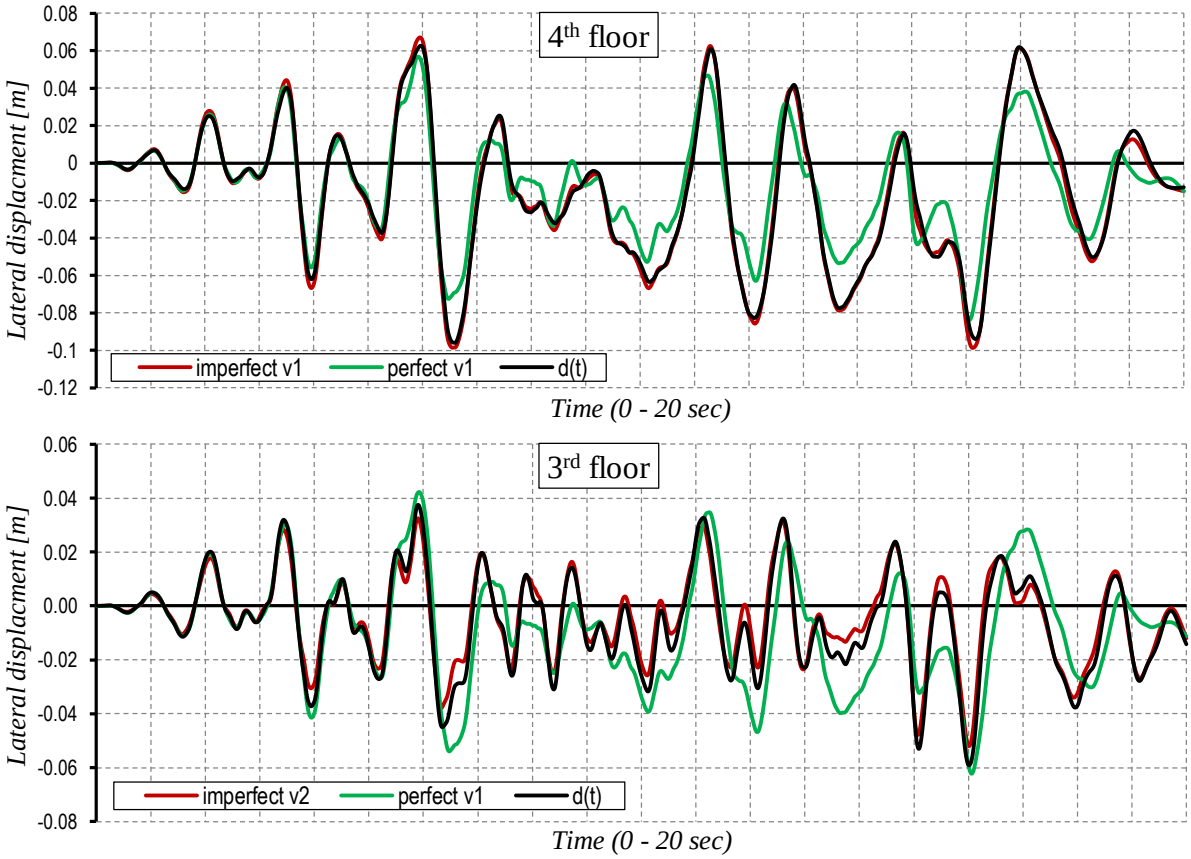

Figure 4.6; *Displacements of slabs recreated by Schmidt decomposition*

The analysis of the imperfect models yielded important experiences in the previous paragraphs. However, it is important to emphasize, that the modal responses are computed using the stiffness of the initial perfect or imperfect configuration with a linear analysis. As the force displacement curve of a deformed brace is strongly nonlinear, see *Figure 2.2*, with the straightening of the bar we can expect the significant increase of the instantaneous stiffness, step after step, even in case of small displacements. This change can substantially

affect the modal response as it has been described before. Consequently, the modal response analysis results presented so far shall not be considered quantitatively accurate. Instead, these results provide a basis for the characterization of a CBF with a developed weak storey.

4.1.3. Wavelet transformation of the seismic response

So far we have identified evidence in the displacement response of a selected CBF to the severe change of the dynamic characteristics caused by the deterioration of the braces. From the same displacement results further information can be extracted to better confirm the changing nature of the seismic response of CBFs. In the following the horizontal displacement results of multiple buildings are analysed with an appropriate signal processing tool.

The main objective of the wavelet transformation [71][72] is to decompose a random signal into elementary contributions. The wavelet transform measures the similarity of the analysed signal function and a series of wavelets with different translation in time and resolution in the frequency domain. The wavelet transform, *W(a,b),* of the signal *x(t)* is given by:

$$W(a,b) = \frac{1}{\sqrt{a}} \int g^{*}\left(\frac{t-b}{a}\right) \cdot x(t)\, dt \tag{4.4}$$

where *g*(t)* is the mother wavelet function which generates the family of the wavelets. The mother wavelet is dilated by parameter *a* and translated by *b* which vary continuously so that a series of son wavelets are created. One possible choice as the mother wavelet is the Morlet function which is a modified version of the Gabor wavelet:

$$g(t) = \exp\left[\frac{-\beta^2 (t-b)^2}{a^2}\right] \cdot \cos\frac{\pi(t-b)}{a} \tag{4.5}$$

This complex expression defines a harmonic function that decays exponentially on both sides over a time interval around *t=b,* see *Figure 4.7*. The parameter β defines the length of the envelope wave. By evaluating Eq. (4.4) on a series of son wavelets in a fixed time and frequency domain we can map the instantaneous participation of the frequency components of the analysed signal. The diagram depicting the results is called a scalogram which is analogue with the spectrogram created by Fourier transformation but the time and frequency axes are both variables, therefore the results are represented by a colormap.

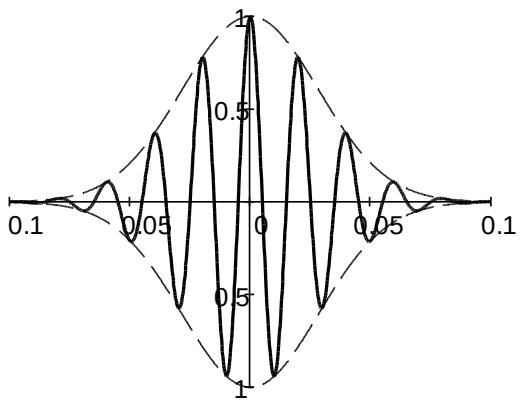

Figure 4.7*; Morlet mother wavelet (a=0.04, b=0, β=1)*

In our present investigation, we consider as input signal, *x(t)*, the lateral displacements of the 4th floor depicted in *Figure 4.3* at first. Also we can decompose the ground acceleration record to see whether it is really random, or it particularly excites certain frequencies and by it, affects the response. Considering the former case, the wavelet transform of the displacements of the top floor of the 4-storey CBF does not show sharp margins in *Figure 4.8*. The shape is more cloud-like. This is due to the fact that the seismic excitation and the displacement both miss any kind of harmonic regularity. Furthermore, the displacement diagram only has a few waves over the 20 second time series and this also leads to a bad resolution. Nonetheless, the local maxima are denoted by a white line on the scalogram and this line shows that after the incipient featureless noise the characteristic frequency decreases from about 0,77 Hz to 0,41-0,43Hz throughout the series. The initial frequency roughly complies with the natural frequency of the perfect structure where the buckled bars in compression are neglected (0.84 Hz) while the later is in agreement with the result in *Table 4.1* (0.46 Hz) corresponding to a model with developed imperfection (50 cm) on the 4th floor. In the meantime the wavelet transform of the accelerogram, see *Figure 4.9*, does not show any tendentious excitation of distinguished frequencies, so our results are not affected by particular excitation.

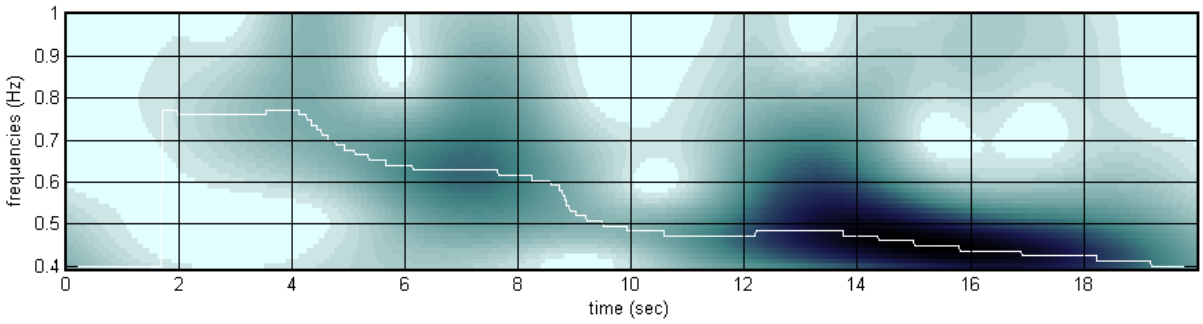

Figure 4.8*; Wavelet transform of the lateral displacements of the top floor*

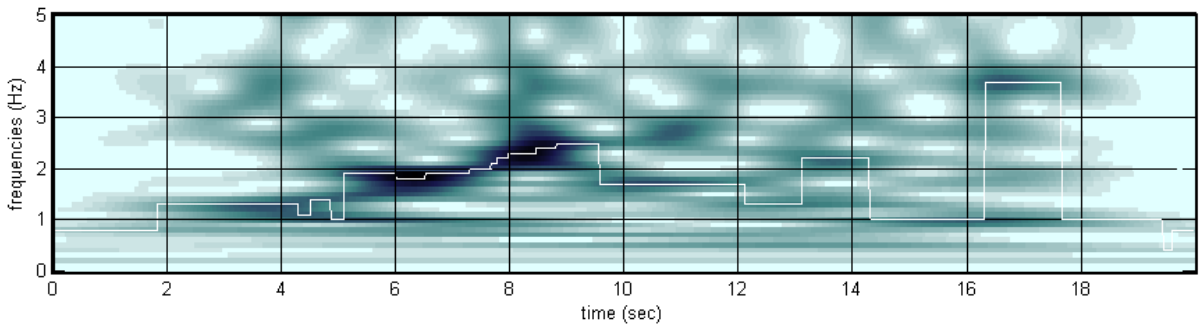

Figure 4.9*; Wavelet transform of ground acceleration record*

In order to derive further conclusions, it is necessary to show, that the response of several other buildings, that exhibit weak storey behaviour, can be described and approximated by the triangular imperfect models. In *Figure 4.10* the maximum interstorey drift and the wavelet transform results of the lateral displacements observed on the weak storeys are presented for two buildings in three more cases. The corresponding imperfect modal shapes of the buildings and the frequency results are depicted in *Figure 4.11*. In CBF-6 accelerogram 1 scaled by 0.75 causes the development of a weak storey on the top floor in the 4 – 16 second interval. Meanwhile the fundamental frequency of the 6th storey's motion decreases from 0.57 Hz to 0.4 Hz. The modal response analysis of the perfect model yields

0.61 Hz for the first mode and the introduction of the triangular imperfection on the top gives 0.4 Hz with a modal shape of large motion of the top.

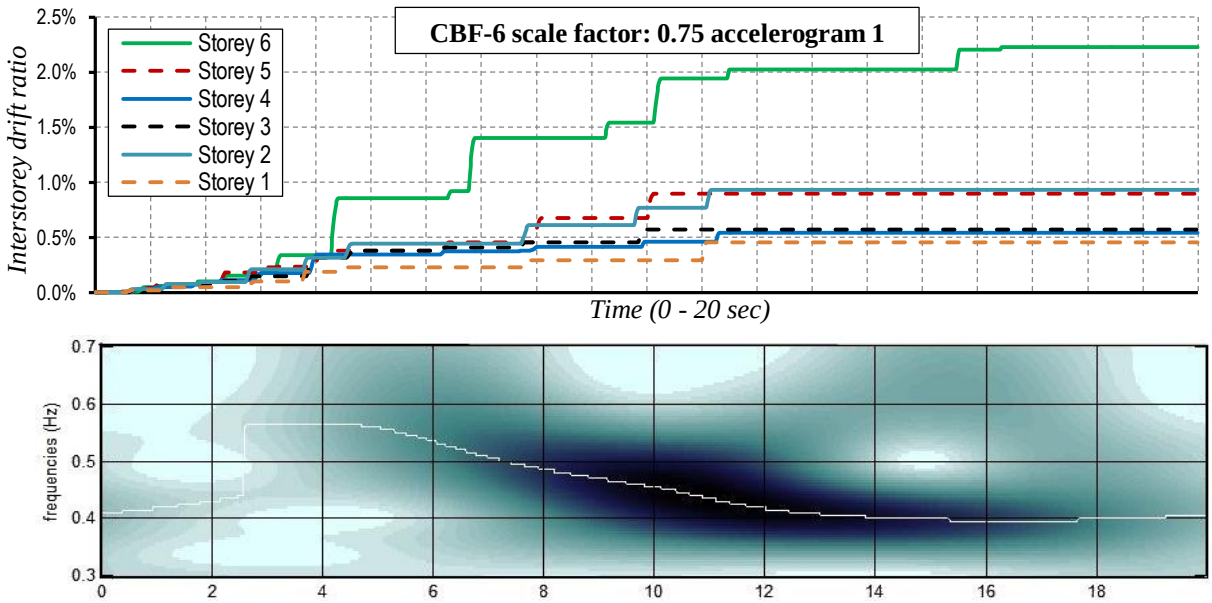

Figure 4.10/a; *Maximum interstorey drift ratios and wavelet transforms of top floor displacements*

In the same CBF accelerogram 6 causes the appearance of weak storeys on the top and moderately on the 5th floor also. The gradual development of significant drifts begins after the 12th second. The wavelet transform becomes dark around the white peak line only in the second half of the time period, showing that this is where the motion gets strongly governed by the component with the peak frequency. The white line monotonically decreases below 0.4 Hz. The modal analysis of an imperfect model with 50 cm triangular imperfection of the top and 25 cm on the 5th floor (corresponding to the maximum realised drifts) yields 0.35 Hz for the imperfect first mode.

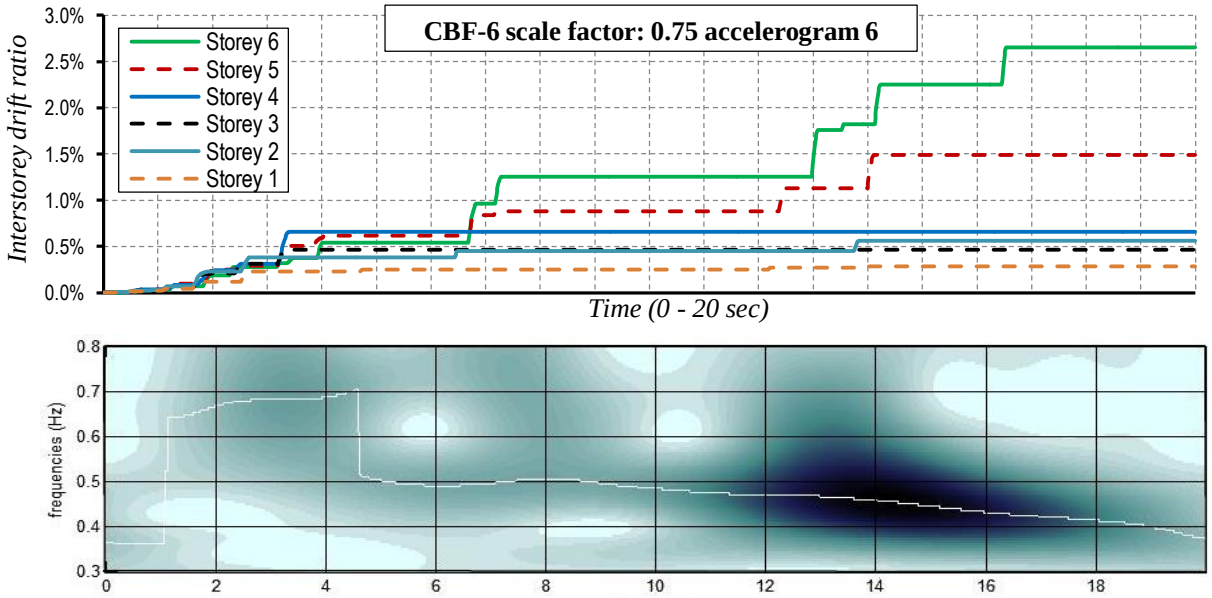

Figure 4.10/b; *Maximum interstorey drift ratios and wavelet transforms of top floor displacements*

In the third case, in CBF-8 accelerogram 1 with a scale of 0.75 results in weak storeys on the 7th and 8th storey also. Between 8 and 12 seconds the development of the weak storey on the 7th is prominent. By introducing the triangular imperfection to this floor in modal analysis the frequency of the fundamental mode decreases from 0.48 Hz to 0.38 Hz. This

change can be observed in the scalogram also. After the 12th second the maximum interstorey drift of the 8th floor catches up with the 7th gradually. In the meantime the scalogram around the peak line becomes lighter showing the decreasing importance of the component and at the end the peak drops down abruptly. This disturbance is again not surprising considering that the frequency of a model with the same imperfection on the top two floors is 0.28 Hz.

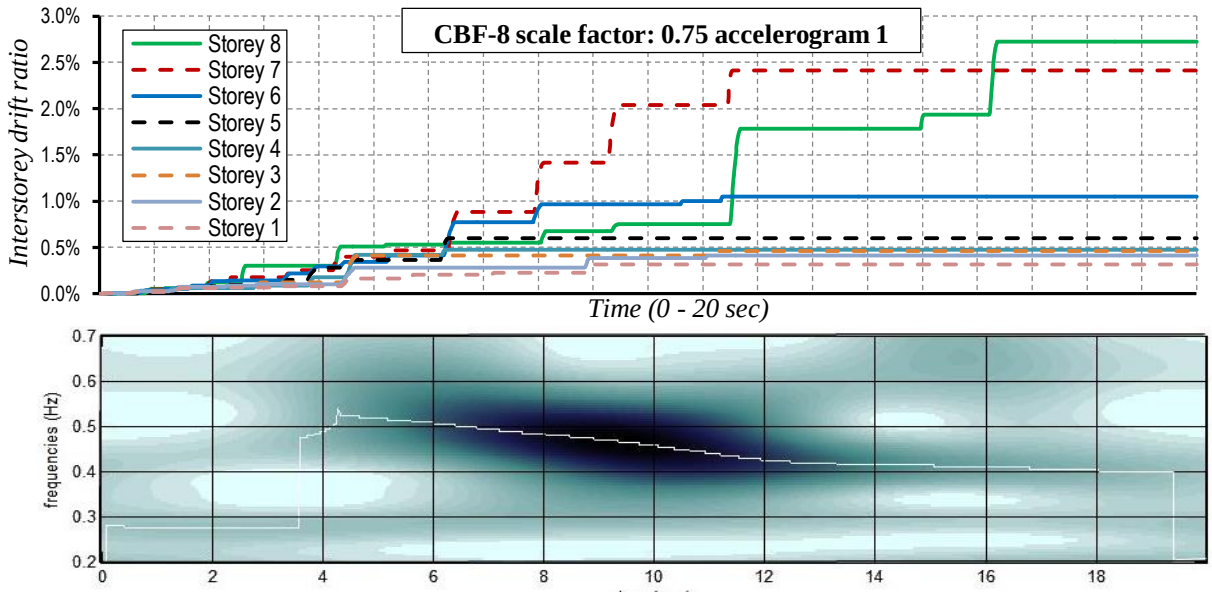

Figure 4.10/c; *Maximum interstorey drift ratios and wavelet transforms of top floor displacements*

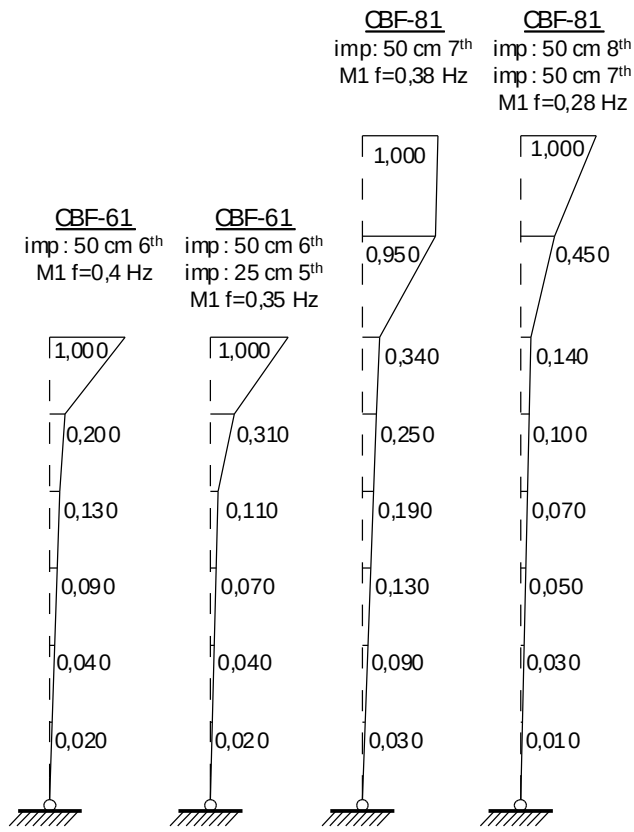

Figure 4.11; *Mode shapes of imperfect 6 and 8-storey models*

In all of the presented cases a good correlation has been found between the identification of the weak storeys, the gradually changing nonlinear response and the imperfect models, which are quasi snapshots during the response. This permits us to

conclude, that the presented process of the development and the properties of the weak storey behaviour are accounted for in the actual response of a CBF. Consequently, these properties, along with the fracture life of the dissipative members, presented in the second chapter, shall be taken into consideration in some way in a standardized design procedure.

4.1.4. Development of the weak storey behaviour

Upon the different features and properties of the weak storey behaviour, presented so far, the process of the development can be ascertained. *Figure 4.12* depicts an organigram of this process. The occurrence of plastic yield of the braces on one floor, results in the permanent triangular deformation of the diagonals. The initial localization of plasticity on one or very few floors can be caused by the overstrength relations of the floors [12], higher mode effects [51] or random effects of the seismic excitation [52], but in the cluttered response of a building it is more likely than the simultaneous plastic deformation anyway.

The triangular deformation, on one hand, devolves the lateral loads on the columns that become bent. On the other hand, as the flexural stiffness of the columns is significantly lower than the axial of the braces, the deformation also causes a crucial drop of the storey shear stiffness. The resulting irregularity of the horizontal stiffness along the building height modifies the global dynamic behaviour of the building and facilitates the localization of large relative drifts on the storey under consideration, which is just further amplified by the decoupling of the modal response. With the large drifts of the storey, plastic deformations cumulate in the hinges at the middle of the braces, the bars deteriorate, the resistance of the braces decrease and further plastic yield is facilitated.

This process is a recurring loop gradually increasing the damage of the weak storey. Hence the development of the weak storey mechanism can be regarded as auto amplifying phenomenon in case of cyclic seismic action. The loop is broken by the collapse of the weak storey. This can happen either by not having adequate columns on and connected to the weak storey or by the fatigue failure of the braces and gussets. The presented loop evidently leads to failure if a sufficiently large number of cycles are provided. Yet, as the number of cycles during a seismic action is limited, by preventing excess brace deformations and providing flexural column resistance and stiffness by choosing adequately large cross sections, the gradual development of the weak storey may be restrained.

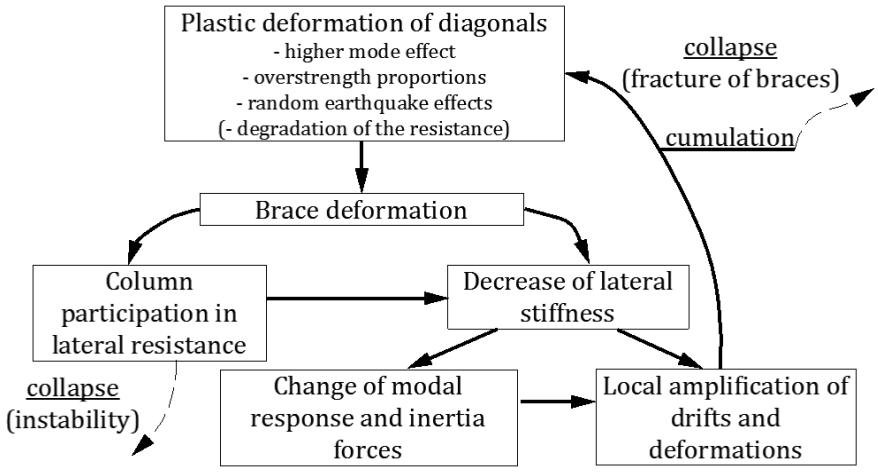

Figure 4.12*; Organigram of the weak storey behaviour of CBF-s*

4.2. Causes of the non-balanced dissipation and early failure in Eurocode 8 CBF designs

4.2.1. Gradual qualitative change of the seismic response

The uniformity condition imposed to the overstrength factors of every floor by Eq. (1.30) is an attempt in Eurocode to evade the occurrence of localized dissipation on a weak storey by promoting the simultaneous yielding of the braces on multiple, or if possible, on every floor in a global plastic mechanism. The maximum and the minimum of the storey overstrength, must not be different by more than 25%. With a design that respects this condition and which is also economic, not permitting unnecessarily large overstrength, we aim to make the axial resistances of all the diagonals just slightly larger than the effects. However, if the maximum axial effects change during the seismic action, the application of the uniformity condition becomes unclear.

As it has been described before the triangular deformation of the braces affects the equivalent modal loading and also devolves some of this loading on the continuous columns. The former effect modifies the axial forces of every diagonal in the overall building and the later decreases the axial effects in the braces of the weak storey. In such conditions the storey overstrengths have to change significantly, so that the uniformity condition gets violated. In *Tables 4.2/a* and *4.2/b* the change of the horizontal forces in the relevant first and second modes are presented. We can see that the change is rather rapid, even 20 cm triangularity can cause significant alteration. This out-of-plane deformation does not correspond to a fully developed weak storey, so the violation of the uniformity condition can be expected even at minor differences from the perfect structural arrangement.

Table 4.2/a; *Change of equivalent lateral forces [kN] of the first mode due to increasing triangular imperfection on the top floor*

storey	*Magnitude of imperfection on top floor [cm]*					
	perfect	*10*	*20*	*30*	*40*	*50*
4	490	498	442	336	274	263
3	361	348	176	78	44	32
2	228	221	106	45	23	16
1	103	101	48	20	11	8

Table 4.2/b; *Change of equivalent lateral forces [kN] of the second mode due to increasing triangular imperfection on the top floor*

storey	*Magnitude of imperfection on top floor [cm]*					
	perfect	*10*	*20*	*30*	*40*	*50*
4	-365	-367	-295	-199	-141	-108
3	184	254	456	556	594	610
2	376	335	382	428	446	452
1	256	203	196	211	217	219

In the hypothetical case of an equivalent triangular imperfection of the braces on every floor the distribution shape of the modal loads does not change with the gradual deterioration, only the magnitudes of the forces. This behaviour corresponds to the desired global dissipative behaviour. In this case the response of the perfect and the imperfect

building is similar. Therefore, with the analysis of the perfect structure, the uniform brace deterioration and the global dissipative behaviour are indirectly supposed. Proving by the uniformity condition that in this particular case the occurrence of the weak storey behaviour is not expected, does not exclude the various and probable cases where incipient random deformations cause the gradual development of a weak storey. In the Eurocode 8 design process the verifications are carried out referring to an elastic state of structure, which corresponds to low or reduced intensity seismic action. Conversely, in an inelastic state closer to failure, the requirements of the standard are not appropriate. Consequently, the uniformity condition is not adequate to drive the structure towards a distributed dissipation on every floor in all circumstances.

4.2.2. Underestimated bending of the columns

The seismic analysis of a perfect CBF model with any linear static procedure yields merely, or at least dominantly axial forces in the columns due to the truss action of the lateral resisting members. However, the triangular deterioration of the braces, as it has been described before, devolves the storey shear on the continuous columns that become bent. As ordinary analysis does not provide such internal forces, or at least not in the possibly realizable magnitude, the normal force resistance of the columns with regard to the simultaneous bending in Eq. (1.33) can be overestimated which leads to the undersizing of the column cross-sections. Moreover, the columns may be subjected even to plastic deformation which necessitates the use of ductile columns. This leads to an even more rigorous demand.

Some design codes impose simple requirements to the cross sections of columns of braced frames that account for the expected flexural effects. For example, the aim of *Eqs. (2.21, 2.22, 2.23)* is to avoid the occurrence of plastic hinges away from the column ends. For the design of special concentrically braced frames (SCBF) [44] specific regulations have to be respected also as it has been mentioned in Section 2.1.2. Conversely, in Eurocode 8, there are no additional requirements for the columns, and the increase of the bending moments due to the deterioration of the braces is not incorporated in the design either. Yet, the principle of capacity design would require the non-dissipative columns to withstand the elevated internal forces to permit the dissipation in the braces without structural failure.

As there are no imposed requirements to the flexural resistance or stiffness [53] of the columns it is possible not to have any continuous columns at all, as the truss action is not affected by the hinged splices of the columns. If all the column splices are hinged, the bending cannot cause the underdesign of the columns. For the sake of comparison the IDA computations were conducted on the model of CBF41 again, but with exclusively hinged connections between every member of the structure. In *Figure 4.13/a* the original results (continuous columns on the facades) are presented and the *b* diagram depicts the result obtained with the hinged model. In terms of seismic design according to Eurocode 8 the solutions identically respect the requirements. On the behaviour of the two models, however, a clear discrepancy can be observed. Up until 0.50 scale factor the two models exhibit roughly the same response. At higher scale factors the differences of the drift maxima on the four floors is moderate and the rise of the curves is roughly parallel for the original continuous-column model. Conversely, the behaviour of the hinged-column model is

cluttered; the curves do not show any similarity and failure is attained at a lower scale factor by another storey than of the continuous-column model.

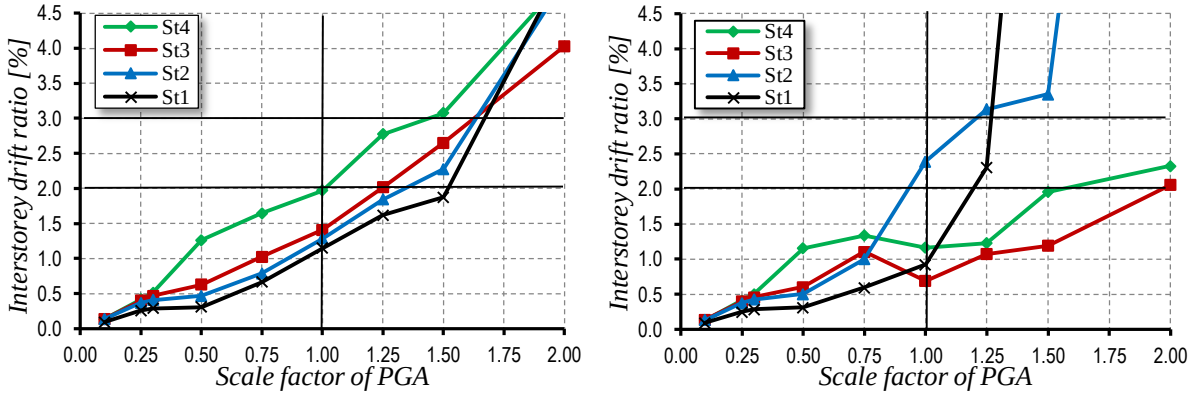

a) continuous columns *b) hinged columns*

Figure 4.13*; IDA diagrams CBF-4 with continuous and hinged column splices (averages of 7 records)*

Apparently, the seismic design process of Eurocode 8 for CBF-s does not describe accurately the behaviour of the structure. Significant effects on the continuous columns are not quantified properly, or in case of hinged column splices, the important participation of the columns in the lateral resistance is neglected.

4.2.3. Global and local slenderness limits of braces

The global and the local slenderness, as well as the material grade, affects the low-cycle fatigue fracture, i.e. the ductility of the braces. Low displacement ductility limits the performance of structures with a well balanced dissipation and the ones with weak storey susceptibility likewise. Therefore, an appropriate selection of ductile brace cross sections can significantly enhance the performance of any CBF regardless of the response to the seismic excitation.

In Section 2.1.1, in *Figure 2.6* it has been presented, that a large but otherwise probable high local slenderness can significantly limit the ductility of a hollow section brace. Eurocode 8 requires the sections to be class 1 that are capable of large plastic deformations without buckling of the plates. In the case of rectangular hollow section braces this means that the breadth-to-thickness ratio can go up to 33 supposing that the yield stress is 235 MPa.

$$\frac{b}{t} \leq 33\varepsilon \text{ with } \varepsilon = \sqrt{\frac{235}{f_y\left[MPa\right]}} \tag{4.6}$$

However, by using the formula of Nip et al. for hot-rolled carbon steel sections, Eq. (2.14), we find that the ductility capacity of a stockier brace with relative global slenderness equal to 1.3 and with a breadth-to-thickness ratio of 30, is about 4.0 that corresponds to only 1.1% interstorey drift ratio in the buildings presented in this article. This drift capacity is low, especially compared to the damage limitation state requirement (2%). Such an early failure can be avoided by imposing a more rigorous condition to the local slenderness than what is defined by Eq. (4.6). According to regulations in the United States [74], in the design of SCBF-s [44] the maximum breadth-to thickness ratio of square hollow section braces is:

$$\frac{b}{t} = 0.64 \cdot \sqrt{\frac{E_s}{f_y}} \tag{4.7}$$

For regular structural steel where the yield stress is 235 MPa this formula gives about 19. Considering again a brace with relative global slenderness of 1.3 but breadth-to-thickness ratio of 19, the ductility capacity obtained is 7.11. This enlarged ductility permits exactly 2% interstorey drift ratio.

Evidently, the cross-sectional classification, employed by Eurocode 3, which characterizes cross sections subjected to static loading, is not appropriate to be implemented for sections under cyclic loading. More rigorous restriction, such as the one in Eq. (4.7) is needed to avoid the early failure of the diagonals. Alternatively, by refined relationships between the slenderness parameters and the ductility, like the ones of Nip et al. presented in 2.1.1, diagrams can be provided that can facilitate the choice of hollow sections to meet specific lateral drift or ductility demands, see *Figure 4.14*.

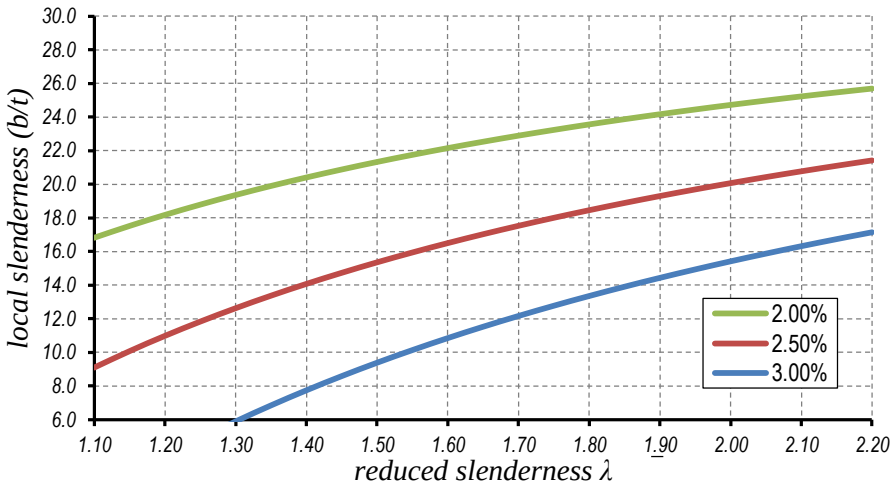

Figure 4.14; *Slenderness limits for imposed storey drift demands (S235, HR-SHS)*

4.2.4. Summary of the existing and necessary requirements on the seismic design of CBFs

Upon all the findings presented so far in the preceding chapters, the following statements can be made about the Eurocode 8 seismic design of CBF-s:

- The buildings are mostly susceptible to exhibit weak storey behaviour;
- The likelihood of the weak storey behaviour increases with the storey umber;
- The weak storey behaviour may lead to the early failure of the primary resisting members of the structure;
- The plastic deformations of the braces may eventually cause a significant change of the dynamic characteristics and the rearrangement of the inertia forces; such effects are not considered in any way in Eurocode 8;
- The incipient elastic behaviour, that the Eurocode 8 design procedure refers to, is significantly different from the inelastic behaviour;
- The uniformity condition, Eq. (1.30), is not adequate to promote the global dissipation as it is not valid in any random state that the structure may undergo during the seismic excitation;
- The analysis of a perfect structural model leads to the underestimation of the bending of the columns that develops with the deterioration of the braces; therefore Eurocode 8 does not safeguard sufficient overstrength in the columns, so it does not comply with the requirements of capacity design;

- The Eurocode 8 design does not make difference between CBF-s with continuous or hinged columns while the performance of the former is better;
- The local slenderness limit of hollow section braces should be more rigorous than Eurocode 3 class 1 to safely provide the adequate ductility of the braces;

The seismic behaviour of a dissipative CBF is not as of a vertical truss, counteracting the lateral seismic load by merely axial forces. Any design approach that assumes truss action incorporates the possibility of the above mentioned problems. The Eurocode 8 seismic design procedure of concentrically braced frames has to be enhanced or amended by new criteria that take into consideration the discussed effects. Firstly, appropriate criteria shall be introduced that aim to increase the ductility capacity of the resistant members and effectively prevent the early failure. Also, the performance of Eurocode 8 CBF designs may be enhanced by introducing conditions as listed below:

- CBF-s need to contain continuous columns that provide flexural resistance to the lateral loading. Though regular analysis methods do not yield relevant bending moment results, imposed limits to columns is a way to allow the development of considerable bending, e.g. examples given in 2.1.2.
- Elevated local slenderness of the hollow-section braces is accountable for low ductility capacity and consequently for the possibility of early collapse. More rigorous criteria, such as Eq. (4.7) may prevent such scenario.
- In the detailing of gusset plates, the requirement of sufficient clearance that allows the rotation of the diagonal can prevent the fracture of the gusset welds.

In this Chapter certain weaknesses of the Eurocode 8 design procedure of CBF-s has been pointed out. On one hand, some problems related to the detailing, which affect the ductility were drawn attention to, but more importantly, factors contributing to the development of the weak storey behaviour were identified. It is clear, that the EC8 criteria need revision. However, in the authors point of view, it is not the basic capacity design approach that permits rather high behaviour factors that needs to be modified. Instead, the criteria imposed upon the uniformity of the storey overstrengths and the requirements of the columns need to be replaced. With such modifications the weak storey behaviour may be avoided and the expected high performance of the structure can be attained.

In the following chapter a possible method will be elaborated that aims to promote the well distributed dissipation on every floor of a CBF. The method will be applied for the redesign of the buildings presented in 3.1 and the performance of the new designs will be compared to the originals to verify the methods suitability.

Chapter 5

Robust Seismic Brace Design method

Principles, Formulation and Application

In this chapter the findings of the previous descriptive chapters are turned into requirements and new criteria imposed upon the seismic design of CBF-s. Firstly, the concepts of the new criteria are elaborated and the principles of the Robust Seismic Brace Design method are established. This is followed by a thorough investigation of the internal and external plastic work of the CBF members and loads in plastic collapse mechanisms, which are in the focus of the method. The robust performance of the new method is demonstrated by the redesign of the various CBF-s presented and found to have weak storeys in Chapter 3. In the end, simplified alternatives of the method are also given and their suitability is examined.

5.1. Principles of the Robust Seismic Brace Design method

5.1.1. Requirements imposed to the design method

In previous chapters the inelastic seismic response of CBF-s has been introduced in detail and upon the findings the Eurocode 8 design procedure of braced frames has been critically discussed. In the following the most important requirements of an enhanced design method will be defined via a brief summary of the explored response.

In a real seismic event, experiencing, and therefore expecting equal and simultaneous displacement response of the storeys corresponding to the global plastic mechanism is unlikely. Conversely, it is a lot more probable that plastic deformations occur separately on one or a few floors at a time than simultaneously on every. What may be required however, is well distributed dissipation among all the floors. The participation is favourable if the degradation of the braces, and therefore the realized interstorey drift maxima is closely the same on every floor.

The degradation of the braces is the consequence of the plastic deformations at mid length due to inelastic buckling and the tensile yield. Together, the axial elongations and the development of the plastic hinge at the mid sections result in having triangular-shape, imperfect braces, see *Figure 5.1*. The amplitude of the triangular imperfection is coherent with the development of a weak storey. The gradually increasing triangularity of the diagonals results in the decrease of the axial force of the braces and devolves the seismic loading on the columns. The columns counteract the loading by bending, insofar as they are continuous at least at one end. So, the bending develops even as a result of moderate plastic deformation of the braces, not only in a storey collapse mechanism. Therefore, a braced frame is no longer a truss when subjected to seismic action, developing only axial forces. So, continuous columns with adequate flexural reserve are indispensable in a CBF.

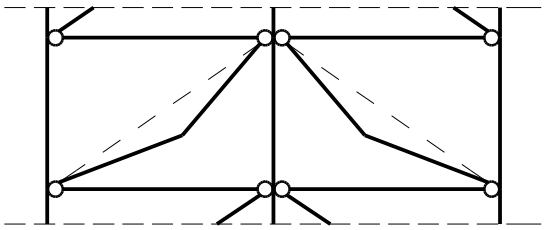

Figure 5.1*; Triangular deformation of braces due to repeated plastic deformations*

The flexural stiffness of the columns does not make up for the loss of lateral stiffness due to the brace degradation, so in the global model of the CBF the lateral stiffness of the weak storey is significantly lower than of the other floors. This modification of the structural system causes qualitative changes in the modal response of the building. A significant, but disproportional change of the stiffness of the system depicted in *Figure 5.2* alters the modal shapes and the natural frequencies also. The modes are uncoupled into modes that are primarily the motions of the slabs above the weak storey or in the contrary, motion of the ones below. In *Figure 5.2* only the first two modes are presented as these are the ones that have decisively large modal mass participation factors, the higher modes are mostly negligible. The first mode has a significantly higher period than the second mode. So, if we compute the maximum displacement response of the building considering the design displacement spectrum, see Eq. (1.19), and the combination of the modes we can find that the response is strongly governed by the first imperfect mode.

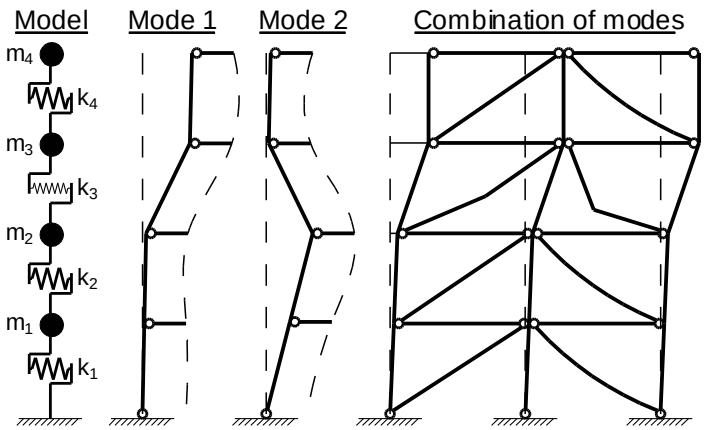

Figure 5.2*; Modal response of a CBF with a weak storey (modelled by triangular braces)*

The localization of the drifts on the weak storey may lead to even further degradation of the braces, decrease of the stiffness and consequently to the gradual self-amplification of the weak storey phenomenon.

The occurrence of a weak storey may result in the collapse of the building. However, if adequate resistance is provided by the columns, the building may be able to resist the seismic demands, though exhibiting localized displacements and unfavourable dissipative behaviour. A regular floor is expected to have moderate interstorey drifts in the range of its design seismic demand. Close to the resistance limit however, the drifts may grow abruptly, resulting in an asymptotic curve. Conversely, a weak storey can exhibit larger drifts even in case of low seismic action, but the development of the drifts may be limited at a certain level. These two response possibilities are depicted in *Figure 5.3*, but may also be observed on the examples presented in Chapter 3.

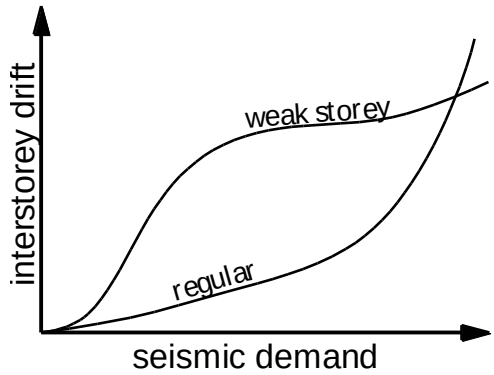

Figure 5.3*; Response alternatives to growing seismic demand*

The performance of the weak storey can be adequate, if the early development of the interstorey drifts does not exceed acceptable levels i.e. drifts that disturb serviceability or damage secondary structures. So, the weak storey behaviour shall be distinguished from the weak storey collapse. The weak storey behaviour is the prominent localization of lateral drifts on a certain floor(s) that may or may not cause early failure but is inevitably unfavourable. Furthermore, the fact that the drifts on the weak storey may not grow proportionally with the seismic action indicates, that the likelihood of the weak storey behaviour could be analyzed without the exact definition of the magnitude of the seismic loading. The weak storey behaviour can be regarded as an inherent susceptibility of a CBF that can be identified by the comparison of one floor to the others and not to a given seismic demand.

Upon the description of the behaviour and the response of CBF-s to seismic actions presented above, an effective design method should:

- Take into consideration the change of the modal behaviour due to the brace deterioration and the resulting response of the CBF;
- Quantify the participation of the columns and impose requirements to their performance in the lateral resistance of a storey;
- Prevent the occurrence of the weak storey collapse mechanism independently of the intensity of the design seismic action;
- Prevent the occurrence of the weak storey behaviour by unifying the (maximum) interstorey drifts on every floor;

In the following, 5.1.2 and 5.1.3 Sections propose two criteria that lead to respecting the above principles starting from a design made by classical spectral analysis.

5.1.2. Criterion 1: preventing the weak storey collapse mechanism

Let us suppose that for a given CBF structure we compute the storey shear effects for each storey conducting an analysis that complies with Eurocode 8 provisions. Also, we determine the lateral resistance of each storey coming from the braces only and in a second case the total storey shear resistance involving also the columns. Dividing the resistances with the effects the results can be depicted in a diagram like *Figure 5.4*. As the resistance over the effect is the definition of the overstrength in seismic design, the horizontal axis is denoted by Ω, representing the overstrength and along the vertical axis the storeys are presented one above the other. The maximum and the minimum of the overstrength yielded by the braces is indicated by two red dashed lines. The Eurocode 8 criterion for the uniformity of the overstrength requires that these do not differ by more than 25%, see Eq. (1.29). But, in order to bridge the gap between the two levels sufficient reserve is needed, provided by continuous columns. In the figure, on storey 3 this reserve is not accounted for. The resistance of the storey is depleted before every brace can attain yield.

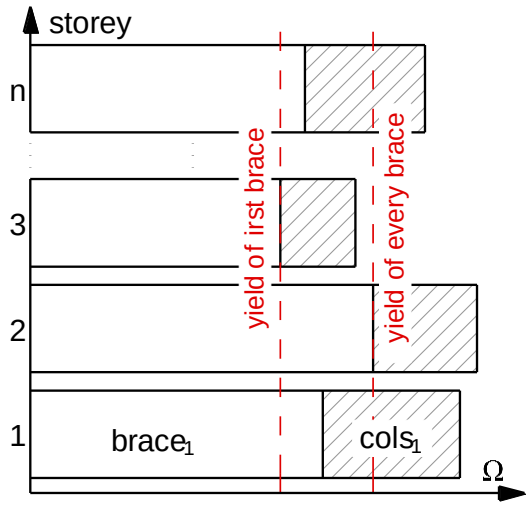

Figure 5.4; *Overstrength relations of a multi-storey CBF*

One of the primary objectives of the redesign method is therefore to secure adequate resistance on every storey that exceeds the resistance corresponding to the yield of every brace i.e. the global plastic mechanism. As we wish to determine the combined resistance of the braces and the columns that corresponds to the CBF behaviour in the inelastic range, the

analysis shall not be elastic; instead plastic analysis is more appropriate. As it has been mentioned in Chapter 1, the traditional nonlinear static method used for seismic analysis is the pushover analysis. In pushover analysis the ultimate resistance is approached applying the static principle of plasticity [74]. The lateral loading is monotonically increased as long as it results in a statically admissible internal force filed i.e. the structure is in equilibrium. The largest possible loading corresponds to the development of the collapse mechanism. In the present method the kinematic principle will be applied. Let us consider several kinematically admissible collapse mechanisms of a CBF and compare them. According to theory, the realized mechanism is the one that corresponds to the smallest lateral loading. The considered plastic mechanisms have to be obviously the favourable global mechanism and the unfavourable weak storey mechanisms. Partial mechanisms that involve several, but not every storey in the plastic deformation may be considered also. However, in the basic idea of the present method the partial mechanisms are not considered. Consequently, the global mechanism and *n* storey mechanisms (in an n-storey CBF) have to be computed considering a lateral loading that corresponds to the inelastic response of the CBF. It has to be noted though, that if we consider the inelastic response of a CBF, various load arrangements are possible. The deterioration of the braces on the ith storey results in a response, where only the floors above the weak storey sway with large amplitudes. The equivalent seismic load pattern corresponding to this response is having concentrated forces at the slabs from the ith storey up to the top, see *Figure 5.5*. If the masses are equal (the case of not equal masses will be considered later on), the forces are also equal, so the loading can be characterised simply by one λ parameter. This load pattern is also favourable to promote the development of the weak storey; therefore this simplification is for the benefit of safety.

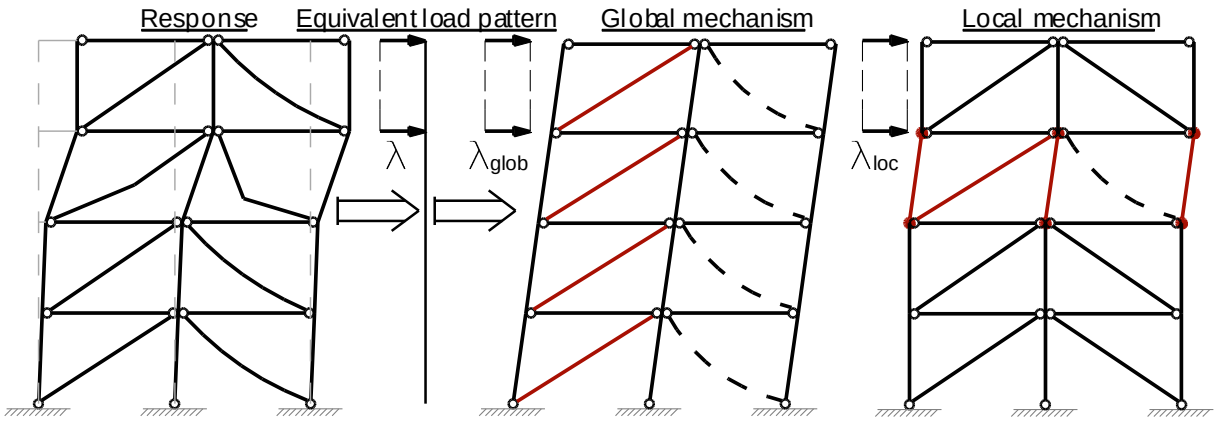

Figure 5.5*; Equivalent lateral loading of CBF with developed weak storey*

In an n-storey CBF *n* different load patterns can be analysed each ranging from the top down to a particular storey. For each load pattern, the load parameter corresponding to the formation of the global, λ_{glob}, and the local, λ_{loc}, plastic mechanism can be computed i.e. *n* parameter pairs can be calculated. If the local load multiplier is larger than the global, then according to the kinematic principle, the occurrence of a storey collapse is prevented. So, in order to secure that all the storeys have enough reserve so that no localized collapse shall occur, the following criterion has to be met:

$$\frac{\lambda_{loc,i}}{\lambda_{glob,i}} \geq 1.0 \quad \text{where } i=1..n \tag{5.1}$$

Important characteristic of the requirement above is that for the evaluation the magnitude of seismic loading is not given, but instead it is the unknown load multiplier that

has to be determined. The plastic analysis method to be conducted and the requirement of Eq. (5.1) itself:

- Takes into consideration the variation of the modal behaviour due to the brace deterioration and the resulting response of the CBF.
- Quantifies the participation of the columns and imposes requirements to their performance in the lateral resistance of a storey.
- Is required to prevent the occurrence of the weak storey collapse mechanism.
- Can be carried out independently of the design seismic intensity.

5.1.3. Criterion 2: unifying the maximum drifts, promoting distributed dissipation

Although the condition of Eq. (5.1) is necessary to prevent weak storey collapse, it is not sufficient to keep the differences of the interstorey drifts on all the floors within an acceptable range. The reason is the following. Eq. (5.1) can be satisfied by enlarging either the brace or the column cross sections as they are both involved in the plastic resistance of a certain storey. If in an extreme case the resistance is only given by the brace and the columns are negligible (or hinged at both ends), the load corresponding to the yield of the brace is equal to the ultimate plastic resistance of the storey. As the method under consideration aims to prevent the attainment of the storey resistance, the brace yield will not be reached either and the storey remains elastic throughout the seismic action. Conversely, if all the resistance is provided by the columns and the braces are neglected, the lateral displacement on this certain floor will be a lot larger than on other floors. The bending of the columns permits substantially larger displacements than the stiff bracing. Such a floor has the tendency to exhibit the weak storey behaviour as it has been presented before in *Figure 5.3*. The anticipated responses of these two extreme cases are depicted in *Figure 5.6* along with the theoretical behaviour of a regular, well designed floor. The two cases may be satisfactory, satisfying all resistance design criteria, but certainly they are both unfavourable because they impair the dissipative behaviour of the CBF. In the former case the floor is not exploited in the dissipation, whereas the latter case is too much involved by developing weak storey behaviour.

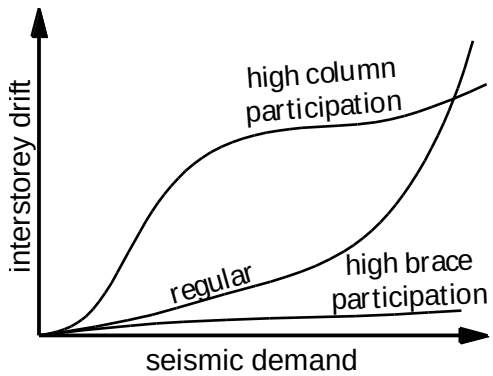

Figure 5.6; *Improper brace or column participation in storey resistance*

If the ratio of the local and global load multipliers is high i.e. significantly larger than 1.0, then the storey may be overdesigned, not participating in the dissipation. Nevertheless, defining an upper bound value to the ratio is arguable. Firstly, the upper bound may create design situations where the structural dimensions, that were found by conducting the standard analysis that takes into consideration the intensity of the seismic loading and stability of compression members, has to be decreased. As the redesign method under

discussion is independent of the seismic intensity, such alteration is questionable. The method should only be used to reinforce the presumably weak storeys. Furthermore, the fact, that there are several or strong continuous columns on a floor (e.g. moment resisting frames) can raise the ratio of Eq. (5.1) far beyond 1.0, but this does not necessarily mean that the desired yield of the brace is not attained. In fact, such a storey is favourable as it provides large reserve in the columns.

The objective with the introduction of a second criterion is to avoid cases where too large or in the contrary too small inelastic deformations can be expected. For such investigation the elasto-plastic behaviour of a weak storey needs to be examined. In the following this behaviour is used to estimate the cyclic inelastic behaviour of soft storeys. In *Figure 5.7* the shear force of a storey, denoted by the λ multiplier, and the interstorey drift of the same floor are depicted by the two axes of the presented diagrams. Apart from the load multiplier corresponding to the elastic limit, and the development of the full plastic storey mechanism, the global load multiplier is also indicated. The black line represents the theoretical (pushover) curve of a storey with one, straight brace. This curve exhibits a large stiffness up until the attainment of the tensile yield of the brace. After this, large drifts are realized while the local resistance, including the columns is reached.

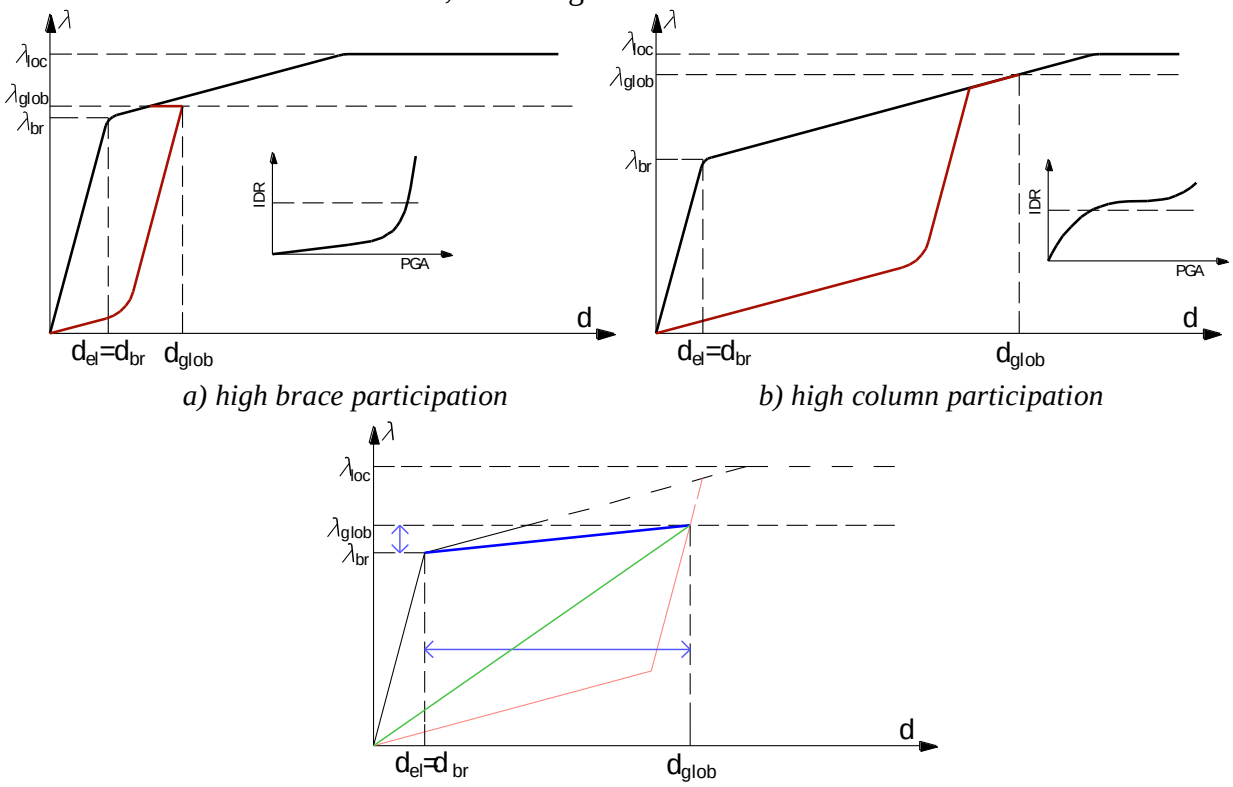

Figure 5.7; *Theoretical elasto – plastic force – displacement curves of braced storey*

The two unfavourable storey responses depicted by *Figure 5.6* are represented in the load multiplier – storey drift format in the *a)* and *b)* diagrams of *Figure 5.7*. If the brace resistance, or in other words the elastic limit, is close to λ_{glob}, large inelastic deformations and triangular brace deterioration cannot be realized and the displacements corresponding to the elastic limit and the development of the global mechanism are close to each other. Conversely, in the case of the *b)* diagram when significant involvement of the columns is needed to respect the first criterion of Eq. (5.1), the inelastic displacements and the

deterioration are larger. Visibly, the inelastic storey drifts that we may expect are in correlation with the position of the global load multiplier in the [λ_{br}, λ_{loc},] range.

Regarding the drift corresponding to the yield of the brace, d_{br}, if the yield stress is the same on every storey, then this drift also has to be closely the same constant on every storey. In order to promote a uniform response on every floor, it needs to be ensured, that the inelastic drift corresponding to the attainment of the global mechanism, d_{glob}, is also closely the same on every floor [76]. Therefore, the following ratio has to be quasi constant for all the storeys:

$$\frac{d_{br,i}}{d_{glob,i}} = const \tag{5.2}$$

Let us consider the initial stiffness up to the elastic limit and the secant stiffness of the inelastic response depicted by a green line in *Figure 5.7/c*. The ratio of the stiffness values, denoted by β, describes the relative stiffness loss resulted by the deterioration of the brace.

$$\frac{\frac{\lambda_{br}}{d_{br}}}{\frac{\lambda_{glob}}{d_{glob}}} = \beta \tag{5.3}$$

This sort of stiffness loss has been addressed before in Section 4.1.2 where using elastic imperfect models it has been shown, that the localized change of the stiffness changes the modal behaviour in a way that it promotes the development of the weak storey, whereas the simultaneous and proportional decrease of the stiffness on every floor has no such effect. In the later case the CBF maintains the modal behaviour ideal for the occurrence of distributed dissipation with the involvement of every floor. Consequently, we may assume that to obtain a favourable CBF design, without weak storey susceptibility when subjected to seismic action, β has to be the same on every floor. Therefore, by rearranging Eq. (5.3) we may find that the ratio of the λ_{br} and λ_{glob} is equal to the product of ideally constant values, so the ratio itself has to be constant in a CBF that does not exhibit weak storey behaviour. The ratio somehow expresses the involvement of the brace of a given floor in the resistance to the loading corresponding to the global mechanism, therefore it has been named Brace Performance Ratio (hereinafter BPR). As a second design criterion, additional to Eq. (5.1), it is required that the maximum and minimum BPR do not differ by more than 0.1.

$$BPR_i = \frac{\lambda_{br,i}}{\lambda_{glob,i}} = \beta_i \frac{d_{br,i}}{d_{glob,i}} \text{ and } BPR_{\min} + 0.1 \geq BPR_{\max} \tag{5.4}$$

It is obvious that if the BPR is close to 1.0, then the bracing is overdesigned, column resistance is barely needed and the storey is not involved in the plastic dissipation. For this reason it is recommended that the maximum BPR shall not exceed 0.9, or in other words, at least 10% of the resistance to the loading defined by λ_{glob} has to be provided by continuous columns. It has to be noted that the above values, 0.1 and 0.9, are empirically determined. They have been defined upon the results that are to be presented later on in this chapter.

5.1.4. Application of the Robust Seismic Brace Design criteria

The reinforcement of a CBF to satisfy the two criteria of Eq. (5.1) and Eq. (5.4) may influence the buildings adequacy to Eurocode 8 requirements. The uniformity condition of the storey overstrengths, Eq. (1.29), can be violated as the reinforcement of the braces may significantly increase the maximum overstrength. Therefore, the newly introduced criteria aim to replace the uniformity condition. The requirement for the columns and beams, Eq. (1.32), may be moderately affected if the minimum storey overstrength is increased by the redesign, but this should be limited given that the redesign does not involve every brace. Nevertheless, the need of considerable lateral storey shear resistance yielded by the bending of the columns may require larger column cross sections than Eq. (1.32).

As the seismic response of a building is random, closely chaotic, the introduced criteria do not aim to promote the unlikely simultaneous yield of the braces on every floor. Conversely, they provide a barrier within which plastic deformations can be realized in the diagonals of multiple storeys. It assures that the CBF tends to exhibit distributed dissipation with the involvement of every storey regardless of the loading history and any instantaneous plastic deformation scheme. The CBF that fulfils Eq. (5.1) and Eq. (5.4) is deemed to be robust in terms of being able to exhibit a controlled dissipative behaviour under any seismic effect within its design intensity range. For this reason the redesign procedure has been named as the Robust Seismic Brace Design (henceforth RSBD) method.

The RSBD redesign method has to be conducted in the following steps:

- Initial design of the structure according to related codes i.e. Eurocode 3 and Eurocode 8 considering the response spectra, behaviour factor, conducting an elastic analysis and dimensioning the members according to its internal force results. In the seismic design Eq. (1.29) can be neglected.
- For n different loading patterns, considering the global and n local plastic mechanisms computation of n $\lambda_{glob,i}$ and $\lambda_{loc,i}$ parameter pairs. Computation of the $\lambda_{br,i}$ load multiplier of the braces for n local mechanisms.
- Reinforcement of the braces to respect the condition given for the BPR, Eq. (5.4). Attention is to be paid that the modification of one brace does not only change the corresponding local load multiplier and the brace participation ratio of that floor, but also all the global multipliers and every other BPR in the same time.
- Reinforcement of the columns or introduction of more continuous column splices in the building to satisfy the condition of Eq. (5.1).

5.2. Formulation of the Robust Seismic Brace Design method

As it has been presented previously, the RSBD method is based on plastic analysis, in which various load multipliers need to be computed with the application of the kinematic principle. Therefore, to determine the multipliers internal and external works have to be calculated. In the following, the basic assumptions, the work of the plastic members and the loads will be determined and the load multipliers will be expressed.

5.2.1. Geometry and material model

In *Figure 5.8* the deformed shape of a braced bay is presented, depicting the relevant parameters that describe the geometry. The storey height and the column spacing are denoted by H and B respectively. The initial length of the diagonal concentric braces is L and the elongation due to the lateral drift is ΔL. In conjunction with the elongation of the diagonal vertical shortening and lateral drift are realized also, that are denoted by ΔH and ΔB. The later is the interstorey drift as it can be expressed as the difference between the lateral displacements of the floor slabs above and under, denoted by X_i and X_{i+1}. The vertical shortening can be expressed as follows:

$$\Delta H = H - H \cdot \cos \Delta\varphi \tag{5.5}$$

The cosine of the angle of the drift can be well approximated by its truncated Taylor series as the considered displacements in the present analysis are inherently small. Furthermore the angle itself is closely equal to the ratio of the interstorey drift and the storey height, supposing that the sinus of the angle and the angle itself are equal.

$$\cos \Delta\varphi \approx 1 - \frac{\varphi^2}{2} \tag{5.6}$$

$$\sin \Delta\varphi \approx \Delta\varphi \approx \frac{\Delta B}{H} \tag{5.7}$$

Substituting Eq. (5.6) and Eq. (5.7) into Eq. (5.5) we get:

$$\Delta H = H - \cos \Delta\varphi \cdot H = H \cdot \left(1 - 1 + \frac{\Delta\varphi^2}{2}\right) = H \frac{\Delta\varphi^2}{2} = \frac{\Delta B^2}{2H} \tag{5.8}$$

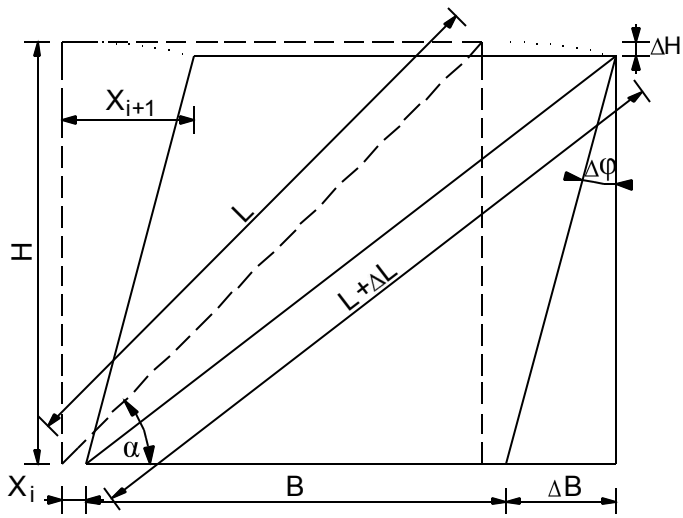

Figure 5.8; *Geometry model of collapse mechanism*

To express the lateral drift by the elongation of the diagonal we consider that:

$$\left(L+\Delta L\right)^2=\left(B+\Delta B\right)^2+\left(H-\Delta H\right)^2 \tag{5.9}$$

By neglecting the small vertical shortening we get:

$$\Delta B=\sqrt{\left(L+\Delta L\right)^2-H^2}-B\approx\frac{\Delta L}{\cos\alpha} \tag{5.10}$$

In plastic analysis according to the theorem of constant stresses [74], in a plastic mechanism the stress field does not change. This means that the internal work of the structure consists of only the dissipation of the plastic members; elastic deformations and reversible elastic work are not realized. This provides the possibility of considering a simple rigid – perfectly plastic material model in the following calculations, where yield stress is f_y.

5.2.2. Internal work of the braces

The relative lateral drift of two adjacent floor slabs in a CBF forces axial elongation on the brace which leans in the direction of the drift. Meanwhile the brace in compression buckles see *Figure 5.9*. Assuming rigid plastic behaviour, the buckling is realized by the formation of a plastic hinge at the mid-section of the compression brace. All the plastic deformations are located in this plastic hinge, the two segments of the brace remain undeformed. The buckled shape causes the bending of the bar, therefore the internal work of the compression brace is realized by the work of the combined axial force and bending effect on the plastic deformations of the hinge. It has to be noted, that the real inelastic buckling behaviour of the compression brace is a lot more complex, as it has been briefly introduced in Chapter 2. Here, with the perfectly plastic cross-sectional model we aim to give a strong, upper bound estimation of the compression braces performance. The tensile brace is subjected merely to axial force that performs work on the elongation. In the following, expressions will be given for the deformations, the internal forces under consideration and also for the plastic internal work of the braces.

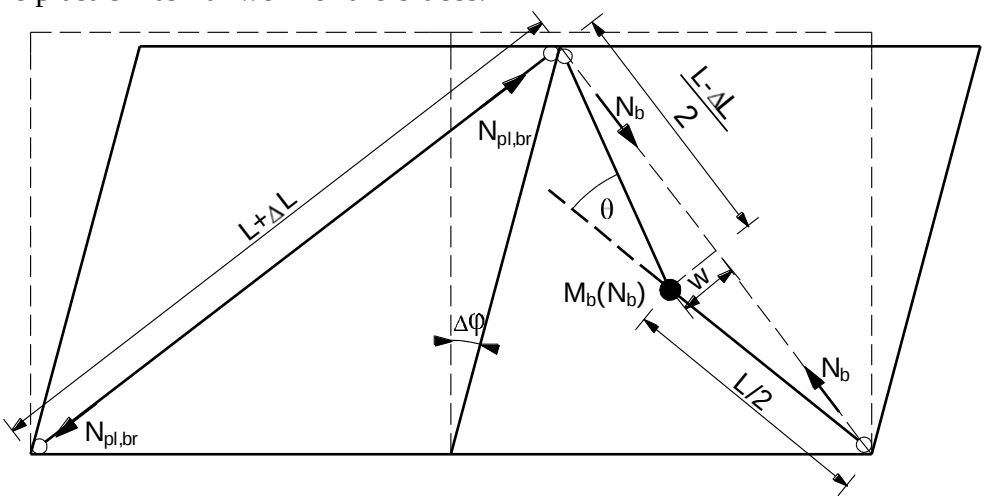

Figure 5.9; *Deformation and internal forces of braces*

The rotation of the plastic hinge can be computed by the use of the out-of-plane deformation, denoted by w. In the analysis an initial local imperfection, w_0 is also considered, but at the computation of the plastic rotation angle of the hinge, θ, it is subtracted as it describes the undeformed imperfect shape of the brace. The connection between the

axial shortening and the out-of-plane deformation can be expressed from the triangular geometry depicted in *Figure 5.9*:

$$\left(\frac{L}{2}\right)^2 = \left(\frac{L-\Delta L}{2}\right)^2 + \Delta w^2 \Rightarrow \Delta w(\Delta L) = \sqrt{\frac{\Delta L}{2}\left(L - \frac{\Delta L}{2}\right)} \tag{5.11}$$

The total out-of -plane deformation, considering a w_0=L/200 initial imperfection also, is:

$$w(\Delta L) = \Delta w(\Delta L) + w_0 = \sqrt{\frac{\Delta L}{2}\left(L - \frac{\Delta L}{2}\right)} + \frac{L}{200} \tag{5.12}$$

The rotation angle of the plastic hinge θ can be expressed as follows:

$$\theta(\Delta L) = 2 \cdot \arctan\left[\left(w(\Delta L) - w_0\right) \cdot \frac{2}{L - \Delta L}\right] \tag{5.13}$$

The analysed braced frames all have square hollow section braces. The geometry of these cross-sections is approximated in a way that the filleting of the corners is neglected. Therefore, the only two parameters that are used to describe the cross-section of the braces is the external size, *a*, and the plate thickness, *t*. The area and the plastic section modulus are calculated with the *a* and *t* parameters as follows:

$$A_{br} = a^2 - (a - 2t)^2 \tag{5.14}$$

$$Q_{pl,br} = \frac{a^3}{4} - (a - 2t) \cdot \left(\frac{a}{2} - t\right)^2 \tag{5.15}$$

The plastic axial resistance of the section is defined as below:

$$N_{pl,br} = A_{br} \cdot f_y \tag{5.16}$$

The plastic moment resistance is:

$$M_{pl,br} = Q_{pl,br} \cdot f_y \tag{5.17}$$

The plastic deformations in the hinge are resulted by the simultaneous effect of the compression and the bending of the brace. Also, the bending is dependent of the axial force as it is resulted by the eccentricity of the axial force to the mid-section of the brace:

$$M_{br}\left(N_{c,br}\right) = N_{c,br} \cdot w(\Delta L) \tag{5.18}$$

Besides, the bending and the axial force together result in the entirely plastic normal stress distributions depicted in *Figure 5.10*. The stress distribution in the plastic hinge is asymmetric as the axial compression enlarges the negative stress zone. The bending moment, besides Eq. (5.18), can also be determined by considering that the axial force – moment interaction defines a point on the yield surface of the cross section. To express the moment, let us subtract $S(N_b)$, the first moment of the hatched area, A_N, on which the normal force is realized, from the plastic section modulus:

$$M_{br}\left(N_{c,br}\right) = M_{pl,br} - S(N_{c,br}) \cdot f_y = \left[Q_{pl,br} - S(N_{c,br})\right] \cdot f_y \tag{5.19}$$

By the use of Eq. (5.18) that expresses the equilibrium and Eq. (5.19), which is a representation of the plasticity condition, an expression can be given from which the axial force can be computed for any given axial shortening.

$$\left[Q_{pl,br} - S(N_{c,br})\right] \cdot f_y - N_{c,br} \cdot w(\Delta L) = 0 \tag{5.20}$$

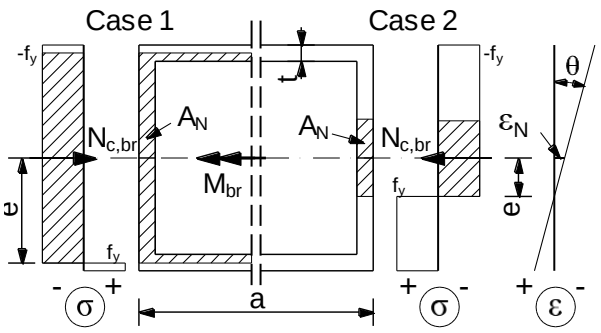

Figure 5.10; *Normal stress distributions and deformation diagram of SHS brace cross-section*

For the resolution of Eq. (5.20) the expression of the first moment of area, $S(N_b)$, has to be defined. In terms of the layout of the A_N area two cases can be distinguished. In case 1 the normal force is large enough to expand the area needed for the normal resistance into the flanges of the section. In case 2 the area is confined to the webs only. The eccentricity of the neutral axis, denoted by e, is calculated in the two cases as follows:

$$e(N_{c,br}) = \begin{cases} \dfrac{a}{2} - \dfrac{A_{br} - N_{c,br}/f_y}{2a} & if, N_{c,br} > (a-2t)t \cdot f_y \\ \dfrac{N_{c,br}}{4t \cdot f_y} & if, N_{c,br} \le (a-2t)t \cdot f_y \end{cases} \tag{5.21}$$

The equation for the first moment of area using the eccentricity defined above is:

$$S(N_{c,br}) = \begin{cases} \left[e(N_{c,br})\right]^2 a - \dfrac{(a-2t)^3}{4} & if, N_{c,br} > (a-2t)t \cdot f_y \\ \left[e(N_{c,br})\right]^2 \cdot 2t & if, N_{c,br} \le (a-2t)t \cdot f_y \end{cases} \tag{5.22}$$

By substituting Eq. (5.22) into Eq. (5.20) the axial force can be computed from the shortening of the brace and with Eq. (5.19) the bending moment can be determined. In the diagrams of *Figure 5.11* the normalised axial force and the normalised bending moment are depicted in a 0 – 1% shortening range for an SHS100×4 brace with length L=6708 mm. As the shortening grows, the triangular out-of-plane buckling increases and the axial force in the bar decreases as it can be expected. Though the material is rigid plastic, at 0 shortening the normal force is not equal to the plastic resistance since the w_0 initial imperfection has been considered. The decay of the axial force is fast and this gives a similarly rapid rise to the bending moment. Therefore, apart from cases of very small displacements, the internal work of the compression braces is primarily defined by the bending of the plastic hinge.

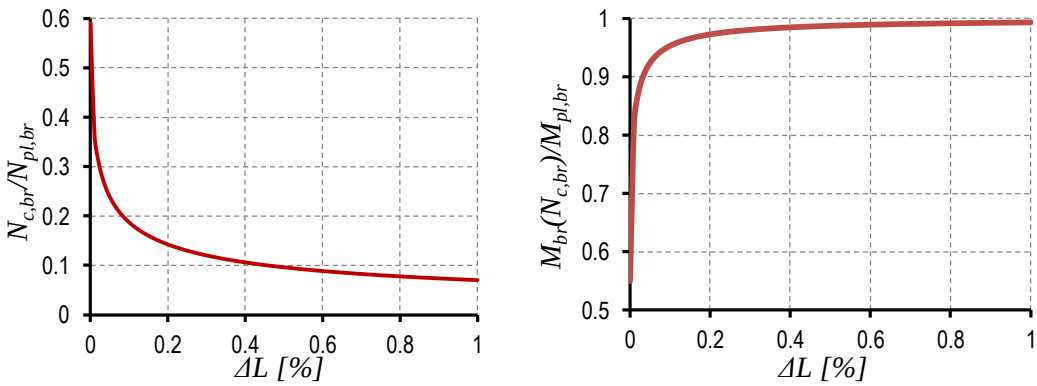

a) decrease of axial force *b) increase of bending moment*

Figure 5.11; *Change of the axial force and the bending moment of brace with the shortening*

Eqs. (5.19) (5.21) and (5.22) define a nonlinear yield surface in a rather complex way. In Eurocode 3 the interaction of the axial forces and bending moments is provided also, but in the following simplified form. The moment resistance shall not be decreased by the effect of the normal force if:

$$N_{c,br} \leq 0.25 N_{pl,br} \text{ and } N_{c,br} \leq \frac{0.5 \cdot a \cdot t \cdot f_y}{\gamma_{M0}} \tag{5.23}$$

where γ_{M0}=1.0. Otherwise the interaction is defined by the linear formula presented below:

$$M_{br}(N_{c,br}) = M_{pl,br} \cdot \frac{1-n}{1-0.5 \cdot a_w} \text{ with } n = \frac{N_{c,br}}{N_{pl,br}} \text{ and } a_w = \frac{A_{br} - 2a \cdot t}{A_{br}} \tag{5.24}$$

In *Figure 5.12* the curves of the yield surface and the Eurocode interaction formula are depicted for the sake of comparison. As it can be seen, in the range of smaller axial forces, the interaction curve of Eurocode suggests that the bending moment resistance is independent of the axial force. Unfortunately, due to the fast decay of the axial force presented in *Figure 5.11/a*, this is the range in which the normal force of the compression brace can be expected. Therefore, here the use of the nonlinear yield condition is favoured.

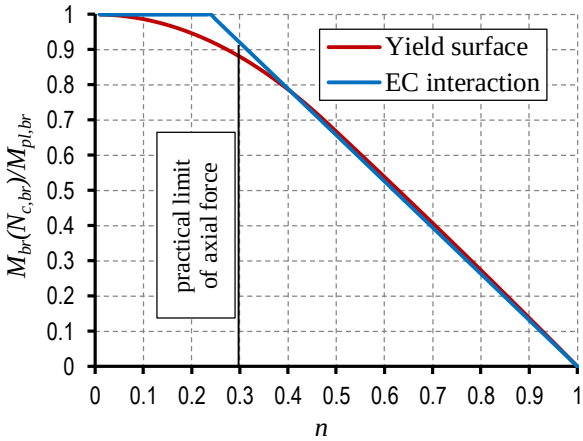

Figure 5.12*; Nonlinear yield surface and EC3 interaction curve of SHS section*

The appropriateness of the yield condition can be identified by first determining the tangent of the curve by the derivative of the function in Eq. (5.19). Substituting Eq. (5.21) and Eq. (5.22) into Eq. (5.19) and considering case 2 we get for the inclination of the tangent of the nonlinear yield surface:

$$M_{br}\left(N_{c,br}\right) = \left[Q_{pl,br} - \left[\frac{N_{c,br}}{4t \cdot f_y} \right]^2 \cdot 2t \right] \cdot f_y = Q_{pl,br} \cdot f_y - \frac{N_{c,br}^{\ 2}}{8t \cdot f_y} \tag{5.25}$$

$$\frac{dM_{br}\left(N_{c,br}\right)}{dN_{c,br}} = -\frac{N_{c,br}}{4t \cdot f_y} = -e(N_{c,br}) \tag{5.26}$$

In case 1, neglecting the constants at the beginning as they have no influence on the derivative:

$$M_{br}\left(N_{c,br}\right)=\left[\cancel{Q_{pl,br}}-\left[e(N_{c,br})\right]^2 a+\cancel{\frac{(a-2t)^3}{4}}\right]\cdot f_y$$

$$\Rightarrow\left[\frac{a}{2}-\frac{A_{br}-N_{c,br}/f_y}{2a}\right]^2 a\cdot f_y \tag{5.27}$$

$$-\frac{a^3 f_y}{4}+\frac{A_{br}\cdot a\cdot f_y}{2}-\frac{N_{c,br}a}{2}-\frac{A_{br}^2\cdot f_y}{4a}+\frac{A_{br}N_{c,br}}{2a}-\frac{N_{c,br}^2}{4a\cdot f_y}$$

$$\frac{dM_{br}\left(N_{c,br}\right)}{dN_{c,br}}=-\frac{a}{2}+\frac{A_{br}}{2a}-\frac{N_{c,br}}{2a\cdot f_y}=-e(N_{c,br}) \tag{5.28}$$

As it can be seen, the inclination of the tangent in any point of the nonlinear yield surface is equal to the negative eccentricity of the neutral axis. Let us also determine the relation between the plastic deformations regarding *Figure 5.10*. One can see that the connection between the axial deformation, ε_N, and the rotation of the hinge, θ, is defined again by the eccentricity. However, the eccentricity is not constant, and as the braces are expected to perform in the low axial force high bending moment range corresponding to case 2, it should not even be approximated with a constant. Therefore, the connection can only be expressed in the incremental form below:

$$d\theta=\frac{d\varepsilon_N}{e(N_{c,br})}\Rightarrow\frac{d\theta}{d\varepsilon_N}=\frac{1}{e(N_{c,br})} \tag{5.29}$$

Taking a look at Eqs. (5.26) and (5.28) as well as Eq. (5.29) we can see that the plastic deformations are orthogonal to the tangent of the yield surface in every point. Therefore, the nonlinear yield surface satisfies the normality rule [74] which makes it appropriate to use in plastic analysis.

The objective of this investigation of the brace plasticity is to compute the plastic work of both the tensile and the compression diagonal and to relate this to an appropriately chosen parameter, e.g. the axial shortening. The internal work of the tensile brace can be computed by a very simple equation as the axial force is constant.

$$\Delta W_{t,br}\left(\Delta L\right)=N_{pl,br}\cdot\Delta L=A_{br}\cdot f_y\cdot\Delta L \tag{5.30}$$

Conversely, in the case of the compression bar the axial force, the bending moment and the plastic deformation are all functions of the shortening, so the internal plastic work is expressed in incremental form. In the equation the work of the axial force and the bending are calculated separately.

$$\begin{aligned}dW_{c,br}\left(\Delta L\right)&=N_{c,br}\cdot d\varepsilon_N+M_{br}\left(N_{c,br}\right)\cdot d\theta\\ dW_{c,br}\left(\Delta L\right)&=N_{c,br}\cdot e\left(N_{c,br}\right)\cdot d\theta\left(\Delta L\right)+M_{br}\left(N_{c,br}\right)\cdot d\theta\end{aligned} \tag{5.31}$$

In *Figure 5.13/a* the internal work i.e. the plastic energy dissipation of the tensile and the compressive brace is plotted against the axial percentile elongation of the bar. The work is normalised with the maximum work of the tensile brace. For the compression brace, the curve can be computed by the step-by-step evaluation of the incremental expression above. As it can be seen, the dissipation of the compression brace, compared to the tensile, is rather small, about 15%. However, the ratio of the compressive dissipation may not be this small on

every floor of a CBF as the compressive dissipation depends also on the slenderness of the brace and not only the cross-sectional area. A stockier brace is expected to dissipate more energy. *Figure 5.13/b* depicts the dissipation of the compression brace as a function of the reduced slenderness, which has been changed by modifying the cross.sectional sizes and keeping the length constant. The interval of the considered slenderness is equal to the range permitted for seismic resistant braced frames by Eurocode 8. As it can be seen, the effect on the dissipation is moderate. By taking into account the compression braces, the effect of the overstrength provided by the application of stockier braces instead of slender ones can be analysed. However, in the present study this effect is estimated to be negligible. It has to be noted also, that the work of the compressive brace presented here, is strong an upper bound estimation as at the plastic hinge in reality the warping of the plates, and in cyclic loading, the appearance of small cracks result in the decrease of the resistance of the section. The decreased internal forces dissipate less energy than the perfectly plastic cross-sectional model. Therefore, we expect the compression braces to dissipate even less energy compared to the tensile brace than what we have estimated here.

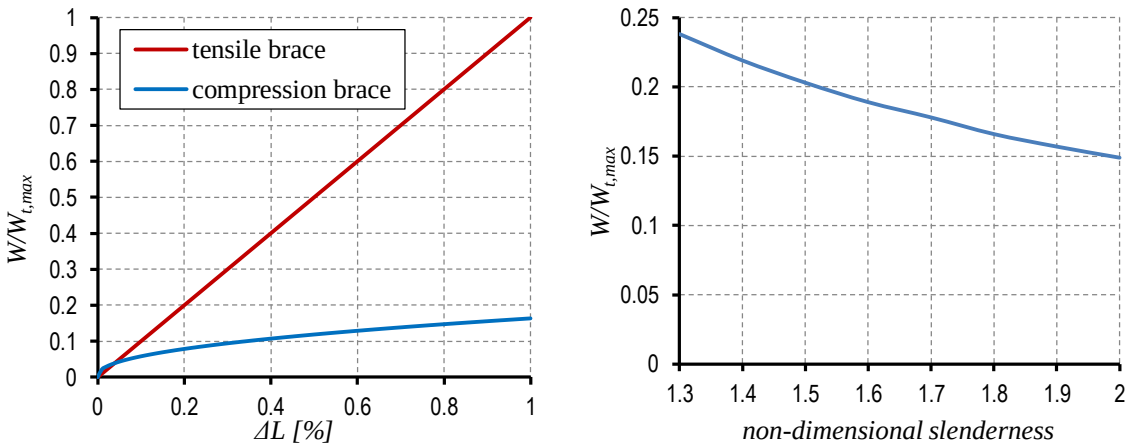

a) tension and compression *b) effect of slenderness on the dissipation*

Figure 5.13*; Dissipation of tensile and compression braces*

By neglecting the dissipation of the compression braces in the plastic analysis we introduce a not particularly large, but roughly proportional decrease of the plastic internal work of the braces on every storey in a CBF. This simplification is very favourable in terms of computation as it reduces the evaluation of the work of the braces to Eq. (5.30) only. Therefore, in our future analysis only the tensile braces will be considered at the determination of the internal work of the braces. However, we note that the possibility to refine the calculations with regard to the compression bars has been hereby presented.

5.2.3. Internal work of the columns

In the columns the plastic yield of the cross section is caused by the combined axial compression and flexural effects, similarly to the already presented braces. The main difference, compared to the previous case, is that in the columns the normal force is a constant parameter, not a function of the deformation and this constant axial force can be expected to be larger than 0.4 – 0.5 times the plastic axial resistance. This is usually true for the majority of the columns of a building. The most common cross-sectional types for columns in steel buildings are the various wide-flange H sections (HEB, HEM, HD); also in the examples these sections are applied. In order to simplify the model of the H-section the filleting of the corners is neglected. Supposing that the section is symmetrical to both principal axes, for the definition of the geometry four parameters are needed: the height h, the breadth b and the thickness of the web and the flanges, t_w and t_f, see *Figure 5.14*. Using these parameters, the area and the plastic section moduli for both axes are computed with the following expressions:

$$A_c = t_w \cdot h + 2\left(b - t_w\right)t_f \tag{5.32}$$

$$Q_{pl,y,c} = t_w\left(\frac{h}{2} - t_f\right)^2 + b \cdot t_f\left(h - t_f\right) \tag{5.33}$$

$$Q_{pl,z,c} = 2b \cdot t_f \frac{b}{4} + \left(h - 2t_f\right)\frac{t_w^2}{4} \tag{5.34}$$

The plastic axial and flexural resistances are:

$$N_{pl,c} = A_c \cdot f_y \tag{5.35}$$

$$M_{pl,y,c} = Q_{pl,y,c} \cdot f_y \tag{5.36}$$

$$M_{pl,z,c} = Q_{pl,z,c} \cdot f_y \tag{5.37}$$

Let us determine the axial force - uniaxial bending yield surfaces are the same way as before, by decreasing the plastic section modulus with the first moment of the A_N area i.e. the area on which the normal force is distributed:

$$M_{y,c}\left(N_c\right) = M_{pl,y,c} - S_y(N_c) \cdot f_y = \left[Q_{pl,y,c} - S_y(N_c)\right] \cdot f_y \tag{5.38}$$

$$M_{z,c}\left(N_c\right) = M_{pl,z,c} - S_z(N_c) \cdot f_y = \left[Q_{pl,z,c} - S_z(N_c)\right] \cdot f_y \tag{5.39}$$

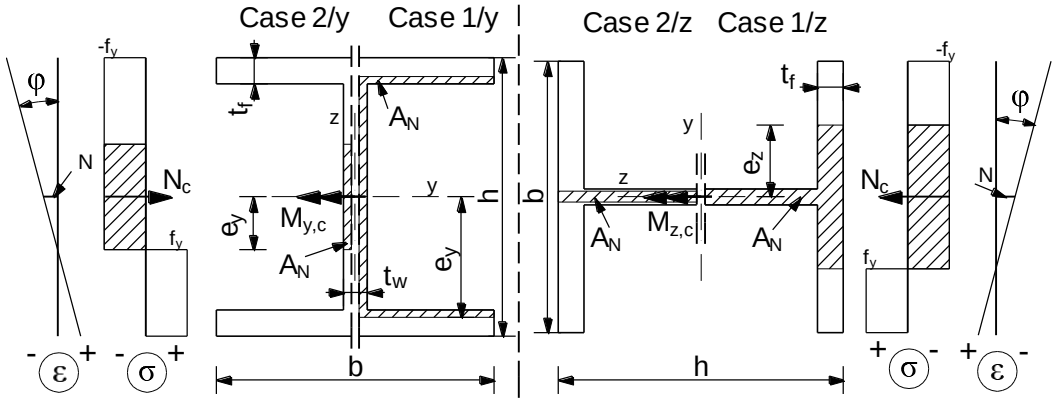

Figure 5.14*; Normal stress distributions and deformation diagrams of column H-section*

First, the eccentricity of the neutral axis has to be computed. Depending on the position of the column, it can be bent about the y or the z principal axis. Regarding the magnitude of the normal force, two cases can be distinguished; the distribution area of the normal force is either confined to the web of the section (Case 2) or extends into the flanges also (Case 1). Due to the usually elevated axial effect of the columns, Case 1 can be anticipated in most columns of a CBF.

$$e_y(N_c)=\begin{cases}\dfrac{h}{2}-t_f+\dfrac{N_c-(h-2t_f)t_w\cdot f_y}{2b\cdot f_y} & if, N_c>\left(h-2t_f\right)t_w\cdot f_y\\ \dfrac{N_c}{2t_w\cdot f_y} & if, N_c\le\left(h-2t_f\right)t_w\cdot f_y\end{cases} \tag{5.40}$$

$$e_z(N_c)=\begin{cases}\dfrac{t_w}{2}-\dfrac{N_c-h\cdot t_w\cdot f_y}{4t_f\cdot f_y} & if, N_c>h\cdot t_w\cdot f_y\\ \dfrac{N_c}{2h\cdot f_y} & if, N_c\le h\cdot t_w\cdot f_y\end{cases} \tag{5.41}$$

The equations of the first moment of area using the eccentricity are:

$$S_y\left(N_c\right)=\begin{cases}\left[e_y(N_c)\right]^2 b-\dfrac{\left(b-t_w\right)\cdot\left(h-2t_f\right)^2}{4} & if, N_c>\left(h-2t_f\right)t_w\cdot f_y\\ \left[e_y(N_c)\right]^2\cdot t_w & if, N_c\le\left(h-2t_f\right)t_w\cdot f_y\end{cases} \tag{5.42}$$

$$S_z\left(N_c\right)=\begin{cases}\left[e_z(N_c)\right]^2\cdot 2t_f+\dfrac{\left(h-2t_f\right)\cdot t_w^2}{8} & if, N_c>h\cdot t_w\cdot f_y\\ \left[e_z(N_c)\right]^2\cdot h & if, N_c\le h\cdot t_w\cdot f_y\end{cases} \tag{5.43}$$

As in this case the axial force is predefined parameter, not dependent on the deformation, the moment corresponding to the full plastic yield can be calculated with the equations above. The plastic work can be expressed by the internal forces as the sum of the work of the axial force on the ε_N deformation and of the moment on the φ rotation. Regarding that the connection of the axial deformation and the rotation given by Eq. (5.29) is valid here also, the expressions can be rewritten:

$$\Delta W_{y,c}\left(\Delta\varphi\right)=N_c\cdot\varepsilon_N+M_{y,c}\left(N_c\right)\cdot\Delta\varphi=\left(N_c\cdot e_y\left(N_c\right)+M_{y,c}\left(N_c\right)\right)\cdot\Delta\varphi \tag{5.44}$$

$$\Delta W_{z,c}\left(\Delta\varphi\right)=N_c\cdot\varepsilon_N+M_{z,c}\left(N_c\right)\cdot\Delta\varphi=\left(N_c\cdot e_z\left(N_c\right)+M_{z,c}\left(N_c\right)\right)\cdot\Delta\varphi \tag{5.45}$$

In order to investigate the effect of the axial force on the plastic dissipation of a column section, in *Figure 5.15* the normalized axial force against the internal work of the H section divided by the work of the section in pure bending is presented. The work in pure bending is:

$$\Delta W_{pl,y,c}\left(\Delta\varphi\right)=Q_{pl,y,c}\cdot f_y\cdot\Delta\varphi \tag{5.46}$$

$$\Delta W_{pl,z,c}\left(\Delta\varphi\right)=Q_{pl,z,c}\cdot f_y\cdot\Delta\varphi \tag{5.47}$$

It is noted, that the two diagrams are independent of the rotation itself, because dividing Eq. (5.44) or (5.45) by Eq. (5.46) or (5.47) we can simplify with the rotation.

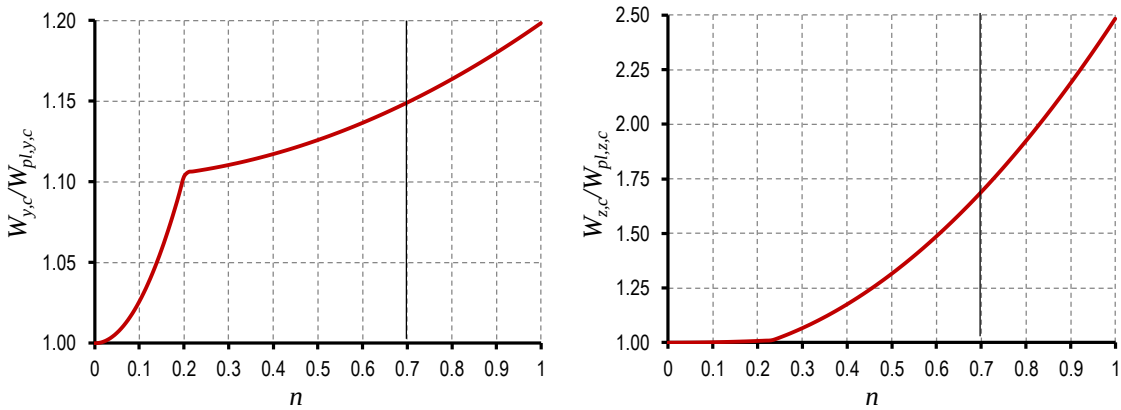

a) bending about y axis *b) bending about z axis*

Figure 5.15*; Dissipation of column cross section as a function of the axial force*

Both curves of *Figure 5.15* can be divided into two parts. When the section is bent about the y axis the internal work grows rapidly while the area of the normal force distribution is in the web as both the eccentricity and the axial force is growing. Beyond the point where the eccentricity reaches the flange plates, only the axial force keeps changing significantly, so the increase of the work becomes more moderate. Conversely, in the case of bending about the z axis, the rotational work is not modified significantly by the normal force as long as the A_N area is located within the web. However, after the area reaches the flanges also, the eccentricity grows rapidly and this leads to the rise of the internal work. Though the increase is significant in the later case, it has to be noted, that the values roughly over 0.7 normalized axial force are practically not attainable as the normal force usually does not exceed this rate in actual examples.

The model that has been presented so far for the determination of the column plastic work on one hand overestimates the actual work, as in reality the local buckling of the walls precedes the development of the full plastic deformation. On the other hand, its dependence on the axial force may cause difficulties further on. The axial force of the columns is primarily defined by the gravity loads, but the lateral seismic loading also causes significant tension or compression in the columns of the braced bay, see *Figure 5.16*. Consequently, the axial force is unknown as the λ load multiplier is also unknown, and λ cannot even be expressed from the equations given for the work of the column above. Therefore, the dependence of the internal work on the load multiplier could prevent the definition of easy-to-use formulas as it will be demonstrated later.

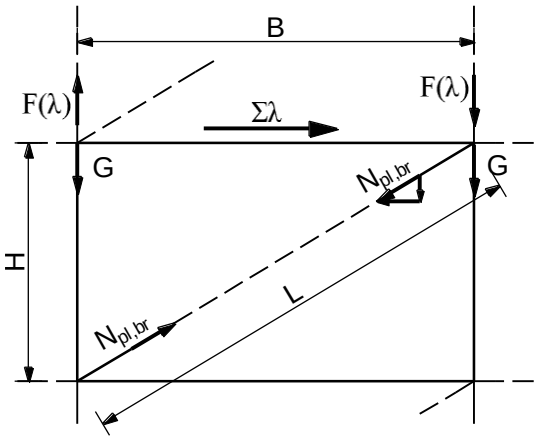

Figure 5.16*; Forces acting on a braced bay*

As the objective of the RSBD method is to give easy but effective conditions for the redesign of CBF-s, it is necessary to resolve this dependence. One possible solution is to consider a shear building model, where only the lateral equilibrium equations are satisfied [75]. In the following we come back again to the Eurocode 3 axial force – moment interaction curves to give another solution.

In Eurocode 3 the interaction of the axial force and the bending moment for both axes of an H-section is defined similarly to SHS sections. For bending about the first principal axis, y, the bending resistance is not decreased by the axial force if:

$$N_c \leq 0.25 N_{pl,c} \text{ and } N_c \leq \frac{0.5 \cdot h_w \cdot t_w \cdot f_y}{\gamma_{M0}} \tag{5.48}$$

where h_w is the height of the web of the section (h-2×t_f). For bending about the z axis the resistance is not decreased if:

$$n \leq a \text{ with } n = \frac{N_c}{N_{pl,c}} \text{ and } a = \frac{A_c - 2b \cdot t_f}{A_c} \leq 0.5 \tag{5.49}$$

If the criteria of Eqs. (5.44) or (5.45) are not met, the moment resistance is to be decreased with a linear expression in case of the y axis and a quadratic in case of the z.

$$M_{y,c}(N_c) = M_{pl,y,c} \cdot \frac{1-n}{1-0.5 \cdot a} \tag{5.50}$$

$$M_{z,c}(N_c) = M_{pl,z,c} \cdot \left[1 - \left(\frac{n-a}{1-a}\right)^2\right] \tag{5.51}$$

In *Figure 5.17* the yield surfaces and the interaction curves are presented for both axes. The difference of the two approaches for the y axis is less than it was for the SHS section of the brace. Considering, that the normalized axial force in the columns is usually larger than 0.4, both methods give practically the same result. The two curves corresponding to the bending about the z axis are even better matches.

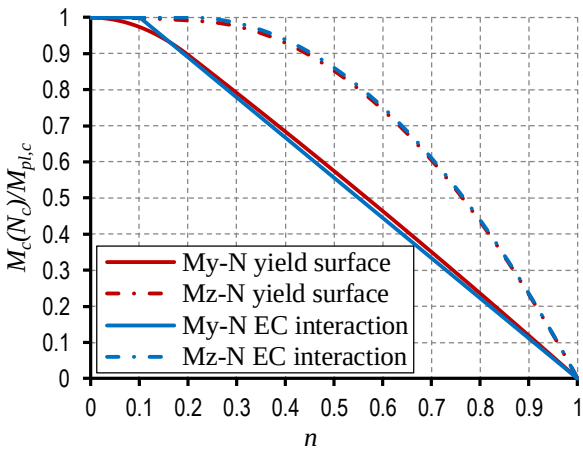

Figure 5.17*; Nonlinear yield surfaces and EC3 interaction curves of H-section*

Considering the bilinear interaction curve and denoting the end of the constant moment part by N_{lim}, given by Eq. (5.48), on the normal force axis, the bending is:

$$M_{y,c}(N_c)=\begin{cases} M_{pl,y,c} & N_c \le N_{\lim} \\ \dfrac{N_{pl,c}-N_c}{N_{pl,c}-N_{\lim}} M_{pl,y,c} & N_c > N_{\lim} \end{cases} \tag{5.52}$$

As it has been presented before in Eqs. (5.26) and (5.28), the eccentricity of the neutral axis can be determined by derivation of the expression above. With the eccentricity, the axial deformation can be calculated, see Eq. (5.29).

$$e_y\left(N_c\right)=\begin{cases} 0 & N_c \le N_{\lim} \\ \dfrac{M_{pl,y,c}}{N_{pl,c}-N_{\lim}} & N_c > N_{\lim} \end{cases} \tag{5.53}$$

Expressing the work of the columns the same way as before in Eq. (5.44) we get:

$$\Delta W_{y,c}\left(\Delta\varphi\right)=\left(M_{y,c}\left(N_c\right)+N_c\cdot e_y\left(N_c\right)\right)\Delta\varphi=$$

$$=\begin{cases} M_{pl,y,c}\cdot\Delta\varphi & N_c \le N_{\lim} \\ \left(\dfrac{N_{pl,c}}{N_{pl,c}-N_{\lim}} M_{pl,y,c} - \cancel{\dfrac{N_c}{N_{pl,c}-N_{\lim}} M_{pl,y,c}} + \cancel{N_c \dfrac{M_{pl,y,c}}{N_{pl,c}-N_{\lim}}}\right)\Delta\varphi & N_c > N_{\lim} \end{cases} \tag{5.54}$$

$$\Delta W_{y,c}\left(\Delta\varphi\right)=\begin{cases} M_{pl,y,c}\cdot\Delta\varphi & N_c \le N_{\lim} \\ \dfrac{N_{pl,c}}{N_{pl,c}-N_{\lim}} M_{pl,y,c}\cdot\Delta\varphi & N_c > N_{\lim} \end{cases} \tag{5.55}$$

As it can be seen, the bilinear interaction curve simplifies the strong dependence of the plastic work on the axial force into two intervals. The choice of the suitable expression from Eq. (5.55) still depends on the axial force, but this can only lead to a two-step iteration i.e. supposing one scenario, verifying the assumption and perhaps modify the choice. The use of the Eurocode 3 interaction curve for the y axis is therefore favourable as it is bilinear. In order to be able to do the same simplification for the columns bent about the z axis, that interaction curve has to be bilinearised also. In order to do so, an appropriately chosen n_{lim} needs to be determined, which is the limit axial force as before in normalised format. Let us compute the difference of the nonlinear interaction curve and its bilinear approximation as the integral of the square of the differences:

$$diff=\int_0^1\left[\left(1-\left(\frac{n-a}{1-a}\right)^2\right)-\frac{n_{pl,c}-n}{n_{pl,c}-n_{\lim}}\right]^2 dn \tag{5.56}$$

Defining n_{lim} to make the above difference minimal gives an optimal definition of the bilinear interaction curve. For most H-section columns used in the CBF-s of the present research the limit has been found to be between 0.45 and 0.5. The bilinearisation of the M_z – N interaction curve leads to having the same expression for the work of the column when bent about the z axis as the one given for y axis in Eq. (5.55). Nevertheless, the calculation of the work of the columns is still not definite due to a particular characteristic of CBF-s.

The internal work of the columns is considered only in storey mechanisms and obviously only on the floor of the mechanism itself. In a building all the columns, a total number of *m*, may participate in the lateral resistance depending on the stiffness of the column splices. The peak values of the bending moment diagram, see *Figure 5.18*,

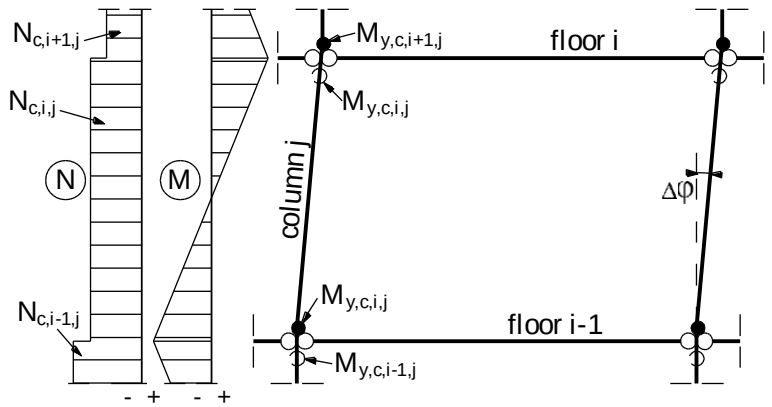

Figure 5.18*; Internal forces and plastic hinges of columns in storey mechanism*

are located at the floor slabs. As the beams are usually connected to the columns, in a conventional CBF, by hinges, the moment peaks may form a plastic hinge right above or under the floor slabs, where the cross-sections may be different. Furthermore, for the determination of the plastic moment resistance the significant axial forces in the columns have to be considered also. As these increase at every floor slab, the resistance of the column below a certain slab is not necessarily larger than the one above. Consequently, attention is to be paid to appropriately select the smallest resistance at both floor slabs of the analysed storey. For each column a pointer vector can be defined that identifies which column cross-sections work has to be considered in the computation. The pointer vector, *J*, can have zero or one values. The vector for the jth column on the ith floor, assuming bending about the y axis is:

$$\mathbf{J}_{i,j} = \begin{bmatrix} if\ M_{y,c,i-1,j} < M_{y,c,i1,j}\ then\ 1,\ otherwise\ 0 \\ if\ M_{y,c,i-1,j} > M_{y,c,i1,j}\ then\ 1,\ otherwise\ 0 \\ if\ M_{y,c,i+1,j} > M_{y,c,i1,j}\ then\ 1,\ otherwise\ 0 \\ if\ M_{y,c,i+1,j} < M_{y,c,i1,j}\ then\ 1,\ otherwise\ 0 \end{bmatrix} \tag{5.57}$$

It is important, that in the case of hinged column splices, the corresponding member or members are considered to be zero in the vector above. By the pointer vector, the total internal work of a column is computed as follows:

$$\Delta W_{col,i,j}(\Delta\varphi) = \left[\Delta W_{y,c,i-1,j}(\Delta\varphi) \quad \Delta W_{y,c,i,j}(\Delta\varphi) \quad \Delta W_{y,c,i,j}(\Delta\varphi) \quad \Delta W_{y,c,i+1,j}(\Delta\varphi)\right] \cdot \mathbf{J}_{i,j} \tag{5.58}$$

This equation can be rewritten by factoring the φ rotation:

$$\Delta W_{col,i,j}(\Delta\varphi) = \left[M^{sub}_{y,c,i-1,j} \quad M^{sub}_{y,c,i,j} \quad M^{sub}_{y,c,i,j} \quad M^{sub}_{y,c,i+1,j}\right]\Delta\varphi \cdot \mathbf{J}_{i,j} \tag{5.59}$$

where M^{sub} is a moment resistance substituting the one given by Eq. (5.52):

$$M^{sub}_{y,c} = \begin{cases} M_{pl,y,c} & N_c \le N_{\lim} \\ \dfrac{N_{pl,c}}{N_{pl,c} - N_{\lim}} M_{pl,y,c} & N_c > N_{\lim} \end{cases} \tag{5.60}$$

The previous three equations are valid for columns bent about the z axis also with the appropriate changes in the lower indices. For every column the product of the substituting moments and the pointer vector can be interpreted as a total moment that has to be used for the determination of the plastic work:

$$M_{col,i,j} = \begin{matrix} \left[M^{sub}_{y,c,i-1,j} \quad M^{sub}_{y,c,i,j} \quad M^{sub}_{y,c,i,j} \quad M^{sub}_{y,c,i+1,j} \right] \\ or \\ \left[M^{sub}_{z,c,i-1,j} \quad M^{sub}_{z,c,i,j} \quad M^{sub}_{z,c,i,j} \quad M^{sub}_{z,c,i+1,j} \right] \end{matrix} \cdot \mathbf{J}_{i,j} \tag{5.61}$$

By substituting Eqs. (5.61) and (5.7) into Eq. (5.59) and by summing up all the columns, the internal work of the columns in the storey mechanism is expressed as a function of the lateral drift as follows:

$$\Delta W_{col,i}\left(\Delta B\right) = \sum_{j=1}^{m} M_{col,i,j} \cdot \frac{\Delta B_i}{H_i} \tag{5.62}$$

5.2.4. External work of the lateral loading

In the RSBD method the seismic loading is defined as horizontal concentrated forces applied at the height of the floor slabs. The forces are defined by an unknown parameter, denoted by λ, and to account for the variability of the masses, it is multiplied by a reduced mass vector, m_p. This vector is defined as the sum of the masses on a storey divided by the smallest of all the storey masses. If the mass is constant along the height, the vector is an identity vector; otherwise it shows the ratio of the overweight of the particular floors.

$$mp_i = \frac{\sum_j m_{i,j}}{\min\left(\sum_j m_{i,j}\right)} \tag{5.63}$$

The loading is distributed from the top down to the floor under investigation. In an n storey-tall building n different load patterns can be defined. The i index appended to the load parameter refers to a distribution ranging from the ith storey up. According to the basic idea of the RSBD method, the works are computed for global and local plastic mechanisms, so for the n load arrangements n load multiplier pairs, $\lambda_{glob,i}$ and $\lambda_{loc,i}$, have to be calculated.

Figure 5.19 depicts the relevant external loads of a CBF. Both the global and the storey mechanism are predefined; their shape is described by the ΔB_i lateral displacement, which is equal on every storey if the storey heights are equal in the whole building. In the local mechanism the lateral forces are equally displaced, their work is:

$$\Delta W_{\lambda,loc,i}\left(\Delta B\right) = \Delta B_i \cdot \lambda_{loc,i} \cdot \sum_{k=i}^{n} mp_k \tag{5.64}$$

In the global mechanism the lateral displacement increases with the height of the building. Therefore, for every concentrated loading involved in the mechanism, the lateral displacement has to be calculated individually. The external work can be computed as follows:

$$\Delta W_{\lambda,glob,i}\left(\Delta B\right) = \lambda_{glob,i} \cdot \sum_{k=i}^{n}\left(mp_k \cdot \sum_{l=1}^{k} \Delta B_l \right) \tag{5.65}$$

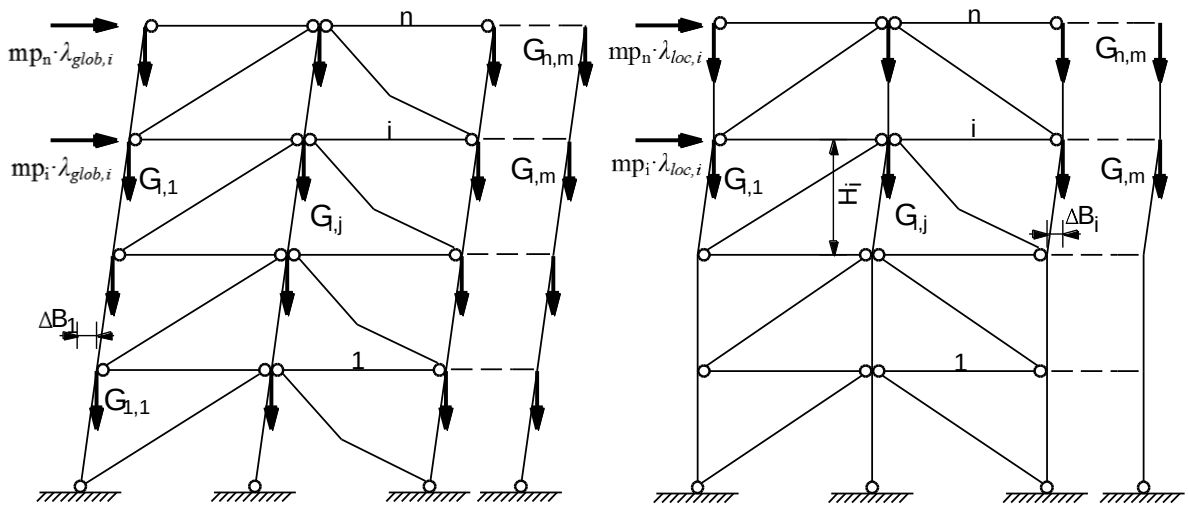

Figure 5.19*; External work of lateral loading and gravity forces*

5.2.5. External work of the gravity forces

On the n floors the m columns create $n \times m$ beam-column intersections and the gravity forces are concentrated into these intersections. The gravity forces perform their work on vertical displacements of which two kinds can be distinguished. Firstly, in both mechanisms due to the nonlinear approximation of the geometry, see Eqs. (5.6) and Eq. (5.8), the vertical, rigid-body displacements of the slabs can be calculated. This displacement accounts for the second-order work of the gravity forces. Moreover, in a storey mechanism the axial shortening that is realized in the plastic hinges of the columns also results in vertical displacement of the gravity forces. In *Figure 5.20* the vertical displacement due to the column displacement and deformation is depicted. The figure corresponds to a column that is continuous at both ends. If one or both splices are hinged, then there is no plastic shortening on these ends. By the use of the pointer vector already presented before, the total shortening of a column, assuming the bilinearization of the M-N curve, is:

$$\Delta\varepsilon_{N,i,j} = \begin{bmatrix} e_{y,i-1,j} & e_{y,i,j} & e_{y,i,j} & e_{y,i+1,j} \end{bmatrix} \cdot \mathbf{J}_{i,j} \cdot \Delta\varphi = e_{col} \cdot \Delta\varphi \tag{5.66}$$

The product of the eccentricities and the pointer vector can be denoted by a total eccentricity, similarly as it has been done with the moments in Eq. (5.61). Thus the work of a concentrated P force applied on the top of a column is:

$$\begin{aligned} \Delta W_P(\Delta\varphi) &= P\left(\Delta H + e_{col} \cdot \Delta\varphi \cdot \cos\Delta\varphi\right) = P\left[H\frac{\Delta\varphi^2}{2} + e_{col} \cdot \Delta\varphi \cdot \left(1 - \frac{\Delta\varphi^2}{2}\right)\right] = \\ &= P\left[H\frac{\Delta\varphi^2}{2} + e_{col} \cdot \Delta\varphi - e_{col}\frac{\Delta\varphi^3}{2}\right] \end{aligned} \tag{5.67}$$

In the expression above the third member in the brackets is very small compared to the first two, therefore it can be neglected. Considering all the concentrated gravity forces and columns and substituting Δφ by Eq. (5.7), the work of the columns in a storey mechanism is:

$$\Delta W_{G,loc,i}(\Delta B) = \sum_{k=i}^{n}\sum_{l=1}^{m}\left[G_{k,l} \cdot \left(\frac{\Delta B_i^2}{2H_i} + e_{col,l} \cdot \frac{\Delta B_i}{H_i}\right)\right] \tag{5.68}$$

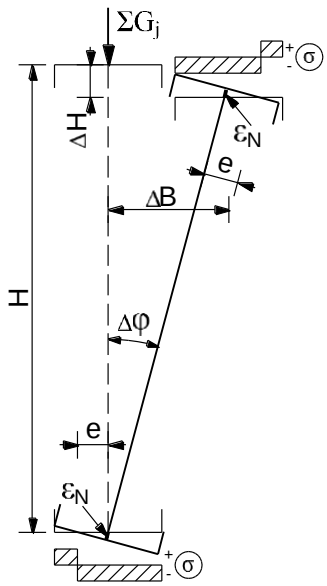

Figure 5.20*; Displacements and deformations of a column in a storey mechanism*

In the global plastic mechanism every gravity force has to be taken into consideration. The vertical displacements, coming only from the second order shortening this time, are the same on the one floor, but with the height they increase. The work of the gravity forces are computed with the formula below:

$$\Delta W_{G,glob}\left(\Delta B\right)=\sum_{k=1}^{n}\left[\sum_{l=1}^{m}G_{k,l}\cdot\frac{\left(\sum_{k=1}^{i}\Delta B_k\right)^2}{2\sum_{k=1}^{i}H_k}\right] \tag{5.69}$$

5.2.6. Energy equivalence, determination of load multipliers

In order to express the load multipliers needed to evaluate the two criteria of the RSBD method we consider the equivalence of the external and the internal works in both the local and global mechanisms. In case of the global mechanism the equation is as follows:

$$\Delta W_{\lambda,glob,i}+\Delta W_{G,glob}=\sum_{i}\Delta W_{t,br,i} \tag{5.70}$$

Substituting Eqs. (5.30), (5.65) and (5.69) into Eq. (5.70) we get:

$$\lambda_{glob,i}\cdot\sum_{k=i}^{n}\left(mp_k\cdot\sum_{l=1}^{k}\Delta B_l\right)+\sum_{k=1}^{n}\left[\sum_{l=1}^{m}G_{k,l}\cdot\frac{\left(\sum_{k=1}^{i}\Delta B_k\right)^2}{2\sum_{k=1}^{i}H_k}\right]=\sum_{i}N_{pl,br,i}\cdot\Delta B_i\cdot\cos\alpha_i \tag{5.71}$$

In case of the local mechanism the energy equivalence is as the following:

$$\Delta W_{\lambda,loc,i}+\Delta W_{G,loc,i}=\Delta W_{t,br,i}+\Delta W_{col,i} \tag{5.72}$$

Substituting Eqs. (5.30), (5.62), (5.64) and (5.68) into Eq. (5.72) we get:

$$\Delta B_i \cdot \lambda_{loc,i} \cdot \sum_{k=i}^{n} mp_k + \sum_{k=i}^{n}\sum_{l=1}^{m}\left[G_{k,l} \cdot \left(\frac{\Delta B_i^2}{2H_i} + e_{col,l} \cdot \frac{\Delta B_i}{H_i}\right)\right] = \\ = N_{pl,br,i} \cdot \Delta B_i \cdot \cos\alpha_i + \sum_{j=1}^{m} M_{col,i,j} \cdot \frac{\Delta B_i}{H_i} \tag{5.73}$$

The equation above can be further simplified by collating the work of the columns and the gravity forces. Let us emphasize these parts of the equation. Furthermore, let us consider only one column, where the gravity forces to be considered are simply denoted by G, the eccentricity is e_y and the moment is $M_{y,c}^{sub}$:

$$\ldots + G \cdot \left(\frac{\Delta B_i^2}{2H_i} + e_y \cdot \frac{\Delta B_i}{H_i}\right) = \ldots + M_{y,c}^{sub} \cdot \frac{\Delta B_i}{H_i} \tag{5.74}$$

Substituting Eq. (5.53) and (5.60) into Eq. (5.74) we get:

$$\ldots + G \cdot \frac{\Delta B_i^2}{2H_i} = \ldots + \left\{\begin{matrix} M_{pl,y,c} & N_c \le N_{\lim} \\ \dfrac{N_{pl,c}}{N_{pl,c} - N_{\lim}} M_{pl,y,c} & N_c > N_{\lim} \end{matrix}\right\} \cdot \frac{\Delta B_i}{H_i} - \\ -G \cdot \left\{\begin{matrix} 0 & N_c \le N_{\lim} \\ \dfrac{M_{pl,y,c}}{N_{pl,c} - N_{\lim}} & N_c > N_{\lim} \end{matrix}\right\} \cdot \frac{\Delta B_i}{H_i} \tag{5.75}$$

By re-arranging the equation we get:

$$\ldots + G \cdot \frac{\Delta B_i^2}{2H_i} = \ldots + \left\{\begin{matrix} M_{pl,y,c} & N_c \le N_{\lim} \\ \dfrac{N_{pl,c} - G}{N_{pl,c} - N_{\lim}} M_{pl,y,c} & N_c > N_{\lim} \end{matrix}\right\} \cdot \frac{\Delta B_i}{H_i} \tag{5.76}$$

On the right side of the expression above we can see a modified version of the substituting moment defined by Eq. (5.60). Here the moment is reduced by the effect of the gravity forces. Let us denote the total reduced column moment as defined by Eq. (5.61), after the operation with the pointer vector, as $M_{red,i,j}$ referring to the total reduced moment of a column. With this new column representation Eq. (5.73) is:

$$M_{red,i,j} = \begin{matrix} \left[M_{y,c,i-1,j}^{red} \quad M_{y,c,i,j}^{red} \quad M_{y,c,i,j}^{red} \quad M_{y,c,i+1,j}^{red}\right] \\ or \\ \left[M_{z,c,i-1,j}^{red} \quad M_{z,c,i,j}^{red} \quad M_{z,c,i,j}^{red} \quad M_{z,c,i+1,j}^{red}\right] \end{matrix} \cdot \mathbf{J}_{i,j} \tag{5.77}$$

$$\Delta B_i \cdot \lambda_{loc,i} \cdot \sum_{k=i}^{n} mp_k + \sum_{k=i}^{n}\sum_{l=1}^{m} G_{k,l} \cdot \frac{\Delta B_i^2}{2H_i} = N_{pl,br,i} \cdot \Delta B_i \cdot \cos\alpha_i + \sum_{j=1}^{m} M_{red,i,j} \cdot \frac{\Delta B_i}{H_i} \tag{5.78}$$

From Eq. (5.71) and Eq. (5.78) both the global and the local multipliers can be expressed explicitly. However, it has to be noted, that for the determination of the local multiplier a two-step iteration may be needed as the reduced moment depends on the axial force, which is affected by the lateral loading for certain columns.

$$\lambda_{glob,i} = \frac{\sum_i N_{pl,br,i} \cdot \Delta B_i \cdot \cos\alpha_i - \sum_{k=1}^{n} \left[\sum_{l=1}^{m} G_{k,l} \cdot \frac{\left(\sum_{k=1}^{i} \Delta B_k \right)^2}{2 \sum_{k=1}^{i} H_k} \right]}{\sum_{k=i}^{n} \left(mp_k \cdot \sum_{l=1}^{k} \Delta B_l \right)} \tag{5.79}$$

$$\lambda_{loc,i} = \frac{N_{pl,br,i} \cdot \Delta B_i \cdot \cos\alpha_i + \sum_{j=1}^{m} M_{red,i,j} \cdot \frac{\Delta B_i}{H_i} - \sum_{k=i}^{n} \sum_{l=1}^{m} G_{k,l} \cdot \frac{\Delta B_i^2}{2H_i}}{\Delta B_i \cdot \sum_{k=i}^{n} mp_k} \tag{5.80}$$

The formula for the calculation of λ_{br}, which is necessary for the determination of the BPR is Eq. (5.80) neglecting the participation of the columns:

$$\lambda_{br,i} = \frac{N_{pl,br,i} \cdot \Delta B_i \cdot \cos\alpha_i - \sum_{k=i}^{n} \sum_{l=1}^{m} G_{k,l} \cdot \frac{\Delta B_i^2}{2H_i}}{\Delta B_i \cdot \sum_{k=i}^{n} mp_k} \tag{5.81}$$

So far the formulas have been derived with respect to second order effects i.e. supposing that the lateral displacement is not infinitesimal. In classical limit state analysis the work is calculated by introducing an infinitesimally small variation of the geometrically admissible displacement field to the initial perfect geometry. In the present study this variation is defined by the lateral drift, *ΔB*. When *ΔB* is infinitesimally small, i.e. closely zero, it eliminates the second order works of the gravity forces, resulting in the following, simplified expressions for the load multipliers:

$$\lambda_{glob,i}^{\lim A} = \frac{\sum_i N_{pl,br,i} \cdot \cos\alpha_i}{\sum_{k=i}^{n} \left(mp_k \cdot \sum_{l=1}^{k} l \right)} \tag{5.82}$$

$$\lambda_{loc,i}^{\lim A} = \frac{N_{pl,br,i} \cdot \cos\alpha_i + \sum_{j=1}^{m} M_{red,i,j} \cdot \frac{1}{H_i}}{\sum_{k=i}^{n} mp_k} \tag{5.83}$$

$$\lambda_{br,i}^{\lim A} = \frac{N_{pl,br,i} \cdot \cos\alpha_i}{\sum_{k=i}^{n} mp_k} \tag{5.84}$$

In the seismic response of building structures the drifts are moderate though, but hardly infinitesimally small. Consequently, the large gravity forces may substantially affect the results that we could obtain with the presented first order limit state analysis. In order to examine and validate this effect, various separated storeys of CBF61 and 81 were analysed by means of pushover analysis and also, to a series of predefined lateral displacements, the storey shear has been computed by Eq. (5.80). A schematic model for the pushover analysis is presented in *Figure 5.21/a*. As it can be seen the storeys above and below a specific storey were replaced by equivalent springs and besides the constant gravity forces the parametric

lateral loading has been applied. In *Figure 5.21/b* only two characteristic pushover curves (of CBF61, 6th and 4th floor) and the corresponding results of Eq. (5.80) are depicted as the results of the various other floors strongly overlap.

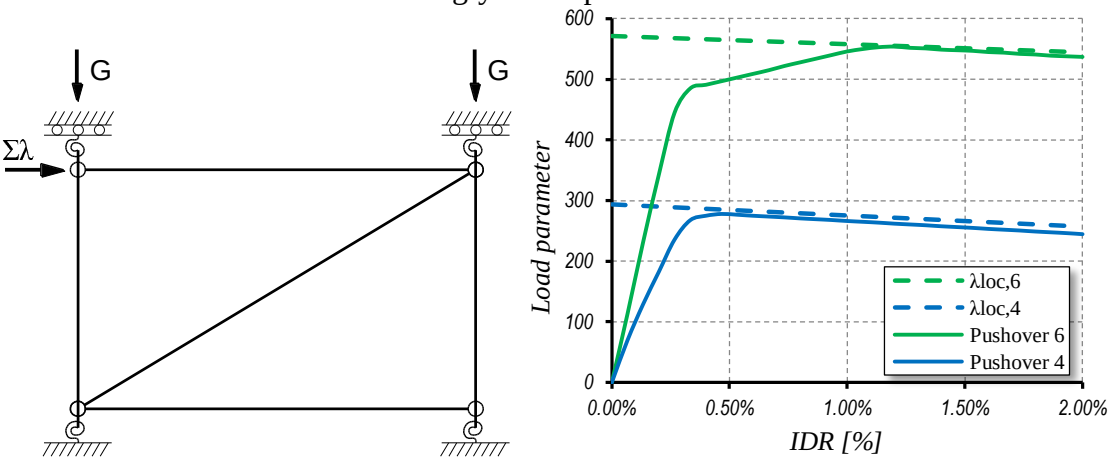

a) schematic model for Pushover analysis *b) Pushover and 2nd order RSBD curves*

Figure 5.21*; Storey pushover and 2nd order RSBD results*

As it can be seen in the diagram above, the local load multiplier results of the RSBD analysis may give a good upper estimate of the pushover curves beyond a certain interstorey drift. The depicted interstorey drift ratio range is realizable in a seismic situation and in this range the decrease of the load multiplier may be more than 10% of the results that can be obtained by limit analysis (0.00%). Furthermore, in later paragraphs of this chapter it will be demonstrated, that by limit analysis unnecessarily conservative designs can be obtained. Consequently, for the above reasons it is recommended that the RSBD method is applied with second order computations, considering Eqs. (5.79) (5.80) and (5.81) and a predefined lateral drift. The redesigns that are to be introduced in the following were obtained considering 2% lateral drift, which is the acceptance limit, unless specified otherwise.

5.3. Application of the Robust Seismic Brace Design method

Both the reason of the development and the underlying ideas of the RSBD method were the observed results coming from a series of CBF analyses, which were presented in Chapter 3. In order to verify the viability of the redesign method in the following we will attempt to enhance the response of all the introduced CBF-s by making modification so that the buildings comply with the RSBD criteria. On one hand the original designs will be evaluated with the RSBD method to see whether the method is capable to identify the problematic storeys. This will be followed by the redesign of the CBF-s and the same IDA process that can demonstrate the sufficiency of the RSBD method. Besides the CBF – CBF (type 1) and MRF – CBF (type 2) buildings and the irregular examples (q=5 and irregular mass), redesigns where only the braces or the columns are modified and redesigns where the limit analysis RSBD method is applied will also be presented.

5.3.1. Performance of the reinforced type 1 and type 2 CBF-s

Below for each CBF structure two tables and two IDA diagrams are presented. The tables show the important cross sections, the storey overstrength and the RSBD method load multiplier and BPR results. In the first table, which corresponds to the original EC8 design, the inadequacies of the load multipliers (first criterion) and the maximum and minimum BPR (second criterion) are in bold letters. In the second table, the modified cross sections and also the maximum and minimum BPR are bold. Below each table the ratio of the largest and smallest storey overstrength, required to be below 1.25 by Eurocode 8 is also indicated.

Taking a look at the numerous examples below, one can see that the RSBD method fairly accurately indicates the location of the weak storey(s) in the EC8 designs. Furthermore, the more amplified the weak storey phenomenon is, the more the RSBD criteria are violated. One may also notice that in the type 2 (MRF – CBF) buildings the weak storey behaviour is mitigated and therefore they require less reinforcement of the columns, but mostly the same of the braces, compared to the type 1 (CBF – CBF) structures. As the reinforcement of the braces of any floor increases the global load multiplier, during the redesign process the need of reinforcing floors below the ones that were found to be weak in the first (a) tables arises. This shows that with the RSBD method cases where the reinforcement causes the weak storey occurrence to shift to another storey, as it was demonstrated in Chapter 3, 3.3.2, can be successfully prevented. The reinforced CBF-s usually do not meet the requirement of the uniformity condition. Nevertheless, the response of each and every building provides lot slimmer families of curves than of the original designs, which shows that a favourable, well distributed dissipative behaviour is realized with the redesign. These RSBD designs are also adequate, early failure is not observed; in fact the buildings tend to be a lot better performing than necessary, reaching failure at elevated scale factors. The failure typically occurs on the first and second floors in the form of rapid increase of the storey drifts that refers to collapse by instability. This however is not weak storey collapse as it is not preceded by weak storey behaviour. After all, a bent cantilever beam is also expected to break only in one cross section close to the restrain.

In the cases of CBF82,101 and 102 one can observe that the top floor is presumably over reinforced by the RSBD method as the curve of this storey deviates from the rest towards the lower drift regions. Nevertheless, the discrepancy under consideration only occurs at high scale factors in the diagrams and it has a moderate effect on the response.

Table 5.1a; *CBF41-EC8*

storey	*int.col.*	*ext.col.*	*brace*	*Ω*	λ_{loc}	λ_{glob}	$\frac{\lambda_{loc}}{\lambda_{glob}}$	*BPR*
4	HEA 160	HEA 140	100×4	1.05	**342.5**	**471.6**	**0.73**	**0.70**
3	HEB 180	HEA 200	100×6.3	0.99	291.8	269.5	1.08	0.91
2	HEB 220	HEB 200	100×8	0.97	255.5	209.6	1.22	**0.95**
1	HEB 260	HEB 240	100×10	0.99	193.1	188.7	1.02	0.95

$\Omega_{max}/\Omega_{min}$=1.08

Table 5.1b; *CBF41-RSBD*

storey	*int.col.*	*ext.col.*	*brace*	*Ω*	λ_{loc}	λ_{glob}	$\frac{\lambda_{loc}}{\lambda_{glob}}$	*BPR*
4	HEA 160	**HEA 200**	**100×5**	**1.30**	510.2	490.4	1.04	**0.84**
3	HEB 180	**HEA 220**	100×6.3	0.99	369.9	280.2	1.32	0.88
2	HEB 220	**HEB 240**	100×8	0.97	307.8	217.9	1.41	**0.91**
1	HEB 260	**HEB 260**	100×10	0.99	211.5	196.1	1.08	0.91

$\Omega_{max}/\Omega_{min}$=1.34

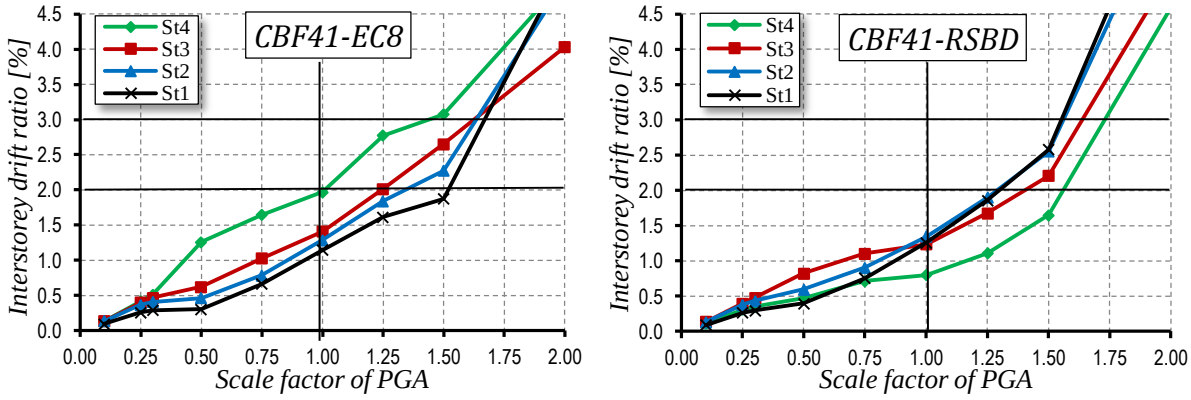

Figure 5.22; *IDA diagrams of 4-storey CBFs (averages of 7 records)*

Table 5.2a; *CBF42-EC8*

storey	*int.col.*	*ext.col.*	*brace*	*Ω*	λ_{loc}	λ_{glob}	$\frac{\lambda_{loc}}{\lambda_{glob}}$	*BPR*
4	HEA 180	HEA 200	100×4	1.09	**427.9**	**467.2**	**0.92**	**0.63**
3	HEB 180	HEB 200	100×6	0.97	355.0	267.0	1.33	0.77
2	HEB 220	HEB 220	100×8	1.00	321.6	207.6	1.55	**0.84**
1	HEB 260	HEB 280	100×10	1.04	226.1	186.9	1.21	0.84

$\Omega_{max}/\Omega_{min}$=1.12

Table 5.2b; *CBF42-RSBD*

storey	*int.col.*	*ext.col.*	*brace*	*Ω*	λ_{loc}	λ_{glob}	$\frac{\lambda_{loc}}{\lambda_{glob}}$	*BPR*
4	HEA 180	HEA 200	**100×5**	**1.33**	516.6	483.7	1.07	**0.75**
3	HEB 180	HEB 200	100×6	0.98	375.6	276.4	1.36	0.75
2	HEB 220	HEB 240	100×8	1.00	336.4	215.0	1.56	**0.82**
1	HEB 260	HEB 280	100×10	1.05	232.7	193.5	1.20	0.81

$\Omega_{max}/\Omega_{min}$=1.36

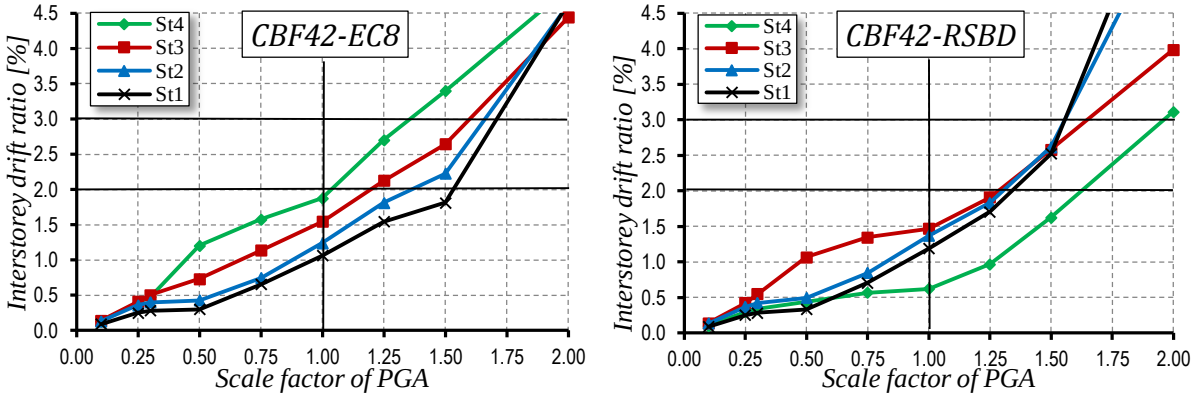

Figure 5.23; *IDA diagrams of 4-storey CBFs (averages of 7 records)*

Table 5.3a; *CBF61-EC8*

storey	*int.col.*	*ext.col.*	*brace*	*Ω*	λ_{loc}	λ_{glob}	$\frac{\lambda_{loc}}{\lambda_{glob}}$	*BPR*
6	HEA 160	HEA 160	90×5	1.00	**364.4**	**513.6**	**0.71**	**0.70**
5	HEB 180	HEA 180	100×6	0.98	**265.0**	**280.1**	**0.95**	0.81
4	HEB 220	HEB 200	100×8	1.04	245.7	205.4	1.20	0.91
3	HEB 240	HEB 220	100×10	1.04	230.7	171.2	1.35	**0.96**
2	HEB 280	HEB 240	100×10	1.01	197.7	154.1	1.28	0.90
1	HEB 300	HEB 280	120×10	1.00	148.8	146.7	1.01	0.90

$\Omega_{max}/\Omega_{min}$=1.06

Table 5.3b; *CBF61-RSBD*

storey	*int.col.*	*ext.col.*	*brace*	*Ω*	λ_{loc}	λ_{glob}	$\frac{\lambda_{loc}}{\lambda_{glob}}$	*BPR*
6	HEA 160	**HEA 200**	**100×6**	**1.32**	545.3	537.8	1.01	0.89
5	HEB 180	**HEA 200**	**100×6.3**	1.00	335.0	293.4	1.14	**0.84**
4	HEB 220	HEB 200	100×8	1.00	257.6	215.1	1.20	0.87
3	HEB 240	HEB 220	100×10	1.02	230.7	179.3	1.29	**0.91**
2	HEB 280	HEB 240	100×10	0.96	197.7	161.4	1.23	0.86
1	HEB 300	HEB 280	120×10	0.97	148.8	153.7	0.97	0.86

$\Omega_{max}/\Omega_{min}$=1.38

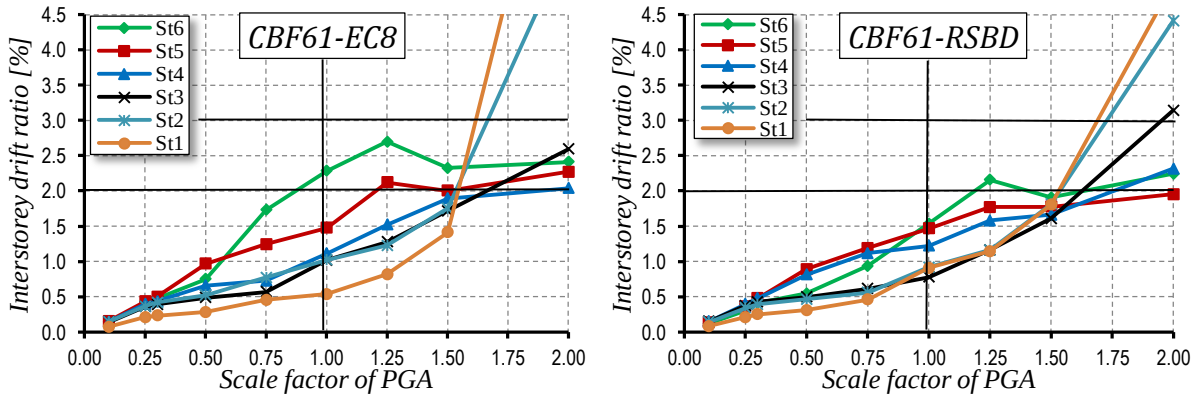

Figure 5.24; *IDA diagrams of 6-storey CBFs (averages of 7 records)*

Table 5.4a; *CBF62-EC8*

storey	*int.col.*	*ext.col.*	*brace*	*Ω*	λ_{loc}	λ_{glob}	$\frac{\lambda_{loc}}{\lambda_{glob}}$	*BPR*
6	HEA 180	HEA 180	90×5	1.00	**436.9**	**513.9**	**0.85**	**0.62**
5	HEB 180	HEB 180	100×6	0.98	343.1	280.3	1.22	0.72
4	HEB 240	HEB 200	100×8	1.01	316.2	205.5	1.54	0.80
3	HEB 260	HEB 240	100×10	1.04	300.6	171.3	1.75	**0.84**
2	HEB 280	HEB 260	100×10	0.99	272.6	154.2	1.77	0.78
1	HEB 320	HEB 320	120×10	1.00	186.0	146.8	1.27	0.78

$\Omega_{max}/\Omega_{min}$=1.06

Table 5.4b; *CBF62-RSBD*

storey	*int.col.*	*ext.col.*	*brace*	*Ω*	λ_{loc}	λ_{glob}	$\frac{\lambda_{loc}}{\lambda_{glob}}$	*BPR*
6	HEA 180	**HEB 180**	**100×5**	**1.15**	524.5	528.1	0.99	**0.70**
5	HEB 180	HEB 180	**100×6.3**	1.00	385.2	288.1	1.34	0.76
4	HEB 240	HEB 200	100×8	1.00	320.6	211.3	1.52	0.78
3	HEB 260	HEB 240	100×10	1.03	300.6	176.0	1.71	**0.81**
2	HEB 280	HEB 260	100×10	0.97	272.6	158.4	1.72	0.76
1	HEB 320	HEB 320	120×10	0.98	186.0	150.9	1.23	0.76

$\Omega_{max}/\Omega_{min}$=1.19

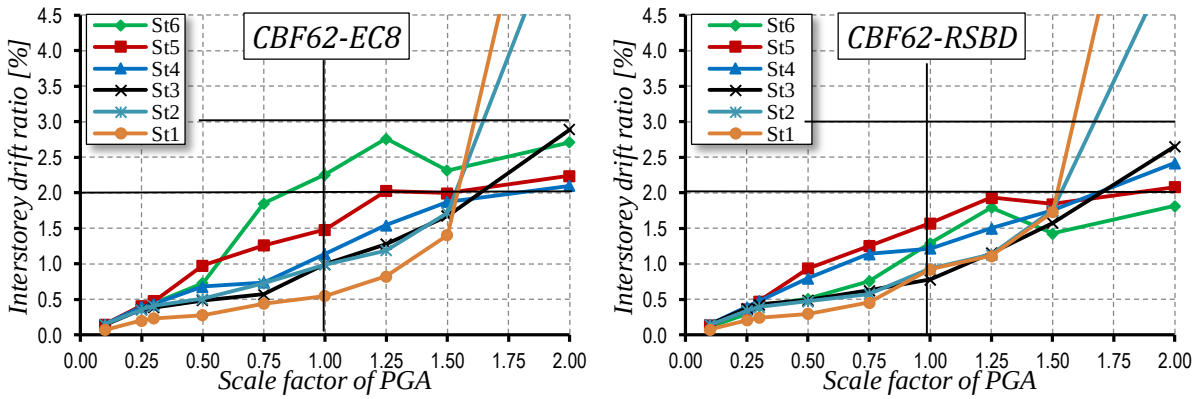

Figure 5.25; *IDA diagrams of 6-storey CBFs (averages of 7 records)*

Table 5.5a; *CBF81-EC8*

storey	*int.col.*	*ext.col.*	*brace*	*Ω*	λ_{loc}	λ_{glob}	$\frac{\lambda_{loc}}{\lambda_{glob}}$	*BPR*
8	HEA 160	HEA 160	90×5	0.99	**402.0**	**609.5**	**0.66**	**0.53**
7	HEB 180	HEA 180	100×6.3	1.05	**296.3**	**325.1**	**0.91**	0.67
6	HEB 220	HEB 200	100×8	1.01	245.0	232.2	1.05	0.71
5	HEB 240	HEB 220	100×10	1.10	229.0	187.5	1.22	0.77
4	HEB 280	HEB 240	120×10	1.01	217.5	162.5	1.34	**0.88**
3	HEB 300	HEB 280	120×10	0.98	192.3	147.8	1.30	0.78
2	HEM 240	HEB 320	140×10	0.98	210.8	139.3	1.51	0.85
1	HEM 240	HEM 240	140×10	1.00	147.2	135.5	1.09	0.74

$\Omega_{max}/\Omega_{min}$=1.07

Table 5.5b; *CBF81-RSBD*

storey	*int.col.*	*ext.col.*	*brace*	*Ω*	λ_{loc}	λ_{glob}	$\frac{\lambda_{loc}}{\lambda_{glob}}$	*BPR*
8	HEA 160	**HEA 240**	**100×6.3**	**1.40**	689.3	662.2	1.04	0.70
7	HEB 180	**HEA 240**	**100×8**	1.21	471.3	353.2	1.33	0.78
6	HEB 220	HEB 200	**100×10**	1.22	309.2	252.3	1.23	0.80
5	HEB 240	HEB 220	100×10	1.11	242.6	203.8	1.19	0.77
4	HEB 280	HEB 240	120×10	1.17	217.5	176.6	1.23	**0.80**
3	HEB 300	HEB 280	120×10	1.07	192.3	160.5	1.20	0.72
2	HEM 240	HEB 320	140×10	1.08	210.8	151.4	1.39	0.79
1	HEM 240	HEM 240	140×10	0.98	147.4	147.2	1.00	**0.69**

$\Omega_{max}/\Omega_{min}$=1.43

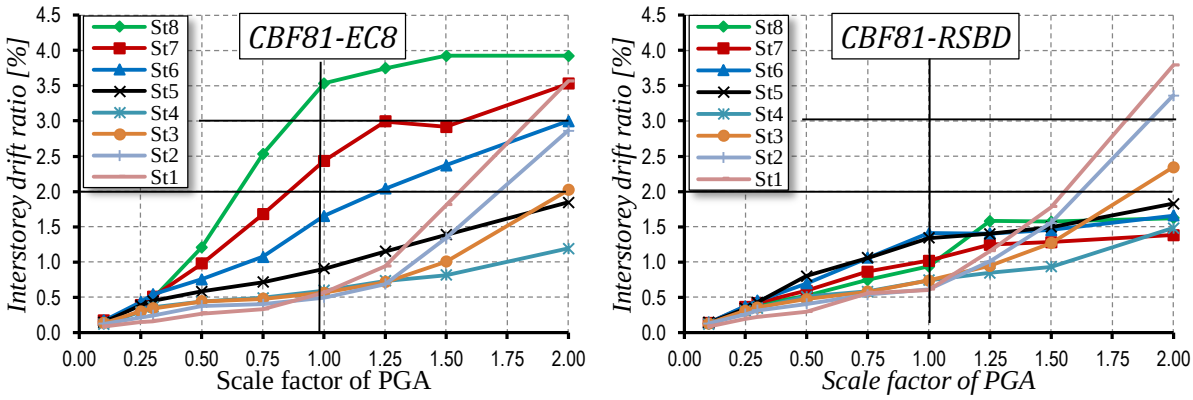

Figure 5.26; *IDA diagrams of 8-storey CBFs (averages of 7 records)*

Table 5.6a; *CBF82-EC8*

storey	*int.col.*	*ext.col.*	*brace*	*Ω*	λ_{loc}	λ_{glob}	$\frac{\lambda_{loc}}{\lambda_{glob}}$	*BPR*
8	HEA 180	HEA 200	90×5	1.02	**458.5**	**644.2**	**0.71**	**0.52**
7	HEB 180	HEB 180	100×6.3	0.99	370.3	343.6	1.08	0.66
6	HEB 220	HEB 200	100×8	0.99	310.5	245.4	1.27	0.70
5	HEB 260	HEB 240	100×10	1.03	306.0	198.2	1.54	0.77
4	HEB 280	HEB 260	120×10	1.13	308.6	171.8	1.80	**0.88**
3	HEB 300	HEB 300	120×10	1.03	282.0	156.2	1.81	0.79
2	HD320×158	HD320×158	140×10	1.08	306.0	147.2	2.08	0.86
1	HD360×179	HD320×158	140×10	1.01	198.7	143.2	1.39	0.76

$\Omega_{max}/\Omega_{min}$=1.14

Table 5.6b; *CBF82-RSBD*

storey	*int.col.*	*ext.col.*	*brace*	*Ω*	λ_{loc}	λ_{glob}	$\frac{\lambda_{loc}}{\lambda_{glob}}$	*BPR*
8	**HEB 180**	**HEB 180**	**110×6.3**	**1.55**	691.6	714.9	0.97	0.72
7	HEB 180	HEB 180	**100×8**	1.21	443.0	386.6	1.15	0.74
6	HEB 220	HEB 200	**100×10**	1.24	365.9	276.1	1.33	0.82
5	HEB 260	HEB 240	100×10	1.12	319.6	223.0	1.43	0.74
4	HEB 280	HEB 260	120×10	1.18	316.6	193.3	1.64	**0.82**
3	HEB 300	HEB 300	120×10	1.07	288.7	175.7	1.64	0.74

storey	*int.col.*	*ext.col.*	*brace*	*Ω*	λ_{loc}	λ_{glob}	$\frac{\lambda_{loc}}{\lambda_{glob}}$	*BPR*
2	HD 320x158	HD 320x158	140×10	1.10	306.0	165.7	1.85	0.76
1	HD 360x179	HD 320x158	140×10	1.00	203.7	161.1	1.26	**0.71**

$\Omega_{max}/\Omega_{min}$=1.55

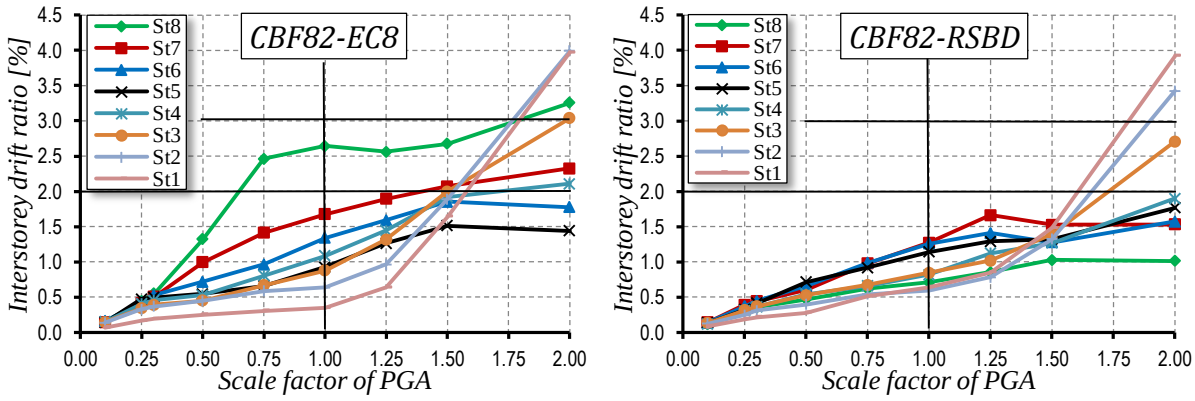

Figure 5.27; *IDA diagrams of 8-storey CBFs (averages of 7 records)*

Table 5.7a; *CBF101-EC8*

storey	*int.col.*	*ext.col.*	*brace*	*Ω*	λ_{loc}	λ_{glob}	$\frac{\lambda_{loc}}{\lambda_{glob}}$	*BPR*
10	HEA 160	HEA 160	100×5	0.98	**425.2**	**793.0**	**0.54**	**0.45**
9	HEB 180	HEA 180	100×8	1.00	**332.7**	**417.4**	**0.80**	0.62
8	HEB 220	HEB 200	100×10	1.00	**281.2**	**293.7**	**0.96**	0.68
7	HEB 240	HEB 220	120×10	1.11	279.1	233.2	1.20	0.84
6	HEB 280	HEB 260	120×10	1.02	235.5	198.2	1.19	0.76
5	HEB 300	HEB 280	140×10	1.07	233.1	176.2	1.32	0.85
4	HEM 240	HEB 320	140×10	1.01	209.5	161.8	1.29	0.77
3	HEM 240	HEM 240	140×12.5	1.09	224.4	152.5	1.47	**0.88**
2	HEM 260	HEM 260	140×12.5	1.03	203.3	146.9	1.38	0.79
1	HEM 280	HD320×198	150×12.5	0.98	142.3	144.2	**0.99**	0.70

$\Omega_{max}/\Omega_{min}$=1.13

Table 5.7b; *CBF101-RSBD*

storey	*int.col.*	*ext.col.*	*brace*	*Ω*	λ_{loc}	λ_{glob}	$\frac{\lambda_{loc}}{\lambda_{glob}}$	*BPR*
10	HEA 160	**HEA 220**	**100×10**	**1.73**	822.7	832.4	0.99	0.79
9	HEB 180	**HEA 220**	**100×10**	1.27	503.7	438.1	1.15	0.78
8	HEB 220	HEB 200	**110×10**	1.19	353.1	308.3	1.15	**0.80**
7	HEB 240	HEB 220	120×10	1.06	269.1	244.8	1.10	0.76
6	HEB 280	HEB 260	120×10	1.02	235.5	208.1	1.13	0.73
5	HEB 300	HEB 280	140×10	1.03	226.4	185.0	1.22	0.77
4	HEM 240	HEB 320	140×10	0.99	203.8	169.9	1.20	**0.70**
3	HEM 240	HEM 240	150×10	0.98	204.0	160.1	1.27	0.71
2	HEM 260	HEM 260	140×12.5	1.03	205.9	154.1	1.34	0.75
1	HEM 280	HD320×198	150×12.5	1.00	149.6	151.3	0.99	0.72

$\Omega_{max}/\Omega_{min}$=1.76

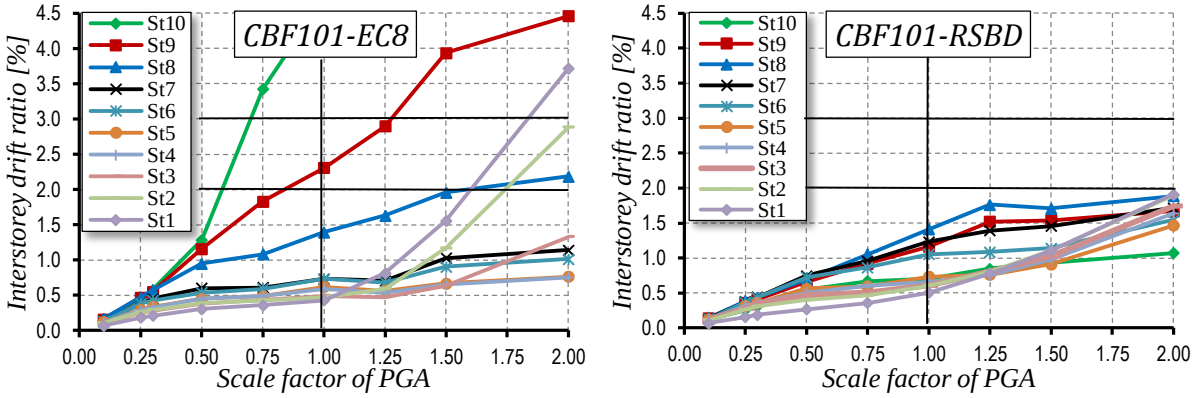

Figure 5.28; *IDA diagrams of 10-storey CBFs (averages of 7 records)*

Table 5.8a; *CBF102-EC8*

storey	*int.col.*	*ext.col.*	*brace*	Ω	λ_{loc}	λ_{glob}	$\frac{\lambda_{loc}}{\lambda_{glob}}$	*BPR*
10	HEA 180	HEB 180	100×5	1.02	**488.4**	**760.8**	**0.64**	**0.47**
9	HEB 180	HEB 180	100×8	1.02	406.5	400.4	1.02	0.65
8	HEB 220	HEB 220	100×10	1.02	347.3	281.8	1.23	0.71
7	HEB 260	HEB 240	120×10	1.10	345.2	223.8	1.54	0.83
6	HEB 280	HEB 280	120×10	1.01	306.0	190.2	1.61	0.75
5	HEB 300	HEB 320	140×10	1.07	309.8	169.1	1.83	**0.85**
4	HD320×158	HD320×158	140×10	1.00	301.1	155.3	1.94	0.76
3	HD320×158	HD360×179	150×10	0.99	309.4	146.3	2.11	0.78
2	HD360×179	HD360×196	140×12.5	1.06	324.7	140.9	2.30	0.82
1	HD360×196	HD400×237	140×12.5	1.00	205.4	138.3	1.48	0.73

$\Omega_{max}/\Omega_{min}$=1.10

Table 5.8b; *CBF102-RSBD*

storey	*int.col.*	*ext.col.*	*brace*	Ω	λ_{loc}	λ_{glob}	$\frac{\lambda_{loc}}{\lambda_{glob}}$	*BPR*
10	**HEB 180**	HEB 180	**100×10**	**1.90**	815.6	821.2	0.99	0.80
9	HEB 180	HEB 180	**100×10**	1.32	503.9	432.2	1.17	0.79
8	HEB 220	HEB 220	**110×10**	1.20	393.5	304.1	1.29	**0.80**
7	HEB 260	HEB 240	120×10	1.09	345.2	241.5	1.43	0.77
6	HEB 280	HEB 280	120×10	1.00	306.0	205.3	1.49	0.70
5	HEB 300	HEB 320	140×10	1.06	309.8	182.5	1.70	0.78
4	HD 320x158	HD 320x158	140×10	0.99	301.1	167.6	1.80	0.71
3	HD 320x158	HD 360x179	150×10	1.00	309.4	157.9	1.96	0.72
2	HD 360x179	HD 360x196	140×12.5	1.04	324.7	152.1	2.14	0.76
1	HD 360x196	HD 400x237	140×12.5	0.98	205.4	149.3	1.38	**0.69**

$\Omega_{max}/\Omega_{min}$=1.94

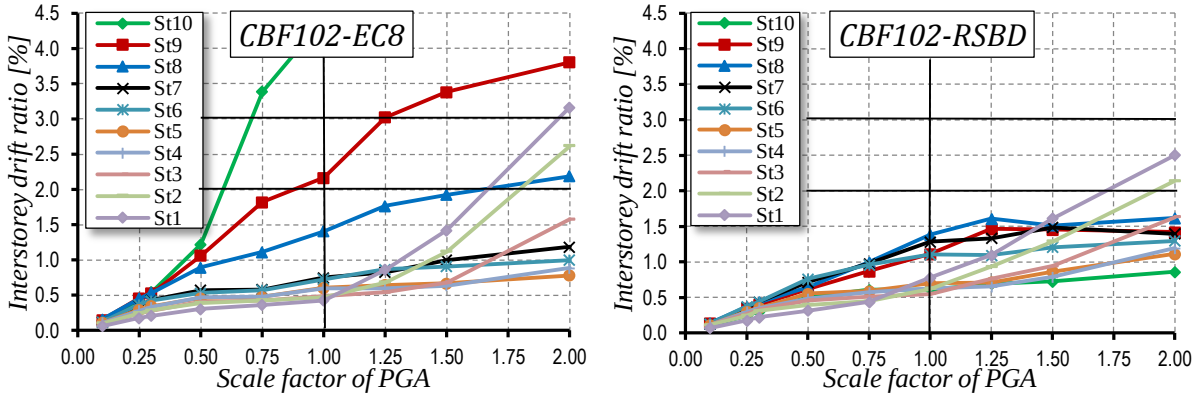

Figure 5.29; *IDA diagrams of 10-storey CBFs (averages of 7 records)*

5.3.2. Performance of CBF-s with only brace or column reinforcement

CBF81-EC8 is an example where the weak storey behaviour is remarkably present on multiple floors, but with the RSBD redesign a quasi ideal response is attained. The family of the curves of the RSBD building is slim and failure drift level is reached beyond 1.5 scale factor, see *Figure 5.26*. This example is appropriate to examine the contribution of the two criteria of the redesign method and to compare solutions where only the braces or the columns are modified.

In the building where only the braces are modified, the first requirement of the RSBD method, Eq. (5.1) is met, but the BPR of the two storeys on the top is significantly higher than the minimum in the building, not complying with Eq. (5.4), see *Table 5.9a*. These two floors are visibly overdesigned as their curves deviate from the rest, exhibiting small lateral displacements. Though the resistance of the reinforced building is adequate, the behaviour is not favourable as the dissipation is not well distributed among all the floors.

In the other case where solely the columns are reinforced the building is clearly not adequate, though the local load multiplier is larger than equal to the global on every floor, see *Table 5.9b*. The BPR results show that the top two floors are under, while the fourth floor is a bit overdesigned with 0.93 BPR. In the corresponding diagram in *Figure 5.30* this response can be observed.

Upon the presented two alternatives it is obvious that the first requirement of the RSBD method, imposed on the load multipliers may be necessary, but it is not satisfactory to provide favourable or adequate designs. Also, it can be concluded that the contribution to the resistance of the braces and the columns is not interchangeable. The resistance depends primarily on the braces. With the reinforcement of the diagonals the local load multipliers can be increased appropriately in the first place. Furthermore, in order to safeguard a good dissipative behaviour, the brace resistance need to be judiciously backed up or partially replaced by the resistance of continuous columns. By satisfying the requirements imposed to the BPR, outlier storey involvements can be ruled out.

Table 5.9a; *CBF81-RSBDbrace*

storey	*int.col.*	*ext.col.*	*brace*	Ω	λ_{loc}	λ_{glob}	$\frac{\lambda_{loc}}{\lambda_{glob}}$	*BPR*
8	HEA 160	HEA 160	**100×10**	**1.90**	724.5	699.9	1.04	**0.94**
7	HEB 180	HEA 180	**100×10**	**1.36**	389.3	373.3	1.04	0.86
6	HEB 220	HEB 200	**100×10**	1.14	282.3	266.6	1.06	0.78
5	HEB 240	HEB 220	100×10	1.01	229.0	215.4	1.06	**0.71**
4	HEB 280	HEB 240	120×10	1.10	217.5	186.6	1.17	0.81
3	HEB 300	HEB 280	120×10	1.01	192.3	169.7	1.13	0.73
2	HEM 240	HEB 320	140×10	1.05	210.8	160.0	1.32	0.81
1	HEM 240	HEM 240	**150×10**	1.06	157.7	155.5	1.01	0.76

$\Omega_{max}/\Omega_{min}$=1.88

Table 5.9b; *CBF81-RSBDcolumn*

storey	*int.col.*	*ext.col.*	*brace*	Ω	λ_{loc}	λ_{glob}	$\frac{\lambda_{loc}}{\lambda_{glob}}$	*BPR*
8	HEA 160	**HEB 220**	90×5	0.99	609.1	609.5	1.00	**0.55**
7	HEB 180	**HEB 220**	100×6.3	1.05	429.7	325.1	1.32	0.71
6	HEB 220	**HEB 220**	100×8	1.01	271.9	232.2	1.17	0.75
5	HEB 240	HEB 220	100×10	1.10	229.0	187.5	1.22	0.82
4	HEB 280	HEB 240	120×10	1.01	217.5	162.5	1.34	**0.93**
3	HEB 300	HEB 280	120×10	0.98	192.3	147.8	1.30	0.84
2	HEM 240	HEB 320	140×10	0.98	210.8	139.3	1.51	0.93
1	HEM 240	HEM 240	140×10	1.00	147.2	135.5	1.09	0.80

$\Omega_{max}/\Omega_{min}$=1.07

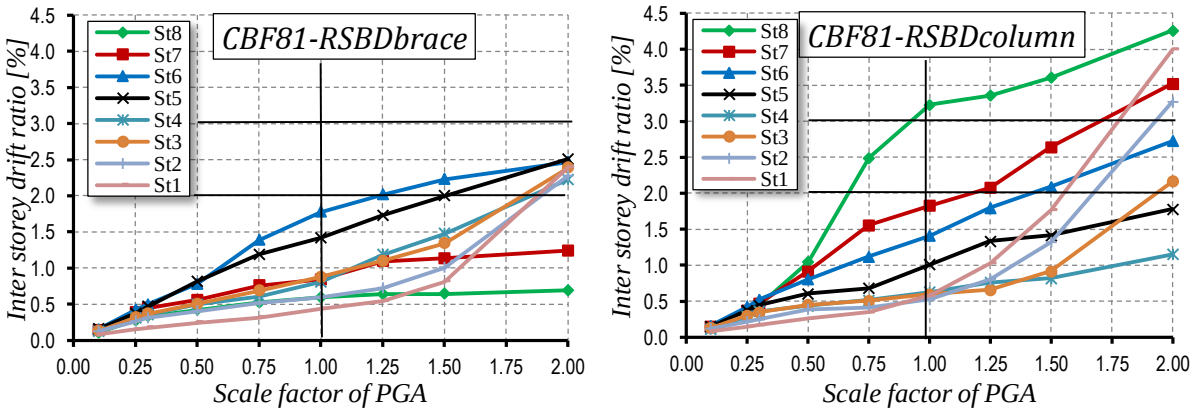

Figure 5.30; *IDA diagrams of 8-storey redesigned CBFs (averages of 7 records)*

5.3.3. Performance of reinforced irregular CBF-s

Regarding the buildings designed initially with behaviour factor q=5, it can be seen that the designs are not necessarily, in every aspect worse than the originals with q=4, see *Figures 5.31, 5.32* and *Figures 5.22, 5.24*. The increase of the drifts is slightly steeper and collapse is attained at smaller scale factors. However, the family of the curves of CBF61Q5-EC8 is slimmer than the one of the original, CBF61-EC8, and also the interstorey drift corresponding to failure is reached at a higher scale factor. The performance of the redesigns is adequate in both presented cases and also slightly better than the redesigns of the original buildings. It has to be noted though that the differences between the designs with behaviour factor 4 or 5 are minor in terms of cross-sectional sizes, see *Table 5.10b* and *5.11b*. The considered examples are therefore a bit more economic with q=5 as the required structural weight is less and also these designs can be just as adequate as the ones with q=4. Yet, the differences that the consideration of a higher behaviour factor provides are found to be small.

The results obtained for the cases where mass irregularities were considered are presented in *Tables 5.12* and *5.13* in *Figures 5.33* and *5.34*. In these cases the discrepancy between the upper floors, where the additional masses are located, and the lower floors is more flagrant than of the regular buildings, see *Figures 5.24* and *5.26*. This, otherwise not surprising statement is valid for both Eurocode originals and redesigns. The 8-storey building, where the mass irregularity is only 20% extra, exhibits a rather satisfactory behaviour after redesign. For the 6-storey CBF however, the family of the curves is broad even after redesign. It has to be emphasized that in this case the mass irregularity is plus 50% on the upper floors. In both examined cases the RSBD method provides designs that are adequate and still have more distributed dissipation than the Eurocode 8 originals.

Table 5.10a; *CBF41Q5-EC8*

storey	*int.col.*	*ext.col.*	*brace*	Ω	λ_{loc}	λ_{glob}	$\frac{\lambda_{loc}}{\lambda_{glob}}$	*BPR*
4	HEA 160	HEA 140	90×4	1.06	**308.2**	**394.2**	**0.78**	**0.64**
3	HEB 180	HEA 180	90×6	1.05	250.7	225.2	1.11	0.81
2	HEB 220	HEB 180	90×8	1.04	218.4	175.2	1.25	**0.87**
1	HEB 260	HEB 220	100×8	0.99	**153.0**	**157.7**	**0.97**	0.79

$\Omega_{max}/\Omega_{min}$=1.06

Table 5.10b; *CBF41Q5-RSBD*

storey	*int.col.*	*ext.col.*	*brace*	Ω	λ_{loc}	λ_{glob}	$\frac{\lambda_{loc}}{\lambda_{glob}}$	*BPR*
4	HEA 160	**HEA 180**	**90×5**	**1.31**	423.8	433.9	0.98	**0.73**
3	HEB 180	**HEA 200**	**90×6.3**	1.07	304.3	247.9	1.23	0.77
2	HEB 220	**HEB 220**	90×8	1.03	248.6	192.8	1.29	0.79
1	HEB 260	**HEB 240**	**100×10**	1.10	185.9	173.6	1.07	**0.83**

$\Omega_{max}/\Omega_{min}$=1.27

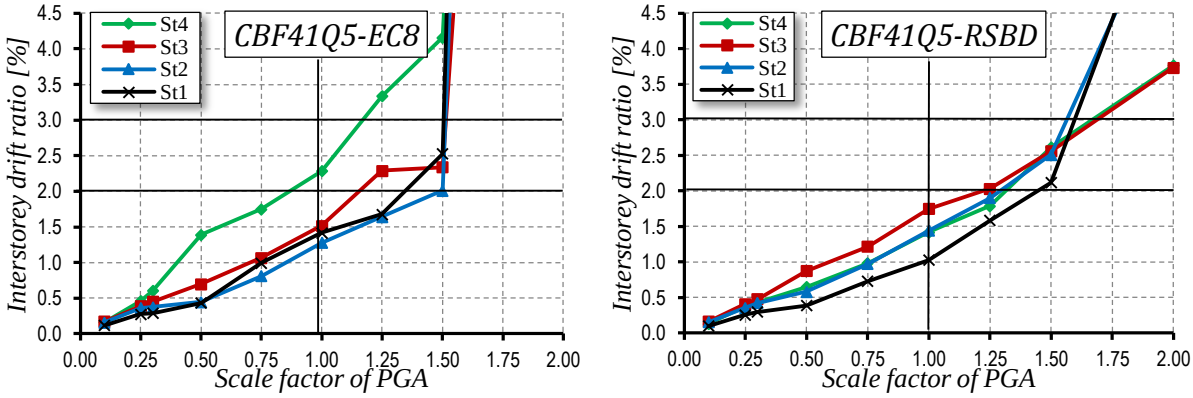

Figure 5.31; *IDA diagrams of 4-storey CBFs (averages of 7 records)*

Table 5.11a; *CBF61Q5-EC8*

storey	*int.col.*	*ext.col.*	*brace*	*Ω*	λ_{loc}	λ_{glob}	$\frac{\lambda_{loc}}{\lambda_{glob}}$	*BPR*
6	HEA 160	HEA 140	100×4	1.05	**347.6**	**482.0**	**0.72**	**0.61**
5	HEB 180	HEA 180	100×6	1.04	269.6	262.9	1.03	0.76
4	HEB 220	HEB 180	110×6.3	1.00	212.1	192.8	1.10	0.76
3	HEB 240	HEB 220	100×8	1.01	200.4	160.7	1.25	0.78
2	HEB 280	HEB 240	100×10	1.06	200.8	144.6	1.39	**0.83**
1	HEB 300	HEB 280	110×10	1.05	144.2	137.7	1.05	0.79

$\Omega_{max}/\Omega_{min}$=1.06

Table 5.11b; *CBF61Q5-RSBD*

storey	*int.col.*	*ext.col.*	*brace*	*Ω*	λ_{loc}	λ_{glob}	$\frac{\lambda_{loc}}{\lambda_{glob}}$	*BPR*
6	HEA 160	**HEA 200**	**100×5**	**1.27**	487.6	496.7	0.98	**0.74**
5	HEB 180	**HEA 200**	100×6	1.04	322.7	270.9	1.19	0.76
4	HEB 220	HEB 180	110×6.3	0.99	221.5	198.7	1.11	0.74
3	HEB 240	HEB 220	100×8	0.98	200.4	165.6	1.21	0.75
2	HEB 280	HEB 260	100×10	1.03	215.5	149.0	1.45	**0.81**
1	HEB 300	HEB 280	110×10	1.01	156.5	141.9	1.10	0.77

$\Omega_{max}/\Omega_{min}$=1.29

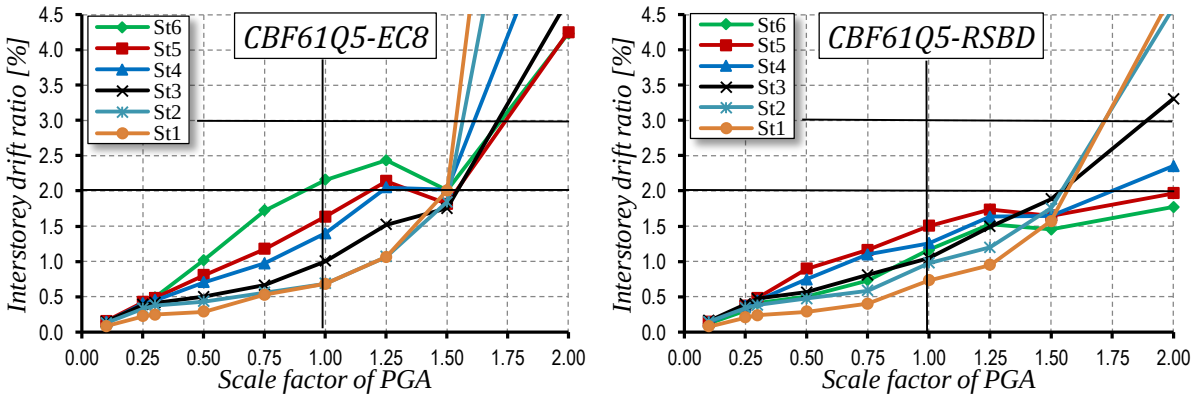

Figure 5.32; *IDA diagrams of 6-storey CBFs (averages of 7 records)*

Table 5.12a; *CBF61M-EC8*

storey	*int.col.*	*ext.col.*	*brace*	*Ω*	λ_{loc}	λ_{glob}	$\frac{\lambda_{loc}}{\lambda_{glob}}$	*BPR*
6	HEA 180	HEA 160	100×6	1.00	**333.8**	**428.1**	**0.78**	**0.67**
5	HEB 220	HEA 200	100×8	0.98	**230.8**	**233.5**	**0.99**	0.75
4	HEB 260	HEB 220	100×10	0.99	198.6	171.2	1.16	0.80
3	HEB 280	HEB 240	120×10	1.00	197.2	151.1	1.30	**0.85**
2	HEB 320	HEB 280	120×10	0.98	182.3	140.1	1.30	0.79
1	HEM 240	HEB 300	140×10	1.01	150.6	135.2	1.11	0.85

$\Omega_{max}/\Omega_{min}$=1.02

Table 5.12b; *CBF61M-RSBD*

storey	*int.col.*	*ext.col.*	*brace*	*Ω*	λ_{loc}	λ_{glob}	$\frac{\lambda_{loc}}{\lambda_{glob}}$	*BPR*
6	HEA 180	**HEA 220**	**100×8**	**1.22**	477.8	445.9	1.07	0.80
5	HEB 220	**HEA 240**	**110×8**	1.02	316.7	243.2	1.30	0.80
4	HEB 260	HEB 220	100×10	0.97	218.8	178.4	1.23	0.77
3	HEB 280	HEB 240	120×10	1.00	197.2	157.4	1.25	**0.81**
2	HEB 320	HEB 280	120×10	0.98	197.0	145.9	1.35	**0.76**
1	HEM 240	HEB 300	140×10	0.98	150.6	140.8	1.07	0.81

$\Omega_{max}/\Omega_{min}$=1.26

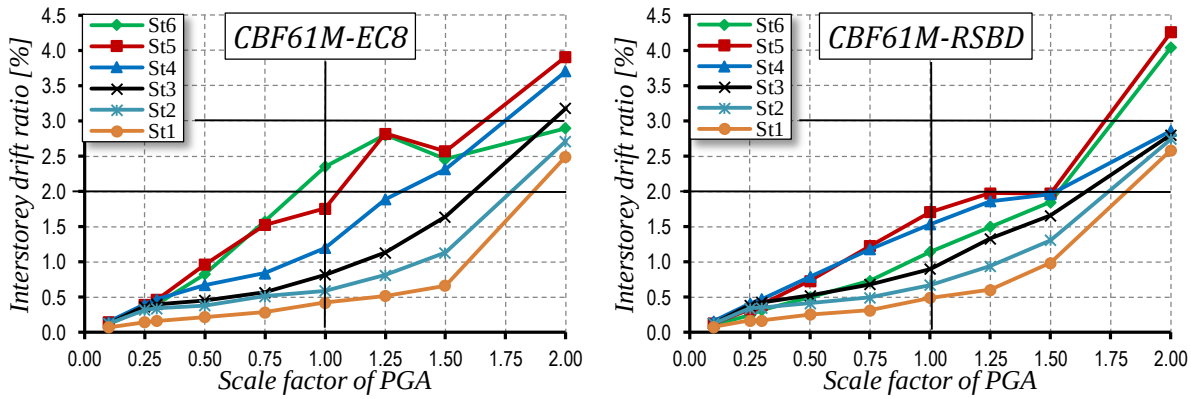

Figure 5.33; *IDA diagrams of 6-storey CBFs (averages of 7 records)*

Table 5.13a; *CBF81M-EC8*

storey	*int.col.*	*ext.col.*	*brace*	*Ω*	λ_{loc}	λ_{glob}	$\frac{\lambda_{loc}}{\lambda_{glob}}$	*BPR*
8	HEA 180	HEA 160	100×5	1.00	**365.9**	**560.7**	**0.65**	**0.54**
7	HEB 200	HEA 200	100×8	1.08	301.9	299.0	1.01	0.76
6	HEB 240	HEB 200	100×10	1.03	231.7	213.6	1.08	0.77
5	HEB 260	HEB 240	140×7.1	1.02	209.9	172.5	1.22	0.78
4	HEB 300	HEB 280	120×10	1.02	209.7	152.9	1.37	0.79
3	HEB 320	HEB 320	140×10	1.09	227.1	140.9	1.61	**0.88**
2	HEM 240	HEM 240	140×10	1.00	211.5	133.9	1.58	0.78
1	HEM 260	HEM 260	150×10	1.00	150.0	130.6	1.15	0.77

$\Omega_{max}/\Omega_{min}$=1.09

Table 5.13b; *CBF81M-RSBD*

storey	*int.col.*	*ext.col.*	*brace*	Ω	λ_{loc}	λ_{glob}	$\frac{\lambda_{loc}}{\lambda_{glob}}$	*BPR*
8	HEA 180	**HEA 240**	**100×8**	**1.44**	629.3	591.9	1.06	**0.76**
7	HEB 200	**HEA 240**	**110×8**	1.20	402.4	315.7	1.27	0.81
6	HEB 240	HEB 200	100×10	1.11	256.7	225.5	1.14	0.79
5	HEB 260	HEB 240	140×7.1	1.02	209.9	182.1	1.15	0.74
4	HEB 300	HEB 280	120×10	1.02	209.7	161.4	1.30	0.75
3	HEB 320	HEB 320	140×10	1.09	227.1	148.7	1.53	**0.83**
2	HEM 240	HEM 240	140×10	1.00	211.5	141.3	1.50	0.74
1	HEM 260	HEM 260	150×10	1.00	150.0	137.9	1.09	0.73

$\Omega_{max}/\Omega_{min}$=1.44

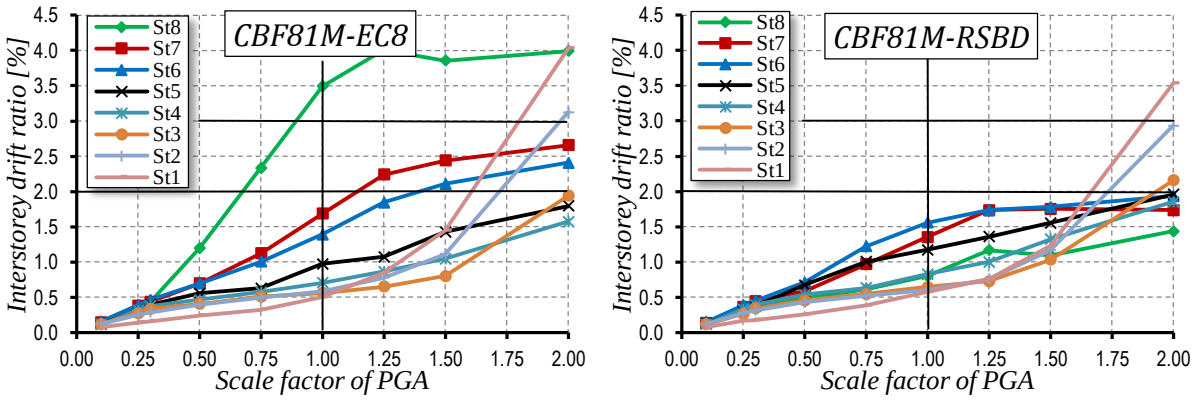

Figure 5.34; *IDA diagrams of 6-storey CBFs (averages of 7 records)*

5.3.4. Performance of CBF-s reinforced by limit analysis RSBD

In the following the type 1 4, 6, 8 and 10-storey CBF-s are redesigned applying the simpler limit analysis formulas i.e. Eqs. (5.82) (5.83) and (5.84). The presented tables only show the obtained redesigns. The changed cross sections are still bold, and any change from the redesigns obtained taking into consideration the second order work of the gravity forces is indicated by red letters. In the figures after the tables the 2nd order and limit analysis RSBD designs are compared via their IDA responses.

As it can be seen the limit analysis mostly entails the further enlargement of the brace and column cross sections that have been reinforced by the 2nd order application of the RSBD method before. Except for the 4-storey CBF this reinforcement does not cause drastic changes. The CBF-s are likewise adequate, but the formerly weak storeys are a bit overdesigned by the limit analysis approach as their curves deviate from the rest towards lower drifts. In addition, this unnecessary and unfavourable alteration is achieved by additional expenses on building material. The case of the 4-storey CBF differs from the rest significantly as response of the limit analysis redesign is remarkably worse than the 2nd order RSBD design. The curves open up like a fan as the scale factor grows and the design is just about adequate. Conversely, the limit analysis design necessitates smaller column sections than the 2nd order RSBD.

The presented examples attest to the fact that it better to conduct the analysis taking into consideration the 2nd order work of gravity forces. However, in most cases the easier-to-evaluate limit analysis RSBD also leads to adequate designs imposing only a reasonably

higher structural weight premium. Therefore, the advantage of the limit analysis RSBD is that its application is easier in exchange of minor changes of the structure and its behaviour.

Table 5.14; *CBF41-RSBD with limit analysis*

storey	*int.col.*	*ext.col.*	*brace*	Ω	λ_{loc}	λ_{glob}	$\frac{\lambda_{loc}}{\lambda_{glob}}$	*BPR*
4	HEA 160	**HEA 200**	**90×6.3**	**1.43**	578.7	568.3	1.02	0.86
3	HEB 180	**HEB 200**	100×6.3	0.99	395.6	324.8	1.22	**0.84**
2	HEB 220	HEB 200	100×8	0.97	343.7	252.6	1.36	0.90
1	HEB 260	HEB 240	100×10	0.99	240.2	227.3	1.06	**0.91**

$\Omega_{max}/\Omega_{min}$=1.47

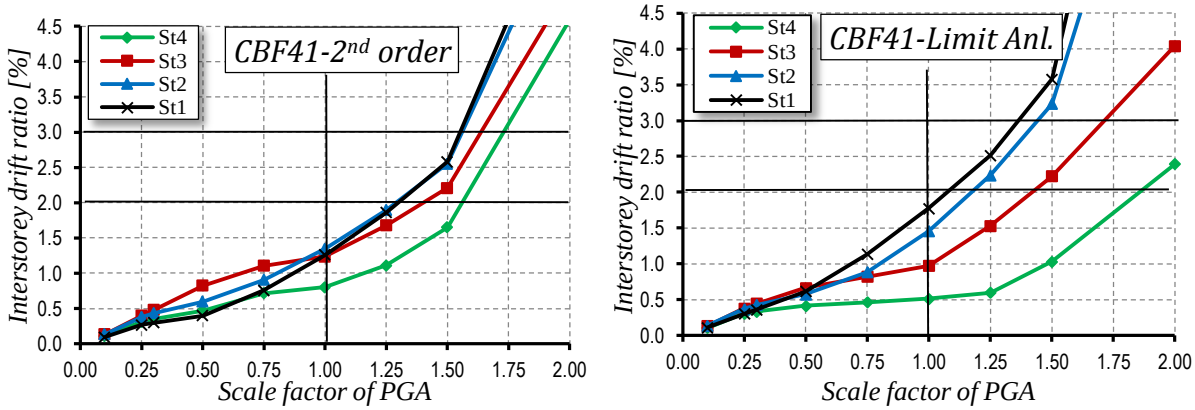

Figure 5.35; *IDA diagrams of 4-storey reinforced CBFs (averages of 7 records)*

Table 5.15; *CBF61-RSBD with limit analysis*

storey	*int.col.*	*ext.col.*	*brace*	Ω	λ_{loc}	λ_{glob}	$\frac{\lambda_{loc}}{\lambda_{glob}}$	*BPR*
6	HEA 160	**HEA 200**	**100×6.3**	**1.42**	632.3	652.1	0.97	0.84
5	HEB 180	**HEB 200**	**100×8**	1.17	439.7	355.7	1.24	**0.90**
4	HEB 220	HEB 200	100×8	1.00	300.2	260.8	1.15	**0.82**
3	HEB 240	HEB 220	100×10	1.02	257.8	217.4	1.19	0.88
2	HEB 280	**HEB 260**	100×10	0.96	239.3	195.6	1.22	0.84
1	HEB 300	HEB 280	120×10	0.97	188.0	186.3	1.01	0.85

$\Omega_{max}/\Omega_{min}$=1.47

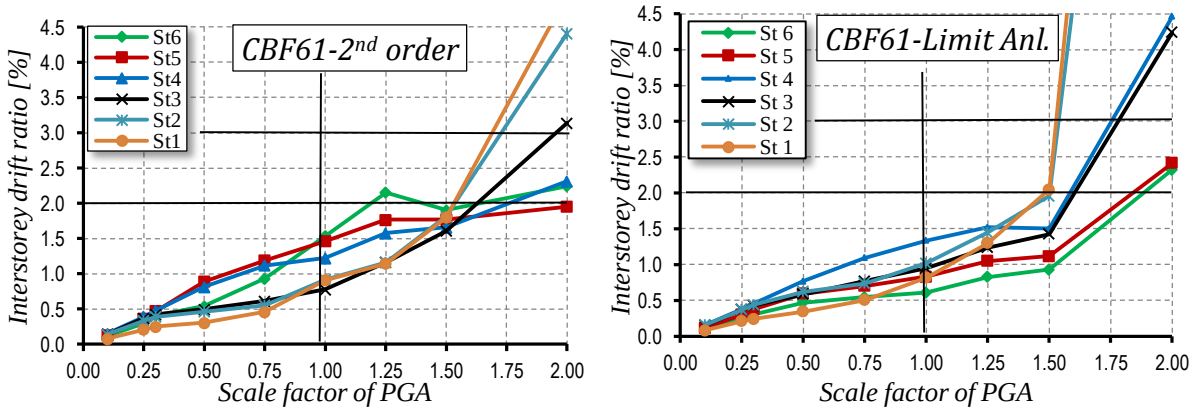

Figure 5.36; *IDA diagrams of 6-storey reinforced CBFs (averages of 7 records)*

Table 5.16; *CBF81-RSBD with limit analysis*

storey	*int.col.*	*ext.col.*	*brace*	Ω	λ_{loc}	λ_{glob}	$\frac{\lambda_{loc}}{\lambda_{glob}}$	*BPR*
8	HEA 160	**HEA 220**	**100×8**	**1.74**	800.2	798.7	1.00	0.76
7	HEB 180	**HEB 200**	**100×8**	1.21	479.7	426.0	1.13	**0.71**
6	HEB 220	HEB 200	**100×10**	1.22	336.3	304.3	1.11	0.75
5	HEB 240	HEB 220	100×10	1.11	269.7	245.7	1.10	0.75
4	HEB 280	HEB 240	120×10	1.17	244.5	213.0	1.15	**0.80**
3	HEB 300	HEB 280	120×10	1.07	219.3	193.6	1.13	0.73
2	HEM 240	HEB 320	140×10	1.08	226.3	182.6	1.24	0.80
1	HEM 240	HEM 240	140×10	0.98	182.4	177.5	1.03	0.72

$\Omega_{max}/\Omega_{min}$=1.77

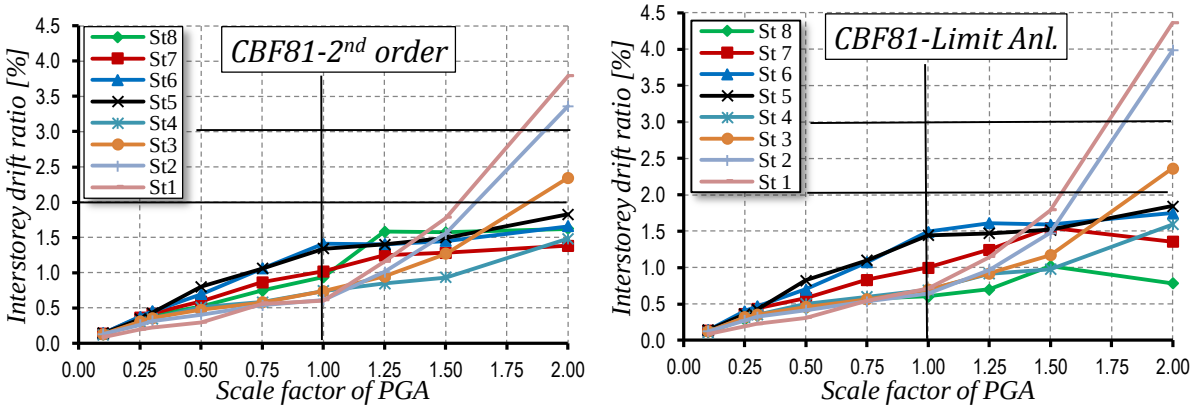

Figure 5.37; *IDA diagrams of 8-storey reinforced CBFs (averages of 7 records)*

Table 5.17; *CBF101-RSBD with limit analysis*

storey	*int.col.*	*ext.col.*	*brace*	Ω	λ_{loc}	λ_{glob}	$\frac{\lambda_{loc}}{\lambda_{glob}}$	*BPR*
10	HEA 160	**HEB 220**	**100×10**	**1.94**	1000.5	986.5	1.01	0.75
9	HEB 180	**HEB 220**	**100×10**	1.27	580.1	519.2	1.12	**0.71**
8	HEB 220	HEB 200	**110×10**	1.19	380.9	365.4	1.04	0.75
7	HEB 240	HEB 220	120×10	1.06	296.1	290.2	1.02	0.73
6	HEB 280	HEB 260	120×10	1.02	262.6	246.6	1.06	0.72
5	HEB 300	HEB 280	140×10	1.03	253.4	219.2	1.16	**0.78**
4	HEM 240	HEB 320	140×10	0.99	230.9	201.3	1.15	0.72
3	HEM 240	HEM 240	150×10	0.98	231.0	189.7	1.22	0.74
2	HEM 260	HEM 260	140×12.5	1.03	223.2	182.7	1.22	0.78
1	HEM 280	HD320×198	150×12.5	1.00	184.0	179.4	1.03	0.76

$\Omega_{max}/\Omega_{min}$=1.98

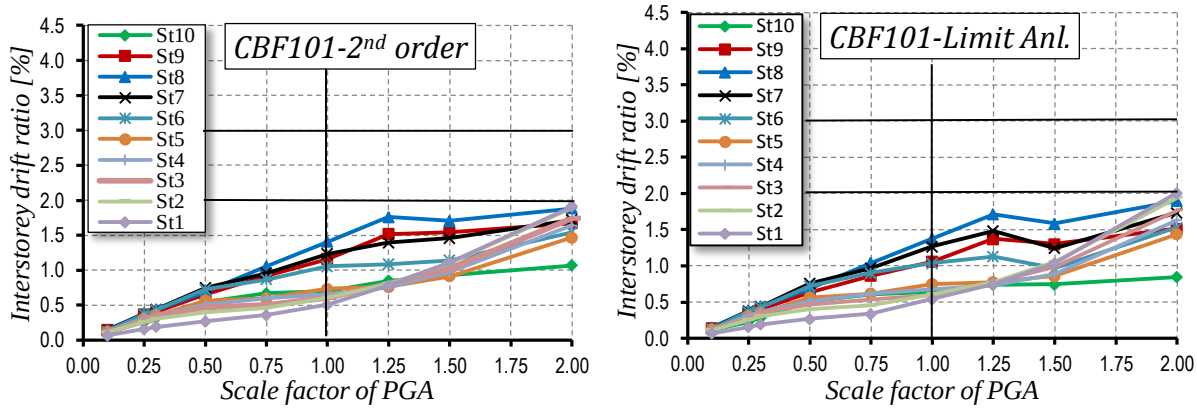

Figure 5.38; *IDA diagrams of 10-storey reinforced CBFs (averages of 7 records)*

5.3.5. Summary on the efficiency of the RSBD method

So far, examining the performance of the original EC8 designs and the RSBD redesigns we have ascertained that the IDA curves of the originals are seemingly broader than of the redesigns. Therefore it would be good to give a measure to this broadness to be able to numerically compare the designs. It is appealing to consider the difference between the maxima and minima of the IDR results, but it may also be necessary to distinguish cases where the curves scatter out like a fan and when only one flagrant curve results in the large difference. Another very important and so far just expected characteristic of the RSBD method is that it provides robust CBF designs that are supposed to reliably resist earthquakes within their design intensity range without sensitivity to any particularity of the excitation. The existence of this alleged characteristic of the method is yet to be demonstrated.

In order to better represent the broadness of the curves the IDR results of the floors for a given scale factor can be considered as values of a discrete random variable, the scatter of which can be described by the standard deviation (hereinafter σ). Therefore, for every acceleration record and every scale factor the σ of the interstorey drifts is calculated as:

$$\sigma_{IDR} = \sqrt{\frac{1}{n}\left[\left(IDR_1 - IDR_\mu\right)^2 + \left(IDR_2 - IDR_\mu\right)^2 + \ldots + \left(IDR_n - IDR_\mu\right)^2\right]} \tag{5.85}$$

where the mean is:

$$IDR_\mu = \frac{1}{n}\left(IDR_1 + \ldots + IDR_n\right) \tag{5.86}$$

As in a low scale factor range the broadness may not be developed and in a high range the results may be distorted by the asymptotic curves corresponding to attained collapse, this analysis is confined to the 0.75 – 1.25 scale factor interval. To represent the broadness of the numerous IDA curves presented before the mean of all the standard deviations in this interval is computed. This way the broadness is expressed by one number, hereinafter referred to as the broadness coefficient that is in IDR unit, see *Figure 5.39*.

To describe the robustness of the obtained results, for a given scale factor the scatter of the broadness for every accelerogram shall be taken. If this scatter is small, the broadness is the same for every earthquake, than the response of the examined CBF is not sensitive to variations of the excitation, therefore it is robust. The broadness has been calculated with the standard deviation before and to compute the scatter of these results, again the σ of these standard deviations is taken for every considered scale factor. The mean of the σ-s is another

number in IDR unit describing the robustness of the CBF-s seismic response therefore it is called robustness coefficient.

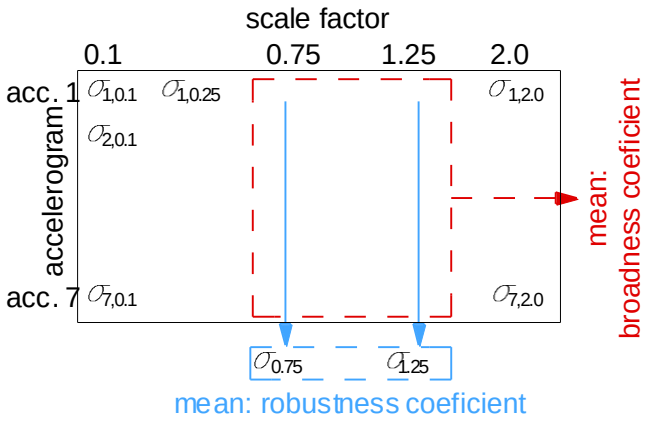

Figure 5.39; *Determination of the broadness and robustness coefficients*

In *Figure 5.40* the broadness and robustness coefficients obtained both for EC8 and RSBD design are presented in two bar charts. As it can be seen, the broadness of the Eurocode 8 designs grows with the building height, whereas with the RSBD method the broadness is kept in an interval of 0.3 – 0.5% IDR for every CBF including the irregular cases as well. Also, the Eurocode 8 design can barely show such a good performance; the broadness of the EC8 design mostly exceeds 0.6% and may go beyond substantial 1.2% relative storey drift. The robustness chart shows that the EC8 designs do not only have broader IDA curves but they are also more sensitive to the particularities of the excitation. The robustness of the EC8 originals is at least 0.20%, but it goes a lot higher up in some cases, while all the RSBD redesigns stay in an astounding 0.1 – 0.16% range. This demonstrates that the RSBD method indeed reliably provides seismic resistant CBF-s.

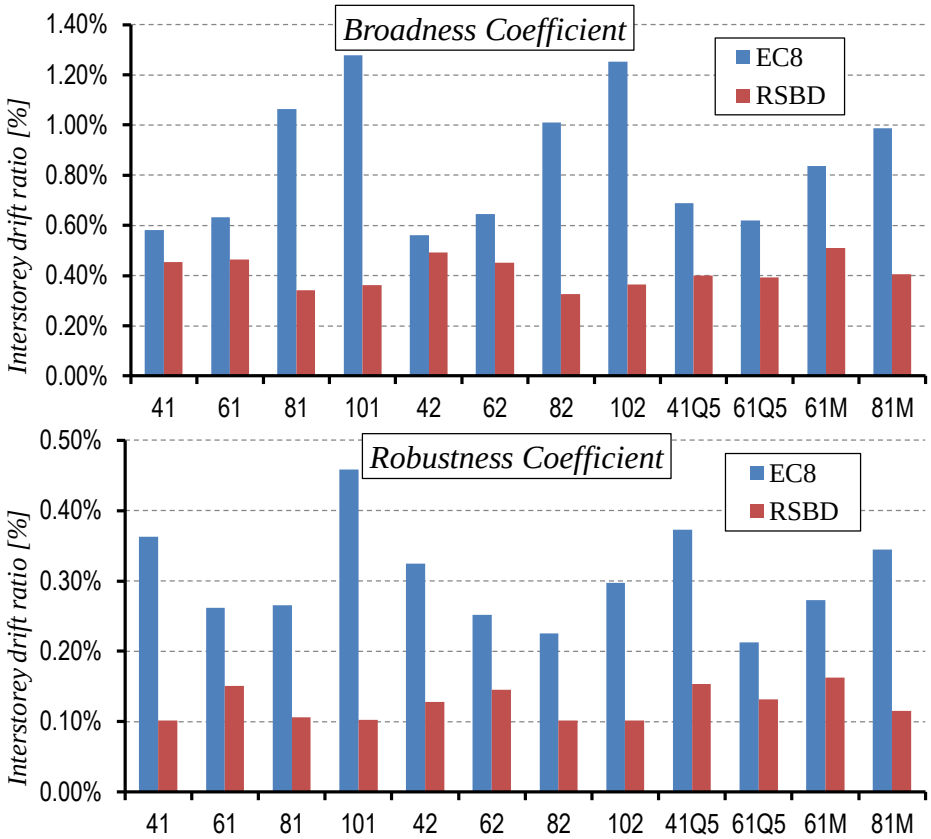

Figure 5.40; *Broadness and robustness coefficients of various CBF-s*

For the sake of further comparison between the original designs *Table 5.18* collects relevant characteristics of the CBF-s. For the original EC8 buildings and for the 2nd order RSBD redesigns the periods, the total steel requirement and the scale factor at which the 2% storey drift is attained are given. For the comparison, the increase of the mass and the failure intensity, and in the last two columns, the decrease of the broadness and the robustness coefficients, see *Figure 5.40*, are provided. In the case of CBF101-RSBD the failure limit as not been attained in the range of analysis, therefore the result there is not available (N.A.).

As it can be seen, the type 1 (CBF – CBF) buildings require in general a larger structural weight premium than the type 2 ones (MRF – CBF). This is due to the fact that the columns need a more significant reinforcement in type 1-s. Nonetheless, the additional material need is not outstanding in any case. The failure intensity is increased in almost every case from an unsatisfactory (<1.0) value to a by far satisfactory one. The increase ranges between 30% up to 200%. This shows that the buildings after redesign are not only adequate, but also possess considerable reserve. The change of the broadness coefficient is somewhat proportional with the change of the failure intensity, showing, that the significant increase in resistance has been achieved mostly by terminating the outlier lateral drifts on weak storeys. The change of the robustness is rather elevated for every considered example (>40%). This demonstrates that the RSBD method does not only enhances the resistance and prevents the development of the weak storeys, but also provides more reliable CBF designs than Eurocode 8.

Table 5.18; *Comparison of EC8 and RSBD CBF designs*

CBF	*period [sec]*	*mass [ton]*	*failure [SF]*	*CBF*	*period [sec]*	*mass [ton]*	*failure [SF]*	*Δmass*	*Δfailure*	*Δbrd.ness*	*Δrbt.ness*
41-EC8	1.13	70.10	1.02	41-RSBD	1.10	72.57	1.31	3.52%	28.4%	-21.9%	-72.1%
61-EC8	1.65	109.09	0.88	61-RSBD	1.60	112.41	1.19	3.04%	35.2%	-26.8%	-42.2%
81-EC8	2.10	160.40	0.60	81-RSBD	2.03	164.35	1.55	2.46%	158.3%	-68.0%	-60.2%
101-EC8	2.54	218.31	0.58	101-RSBD	2.50	221.84	N.A.	1.62%	N.A.	-71.6%	-77.6%
42-EC8	1.19	61.79	1.04	42-RSBD	1.17	62.55	1.29	1.23%	24.0%	-11.9%	-60.6%
62-EC8	1.61	102.25	0.84	62-RSBD	1.58	103.16	1.52	0.89%	81.0%	-30.0%	-42.4%
82-EC8	2.04	150.81	0.60	82-RSBD	2.00	151.26	1.60	0.30%	166.7%	-67.8%	-55.1%
102-EC8	2.41	207.34	0.58	102-RSBD	2.39	208.45	1.72	0.54%	196.6%	-70.8%	-65.8%
41Q5-EC8	1.21	69.63	0.87	41Q5-RSBD	1.17	69.95	1.25	0.46%	43.7%	-42.0%	-58.9%
61Q5-EC8	1.68	108.70	0.93	61Q5-RSBD	1.66	109.02	1.54	0.29%	65.6%	-36.6%	-39.1%
61M-EC8	1.78	123.42	0.88	61M-RSBD	1.74	125.76	1.35	1.90%	53.4%	-38.9%	-40.5%
81M-EC8	2.17	183.34	0.68	81M-RSBD	2.13	185.83	1.67	1.36%	145.6%	-59.0%	-66.7%

5.4. Simplifications of the Robust Seismic Brace Design method

In the previous chapter the reliability of the RSBD method has been substantiated by numerous examples. Though the calculations can be carried out by hand evaluating formulas, it may take a considerable amount of time. Therefore, in the following, by introducing further simplifications we attempt to derive simpler formulas that may be used as preliminary or approximate tools in the seismic design of CBF structures.

Let us consider the already simplified limit analysis approach of the RSBD method and substitute Eqs. (5.82) and (5.84) into the definition of the BPR, Eq. (5.4):

$$BPR_i = \frac{\lambda_{br,i}}{\lambda_{glob,i}} = \frac{\dfrac{N_{pl,br,i} \cdot \cos\alpha_i}{\sum_{k=i}^{n} mp_k}}{\dfrac{\sum_i N_{pl,br,i} \cdot \cos\alpha_i}{\sum_{k=i}^{n}\left(mp_k \cdot \sum_{l=1}^{k} l\right)}} \tag{5.87}$$

Let us suppose that the masses are equal on every floor so that *mp* is an identity vector. This way we get:

$$BPR_i = \frac{\dfrac{N_{pl,br,i}}{(n-i+1)}}{\dfrac{\sum_i N_{pl,br,i}}{\sum_{l=i}^{n} l}} \tag{5.88}$$

In the denominator natural numbers have to be summed. This can be expressed as the sum of the first and the second element multiplied by the half of the number of the elements. Thus the BPR becomes:

$$BPR_i = \frac{N_{pl,br,i}}{(n-i+1)} \cdot \frac{(n+i) \cdot \dfrac{(n-i+1)}{2}}{\sum_i N_{pl,br,i}} \tag{5.89}$$

Let us also suppose the ideal case that the BPR is the same constant on every floor, therefore:

$$BPR = \frac{(n+i)}{2} \cdot \frac{N_{pl,br,i}}{\sum_i N_{pl,br,i}} \tag{5.90}$$

As *i* ranges from 1 to the *n* number of floors, the first fraction is between *n/2* and *n* for any given storey. Consequently, the smallest brace resistance (of the top floor) shall not be smaller than half of the largest resistance (on the first floor) in order to satisfy Eq. (90). Evidently, such a requirement implies substantial reinforcement need on the upper floors in tall CBF structures. This premium may lead to unwanted overdesign of the upper floors, so that these floors eventually do not participate in the dissipation.

Now let us suppose, that the change of the axial resistance need of the braces along the height of the building is linear and on the top exactly the half of the resistance on the ground floor is needed, see *Figure 5.41*.

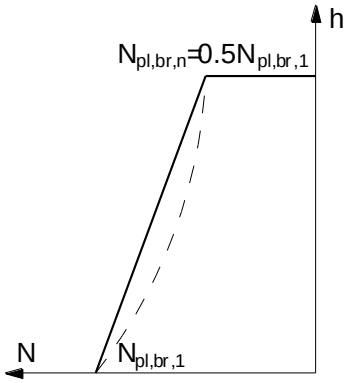

Figure 5.41; *Approximate distribution of axial resistance need of braces*

This demand distribution is not unfamiliar in Eurocode 8 as in section 5.4.2.4 of the standard the envelope of the shear forces of ductile reinforced concrete walls is similar to account for uncertainties in higher mode effects. Given such distribution, the sum of all the brace resistances can be expressed as:

$$\sum_i N_{pl,br,i} = \left(N_{pl,br,1} + N_{pl,br,n}\right)\frac{n}{2} = 1.5N_{pl,br,1}\frac{n}{2} \tag{5.91}$$

Substituting this into Eq. (5.90) we get:

$$BPR = \frac{(n+i)}{2} \cdot \frac{N_{pl,br,i}}{1.5N_{pl,br,1}\frac{n}{2}} = \frac{N_{pl,br,i}}{1.5N_{pl,br,1}} \cdot \frac{n+i}{n} \tag{5.92}$$

Rearranging this expression we get a formula that provides an approximation of the axial resistance need of the braces on every floor:

$$N_{pl,br,i} = BPR \cdot \frac{n \cdot 1.5N_{pl,br,1}}{n+i} \tag{5.93}$$

To give a good estimation of the axial demand of the ground floor brace we assume that the horizontal component of the brace axial force is equal to the base shear of the building, calculated with Eq. (1.38) for example.

$$N_{pl,br,1} = \frac{F_b}{\cos\alpha} \tag{5.94}$$

Furthermore, let us notice, that Eq. (5.93) has the form of the realigned second criterion of the RSBD method, Eq. (5.4), but instead of the horizontal load multiplier the connection is between the oblique axial forces. Therefore, by considering the horizontal component, which is the storey base shear, and distributing it between the loaded floor slabs it is found that:

$$\begin{aligned} \frac{\cos\alpha}{n-i+1} \cdot N_{pl,br,i} &= BPR \cdot \frac{n \cdot 1.5N_{pl,br,1}}{n+i} \cdot \frac{\cos\alpha}{n-i+1} \\ \lambda_{br,i} &= BPR \cdot \lambda_{glob,i} \end{aligned} \tag{5.95}$$

Taking the first criterion, we may say that:

$$\frac{\lambda_{loc,i}}{\lambda_{glob,i}} \geq 1.0$$
$$\lambda_{loc,i} = \lambda_{br,i} + \lambda_{col,i} \geq \lambda_{glob,i} \tag{5.96}$$

Substituting Eq. (5.95) into Eq. (5.96) we get:

$$BPR \cdot \lambda_{glob,i} + \lambda_{col,i} \geq \lambda_{glob,i}$$
$$\lambda_{col,i} \geq (1 - BPR)\lambda_{glob,i} \tag{5.97}$$

Considering the analogy presented in Eq. (5.95) the right side of Eq. (5.97) can be substituted with:

$$(1 - BPR)\lambda_{glob,i} = (1 - BPR)\frac{n \cdot 1.5N_{pl,br,1}}{n+i} \cdot \frac{\cos\alpha}{n-i+1} \tag{5.98}$$

Also, by highlighting the column participation in Eq. (5.83) and still supposing *mp* to be unity vector and that the storey heights are equal we may express λ_{col} as:

$$\lambda_{col,i} = \frac{\sum_{j=1}^{m} M_{red,i,j} \cdot \frac{1}{H}}{n-i+1} \tag{5.99}$$

Substituting Eq. (5.98) and Eq. (5.99) into (5.97) we can express the sum of the continuous columns' bending moment demand (to be determined with respect to the axial force interaction):

$$\frac{\sum_{j=1}^{m} M_{red,i,j} \cdot \frac{1}{H}}{n-i+1} \geq (1 - BPR)\frac{n \cdot 1.5N_{pl,br,1}}{n+i} \cdot \frac{\cos\alpha}{n-i+1}$$
$$\sum_{j=1}^{m} M_{red,i,j} = (1 - BPR)\frac{n \cdot 1.5N_{pl,br,1}}{n+i} \cdot H \cdot \cos\alpha \tag{5.100}$$

For the sake of comparison, the required cross sections of the braces and columns have been determined applying Eqs. (5.94), (5.93) and (5.100) also. The considered examples are CBF41, 61, 81 and 101. In the tables below, the designs obtained with the 2nd order RSBD, the limit analysis RSBD and the lately presented approximate approach are given.

Table 5.19; *CBF41 redesign with various approaches of the RSBD*

storey	*2nd order RSBD*		*limA RSBD*		*approximate RSBD*	
	column	*brace*	*column*	*brace*	*column*	*brace*
4	HEA 200	100×5	HEA 200	90×6.3	HEA 180	100×6
3	HEA 220	100×6.3	HEB 200	100×6.3	HEA 200	110×6.3
2	HEB 240	100×8	HEB 200	100×8	HEB 220	100×8
1	HEB 260	100×10	HEB 240	100×10	HEB 240	100×10

Table 5.20; *CBF61 redesign with various approaches of the RSBD*

storey	*2nd order RSBD*		*limA RSBD*		*approximate RSBD*	
	column	*brace*	*column*	*brace*	*column*	*brace*
6	HEA 200	100×6	HEA 200	100×6.3	HEA 200	110×6.3
5	HEA 200	100×6.3	HEB 200	100×8	HEA 200	120×6
4	HEB 200	100×8	HEB 200	100×8	HEB 200	100×8

3	HEB 220	100×10	HEB 220	100×10	HEB 220	100×10
2	HEB 240	100×10	HEB 260	100×10	HEB 240	100×10
1	HEB 280	120×10	HEB 280	120×10	HEB 280	120×10

Table 5.21; *CBF81 redesign with various approaches of the RSBD*

storey	*2nd order RSBD*		*limA RSBD*		*approximate RSBD*	
	column	*brace*	*column*	*brace*	*column*	*brace*
8	HEA 240	100×6.3	HEA 220	100×8	HEA 220	100×8
7	HEA 240	100×8	HEB 200	100×8	HEA 220	120×8
6	HEB 200	100×10	HEB 200	100×10	HEB 200	100×10
5	HEB 220	100×10	HEB 220	100×10	HEB 220	100×10
4	HEB 240	120×10	HEB 240	120×10	HEB 240	120×10
3	HEB 280	120×10	HEB 280	120×10	HEB 280	120×10
2	HEB 320	140×10	HEB 320	140×10	HEB 320	140×10
1	HEM 240	140×10	HEM 240	140×10	HEM 240	140×10

Table 5.22; *CBF101 redesign with various approaches of the RSBD*

storey	*2nd order RSBD*		*limA RSBD*		*approximate RSBD*	
	column	*brace*	*column*	*brace*	*column*	*brace*
10	HEA 220	100×10	HEB 220	100×10	HEA 220	110×10
9	HEA 220	100×10	HEB 220	100×10	HEA 220	120×10
8	HEB 200	110×10	HEB 200	110×10	HEB 200	120×10
7	HEB 220	120×10	HEB 220	120×10	HEB 220	140×10
6	HEB 260	120×10	HEB 260	120×10	HEB 260	140×10
5	HEB 280	140×10	HEB 280	140×10	HEB 280	150×10
4	HEB 320	140×10	HEB 320	140×10	HEB 320	150×10
3	HEM 240	150×10	HEM 240	150×10	HEM 240	140×12.5
2	HEM 260	140×12.5	HEM 260	140×12.5	HEM 260	150×12.5
1	HD320×198	150×12.5	HD320×198	150×12.5	HD320×198	150×12.5

Looking at the tables, it can be noticed that both simplified approaches result in structural weight premium. This is, on one hand not necessary as the designs obtained with the 2nd order RSBD are appropriate without exception, and on the other hand, this may even lead to unwanted and unfavourable change of the seismic response, as it has been observed in the IDA diagrams of the limit analysis designs. Nevertheless, both simplified approaches reinforce the weak storeys of the EC8 design and give fairly good approximations of the enhanced design of the 2nd order RSBD. The important advantage of the approximate RSBD is that it is very easy and does not require a preliminary EC8 design process like the more accurate forms of the RSBD. The disadvantage is, that the numerous simplifications, such as constant BPR, the brace axial resistance distribution, constant storey height and masses limit the applicability of the approximate RSBD. In the case of the 10-storey CBF the approximate method significantly reinforces every brace compared to 2nd order RSBD solution, which has already been found fairly (over)resistant as the collapse drift limit has not been attained even at 2.0 scale factor. Clearly, as it has been mentioned before as a conclusion of Eq. (5.90), for tall CBF-s the requirement of having more resistance in storey mechanisms than in the global mechanism can be too rigorous especially on the upper floors, where the columns are inherently weaker and do not participate in the lateral resistance as much as the columns on

the lower floors. Therefore, it may be concluded that the current RSBD method has a height limit of application as it tends to result in overdesign on the top floors.

Summary and new scientific results

This dissertation has been dealing with the weak storey behaviour of concentrically braced steel frames subjected to seismic actions. The objectives of the thesis set at the beginning can be grouped around the following issues:

- Description of the response of CBF-s during a seismic action with special attention to the factors related to or indicating the development of a weak storey;
- Identification of the factors facilitating the occurrence of the weak storey behaviour, characterisation of the development of weak storeys;
- Investigation into the performance of CBF-s designed according to Eurocode 8 and identification of the shortcomings of the corresponding parts of the standard; recommendation for enhancements;
- Proposition of a new design method, alternatively new criteria, which are complementary to Eurocode 8 regulations and which successfully prevent the development of weak storeys;

In the following a bulleted list is provided that summarises the findings and the new scientific results of the present dissertation.

In several paragraphs of Chapters 2, 3 and 4 the underlying causes and consequences of the weak storey behaviour are examined. The findings characterising the weak storey behaviour are as follows:

- The weak storey behaviour has a detrimental effect on the seismic performance because it decreases the structures capacity in dissipation and ductility;
- Hollow section members may be prone to early failure due to the local cumulating deformations at mid span;
- The weak storey behaviour, which is the excessively large interstorey drift of one floor, can be distinguished from the weak storey collapse i.e. failure on the weak storey because the later is not necessarily resulted by the former. The weak storey behaviour is unfavourable even if collapse is not attained;
- The weak storey behaviour is partly an inherent susceptibility of the structure, which is just as related to the proportions of stiffness and resistance as the seismic intensity;
- As the weak storey resistance is not simply resistance inadequacy on some floors, ordinary reinforcement may not solve the weak storey problem; just shift it to another floor;
- In order to obtain a satisfactory, well balanced dissipative behaviour, the appropriate selection of both continuous column and brace cross sections is needed, reinforcement of only one member type may not be satisfactory;
- The cumulating plastic deformations cause the deterioration of the braces and this gradually devolves the lateral loading on the columns, therefore the inelastic behaviour of a CBF cannot be characterised by a truss model;

- The brace deterioration also causes a significant drop of the lateral stiffness of the storey it is located on, and this fundamentally affects the response of the structure. The modified modal behaviour contributes to the development of the weak storey;
- The dynamic characteristics of a brace-deteriorated CBF can be approximated by an imperfect model in which the diagonals have a triangular imperfection. This imperfection is resulted by the plastic elongations and is proportional with the realised maximum interstorey drift;
- The interconnected plastic deformations, brace deterioration, change of dynamic response together create a loop that may amplify the weak storey behaviour;

The recognition of several new aspects of the seismic response of CBF-s has paved the way to a critical assessment of the Eurocode 8 regulations. In Chapter 4 the following issues with the standard design procedure have been found:

- The CBF-s designed according to Eurocode 8 are mostly susceptible to exhibit weak storey behaviour;
- The weak storey behaviour may lead to the early failure of the primary resisting members of the structure;
- The plastic deformations of the braces may eventually cause a significant change of the dynamic characteristics and the rearrangement of the inertia forces; such effects are not considered in any way in Eurocode 8;
- The incipient elastic behaviour, that the Eurocode 8 design procedure refers to, is significantly different from the inelastic behaviour;
- The uniformity condition is not adequate to promote the global dissipation as it is not valid in any random state that the structure may undergo during the seismic excitation;
- The analysis of a perfect structural model leads to the underestimation of the bending of the columns that develops with the deterioration of the braces; therefore Eurocode 8 does not safeguard sufficient overstrength in the columns, so it does not comply with the requirements of capacity design;
- The Eurocode 8 design does not make difference between CBF-s with continuous or hinged columns while the performance of the former is better;
- The local slenderness limit of hollow section braces should be more rigorous than Eurocode 3 class 1 to safely provide the adequate ductility of the braces;

Besides the critical assessment, also recommendations have been made to enhance the performance of CBF-s regardless of the presence of weak storeys. These recommendations are:

- CBF-s need to contain continuous columns that provide flexural resistance to the lateral loading. Though regular analysis methods do not yield relevant bending moment results, imposed limits to columns is a way to allow the development of considerable bending;
- Elevated local slenderness of the hollow-section braces is accountable for low ductility capacity and consequently for the possibility of early collapse. More rigorous criteria may prevent such scenario;

- In the detailing of gusset plates, the requirement of sufficient clearance that allows the rotation of the diagonal can prevent the fracture of the gusset welds;

The perhaps most important result of the research presented in this dissertation is the development of the robust seismic brace design method. The most important features of the method are listed below:

- The RSBD method is by definition complementary to the elastic design procedure of Eurocode 8. The method enhances the original designs, so that the weak storey phenomenon is strongly restricted, but seismic demands are in general determined by the initial Eurocode analysis;
- In the RSBD method the stability of the compression members is not considered, which is another reason why it is complementary to the EC8 procedure;
- Takes into consideration the variation of the modal behaviour due to the brace deterioration and the resulting response of the CBF;
- Quantifies the participation of the columns and impose requirements to their performance in the lateral resistance of a storey;
- Prevents the occurrence of the weak storey collapse mechanism independently of the design seismic action;
- Prevents the occurrence of the weak storey behaviour by unifying the (maximum) interstorey drifts on every floor;
- The possibility of second order analysis is incorporated in the RSBD method;
- The first requirement of the redesign method, imposed to the global and local load multipliers, aims to avoid the storey failure before realizing plastic deformations in the designated dissipative members i.e. the braces. This approach is related to the principles of capacity design.

$$\frac{\lambda_{loc,i}}{\lambda_{glob,i}} \geq 1.0 \text{ where } i=1..n$$

- The requirements concerning the brace performance ratios provide a well balanced distribution of the dissipation so that outlier interstorey drifts do not impair the performance of the CBF.

$$BPR_i = \frac{\lambda_{br,i}}{\lambda_{glob,i}} \text{ and } BPR_{\min} + 0.1 \geq BPR_{\max}$$

- Two simplified forms of the RSBD method have been introduced, which provide more conservative designs, but still enhance the original Eurocode 8 design.

The RSBD redesign method has to be conducted in the following steps:

- Initial design of the structure according to related codes i.e. Eurocode 3 and Eurocode 8 considering the response spectra, behaviour factor, conducting an elastic analysis and dimensioning the members according to its internal force results. In the seismic design the uniformity condition can be neglected.
- For n different loading patterns, considering the global and n local plastic mechanisms computation of n $\lambda_{glob,i}$ and $\lambda_{loc,i}$ parameter pairs. Computation of the $\lambda_{br,i}$ load multiplier of the braces for n local mechanisms.

- Reinforcement of the braces to respect the second criterion of the RSBD method. Attention is to be paid that the modification of one brace does not only change the corresponding local load multiplier and the brace participation ratio of that floor, but also all the global multipliers and every other BPR in the same time.
- Reinforcement of the columns or introduction of more continuous column splices in the building to satisfy the first condition.

The presented buildings, that satisfy the two requirements of the RSBD method but violate the uniformity of the storey overstrength condition of Eurocode 8, are adequate and exhibit a favourable dissipation without exception. The original structures designed according to EC 8 mostly do not. Therefore, the RSBD method is recommended to redesign and enhance concentrically braced steel frames.

One possibility of further development of the method is obliterating its dependence on an initial design, making it a complete design procedure. This may be carried out with the definition of design ground acceleration dependant minimum plastic load multipliers that both the local and the global multipliers need to exceed. Also, it had been found that requiring even in tall buildings that the local load multiplier must be larger than the global may be too rigorous. This may provide a limitation in building height to the application of the RSBD method. The limit may be extended by considering only partial mechanisms that extend to several floors instead of the global plastic mechanism. Furthermore, introducing uncertainties such as the real yield stress of the material may necessitate the revision of the two RSBD criteria. These questions may be subjects of further research.

Refrences

[1] U.S. Geological Survey web site http://earthquake.usgs.gov

[2] Farzan N.: The Seismic Design Handbook. Chapman & Hall, New York, 1989.

[3] Dowrick D. J.: Earthquake Resistant Design For Engineers and Architects. 2nd Edition. Wiley & Sons, Chichester, New York, 1987.

[4] EN 1998-1:2004 Eurocode 8: Design of structures for earthquake resistance – Part 1: General rules, seismic actions and rules for buildings

[5] Fardis M. N., Carvalho E., Elnashai A., Faccioli E., Pinto P., Plumier A.: Designers' Guide to EN 1998-1 and 1998-5 Eurocode 8: Design provisions for Earthquake Resistant Structures. Thomas Telford Publishing, London, 2005.

[6] Newmark N. M., Hall W. J.: Earthquake Spectra and Design. Monograph, Earthquake Engineering Research Institute, Berkeley, California, 1982.

[7] Ballio G.: ECCS approach for the design of steel structures against earthquakes. Symposium on Steel Buildings, Luxembourg 1985. IABSE-AIPC-IVBH Report, Vol. 48, pp. 373-380, 1985.

[8] Setti P.: Un metodo per la determinazione del cefficiente di struttura per le costruzioni metalliche in zona sismica. Construzioni Metalliche, N.3, 1985.

[9] Mazzolani F. M., Piluso V.: Theory and Design of Seismic Resistant Steel Frames. E $ FN Spon, 1996. ISBN 0 419 18760 X

[10] EN 1993-1-1:2005 Eurocode 3: Design of steel structures – Part 1-1: General rules and rules for buildings

[11] Paulay T., Priesley M. J.: Seismic Design of Reinforced Concrete and Masonry Buildings. John Wiley @Sons, New York, 1992.

[12] Elghazouli A.Y.: Seismic design procedures for concentrically braced frames. Proc. of the Inst. of Civil Engineers, Structures & Buildings 156, pp. 381-394, 2003.

[13] SEAOC, Vision 2000 – Performance Based Seismic Engineering of Builings. Structural Engineers Association of California, Sacramento, California, 1995.

[14] Krawinkler H., Miranda E.: Performance-Based Earthquake Engineering. In: Earthquake Engineering: From Engineering Seismology to Performance-Based Earthquake Engineering. Eds. Bozorgnia, Bertero. CRC Press, 2004.

[15] Aribert J. M., Vu H. T. : New criteria for taking account of P-Δ effects in seismic design of steel structure. STESSA 2009, Eds.: Sause R., Mazzolani F. M., Ricles J. M. doi.: 10.1201/9780203861592.ch41

[16] Freeman S.A.: The Capacity Spectrum Method as a Tool for Seismic Design, 11th European Conference on Earthquake Engineering, September 6-11th 1998, Paris

[17] Chen W. F., Lui E. M. : Earthquake Engineering for Structural Design. Taylor & Francis Group, Boca Raton, Florida, 2006.

[18] Lestuzzi P., Schwab P., Koller M., Lacave C.: How to chose earthquake recordings for nonlinear seismic analysis of structures. 13th World Conference on Earthquake Engineering, paper 1241, Vancouver, Canada, 2004.

[19] Vamvatsikos D., Cornell C. A.: Incremental Dynamic Analysis. Earthquake Engineering and Structural Dynamics, Vol. 31(3), pp. 491-514, 2002.

[20] Vamvatsikos D., Cornell C. A.: Developing efficient scalar and vector intensity measures for IDA capacity estimation by incorporating elastic spectral shape information. Earthquake Engineering and Structural Dynamics, Vol. 34(13), pp. 1573-1600, 2005.

[21] Bonneville D., Bartoletti S.: Case study 2.3: Concentric braced frame, Lankershim boulevard, North Hollywood. 1994 Northridge Earthquake; Building cas studies; proposition 122: Product 3.2, SSC 94-06, Seismic Safety Commission State of California, pp. 305-324. 1996.

[22] Black G. R., Wenger B. A., Popov E. P.: Inelastic buckling of steel struts under cyclic load reversals. Research report no. UCB/EERC-80/40, Earthquake Engineering Research Center, Berkeley, CA. 1980.

[23] Zayas V. A., Popov E. P., Mahin S. A.: Cyclic inelastic buckling of tubular steel braces. Research report no. UCB/EERC-80/16, Earthquake Engineering Research Center, Berkeley, CA. 1980.

[24] Ikeda K., Mahin S. A.: A refined physical theory model for predicting the seismic behaviour of braced frames. Report UMEE 77R3, Department of Civil Engineering, University of Michigan. 1984.

[25] Lee S., Goel S. C.: Seismic behaviour of hollow and concrete-filled square tubular bracing members. Research report no. UMCE 87-11, University of Michigan, 1987.

[26] Walpole W. R.: Behaviour of cold-formed steel RHS members under cyclic loading. Research report no. 96-4, University of Canterbury, New Zealand, 1996.

[27] Uriz P., Mahin S. A.: Toward earthquake-resistant design of concentrically braced steel-frame structures. Research report no. PEER 2008/08, Pacific Earthquake Research Center, University of California, Berkeley, 2008.

[28] Yang T. Y., Moehle J. P., Stojadinovic B.: Performance evaluation of innovative steel braced frames. Research report no. PEER 2009/103, Pacific Earthquake Research Center, University of California, Berkeley, 2009.
[29] Jin J., El-Tawil S.: Inelastic cyclic model for steel braces. Journal of Engineering Mechanics, Vol. 129, No. 5, pp. 548-557, 2003. doi.: 10.1061/(ASCE)0733-9399(2003)129:5(548)
[30] Han S.-W., Kim W. T., Foutch D. A.: Seismic behaviour of HSS bracing members according to width-thickness ratio under symmetric cyclic loading. Journal of Structural Engineering, Vol. 133, No. 2, pp. 264-273, 2007. doi.: 10.1061/(ASCE)0733-9445(2007)133:2(264)
[31] Shaback B., Brown T.: Behaviour of square hollow structural steel braces with end connections under reversed cyclic axial loading. Canadian Journal of Civil Engineering, 30, pp. 745-754, 2003. doi.: 10.1139/L03-028
[32] Tremblay R., Archambault M.-H., Filiatrault A.: Seismic response of concentrically braced steel frames made with rectangular hollow bracing members. Journal of Structural Engineering, Vol. 129, No. 12, pp. 1626-1636, 2003. doi.: 10.1061/(ASCE)0733-9445(2003)129:12(1626)
[33] Goggins J. M., Broderick B. M., Elghazouli A. Y., Lucas A. S.: Behaviour of tubular steel members under cyclic axial loading. Journal of Constructional Steel Research 62, pp. 121-131, 2005. doi.: 10.1016/j.jcsr.2005.04.012
[34] Nip K. H., Gardner L., Elghazouli A. Y.: Cyclic testing and numerical modelling of carbon steel and stainless steel tubular bracing members. Engineering Structures, Vol. 32, pp. 424-441, 2010. doi.: 10.1016/j.engstruct.2009.10.005
[35] Nip K. H., Gardner L., Elghazouli A. Y.: Ultimate behaviour of steel braces under cyclic loading. Proceedings of the Institution of Civil Engineers, Structures and Buildings, Vol. 166, pp. 219-234, 2013. doi.: 10.1680/stbu.11.00028
[36] Gioncu V., Mazzolani M.: Ductility of Seismic Resistant Steel Structures. Spon Press, London. 2002. ISBN 0-419-22550-1
[37] Gioncu V., Petcu D.: Available rotation capacity of wide-flange beams and beam-columns. Journal of Constructional Steel Research, Vol. 43, pp. 161-217, 1997.
[38] Gioncu V., Petcu D.: Computer program for available ductility analysis of steel structures. Computers and Structures, Vol. 81, pp. 2149-2164, 2003.
[39] Architectural Institute of Japan (AIJ): Load and resistance factor design of steel structures, 1986.
[40] Seismic design of petrochemical plants. prepared by the N. Z. Ministry of Works and Development, Wellington, 1981.
[41] AISC Seismic provisions for structural steel buildings. Chicago, USA, 2002.
[42] Canadian Standard Association CSA S16-01: Limit states design of steel structures. Torontr, Canada, 2001.
[43] Standards New Zealand NZS 3404 Part 1:1997: Steel structures standard. Wellington, New Zealand, 1997.
[44] Cochran M. L., Honeck W. C.: Design of special concentric braced frames. Structural Steel Educational Council, Steel Tips. 2004
[45] Yoo J.-H., Lehman D. E., Roeder C. W.: Influence of connection design parameters on the seismic performance of braced frames. Journal of Constructional Steel Research, Vol. 64, pp. 607-623, 2008.
[46] Lehman D. E., Roeder C. W., Herman D., Johnson S., Kotulka B.: Improved seismic performance of gusset plate connections. Journal of Structural Engineering, Vol 134, No. 6, pp. 890-901, 2008.
[47] Roeder C. W., Lumpkin E. J., Lehman D. E.: A balanced design procedure for special concentrically braced frame connections. Journal of Constructional Steel Research, Vol. 67, No. 11, pp. 1760-1772, 2011
[48] Tremblay R.: Achieving a stable inelastic seismic response for multi-storey concentrically braced steel frames. Engineering Journal, 2003 second quarter, pp. 111-129.
[49] Martinelli L., Perotti F., Bozzi A.: Sesimic design and response of a 14-storey concentrically braced steel building. STESSA 2000 Conference, Montreal, Canada, Mazzolani F., Tremblay R. eds., pp. 327-334.
[50] American Institute of Steel Construction (AISC): Seismic provisions for structural steel buildings. Chicago, 1997.
[51] Chopra A. K., Goel R. K., Chintanapakdee C.: Evaluation of a modified MPA procedure assuming higher modes as elastic to estimate seismic demands. Earthquake Spectra, Vol. 20, No. 3, pp. 757-778, 2004. doi: 10.1193/1.1775237
[52] Györgyi J.: Corrected ground motion functions in the case of near-fault earthquake. The Tenth Int. Conf. on Computational Structures Technology, paper 326, pp.1-10, Valencia, Spain, 2010
[53] Elghazouli A.Y.: Seismic design of steel-framed structures to Eurocode 8. The 14th World Conference on Earthquake Engineering, Beijing, China. 2008.
[54] Longo A., Montuori R., Piluso V.: Failure mode control of X-braced frames under seismic actions. Journal of Earthquake Engineering, 12:728-759. 2008. doi: 10.1080/13632460701572955

[55] Giugliano M. T., Longo A., Montuori R., Piluso V.: Plastic design of CB-frames with reduced section solution for bracing members. Journal of Constructional Steel Research, Vol. 66, pp. 611-621, 2010. doi.: 10.1016/j.csr.2010.01.001
[56] Brandonisio G., Toreno M., Grande E., Mele E., De Luca A.: Seismic design of concentric braced frames. Journal of Constructional Steel Research, 78:22-37, 2012. doi: 10.1016/j.jcsr.2012.06.003
[57] Watanabe A., Hitomi Y., Saeki E., Wada A., Fujimoto M.: Properties of brace encased in buckling-restraining concrete and steel tube. Proc. 9th World Conf. Earthquake Engineering, vol. 4, pp. 719-724, 1988.
[58] Xie Q.: State-of-the-art of buckling restrained braces in Asia. Journal of Constructional Steel Research, 61:727-748, 2005.
[59] Zsarnóczay Á.: Experimental and Numerical Investigation of Buckling Restrained Braced Frames for Eurocode Conform Design Procedure Development. PhD Dissertation, Department of Structural Engineering, Budapest University of Technology and Economics. 2013.
[60] Sause R., Ricles J. M., Roke D., Seo C-Y., Lee K-S.: Design of self-centering steel concentrically-braced frames. Proc. 4th International Conference on Earthquake Engineering, Taipei, Taiwan, paper no. 122, 2006.
[61] Zhu S., Zhang Y.: Seismic analysis of concentrically braced frame system with self-centering friction damping braces. ASCE Journal of Structural Engineering, 134:1, 121-131, 2008.
[62] EN 1991-1-1:2002 Eurocode 1: Actions on structures – Part 1-1: General actions – Densities, self-weight, iposed loads for buildings
[63] EN 1991-1-4:2005 Eurocode 1: Actions on structures – Part 1-4: General actions – Wind actions
[64] Kalkan E., Kunnath S. K.: Adaptive modal combination procedure for nonlinear static analysis of building structures. Journal of Structural Engineering, Vol. 132, No. 11, pp. 1721-1731, 2006. doi.: 10.1061/(ASCE)0733-9445(2006)132:11(1721)
[65] Kalkan E., Kunnath S. K.: Assessment of current nonlinear static procedures for seismic evaluation of buildings. Engineering Structures, Vol. 29, pp. 305-316, 2007. doi.: 10.1016/j.engstruct.2006.04.012
[66] De Ville V.: FINELG: nonlinear finite element analysis program, User's Manual Version 9.0, Ulg et BEG, 2003.
[67] Menegotto M., Pinto P.: Method of analysis for cyclically loaded reinforced concrete plane frames including changes in geometry and nonelastic behaviour of elements under combined normal force and bending. IABSE Symposium on resistance and ultimate deformability of structures acted on by well-defined repeated loads, Lisbon. 1973.
[68] Braconi A et al (2011) OPUS Project final report. European Union, RFCS program
[69] Wilson E. L.: Three-dimensional static and dynamic analysis of structures, A physical approach with emphasis on Earthquake Engineering. Computers and Structures Inc., Berkeley, California. third edition 2002. ISBN 0-923907-00-9.
[70] Merczel D. B, Somja H., Aribert J-M, Lógó, J: On the behavior of concentrically braced frames subjected to seismic loading Periodica Politechnica Civil Engineering, 57/2, 113-122, 2013.
[71] Büssow M.: An algorithm for the continuous Morlet wavelet transform. Mechanical Systems and Signal Processing, Vol. 21, pp. 2970-2979, 2007.
[72] Holschneider M., Kronland-Martinet M., Morlet J., Tchamitchian P.: A real-time algorithm for signal analysis with the help of the wavelet transform. 1988.
[73] ASCE – Federal Emergency Management Agency 356: Prestandard and commentary for the seismic rehabilitation of builidnigs. 2000.
[74] Kaliszky S.: Plasticity. Theory and Engineering Applications. Akadémia Kiadó Budapest, 1989.
[75] Moghaddam H., Hajirasouliha I., Doostan A.: Optimum seismic design of concentrically braced steel frames: concepts and design procedures. Journal of Constructional Steel Research, 61, pp. 151-166, 2005. doi.: 10.1016/j.jcsr.2004.08.002
[76] Priestley M.J.N., Calvi M.C., Kowalsky M.j.:Displacment-Based Seismic Design of Structures. IUSS Press, Pavia, 2007. ISBN 978-88-6198-000-6
[77] Kaliszky S, Lógó J, Merczel B D: Softening and hardening constitutive models and their application to the analysis of bar structures. MECHANICS BASED DESIGN OF STRUCTURES AND MACHINES 39:(3) pp. 334-345. (2011) doi: 10.1080/15397734.2011555733
[78] D. B. Merczel, H. Somja, J.-M. Aribert, M. Hjiaj, J. Lógó: On the weak storey behaviour of concentrically braced frames. Eurodyn 2014 Porto, Portugal, 2014.06.30-2014.07.02. Paper 1629.
[79] D. B. Merczel, H. Somja, J.-M. Aribert, M. Hjiaj, J. Lógó: Plasticity-based method to avoid weak storey behaviour of concentrically braced frames. Eurosteel 2014 Naples, Italy, 2014.09.10-2014.09.12. Paper 683.
[80] D. B. Merczel, H. Somja, J.-M. Aribert, M. Hjiaj, J. Lógó: On the plasticity based seismic design of concentrically braced steel frames. In: C Adam, R Heuer, W Lenhardt, C Schranz (szerk.) Vienna Congress on Recent Advances in Earthquake Engineering and Structural Dynamics 2013 (VEESD 2013). Wien, Ausztria, 2013.08.28-2013.08.30. pp. 1-10. Paper 179.

[81] Merczel Dániel Balázs: On the behaviour of concentrically braced frames subjected to seismic loading. In: Józsa János, Lovas Tamás, Németh Róbert (szerk.) Proceedings of the Conference of Junior Researchers in Civil Engineering 2012. Budapest, Magyarország, 2012.06.19-2012.06.20. Budapesti Műszaki és Gazdaságtudományi Egyetem, pp. 116-125. ISBN: 978-963-313-061-2
[82] Merczel Dániel Balázs: The development of the soft-storey mechanism in concentrically braced steel frames subjected to seismic action. In: Józsa János, Lovas Tamás, Németh Róbert (szerk.) Proceedings of the Second Conference of Junior Researchers in Civil Engineering. Budapest, Magyarország, 2013.06.17-2013.06.18. Budapest: Budapesti Műszaki és Gazdaságtudományi Egyetem
[83] Daniel B. Merczel, Jean-Marie Aribert, Hugues Somja, Mohammed Hjiaj, János Lógó: On the weak storey behaviour of concentrically braced frames. 8th International Conference on Behavior of Steel Structures in Seismic Areas STESSA 2015, Shanghai, China, July 1-3, 2015.
[84] Daniel B. Merczel, Jean-Marie Aribert, Hugues Somja, Mohammed Hjiaj, János Lógó: A method to avoid weak storey mechanisms in concentrically braced frames. 8th International Conference on Behavior of Steel Structures in Seismic Areas STESSA 2015, Shanghai, China, July 1-3, 2015.

Annex

Annex A: Acceleration records used for IDA

Annex B: Details of Eurocode analysis and design of CBF-s

Annex A

Accelerogram 1

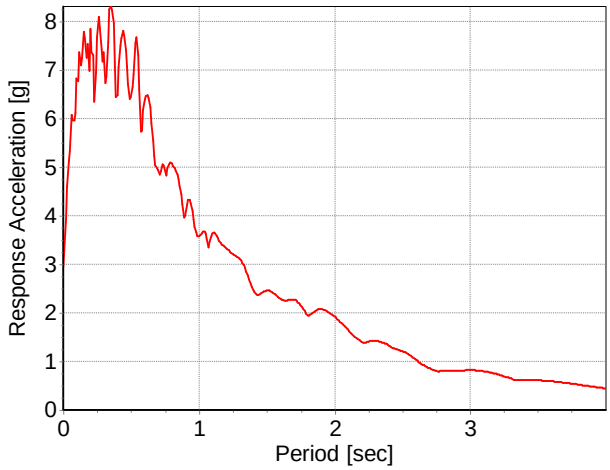

Maximum Acceleration: 2.944g
at time t=9.660sec
Maximum Velocity: 281.408cm/sec
at time t=15.180sec
Maximum Displacement: 131.222cm
at time t=10.830sec

Acceleration RMS: 0.845g
Velocity RMS: 83.301cm/sec
Displacement RMS: 40.909cm

Characteristic Intensity (Ic): 3.474
Specific Energy Density: 138851.852cm2/sec

Sustained Maximum Acceleration (SMA): 2.790g
Sustained Maximum Velocity (SMV): 230.570cm/sec
Effective Design Acceleration (EDA): 2.940g

Predominant Period (Tp): 0.340sec
Mean Period (Tm): 0.427sec

Time series:

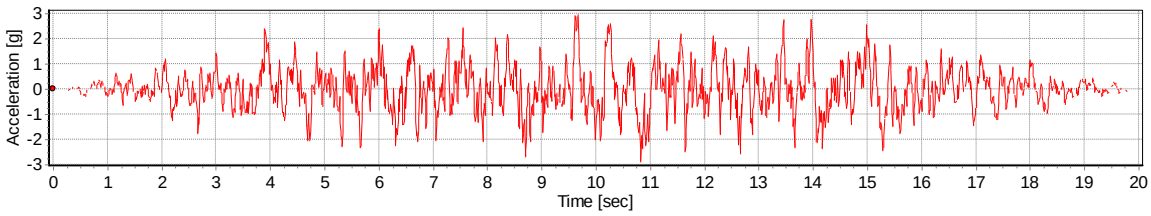

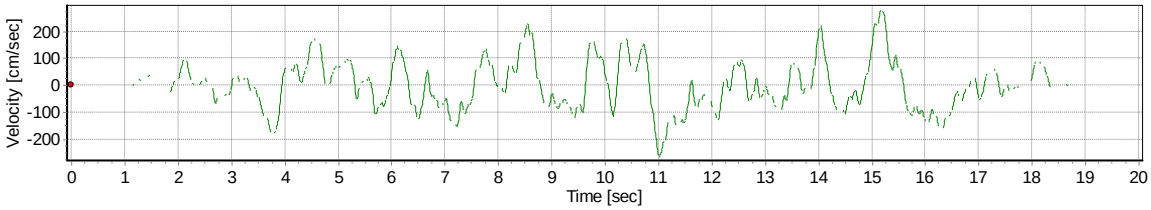

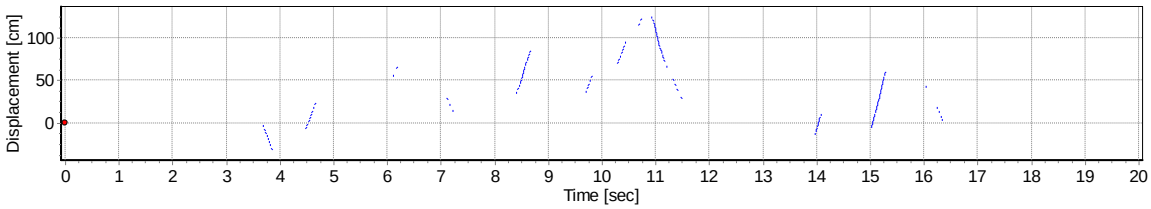

Accelerogram 2

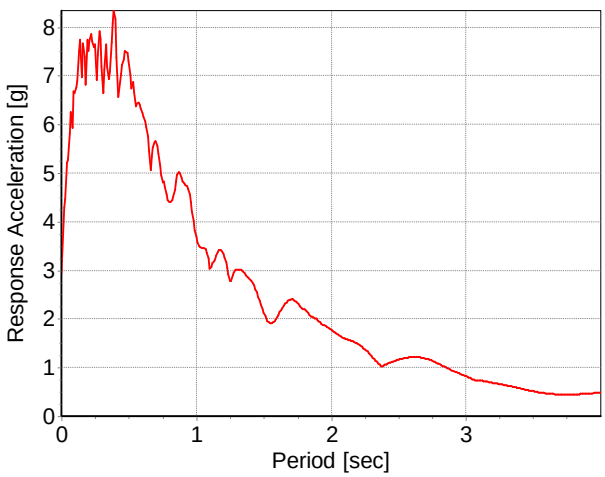

Maximum Acceleration: 2.943g
at time t=7.460sec
Maximum Velocity: 322.775cm/sec
at time t=15.940sec
Maximum Displacement: 145.242cm
at time t=10.790sec

Acceleration RMS: 0.881g
Velocity RMS: 88.454cm/sec
Displacement RMS: 57.478cm

Characteristic Intensity (Ic): 3.698
Specific Energy Density: 156560.414cm2/sec

Sustained Maximum Acceleration (SMA): 2.797g
Sustained Maximum Velocity (SMV): 251.539cm/sec
Effective Design Acceleration (EDA): 2.628g

Predominant Period (Tp): 0.400sec
Mean Period (Tm): 0.441sec

Time series:

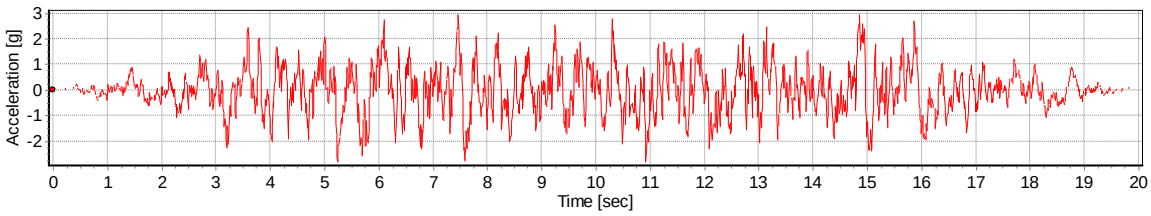

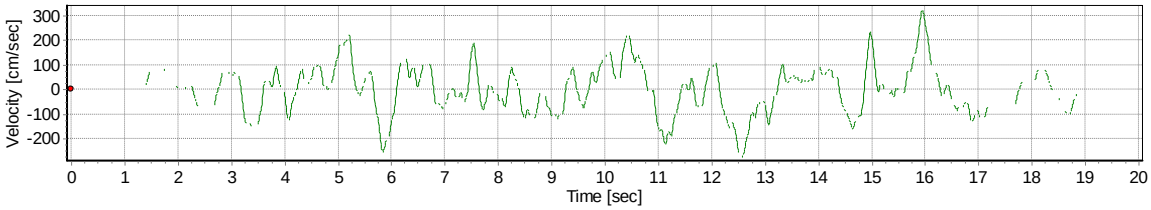

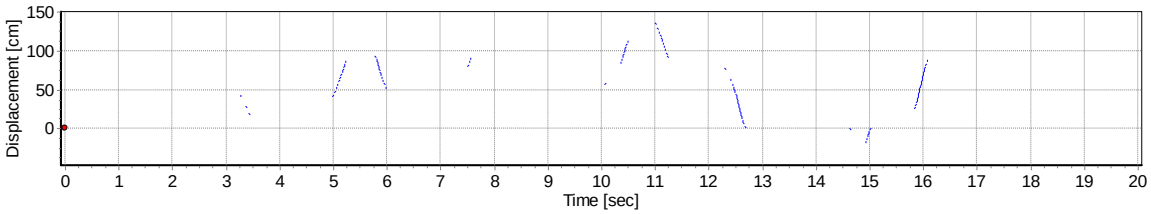

Accelerogram 3

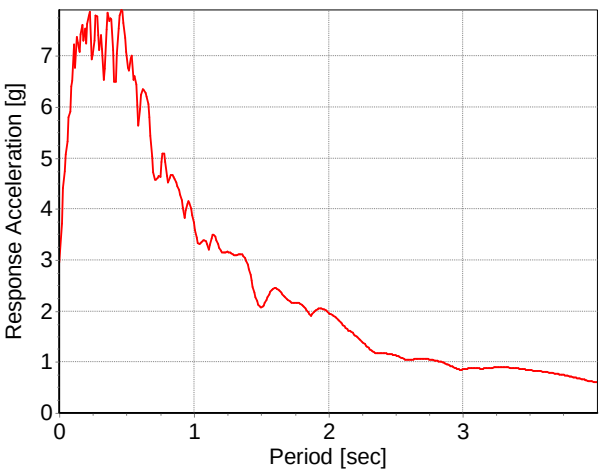

Maximum Acceleration: 2.944g
at time t=10.620sec
Maximum Velocity: 312.570cm/sec
at time t=11.340sec
Maximum Displacement: 112.512cm
at time t=4.830sec

Acceleration RMS: 0.845g
Velocity RMS: 90.150cm/sec
Displacement RMS: 42.184cm

Characteristic Intensity (Ic): 3.475
Specific Energy Density: 162623.410cm2/sec

Sustained Maximum Acceleration (SMA): 2.751g
Sustained Maximum Velocity (SMV): 255.916cm/sec
Effective Design Acceleration (EDA): 2.629g

Predominant Period (Tp): 0.460sec
Mean Period (Tm): 0.439sec

Time series:

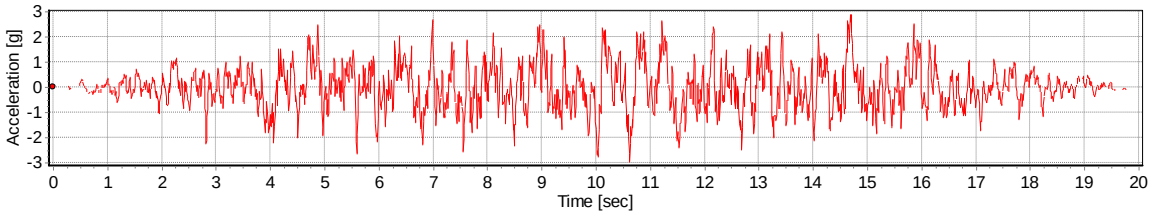

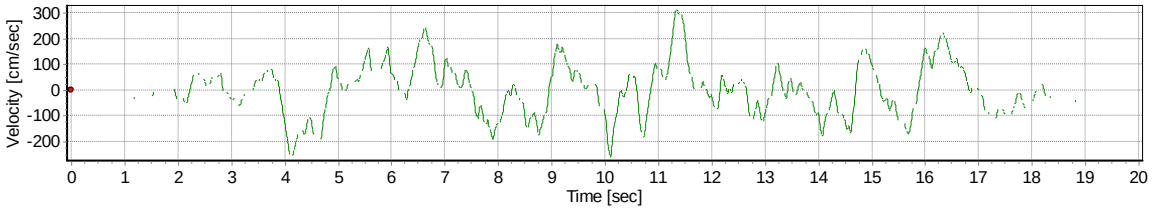

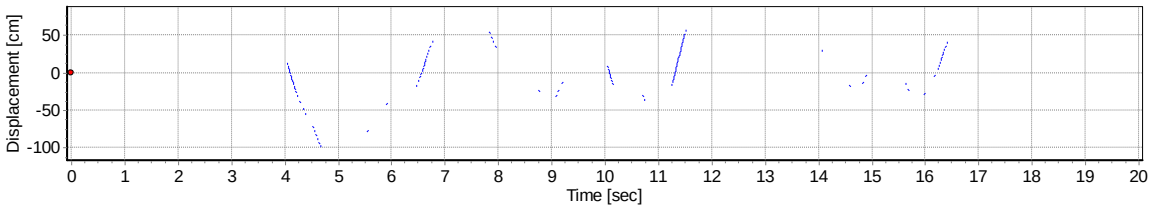

Accelerogram 4

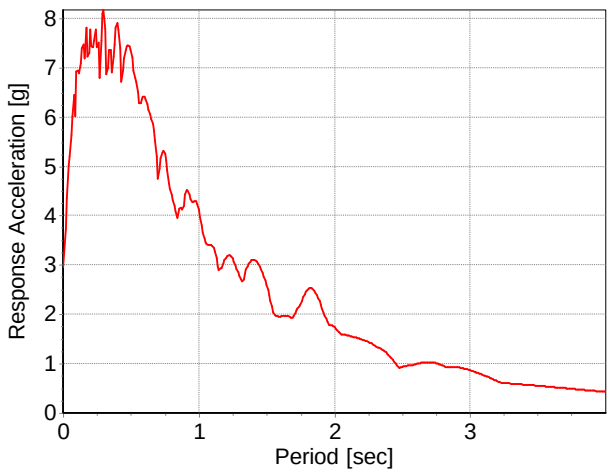

Maximum Acceleration: 2.948g
at time t=7.890sec
Maximum Velocity: 274.624cm/sec
at time t=5.940sec
Maximum Displacement: 116.615cm
at time t=8.880sec

Acceleration RMS: 0.894g
Velocity RMS: 88.202cm/sec
Displacement RMS: 53.380cm

Characteristic Intensity (Ic): 3.781
Specific Energy Density: 155670.330cm2/sec

Sustained Maximum Acceleration (SMA): 2.876g
Sustained Maximum Velocity (SMV): 215.560cm/sec
Effective Design Acceleration (EDA): 2.777g

Predominant Period (Tp): 0.300sec
Mean Period (Tm): 0.426sec

Time series:

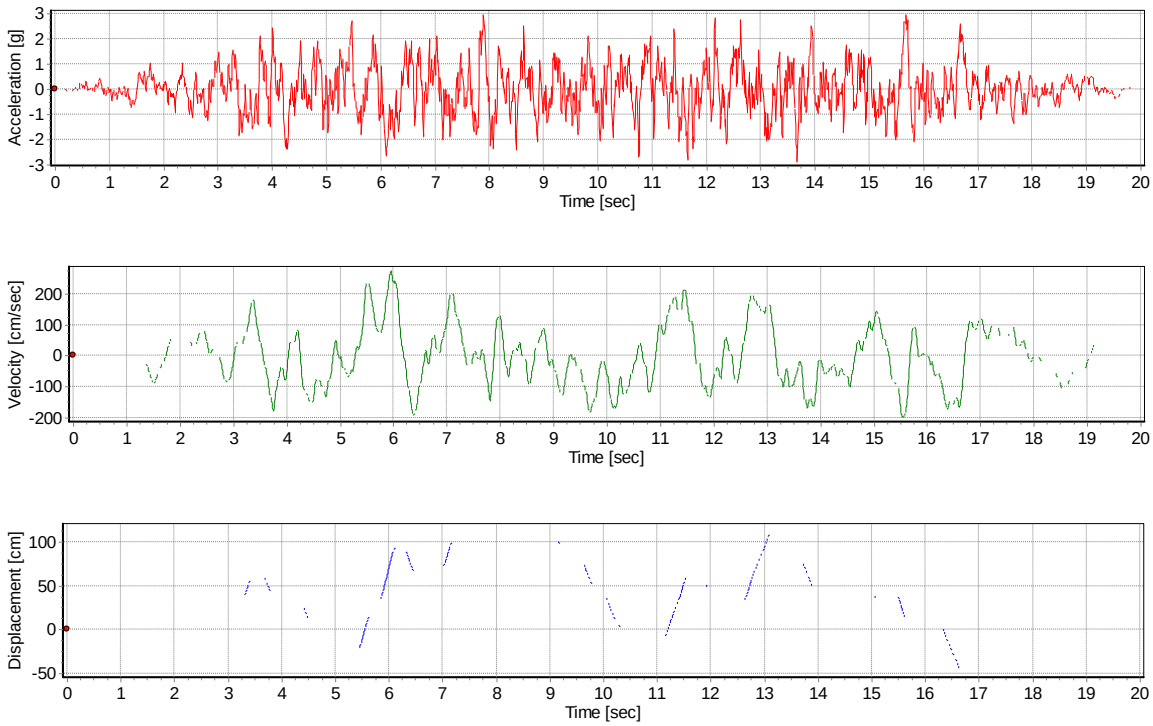

Accelerogram 5

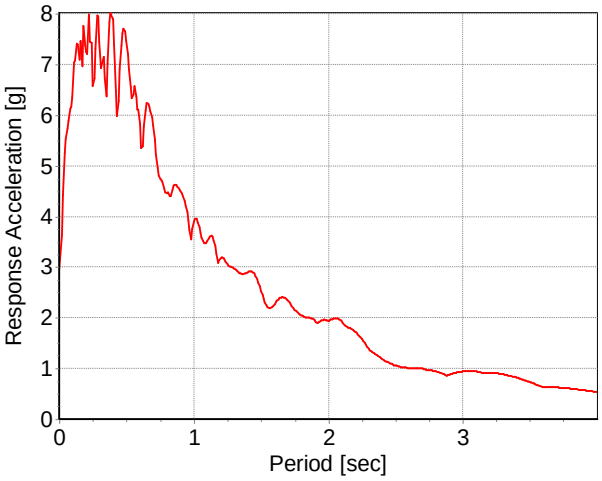

Maximum Acceleration: 2.943g
at time t=10.570sec
Maximum Velocity: 281.020cm/sec
at time t=9.360sec
Maximum Displacement: 170.284cm
at time t=11.890sec

Acceleration RMS: 0.835g
Velocity RMS: 84.709cm/sec
Displacement RMS: 67.712cm

Characteristic Intensity (Ic): 3.415
Specific Energy Density: 143583.960cm2/sec

Sustained Maximum Acceleration (SMA): 2.858g
Sustained Maximum Velocity (SMV): 227.838cm/sec
Effective Design Acceleration (EDA): 2.767g

Predominant Period (Tp): 0.380sec
Mean Period (Tm): 0.430sec

Time series:

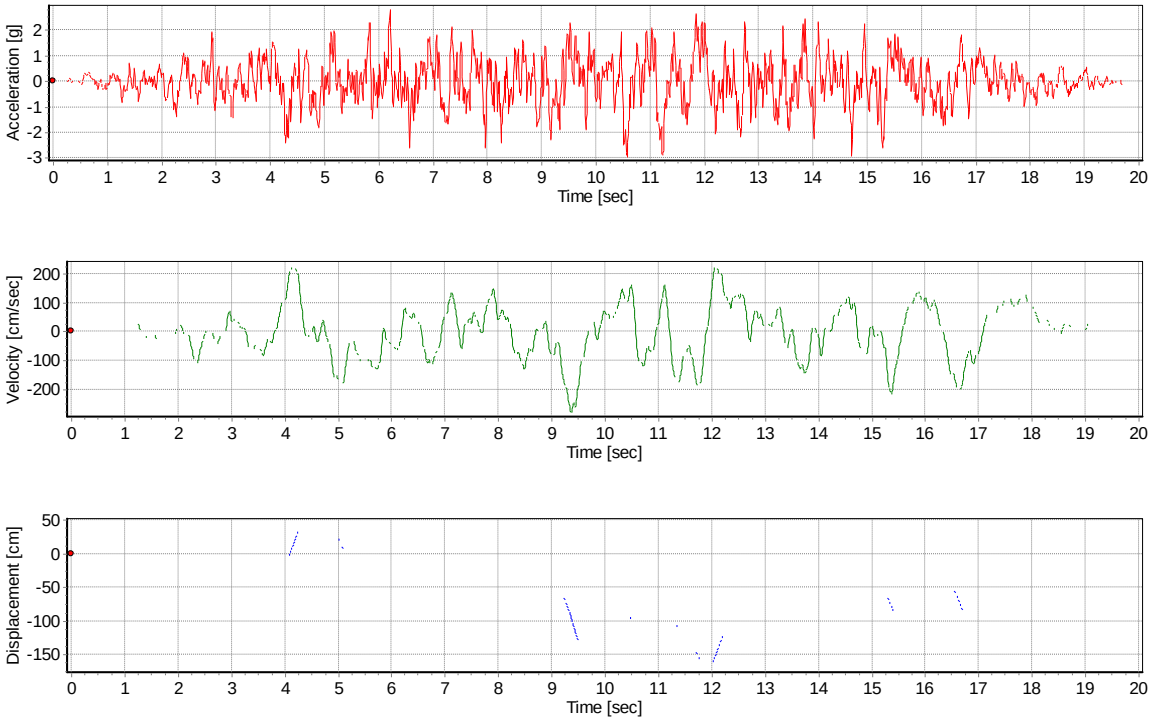

Accelerogram 6

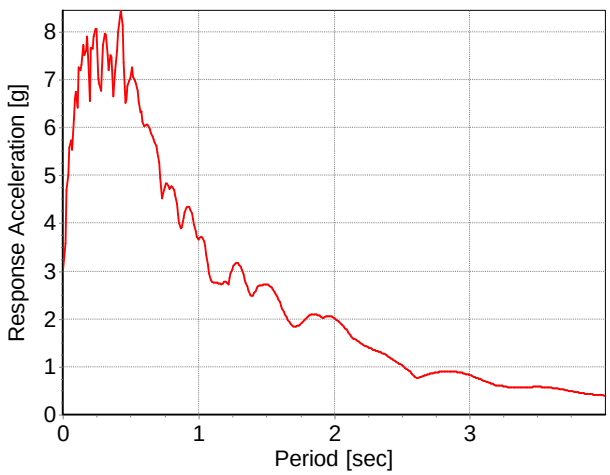

Maximum Acceleration: 2.946g
at time t=8.160sec
Maximum Velocity: 284.823cm/sec
at time t=13.750sec
Maximum Displacement: 134.135cm
at time t=7.430sec

Acceleration RMS: 0.879g
Velocity RMS: 87.955cm/sec
Displacement RMS: 56.510cm

Characteristic Intensity (Ic): 3.688
Specific Energy Density: 154798.067cm2/sec

Sustained Maximum Acceleration (SMA): 2.746g
Sustained Maximum Velocity (SMV): 211.650cm/sec
Effective Design Acceleration (EDA): 2.681g

Predominant Period (Tp): 0.420sec
Mean Period (Tm): 0.425sec

Time series:

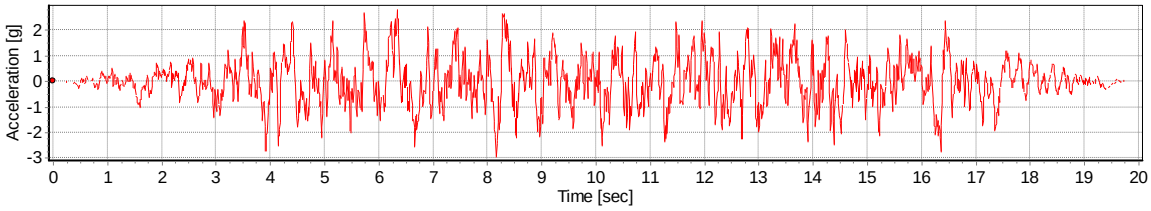

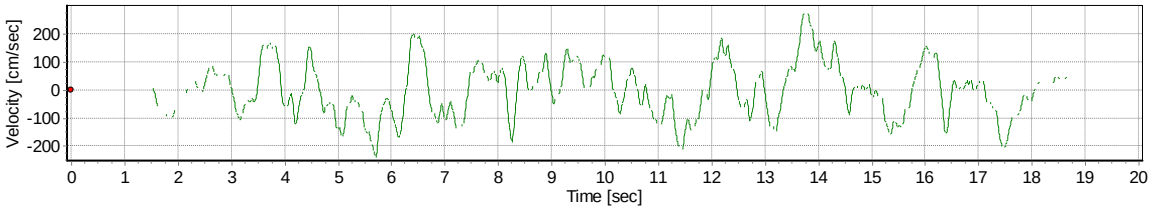

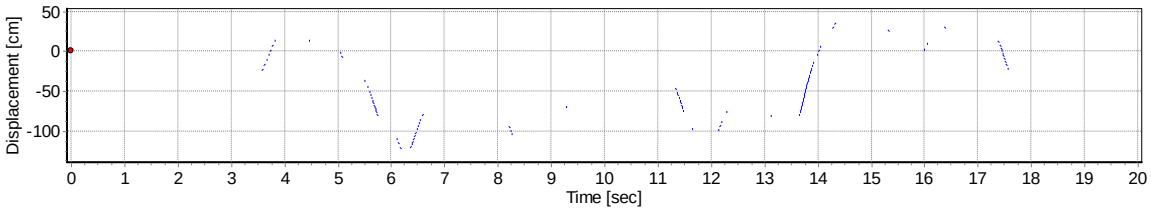

Accelerogram 7

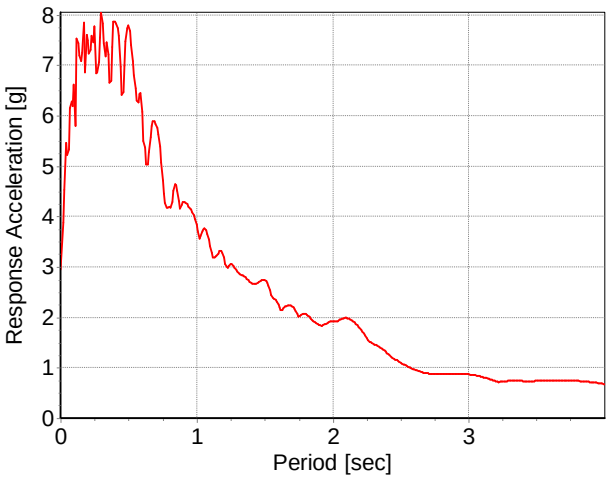

Maximum Acceleration: 2.944g
at time t=11.620sec
Maximum Velocity: 321.298cm/sec
at time t=12.420sec
Maximum Displacement: 100.305cm
at time t=11.900sec

Acceleration RMS: 0.836g
Velocity RMS: 88.697cm/sec
Displacement RMS: 45.033cm

Characteristic Intensity (Ic): 3.418
Specific Energy Density: 157421.560cm2/sec

Sustained Maximum Acceleration (SMA): 2.829g
Sustained Maximum Velocity (SMV): 245.205cm/sec
Effective Design Acceleration (EDA): 2.688g

Predominant Period (Tp): 0.300sec
Mean Period (Tm): 0.430sec

Time series:

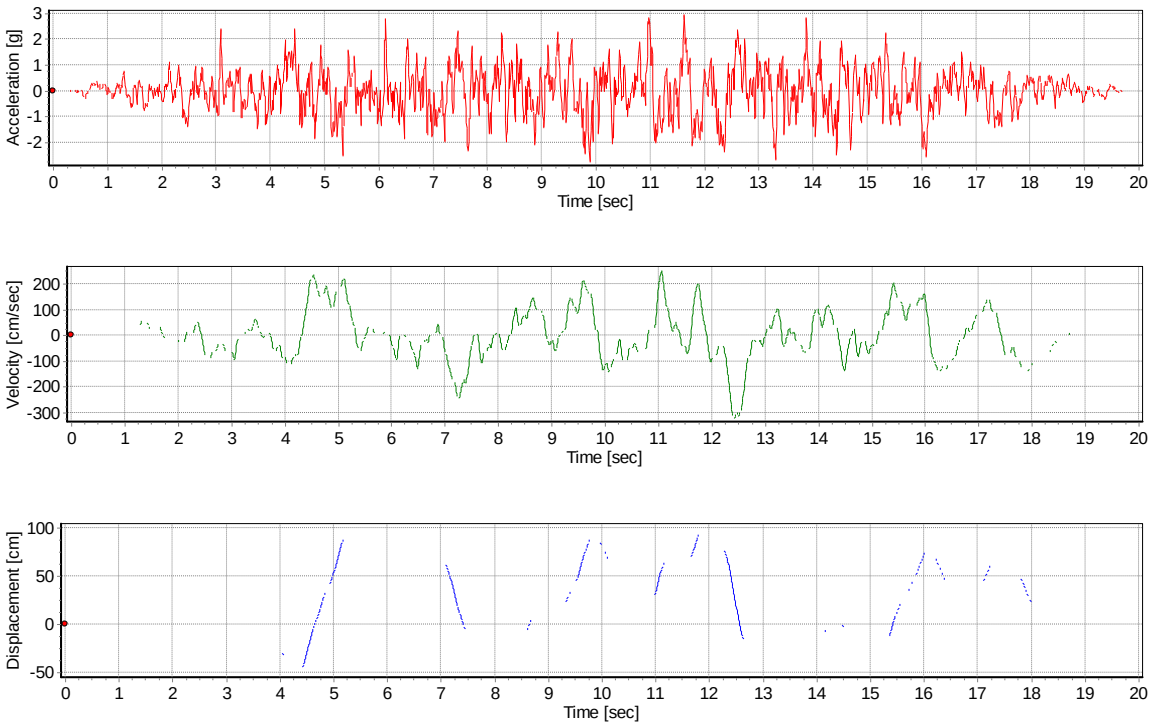

Annex B

Column design results CBF41-EC8

storey	*section*	N_{Ed}	M_{yEd}	M_{zEd}	N_{Rk}	M_{yRk}	M_{zRk}	χ_y	χ_z	*eff.*
4	HEA 140	340.9	2.2	0.9	737.9	40.8	19.9	0.86	0.60	0.85
3	HEA 200	752.4	4.8	1.8	1264.3	100.9	47.9	0.93	0.76	0.82
2	HEB 200	1218.6	5.5	2.0	1835.4	151.0	71.9	0.94	0.77	0.89
1	HEB 240	1743.5	5.5	2.0	2491.0	247.5	117.1	0.96	0.83	0.87
4	HEA 160	491.4	0.0	0.0	911.8	57.6	27.6	0.89	0.66	0.82
3	HEB 180	982.8	0.0	0.0	1534.6	113.1	54.3	0.92	0.73	0.88
2	HEB 220	1474.2	0.0	0.0	2138.5	194.3	92.6	0.95	0.80	0.86
1	HEB 260	1965.6	0.0	0.0	2782.4	301.5	141.5	0.97	0.85	0.83

Column design results CBF42-EC8

storey	*section*	N_{Ed}	M_{yEd}	M_{zEd}	N_{Rk}	M_{yRk}	M_{zRk}	χ_y	χ_z	*eff.*
4	HEA 200	350.2	92.4	2.0	1264.3	100.9	47.9	0.93	0.76	0.90
3	HEB 200	778.4	110.9	3.1	1534.6	113.1	54.3	0.92	0.73	1.01
2	HEB 220	1259.7	121.7	5.5	2138.5	194.3	92.6	0.95	0.80	0.93
1	HEB 280	1819.6	224.8	5.5	3087.9	360.5	168.6	0.98	0.87	1.01
4	HEA 180	295.4	53.9	3.1	1064.6	76.4	36.8	0.91	0.72	0.80
3	HEB 180	586.6	95.5	4.6	1534.6	113.1	54.3	0.92	0.73	0.96
2	HEB 220	586.6	95.5	4.6	1534.6	113.1	54.3	0.95	0.80	0.96
1	HEB 260	1157.4	237.2	7.1	2782.4	301.5	141.5	0.97	0.85	0.94

Column design results CBF61-EC8

storey	*section*	N_{Ed}	M_{yEd}	M_{zEd}	N_{Rk}	M_{yRk}	M_{zRk}	χ_y	χ_z	*eff.*
6	HEA 160	308.1	2.6	8.0	911.8	57.6	27.6	0.89	0.66	0.79
5	HEA 180	671.5	3.5	1.7	1064.6	76.4	36.8	0.91	0.72	0.92
4	HEB 200	1058.5	6.3	2.5	1835.4	151.0	71.9	0.94	0.77	0.78
3	HEB 220	1474.6	7.3	3.4	2138.5	194.3	92.6	0.95	0.80	0.89
2	HEB 240	1917.0	11.0	4.0	2491.0	247.5	117.1	0.96	0.83	0.96
1	HEB 280	2416.0	11.0	4.0	3087.9	360.5	168.6	0.98	0.87	0.93
6	HEA 160	491.4	0.0	0.0	911.8	57.6	27.6	0.89	0.66	0.82
5	HEB 180	982.8	0.0	0.0	1534.6	113.1	54.3	0.92	0.73	0.88
4	HEB 220	1474.2	0.0	0.0	2138.5	194.3	92.6	0.95	0.80	0.86
3	HEB 240	1965.6	0.0	0.0	2491.0	247.5	117.1	0.96	0.83	0.95
2	HEB 280	2457.0	0.0	0.0	3087.9	360.5	168.6	0.98	0.87	0.91
1	HEB 300	2948.4	0.0	0.0	3503.9	439.2	204.5	0.98	0.89	0.95

Column design results CBF62-EC8

storey	*section*	N_{Ed}	M_{yEd}	M_{zEd}	N_{Rk}	M_{yRk}	M_{zRk}	χ_y	χ_z	*eff.*
6	HEA 180	312.6	73.6	1.0	1064.6	76.4	36.8	0.91	0.72	0.96
5	HEB 180	698.6	105.9	1.8	1534.6	113.1	54.3	0.92	0.73	0.92
4	HEB 200	1117.7	117.7	2.9	1835.4	151.0	71.9	0.94	0.77	1.03
3	HEB 240	1578.8	132.4	3.7	2491.0	247.5	117.1	0.96	0.83	0.92
2	HEB 260	2070.8	156.0	4.9	2782.4	301.5	141.5	0.97	0.85	1.02
1	HEB 320	2638.1	229.5	4.9	3790.6	505.0	220.7	0.99	0.89	0.99
6	HEA 180	297.1	63.3	1.2	1064.6	76.4	36.8	0.91	0.72	0.85
5	HEB 180	580.6	91.2	2.6	1534.6	113.1	54.3	0.92	0.73	0.96
4	HEB 240	871.9	128.0	4.1	2491.0	247.5	117.1	0.96	0.83	0.78
3	HEB 260	1156.5	144.2	5.3	2782.4	301.5	141.5	0.97	0.85	0.89
2	HEB 280	1438.5	172.1	7.4	3087.9	360.5	168.6	0.98	0.87	0.98
1	HEB 320	1720.1	325.1	7.4	3790.6	505.0	220.7	0.99	0.89	0.99

Column design results CBF81-EC8

storey	*section*	N_{Ed}	M_{yEd}	M_{zEd}	N_{Rk}	M_{yRk}	M_{zRk}	χ_y	χ_z	*eff.*
8	HEA 160	309.2	2.0	0.0	911.8	57.6	27.6	0.89	0.66	0.53
7	HEA 180	681.5	3.0	1.0	1064.6	76.4	36.8	0.91	0.72	0.92
6	HEB 200	1092.0	6.0	2.0	1835.4	151.0	71.9	0.94	0.77	0.80
5	HEB 220	1539.3	6.0	2.0	2138.5	194.3	92.6	0.95	0.80	0.92
4	HEB 240	2007.7	12.0	4.0	2491.0	247.5	117.1	0.96	0.83	1.01
3	HEB 280	2518.1	13.0	4.0	3087.9	360.5	168.6	0.98	0.87	0.97
2	HEB 320	3047.0	20.0	7.0	3790.6	505.0	220.7	0.99	0.89	0.95
1	HEM 240	3640.3	20.0	7.0	4690.6	497.5	236.4	0.97	0.84	0.96
8	HEA 160	491.4	0.0	0.0	911.8	57.6	27.6	0.89	0.66	0.82
7	HEB 180	982.8	0.0	0.0	1534.6	113.1	54.3	0.92	0.73	0.88
6	HEB 220	1474.2	0.0	0.0	2138.5	194.3	92.6	0.95	0.80	0.86
5	HEB 240	1965.6	0.0	0.0	2491.0	247.5	117.1	0.96	0.83	0.95
4	HEB 280	2457.0	0.0	0.0	3087.9	360.5	168.6	0.98	0.87	0.91
3	HEB 300	2948.4	0.0	0.0	3503.9	439.2	204.5	0.98	0.89	0.95
2	HEM 240	3439.8	0.0	0.0	4690.6	497.5	236.4	0.97	0.84	0.87
1	HEM 240	3931.2	0.0	0.0	4690.6	497.5	236.4	0.97	0.84	0.99

Column design results CBF82-EC8

storey	*section*	N_{Ed}	M_{yEd}	M_{zEd}	N_{Rk}	M_{yRk}	M_{zRk}	χ_y	χ_z	*eff.*
8	HEA 160	301.6	95.8	1.1	1264.3	100.9	47.9	0.93	0.76	0.86
7	HEA 180	685.0	102.8	1.8	1534.6	113.1	54.3	0.92	0.73	0.90
6	HEB 200	1108.7	113.9	2.8	1835.4	151.0	71.9	0.94	0.77	1.01
5	HEB 220	1577.7	144.4	4.2	2491.0	247.5	117.1	0.96	0.83	0.93
4	HEB 240	2071.4	144.4	6.9	2782.4	301.5	141.5	0.97	0.85	1.02
3	HEB 280	2616.6	168.0	6.9	3503.9	439.2	204.5	0.98	0.89	1.01
2	HEB 320	3181.1	175.0	9.7	4728.2	638.7	280.6	0.99	0.89	0.88

storey	section	N_{Ed}	M_{yEd}	M_{zEd}	N_{Rk}	M_{yRk}	M_{zRk}	χ_y	χ_z	eff.
1	HEM 240	3826.7	231.9	9.7	4728.2	638.7	280.6	0.99	0.89	1.03
8	HEA 160	296.1	59.7	1.1	1064.6	76.4	36.8	0.91	0.72	0.82
7	HEB 180	585.7	93.0	1.8	1534.6	113.1	54.3	0.92	0.73	0.95
6	HEB 220	872.7	129.2	2.8	2138.5	194.3	92.6	0.95	0.80	0.92
5	HEB 240	1158.9	140.3	4.2	2782.4	301.5	141.5	0.97	0.85	0.88
4	HEB 280	1445.0	183.3	6.9	3087.9	360.5	168.6	0.98	0.87	0.97
3	HEB 300	1728.6	195.8	6.9	3503.9	439.2	204.5	0.98	0.89	1.03
2	HEM 240	2009.5	215.3	9.7	4728.2	638.7	280.6	0.99	0.89	0.89
1	HEM 240	2292.4	436.1	9.7	5365.1	818.3	395.5	1.00	0.93	0.88

Column design results CBF101-EC8

storey	section	N_{Ed}	M_{yEd}	M_{zEd}	N_{Rk}	M_{yRk}	M_{zRk}	χ_y	χ_z	eff.
10	HEA 160	313.0	2.0	1.0	911.8	57.6	27.6	0.89	0.66	0.57
9	HEA 180	696.5	3.0	1.0	1064.6	76.4	36.8	0.91	0.72	0.94
8	HEB 200	1124.3	6.0	2.0	1835.4	151.0	71.9	0.94	0.77	0.83
7	HEB 220	1599.1	6.0	2.0	2138.5	194.3	92.6	0.95	0.80	0.95
6	HEB 260	2101.3	12.0	4.0	2782.4	301.5	141.5	0.97	0.85	0.91
5	HEB 280	2650.4	14.0	4.0	3087.9	360.5	168.6	0.98	0.87	1.02
4	HEB 320	3215.2	23.0	7.0	3790.6	505.0	220.7	0.99	0.89	1.00
3	HEM 240	3825.7	23.0	7.0	4690.6	497.5	236.4	0.97	0.84	1.01
2	HEM 260	4468.8	18.0	6.0	5160.6	593.1	280.1	0.98	0.86	1.03
1	HD320×198	5147.1	14.0	5.0	5929.1	817.6	359.6	0.99	0.89	0.99
10	HEA 160	491.4	0.0	0.0	911.8	57.6	27.6	0.89	0.66	0.82
9	HEB 180	982.8	0.0	0.0	1534.6	113.1	54.3	0.92	0.73	0.88
8	HEB 220	1474.2	0.0	0.0	2138.5	194.3	92.6	0.95	0.80	0.86
7	HEB 240	1965.6	0.0	0.0	2491.0	247.5	117.1	0.96	0.83	0.95
6	HEB 280	2457.0	0.0	0.0	3087.9	360.5	168.6	0.98	0.87	0.91
5	HEB 300	2948.4	0.0	0.0	3503.9	439.2	204.5	0.98	0.89	0.95
4	HEM 240	3439.8	0.0	0.0	4690.6	497.5	236.4	0.97	0.84	0.87
3	HEM 240	3931.2	0.0	0.0	4690.6	497.5	236.4	0.97	0.84	0.99
2	HEM 260	4422.6	0.0	0.0	5160.6	593.1	280.1	0.98	0.86	0.99
1	HEM 280	4914.0	0.0	0.0	5644.7	697.0	328.3	0.98	0.88	0.99

Column design results CBF102-EC8

storey	section	N_{Ed}	M_{yEd}	M_{zEd}	N_{Rk}	M_{yRk}	M_{zRk}	χ_y	χ_z	eff.
10	HEB 180	315.5	134.5	1.4	1534.6	113.1	54.29	0.92	0.73	0.98
9	HEB 180	720.0	114.7	1.4	1534.6	113.1	54.29	0.92	0.73	0.97
8	HEB 220	1175.7	128.9	2.8	2138.5	194.3	92.57	0.95	0.80	0.88
7	HEB 240	1679.1	160.0	4.2	2491.0	247.5	117.12	0.96	0.83	1.00
6	HEB 280	2227.4	161.5	4.2	3087.9	360.5	168.64	0.98	0.87	0.95
5	HEB 320	2816.3	203.9	7.1	3790.6	505.0	220.69	0.99	0.89	1.01
4	HD320×158	3443.1	202.5	9.9	4728.2	638.7	280.59	0.99	0.89	0.96

storey	*section*	N_{Ed}	M_{yEd}	M_{zEd}	N_{Rk}	M_{yRk}	M_{zRk}	χ_y	χ_z	*eff.*
3	HD360×179	4109.0	186.9	9.9	5365.1	818.3	395.51	1.00	0.93	0.92
2	HD360×196	4794.5	252.1	22.7	5882.1	901.7	436.16	1.00	0.93	1.01
1	HD400×237	5575.7	398.0	22.7	7071.2	1101.2	560.95	1.00	0.94	1.02
10	HEA 180	296.0	63.7	1.4	1064.6	76.4	36.8	0.91	0.72	0.86
9	HEB 180	588.3	103.4	1.4	1534.6	113.1	54.3	0.92	0.73	0.94
8	HEB 220	880.0	138.8	2.8	2138.5	194.3	92.6	0.95	0.80	0.91
7	HEB 260	1168.3	165.7	4.2	2782.4	301.5	141.5	0.97	0.85	0.87
6	HEB 280	1457.2	194.0	4.2	3087.9	360.5	168.6	0.98	0.87	0.96
5	HEB 300	1750.4	228.0	7.1	3503.9	439.2	204.5	0.98	0.89	1.01
4	HD320×158	2039.6	252.1	9.9	4728.2	638.7	280.6	0.99	0.89	0.87
3	HD320×158	2327.1	250.7	9.9	4728.2	638.7	280.6	0.99	0.89	0.99
2	HD360×179	2615.7	347.0	22.7	5365.1	818.3	395.5	1.00	0.93	0.95
1	HD360×196	2900.9	498.5	22.7	5882.1	901.7	436.2	1.00	0.93	0.99

Column design results CBF41Q5-EC8

storey	*section*	N_{Ed}	M_{yEd}	M_{zEd}	N_{Rk}	M_{yRk}	M_{zRk}	χ_y	χ_z	*eff.*
4	HEA 140	295.8	1.0	0.0	737.9	40.8	19.9	0.86	0.60	0.68
3	HEA 180	648.6	1.0	1.0	1064.6	76.4	36.8	0.91	0.72	0.87
2	HEB 180	1038.1	3.0	1.0	1534.6	113.1	54.3	0.92	0.73	0.95
1	HEB 220	1476.5	3.0	1.0	2138.5	194.3	92.6	0.95	0.80	0.88
4	HEA 160	491.4	0.0	0.0	911.8	57.6	27.6	0.89	0.66	0.82
3	HEB 180	982.8	0.0	0.0	1534.6	113.1	54.3	0.92	0.73	0.88
2	HEB 220	1474.2	0.0	0.0	2138.5	194.3	92.6	0.95	0.80	0.86
1	HEB 260	1965.6	0.0	0.0	2782.4	301.5	141.5	0.97	0.85	0.83

Column design results CBF61Q5-EC8

storey	*section*	N_{Ed}	M_{yEd}	M_{zEd}	N_{Rk}	M_{yRk}	M_{zRk}	χ_y	χ_z	*eff.*
6	HEA 140	295.4	0.0	0.0	737.9	40.8	19.9	0.86	0.60	0.67
5	HEA 180	650.2	1.0	0.0	1064.6	76.4	36.8	0.91	0.72	0.85
4	HEB 180	1035.3	3.0	1.0	1534.6	113.1	54.3	0.92	0.73	0.95
3	HEB 220	1447.9	5.0	2.0	2138.5	194.3	92.6	0.95	0.80	0.86
2	HEB 240	1896.4	6.0	2.0	2491.0	247.5	117.1	0.96	0.83	0.93
1	HEB 280	2389.1	6.0	2.0	3087.9	360.5	168.6	0.98	0.87	0.90
6	HEA 160	491.4	0.0	0.0	911.8	57.6	27.6	0.89	0.66	0.82
5	HEB 180	982.8	0.0	0.0	1534.6	113.1	54.3	0.92	0.73	0.88
4	HEB 220	1474.2	0.0	0.0	2138.5	194.3	92.6	0.95	0.80	0.86
3	HEB 240	1965.6	0.0	0.0	2491.0	247.5	117.1	0.96	0.83	0.95
2	HEB 280	2457.0	0.0	0.0	3087.9	360.5	168.6	0.98	0.87	0.91
1	HEB 300	2948.4	0.0	0.0	3503.9	439.2	204.5	0.98	0.89	0.95

Column design results CBF61M-EC8

storey	*section*	N_{Ed}	M_{yEd}	M_{zEd}	N_{Rk}	M_{yRk}	M_{zRk}	χ_y	χ_z	*eff.*
6	HEA 160	424.4	2.6	8.0	911.8	57.6	27.6	0.89	0.66	1.02
5	HEA 200	941.5	3.5	1.7	1264.3	100.9	47.9	0.93	0.76	1.01
4	HEB 220	1470.7	6.3	2.5	2138.5	194.3	92.6	0.95	0.80	0.88
3	HEB 240	1971.5	7.3	3.4	2491.0	247.5	117.1	0.96	0.83	0.98
2	HEB 280	2503.8	11.0	4.0	3087.9	360.5	168.6	0.98	0.87	0.95
1	HEB 300	3095.3	11.0	4.0	3503.9	439.2	204.5	0.98	0.89	1.02
6	HEA 180	737.1	0.0	0.0	1064.6	76.4	36.8	0.91	0.72	0.96
5	HEB 220	1474.2	0.0	0.0	2138.5	194.3	92.6	0.95	0.80	0.86
4	HEB 260	2211.3	0.0	0.0	2782.4	301.5	141.5	0.97	0.85	0.93
3	HEB 280	2702.7	0.0	0.0	3087.9	360.5	168.6	0.98	0.87	1.01
2	HEB 320	3194.1	0.0	0.0	3790.6	505.0	220.7	0.99	0.89	0.95
1	HEM 240	3685.5	0.0	0.0	4690.6	497.5	236.4	0.97	0.84	0.93

Column design results CBF81M-EC8

storey	*section*	N_{Ed}	M_{yEd}	M_{zEd}	N_{Rk}	M_{yRk}	M_{zRk}	χ_y	χ_z	*eff.*
8	HEA 160	394.3	0.0	0.0	911.8	57.6	27.6	0.0	0.89	0.66
7	HEA 200	858.4	2.0	0.0	1264.3	100.9	47.9	2.0	0.93	0.76
6	HEB 200	1356.7	3.0	1.0	1835.4	151.0	71.9	3.0	0.94	0.77
5	HEB 240	1880.9	7.0	2.0	2491.0	247.5	117.1	7.0	0.96	0.83
4	HEB 280	2402.3	8.0	3.0	3087.9	360.5	168.6	8.0	0.98	0.87
3	HEB 320	2960.6	15.0	5.0	3790.6	505.0	220.7	15.0	0.99	0.89
2	HEM 240	3572.3	17.0	5.0	4690.6	497.5	236.4	17.0	0.97	0.84
1	HEM 260	4234.7	11.0	4.0	5160.6	593.1	280.1	11.0	0.98	0.86
8	HEA 180	617.6	0.0	0.0	1064.6	76.4	36.8	0.91	0.72	0.81
7	HEB 200	1235.3	0.0	0.0	1835.4	151.0	71.9	0.94	0.77	0.88
6	HEB 240	1852.9	0.0	0.0	2491.0	247.5	117.1	0.96	0.83	0.90
5	HEB 260	2470.5	0.0	0.0	2782.4	301.5	141.5	0.97	0.85	1.04
4	HEB 300	2961.9	0.0	0.0	3503.9	439.2	204.5	0.98	0.89	0.95
3	HEB 320	3453.3	0.0	0.0	3790.6	505.0	220.7	0.99	0.89	1.03
2	HEM 240	3944.7	0.0	0.0	4690.6	497.5	236.4	0.97	0.84	1.00
1	HEM 260	4436.1	0.0	0.0	5160.6	593.1	280.1	0.98	0.86	1.00

COMPORTEMENT A ETAGE FAIBLE DES OSSATURES EN ACIER A CONTREVENTEMENT CENTRE SOUMIS A DES ACTIONS SISMIQUES

par

Merczel Dániel Balázs

Résumé en français

Presenté devant

Budapest University of Technology and Economics

et

Institut Nationale des Sciences Appliquées Rennes

en vu de l'obtention du grade de

Docteur en Génie Civil

Janvier 2015

1. INTRODUCTION A LA PROBLEMATIQUE DE LA THESE

Les contreventements en acier sont des moyens couramment utilisés pour assurer une rigidité latérale et une résistance aux bâtiments en acier, mais aussi aux bâtiments mixtes acier-béton et aux bâtiments en béton armé, voir *Figure 1*. En outre, ils constituent l'une des solutions recommandées pour un renforcement parasismique. La performance sismique des ossatures contreventées a été étudiée par de nombreux auteurs au cours des dernières décennies, et plusieurs problèmes ont été identifiés en liaison avec la réponse réelle des ossatures, et les méthodes de conception et dimensionnement sismique à spécifier dans les normes ou les codes tels que l'Eurocode 8. Parmi les nombreux sujets, on peut citer entre autres le comportement cyclique des diagonales, les dispositions efficaces et les assemblages de ces diagonales, les exigences imposées à ces mêmes éléments souvent l'objet de controverses, la localisation de déformations inélastiques pouvant conduire à un comportement d'étage faible, etc. La conclusion principale de la plupart des recherches menées sur la performance sismique des ossatures contreventées est de constater que la réponse réelle de ces ossatures peut différer beaucoup de celle des modèles simplifiés préconisés dans les codes. En conséquence, pour obtenir un comportement sismique satisfaisant, ces codes peuvent d'être amendés ou même fondamentalement modifiés. Ce sera le cas de l'Eurocode 8-1 dans le présent travail de thèse.

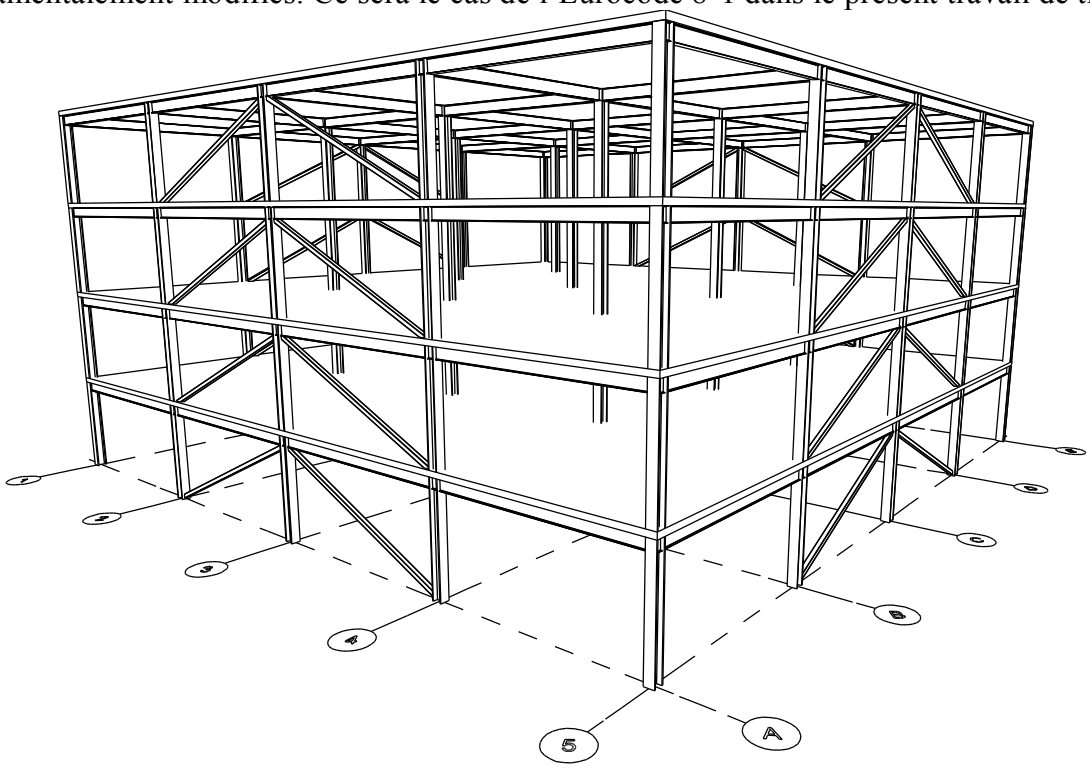

Figure 1; *Bâtiment contreventé*

Afin de se concentrer sur un sujet suffisamment important pour constituer un travail de thèse de doctorat, notre choix a porté sur l'éventualité d'un comportement dissipatif localisé sur un étage de l'ossature. Les objectifs de la recherche sont les suivants:

- Donner une description plus réaliste de la réponse sismique des ossatures contreventées;
- Identifier les facteurs contribuant au développement d'un comportement dissipatif localisé sur un étage;

- Examiner la performance des ossatures contreventées dimensionnées conformément à l'Eurocode 8;
- Identifier les points faibles des règles de l'Eurocode 8 à l'origine de ce comportement insuffisant;
- Proposer une méthode de redimensionnement complémentaire à la procédure actuelle de l'Eurocode 8 faisant appel à d'autres critères, notamment en comportement plastique et élasto-plastique, et vérifier la validité de cette méthode de redimensionnement sur plusieurs exemples d'ossatures démontrant la disparition complète de mécanismes dissipatifs localisés à un ou quelques étages;

Dans la conception habituelle, les ossatures contreventées sont censées générer un mécanisme global plastique lorsqu'elles sont soumises à des actions sismiques, voir la *Figure 2/a*. Selon le sens de ces actions, les diagonales de traction s'allongent plastiquement et celles en compression flambent. Ce mécanisme offre la plus grande dissipation possible dans l'ossature résistante puisque chaque diagonale d'étage contribue à la dissipation de l'énergie sismique. Le mécanisme global fournit donc la plus grande réduction possible des forces internes de l'ossature. En outre, en raison de répartition uniforme des déplacements latéraux de chaque étage, une capacité de déplacement plus importante peut être obtenue. Afin d'utiliser la quantité maximale de dissipation plastique, il convient de s'assurer que toutes les diagonales subissent des allongements plastiques à chaque étage compatibles avec leur ductilité en comportement cyclique alterné. Les éléments non dissipatifs, c'est-à-dire, les poteaux et les poutres doivent rester élastiques. Dans une conception correcte, l'apparition de la plasticité dans les diagonales doit être préservée par une condition de surrésistance imposée aux poteaux et aux poutres, en conformité avec le principe dit de « dimensionnement en capacité ».

Bien que le mécanisme global plastique soit celui que les méthodes de conception simplifiées supposent, il y a le risque qu'un autre mécanisme de ruine se produise. Celui-ci est souvent désigné comme mécanisme d'étage faible, voir la *Figure 2/b*, et il aurait été observé au cours de tremblements de terre récents (Northridge, Christchurch). Dans un mécanisme d'un ou quelque étages faibles, les déformations plastiques sont localisées sur un ou un nombre limité d'étages successifs. Lorsque la diagonale en traction atteint sa limite de résistance plastique, la diagonale comprimée a déjà flambé, si bien que les poteaux doivent apporter leur contribution dans la reprise des forces sismiques horizontales. Alors que dans le cas du mécanisme global plastique les poteaux restent rectilignes, un mécanisme d'étage faible va provoquer la double courbure des poteaux. Si l'action sismique latérale est importante, des rotules plastiques peuvent se former aux extrémités haute et basse des poteaux fléchis, soit au-dessus soit au-dessous des dalles de plancher et un mécanisme plastique local se développe à l'étage. Dans cette situation de mécanisme local, les déplacements latéraux des étages supérieurs sont approximativement égaux au déplacement de l'étage faible. En outre, toute la dissipation plastique du bâtiment se limite à celle de l'étage faible, le reste de l'ossature demeurant inexploitée. En conséquence, la dissipation d'un mécanisme local est de loin inférieure à celle du mécanisme global. En outre, dans un mécanisme local, les poteaux peuvent se trouver soumis à une flexion importante, alors qu'ils ne sont pas conçus à l'origine pour résister de la sorte, mais pour fonctionner comme des éléments de treillis. En raison de la flexibilité des poteaux, le comportement d'étages faibles implique le risque d'une ruine rapide par grand déplacement latéral.

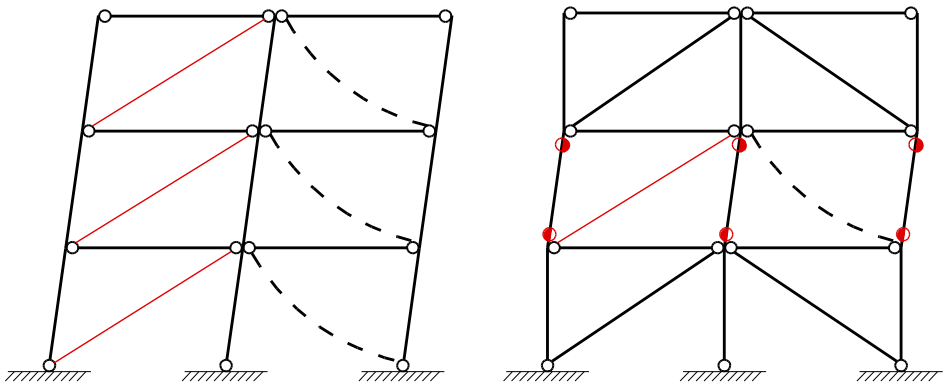

Figure 2; *Mécanisme global et mécanisme local d'un étage faible*

Comme déjà annoncé plus haut, la thèse porte sur l'éventualité du comportement dissipatif d'étages faibles d'ossatures contreventées dimensionnées conformément à l'Eurocode 8. La performance des ossatures contreventées sera évaluée au moyen de l'ADI (Analyse Dynamique Incrémentale). En fait, l'accent sera mis davantage sur l'apparition de mécanismes commençants d'étages faibles que sur la vérification du dimensionnement en résistance, encore que des aspects de résistance en fatigue oligocyclique des diagonales, de résistance en flexion hors-plan des goussets auxquels sont attachées ces diagonales, et de résistance plastique des poteaux en tant qu'éléments comprimés et fléchis ne puissent être négligés dans notre approche.

2. EFFICACITE DES BATIMENTS DIMENSIONNES SELON EUROCODE 8

Dans la littérature existante, il convient de dire que certaines faiblesses des règles de l'Eurocode 8 ont déjà été identifiées. Toutefois, il n'existe pas à notre connaissance d'études approfondies avec des méthodes précises pour se prémunir de l'éventualité de mécanismes dissipatifs locaux d'étages. Afin de pouvoir apprécier l'insuffisance de l'Eurocode 8 à ce sujet, plusieurs bâtiments ont été dimensionnés selon cet Eurocode et seront ultérieurement testés par des simulations numériques de type ADI.

Les bâtiments peuvent se distinguer par leur nombre d'étages, mais également par la disposition spatiale des systèmes résistants à l'action sismique, et aussi par la régularité ou l'irrégularité en élévation et en plan des bâtiments. Dans le présent travail, on a adopté des bâtiments de 4, 6, 8 et 10 étages, désignés par CBF4, CBF6, CBF8 et CBF10 respectivement. Les bâtiments sont identiques dans le plan sans irrégularité géométrique dans ce plan. Ils sont construits sur un réseau orthogonal qui se compose de quatre portées identiques dans les deux directions du plan. Chaque portée est de 6 mètres, qui donne un contour carré en plan de 24 × 24 mètres. La hauteur entre étages est de 3 mètres, voir la *Figure 3*. Deux types de bâtiment ont été étudiés.

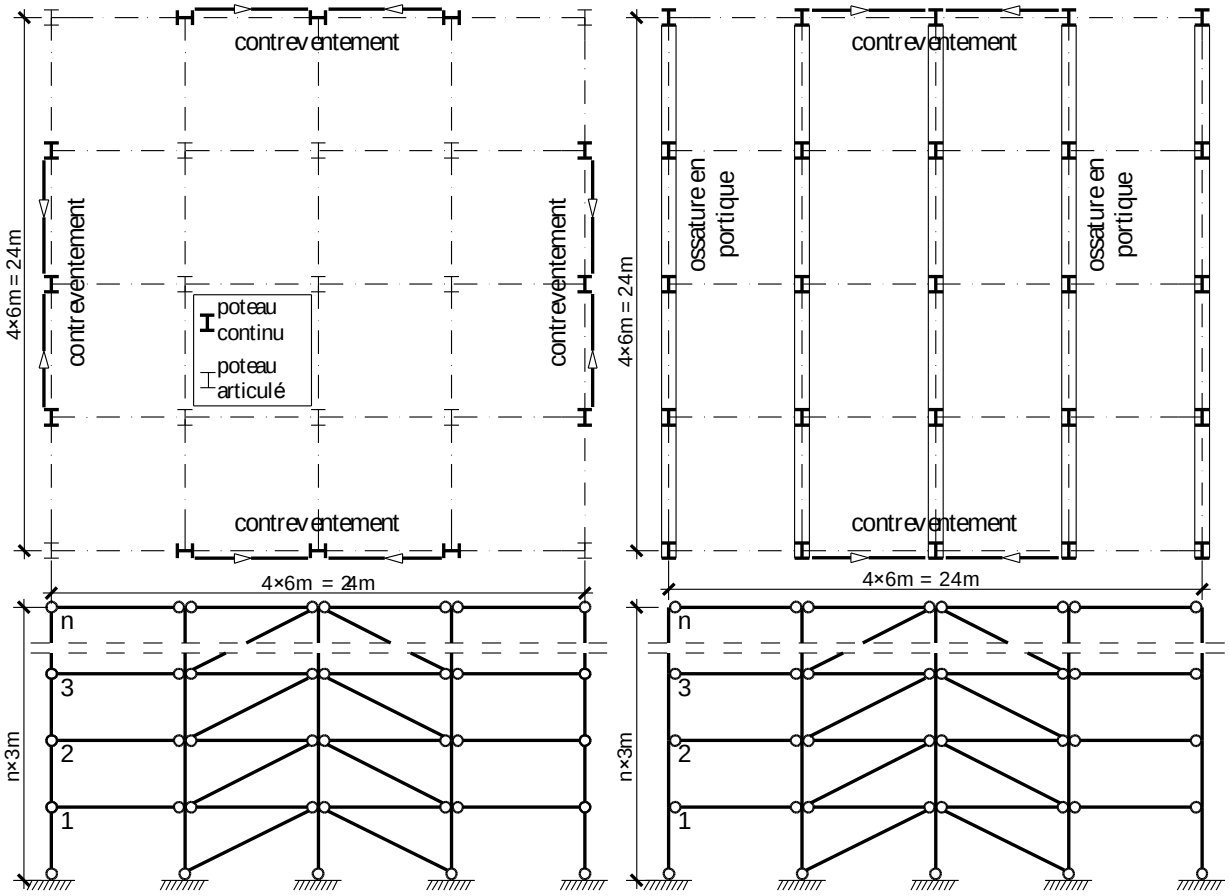

Figure 3; *Plan et élévation des bâtiments*

Dans les bâtiments de type 1, la résistance aux actions latérales est fournie par triangulation par diagonales dans les deux directions. Dans les bâtiments de type 2, on a triangulation par diagonales dans une direction et ossatures en portiques dans l'autre direction orthogonale. Le tableau suivant résume les différents bâtiments étudiés, souligne leurs particularités et donne aussi la période du premier mode de vibration. Dans la désignation, le symbole EC8 veut indiquer que les bâtiments sont dimensionnés ici avec les seules règles de l'Eurocode.

Tableau 1; *Bâtiments contreventés*

Bâtiment	*Caractéristique*	*Période (T_1 sec)*
CBF41-EC8	4 étages, deux ossatures contreventées	1.13
CBF42-EC8	4 étages, portique – ossature contreventée	1.19
CBF61-EC8	6 étages, deux ossatures contreventées	1.65
CBF62-EC8	6 étages, portique – ossature contreventée	1.61
CBF81-EC8	8 étages, deux ossatures contreventées	2.10
CBF82-EC8	8 étages, portique – ossature contreventée	2.04
CBF101-EC8	10 étages, deux ossatures contreventées	2.54
CBF102-EC8	10 étages, portique – ossature contreventée	2.41
CBF41Q5-EC8	4 étages, dimensionnement avec facteur q=5	1.21
CBF61Q5-EC8	6 étages, dimensionnement avec facteur q=5	1.68

CBF61M-EC8	6 étages irrégularité de masse de 50% en partie supérieur	1.78
CBF81M-EC8	8 étages irrégularité de masse de 20% en partie supérieur	2.17

Pour effectuer les calculs de l'analyse dynamique non linéaire (ADI) on a utilisé le logiciel FinelG d'éléments finis. Pour l'action sismique sept accélérogrammes artificiels ont été sélectionnés. La durée de chaque accélérogramme est de 20 secondes avec implicitement les spectres de réponse de ces accélérogrammes calés sur le spectre de dimensionnement de l'Eurocode 8-1, voir *Figure 4*. Avec chaque accélérogramme, plusieurs ADI sont effectuées en faisant croître progressivement l'accélération maximale du sol par un facteur multiplicatif (facteur d'échelle) variant de 0.1 à 2.0, dit « facteur d'échelle », de manière à couvrir un large domaine d'accélérations de part et d'autre de l'accélération de dimensionnement (qui correspond évidement au facteur multiplicatif 1.0)

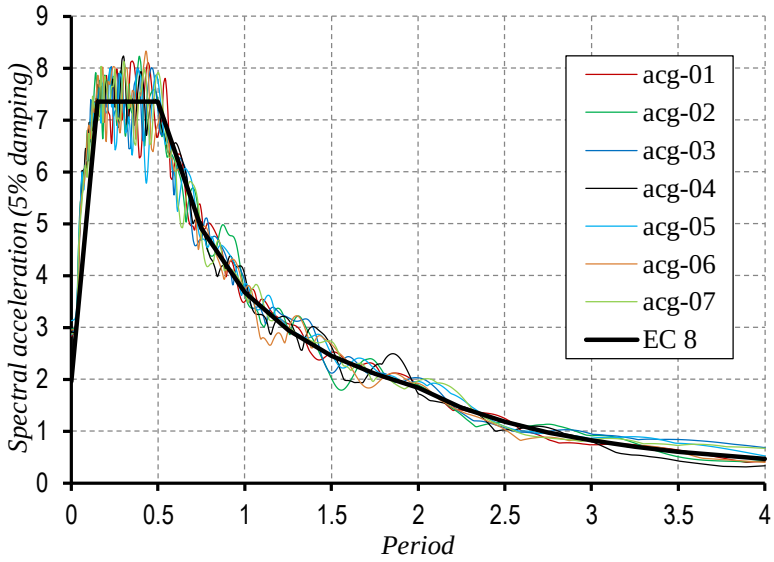

Figure 4; *Spectre de dimensionnement et spectres des accélérogrammes artificiels*

L'interprétation principale du programme de simulations numériques consiste à voir si les ossatures contreventées sont susceptibles ou non de comportement à étages faibles, voire de ruine anticipée de ces étages à des niveaux d'accélération inférieurs à celui de dimensionnement. Afin de faciliter cette interprétation, l'évolution du déplacement relatif maximal entre étages (IDR) en fonction de l'augmentation du facteur d'échelle de l'accélération maximale du sol a été calculée à partir des résultats du calcul numérique. Dans chaque diagramme, les étages sont représentés séparément de sorte que des différences importantes entre réponses d'étages peuvent être facilement visualisées. D'un simple coup d'œil, on peut savoir si les familles de courbes se regroupent dans un faisceau étroit ou sont dispensées, voir *Figure 5*. Dans le domaine de comportement dissipatif, les différences peuvent être parfois grandes, même pour un facteur d'échelle en dessous de la valeur 1.0 de dimensionnement. On peut trouver que la différence maximale entre les déplacements relatifs d'étages est plusieurs fois supérieure à la différence minimale. Dans pareille situation, l'ossature ne présente donc pas une dissipation correctement répartie; il y a des étages qui subissent des incursions plastiques beaucoup plus prononcées que d'autres. Il est également important de noter que le comportement singulier d'un étage supérieur peut se stabiliser au-delà d'une certaine valeur du facteur d'échelle et que d'autres étages peuvent même le rattraper. Dans la plupart des diagrammes ainsi tracés le déplacement relatif de 2% est dépassé pour un facteur d'échelle inférieur à 1.0, qui traduit l'insuffisance du dimensionnement selon l'Eurocode. Pour

précision, la fourchette limite retenus de 2 à 3% pour un déplacement relatif d'étages peut être justifiée sur des bases empiriques de l'endommagement des éléments secondaires (Etats Limites de Dommages), ainsi que la fatigue oligocyclique des diagonales de contreventement, de leurs goussets d'attache et la résistance des autres éléments de l'ossature résistante, en particulier les poteaux (Etats Limites Ultimes).

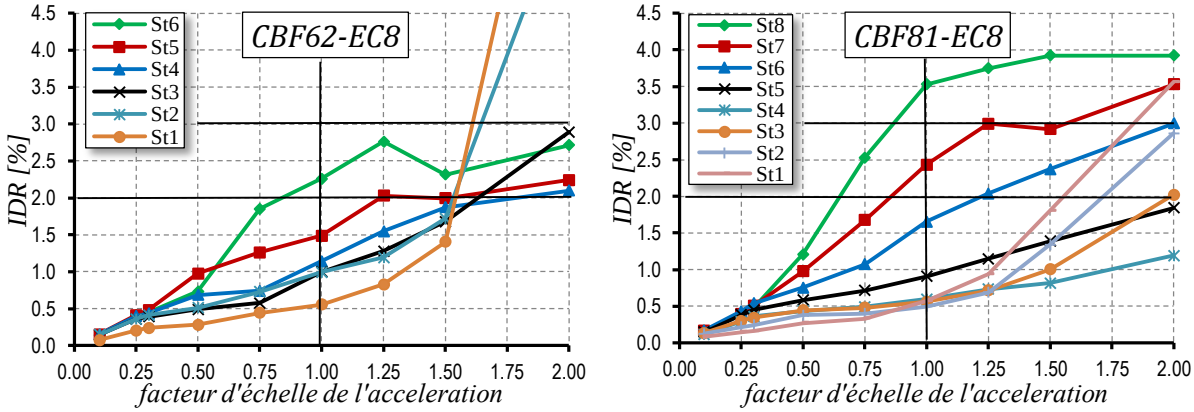

Figure 5; *Diagrammes de l'ADI déduits de l'ADI*

3. ASPECTS A L'ORIGINE AU DEVELOPPEMENT D'ETAGE FAIBLE

Les analyses des bâtiments étudiés ayant montré un comportement plus ou moins prononcé d'étages faibles, la compréhension et la description qualitative des phénomènes à l'origine de ce comportement s'impose de toute évidence. Examinant la déformée du modèle de la *Figure 6* suite à une action sismique, on peut voir que toutes les diagonales ont une forme triangulaire flambée. Dans la section médiane des diagonales de contreventement, des rotules plastiques se sont formées. Sous les cycles répétés de l'action sismique, les déformations plastiques se sont cumulées, facilitant de plus en plus le flambage par rotation de la rotule plastique. Finalement, cela conduit à une géométrie triangulaire de la diagonale. Les allongements plastiques augmentent la longueur des barres; si bien que les diagonales se trouvent être naturellement en compression lorsque le bâtiment est déchargé latéralement de l'excitation sismique. Plus les allongements plastiques se développent, plus la triangularité des diagonales est prononcée.

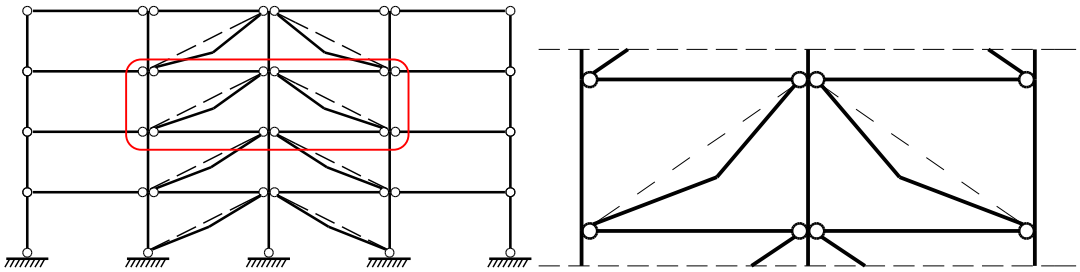

Figure 6; *Déformation plastique des diagonales*

A la *Figure 7*, la courbe de la force axiale - déplacement axial d'une diagonale durant 20 secondes d'excitation cyclique est présentée. Sur cette courbe, plusieurs des pics en traction ne provoquent pas de plasticité, mais seulement en trois cycles, un allongement considérable en traction plastique se produit. Comme la longueur de la diagonale déformée devient plus grande que la longueur d'origine, on constate que le flambement se produit même du côté des déformations positives où on s'attendrait normalement à un comportement de traction. En parallèle, la charge de flambement diminue, conduisant à chaque cycle à des déformations

plastiques cumulées principalement en milieu de la barre avec formation d'une rotule plastique. Avec l'augmentation de la longueur de la barre, le plein développement de la résistance en traction de la diagonale va nécessiter des déplacements axiaux plus importants. Il en résulte, lorsque de petits déplacements en traction ont lieu, que l'effort dans la diagonale est diminué de façon significative, et donc également sa rigidité initiale.

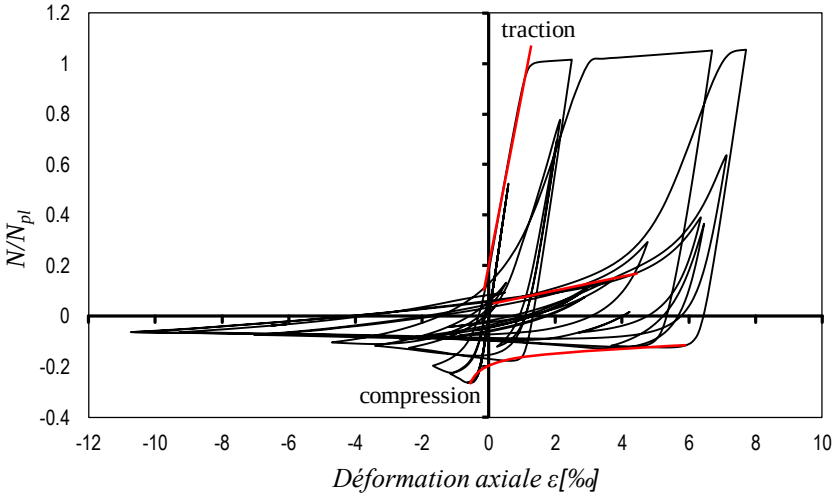

Figure 7; *Courbe force – déformation d'une diagonale en cyclique*

L'accroissement progressif de la triangularité se traduit par une diminution de la force axiale dans les diagonales et un report de la charge sismique sur les poteaux. Or, la rigidité en flexion des colonnes ne permet pas de compenser la perte de rigidité latérale consécutive à la dégradation des diagonales. Ainsi la rigidité latérale de l'étage faible devient nettement inférieure à celle des autres étages. Cette modification de la répartition des raideurs entraîne des changements qualitatifs dans la réponse modale du bâtiment. Une modification significative de la répartition des raideurs du système, voir *Figure 8*, modifie l'allure des modes ainsi que les fréquences naturelles. Les modes se décomposent en modes décrivant le mouvement des dalles au-dessus de l'étage faible et en mode résonance de ceux dessous. Dans la *Figure 8*, seuls les deux premiers modes sont présentés puisqu'ils correspondent aux modes dont les facteurs de participation sont les plus élevés, les modes supérieurs étant pour la plupart négligeables. Le premier mode possède une période sensiblement plus élevé que le second mode. Donc, si on calcule la réponse en déplacement du bâtiment sur base du spectre de réponse en déplacement et de la combinaison des modes, on constate que la réponse est fortement régie par le premier mode imparfait.

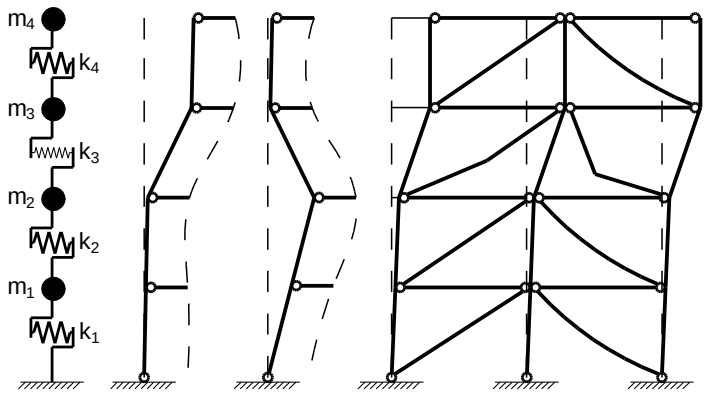

Figure 8; *Réponse d'une portique imparfait*

La triangulation des barres de contreventement induit un report des charges latérales sur les colonnes. Par ailleurs, comme la rigidité en flexion des colonnes est sensiblement inférieure à la raideur axiale des diagonales, ce mode de déformation a également pour conséquence une diminution substantielle de la rigidité au cisaillement latérale. L'irrégularité de la répartition de la raideur horizontale sur la hauteur du bâtiment modifie le comportement dynamique global et induit une localisation de grands déplacements au droit de l'étage considéré. Le phénomène est amplifié par un phénomène de « découplage » de la réponse modale. Les grands déplacements induisent des déformations plastiques qui se cumulent dans des rotules plastiques situées au milieu des barres qui se détériorent avec pour résultat une chute de la résistance rendant ainsi plus aisé le développement et l'accumulation de déformations plastiques.

Ce processus est une boucle récurrente au cours de laquelle les dommages de l'étage faible augmentent progressivement. Ainsi l'initiation du mécanisme étage faible aura pour conséquence d'accentuer le phénomène qui s'amplifie au cours des cycles et donc on peut déduire que le phénomène induit une rupture dans le comportement modal et que cette dernière s'accentue. Ainsi le phénomène s'auto-alimente et a pour conséquence d'accroître la plastification localisée. La boucle est rompue par l'effondrement de l'étage faible. Cela peut se produire soit par ruine des poteaux qui ont une capacité de résistance insuffisante ou sont discontinus soit par fatigue des diagonales et des goussets. La boucle présentée conduit évidemment à la ruine de la structure si cette dernière est soumise à un nombre de cycles suffisants. Le nombre de cycles au cours d'un séisme reste limité. Ainsi en empêchant les déformations dans les diagonales et en offrant une résistance accrue des colonnes en flexion, le développement progressif de l'étage faible peut être empêché.

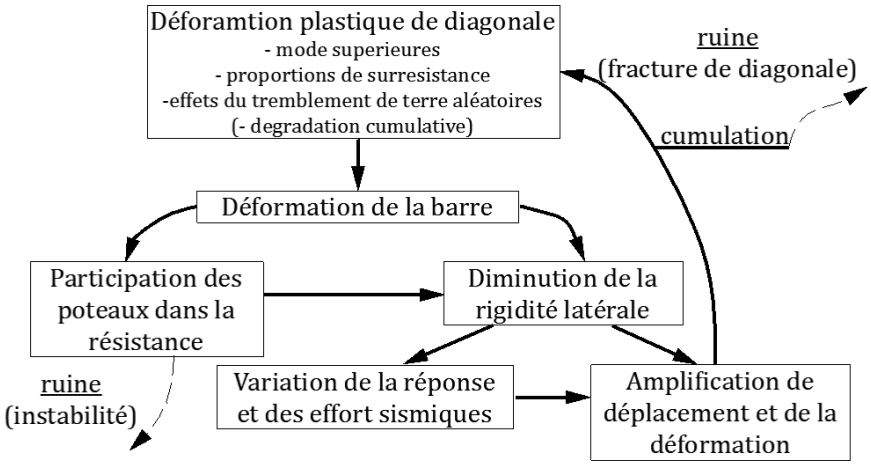

Figure 9; *Organigramme du développement d'étage faible*

La condition dans l'Eurocode 8 pour promouvoir une plasticité simultanée de toutes les barres de traction, assurant de la sorte un comportement plastique global s'exprime en exigeant que le maximum et le minimum de la surrésistance des diagonales (dans la situation sismique de calcul) ne différent pas de plus de 25%.

$$\frac{\Omega_{\max}}{\Omega_{\min}} \leq 1.25 \qquad (1)$$

Dans la situation de calcul de l'Eurocode 8, les vérifications sont effectuées dans l'hypothèse d'un état élastique de la structure, permis par l'utilisation du facteur de comportement conduisant à une action sismique d'intensité réduite. En revanche, dans un état inélastique, proche de la ruine, les exigences de type (1) de la norme ne sont plus adaptées a

priori. Dès l'instant où la plasticité se développe à un niveau de l'ossature, la distribution élastique des forces statiques équivalentes de l'action sismique va se trouver fondamentalement modifié.

Pour s'assurer que les déformations plastiques restent localisées exclusivement dans les diagonales, le dimensionnement des poteaux et des poutres de la structure primaire est effectué en majorant la partie sismique de leurs sollicitations par différents facteurs. Ainsi la résistance axiale de ces éléments, calculée conformément à l'Eurocode 3 en tenant compte d'une interaction éventuelle avec la flexion, $N_{pl,Rd}(M_{Ed})$, doit satisfaire l'exigence ci-après:

$$N_{Rd}\left(M_{Ed}\right) \geq N_{Ed,G} + 1.1 \cdot \gamma_{ov} \cdot \Omega \cdot N_{Ed,E} \text{ où } \Omega = \Omega_{\min} \qquad (2)$$

L'analyse élastique et statique des sollicitations sismiques d'une ossature contreventée sans imperfection des barres ne donne seulement que des forces axiales dans les poteaux et les poutres dans l'hypothèse d'un fonctionnement en treillis. En réalité, la détérioration triangulaire des diagonales, comme cela a été décrit précédemment, conduit à transférer à chaque niveau une part de l'effort tranchant horizontal sismique sur les poteaux (en général continus sur la hauteur), qui se trouvent par conséquent fléchis. Comme l'analyse élastique classique ne fournit pas de forces internes représentatives de cette situation, ou tout au moins pas avec l'amplitude qui convient, la résistance axiale des poteaux est surestimée et conduit à un sous-dimensionnement des sections de ces poteaux. En outre, il n'est pas exclu que les poteaux soient soumis à une déformation plastique, exigeant de leur part un comportement ductile, d'où des exigences de dimensionnement encore plus sévères (par exemple avec une limitation de l'effort normal et de l'élancement).

Sur la base de toutes les observations de la thèse sur le comportement d'ossatures contreventées, les conclusions suivantes peuvent être tirées sur la conception parasismique de l'Eurocode 8:

- Les ossatures montrent une grande sensibilité à faire apparaître un comportement d'étage faible;
- Un comportement d'étage faible peut conduire à une ruine précoce de l'étage et donc de la structure primaire;
- Les déformations plastiques des diagonales peuvent provoquer un changement significatif du comportement dynamique de l'ossature, d'où une redistribution des forces sismiques équivalentes. En aucune façon, ces modifications ne sont considérées dans la procédure de dimensionnement de l'Eurocode 8;
- Le comportement inélastique de l'ossature primaire que l'Eurocode 8 laisse de côté, est significativement différent de son comportement élastique;
- La condition d'uniformité selon la relation Eq. (1), non suffisante sur le plan de la dissipation globale, est également vraisemblablement affectée par le caractère aléatoire de l'excitation sismique qui disparaît lors du dimensionnement au moyen du spectre de réponse;
- L'analyse d'un modèle d'ossature sans imperfections de forme conduit à une sous-estimation de la flexion des poteaux qui se développe avec la détérioration des diagonales; aussi l'Eurocode 8 ne garantit-il pas une surrésistance suffisante pour les poteaux;
- Enfin l'Eurocode 8 ne donne aucune spécification pour les ossatures contreventées au sujet de l'effet de continuité des poteaux en général sur toute la hauteur de l'ossature;

4. MÉTHODE DITE « ROBUST SEISMIC BRACE DESIGN »

La première idée à la base de la méthode RSBD repose sur la nécessité d'utiliser un modèle inélastique d'analyse de la structure à la place du modèle élastique initial. Dans cette situation de comportement, en raison de la détérioration des diagonales, les déplacements se produisent essentiellement au-dessus de l'étage faible. Les forces sismiques équivalentes correspondant à ce mouvement d'ensemble sont alors constantes, réparties du sommet de l'ossature jusqu'à l'étage faible, comme le montre la *Figure 10*. Afin d'éviter une ruine d'étage faible, il convient de vérifier que cette distribution de forces provoque un mécanisme plastique global à un niveau de multiplicateur de charge $\lambda_{glob,i}$ inférieur à celui du multiplicateur $\lambda_{loc,i}$ du mécanisme d'étage local. Dans une ossature contreventée de *n* étages, *n* distributions de forces différentes sont à considérer, si bien que la condition ci-dessous doit être satisfaite pour *n* paires de multiplicateurs :

$$\frac{\lambda_{loc,i}}{\lambda_{glob,i}} \geq 1.0 \quad \text{where } i=1..n \tag{3}$$

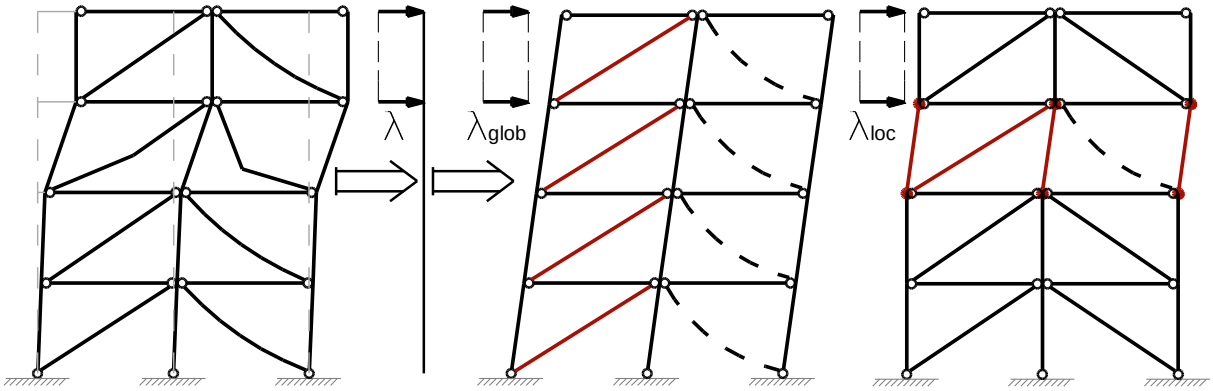

Figure 10; *Modèles de calcul plastique*

La condition (3) peut être satisfaite par le renforcement soit de la diagonale, soit les sections des poteaux, les deux types d'éléments étant impliqués dans la résistance plastique d'un certain étage. Si, dans un cas limite, la résistance n'est donnée que par la diagonale et si celle des poteaux est négligeable (ou si ces poteaux sont articulés aux deux extrémités), l'effort tranchant horizontal correspondant à la plasticité de la diagonale en traction est alors égal à la résistance plastique de l'étage. Comme la méthode vise à empêcher la réalisation d'un mécanisme d'étage, la plasticité de la diagonale ne doit pas être atteinte et donc l'étage reste élastique durant toute l'action sismique. Inversement, si toute la résistance est fournie par les poteaux et si celle des diagonales de l'étage est négligeable, le déplacement latéral au niveau de cet étage sera beaucoup plus grand que sur les autres étages, car la flexibilité des poteaux permet des déplacements plus importants que ceux dûs à la triangulation. On peut considérer qu'un tel plancher a tendance à présenter un comportement d'étage faible. Les réponses de ces deux cas limites sont représentées dans la *Figure 11* avec comparaison au comportement souhaitable d'un étage normal.

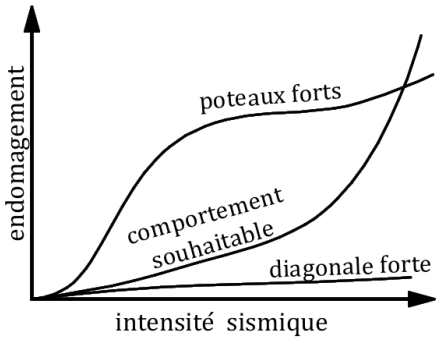

Figure 11; *Réponses possibles d'un étage*

L'objectif d'un deuxième critère est précisément d'éviter des cas où trop ou trop peu de déformations inélastiques vont se produire. Dans ce but, le comportement élasto-plastique d'un étage faible doit être considéré. Sur la *Figure 12*, la force de cisaillement d'un étage, représentée par son multiplicateur λ, et le déplacement relatif d'entre le haut et le bas du même étage constituent les deux axes des diagrammes représentés. La ligne noire représente la courbe de chargement (type « pushover ») d'un étage avec une diagonale rectiligne. La courbe rouge représente le déchargement avec une déformation triangulaire de la diagonale, plus importante sur la figure de droite que sur celle de gauche. Si la résistance de la diagonale, ou en d'autres termes sa limite élastique correspondant au multiplicateur λ_{br}, est proche de λ_{glob}, de grands déplacements inélastiques associés à une forte détérioration triangulaire de la diagonale ne peuvent se produire, et dans ce cas les déplacements correspondant à la limite élastique d_e et à la formation du mécanisme global d_{glob} sont proches l'un de l'autre. Inversement, si λ_{glob} est significativement plus grand que λ_{br}, les poteaux permettent de grands déplacements avant que le mécanisme global ne se développe. Manifestement, la grandeur du déplacement inélastique auquel on peut s'attendre est en étroite corrélation avec la position du multiplicateur de charge global λ_{glob} dans l'intervalle [λ_{br}, λ_{loc}]. C'est la raison pour laquelle un deuxième critère de la méthode consiste à resserrer cet intervalle, autrement dit à imposer que le maximum et le minimum du rapport BPR ci-après ne diffèrent pas de plus de 10%.

$$BPR_{\min} + 0.1 \geq BPR_{\max} \text{ avec } BPR_i = \frac{\lambda_{br,i}}{\lambda_{glob,i}} \tag{4}$$

Il est évident que si le BPR est proche de 1.0, la triangulation est surdimensionnée, le rôle des poteaux est à peine nécessaire et l'étage n'est pas vraiment impliqué dans la dissipation plastique. Pour cette raison, il est recommandé que le BPR maximal ne dépasse pas 0.9.

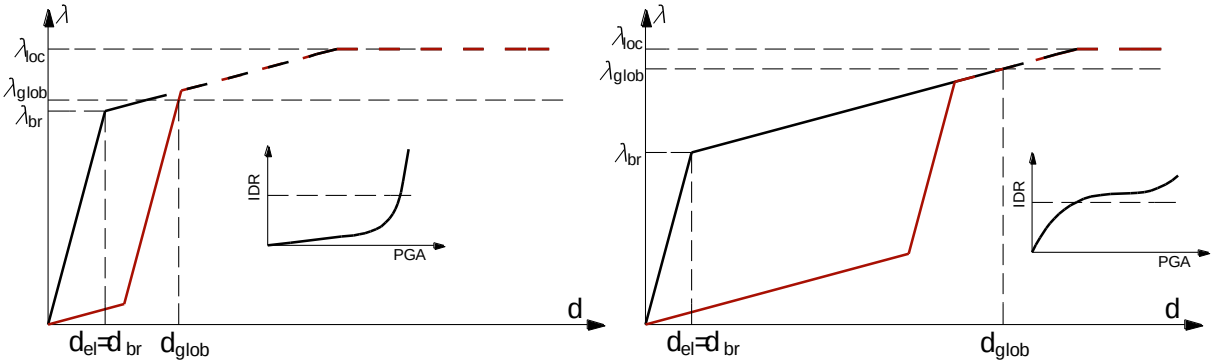

Figure 12; *Étage surdimensionné (à gauche) et étage faible (à droite)*

Afin de disposer des multiplicateurs de charge nécessaires pour évaluer les deux critères de la méthode RSBD, on doit exprimer l'équivalence des travaux extérieurs et intérieurs pour les mécanismes locaux et globaux. Dans le cas d'un mécanisme global l'égalité est la suivante:

$$W_{\lambda,glob,i} + W_{G,glob} = \sum_i W_{t,br,i} \tag{5}$$

Sous forme développée et sans rentrer ici dans tous les détails, cette égalité donne:

$$\lambda_{glob,i} \cdot \sum_{k=i}^{n} \left(mp_k \cdot \sum_{l=1}^{k} \Delta B_l \right) + \sum_{k=1}^{n} \left[\sum_{l=1}^{m} G_{k,l} \cdot \frac{\left(\sum_{k=1}^{i} \Delta B_k \right)^2}{2 \sum_{k=1}^{i} H_k} \right] = \sum_i N_{pl,br,i} \cdot \Delta B_i \cdot \cos \alpha_i \tag{6}$$

Dans le cas d'un mécanisme local, l'égalité est la suivante:

$$W_{\lambda,loc,i} + W_{G,loc,i} = W_{t,br,i} + W_{col,i} \tag{7}$$

Sous forme développée et sans rentrer dans les détails, cette dernière égalité donne:

$$\begin{aligned} \Delta B_i \cdot \lambda_{loc,i} \cdot \sum_{k=i}^{n} mp_k + \sum_{k=i}^{n} \sum_{l=1}^{m} \left[G_{k,l} \cdot \left(\frac{\Delta B_i^2}{2H_i} + e_{col,l} \cdot \frac{\Delta B_i}{H_i} \right) \right] = \\ = N_{pl,br,i} \cdot \Delta B_i \cdot \cos \alpha_i + \sum_{j=1}^{m} M_{col,i,j} \cdot \frac{\Delta B_i}{H_i} \end{aligned} \tag{8}$$

Des relations (6) et (8), les multiplicateurs globaux et locaux peuvent être déduits explicitement. Cependant, il est à noter que, pour la détermination du multiplicateur local un calcul itératif en deux étapes peut être nécessaire dans la mesure où le moment résistant plastique des poteaux peut être réduit par interaction avec la force axiale, laquelle est dépendante des forces sismiques latérales du mécanisme à connaître.

$$\lambda_{glob,i} = \frac{\sum_i N_{pl,br,i} \cdot \Delta B_i \cdot \cos \alpha_i - \sum_{k=1}^{n} \left[\sum_{l=1}^{m} G_{k,l} \cdot \frac{\left(\sum_{k=1}^{i} \Delta B_k \right)^2}{2 \sum_{k=1}^{i} H_k} \right]}{\sum_{k=i}^{n} \left(mp_k \cdot \sum_{l=1}^{k} \Delta B_l \right)} \tag{9}$$

$$\lambda_{loc,i} = \frac{N_{pl,br,i} \cdot \Delta B_i \cdot \cos \alpha_i + \sum_{j=1}^{m} M_{red,i,j} \cdot \frac{\Delta B_i}{H_i} - \sum_{k=i}^{n} \sum_{l=1}^{m} G_{k,l} \cdot \frac{\Delta B_i^2}{2H_i}}{\Delta B_i \cdot \sum_{k=i}^{n} mp_k} \tag{10}$$

La formule pour le calcul de λ_{br}, qui est nécessaire à la connaissance de BPR_i se déduit de la relation (10), en négligeant la participation des poteaux:

$$\lambda_{br,i} = \frac{N_{pl,br,i} \cdot \Delta B_i \cdot \cos \alpha_i - \sum_{k=i}^{n} \sum_{l=1}^{m} G_{k,l} \cdot \frac{\Delta B_i^2}{2H_i}}{\Delta B_i \cdot \sum_{k=i}^{n} mp_k} \tag{11}$$

5. RESULTATS NUMERIQUES ET PERFORMANCE DE LA METHODE RSBD

Ci-après, pour les deux ossatures contreventées déjà considérées plus haut à la figure 5, les résultats de la méthode sont donnés dans les tableaux 2, 3, 4 et 5 et sur les figures 13 et 14 illustrant les réponses en déplacements relatifs d'étages selon l'analyse dynamique incrémentale (ADI). Les tableaux donnent les sections les plus importantes, les sur-résistances et les multiplicateurs de charge de la méthode RSBD. Dans les tableaux 2 et 4, qui correspondent au dimensionnement initial selon l'EC8, les insuffisances des multiplicateurs de charge (premier critère) et les valeurs du BPR maximum et minimum (deuxième critère) sont signalées en caractères gras. Dans les tableaux 3 et 5, les sections modifiées par la méthode RSBD et aussi les nouvelles valeurs du BPR maximum et minimum sont également en gras. Au-dessous de chaque tableau, le rapport entre la plus grande et la plus petite surrésistance des diagonales imposée au plus égal à 1,25 par l'Eurocode 8, est également indiqué.

Examinant ces deux exemples, on peut voir que la méthode RSBD corrige systématique la présence de l'étage(s) faible(s) dans les bâtiments dimensionnés selon l'EC8. En outre, le phénomène d'étage faible est d'autant plus amplifié avec l'EC8 que les critères de la méthode RSBD sont davantage violés. On peut également remarquer que dans le bâtiment de type 2 (contreventé par triangulations dans la direction de l'action sismique et par portiques transversalement), le comportement d'étage faible est atténué. Ce type de bâtiment nécessite moins de renforcement des poteaux, mais en général le même renforcement des diagonales, par rapport aux bâtiments de type 1 (contreventement par triangulations dans les deux directions). Comme le renforcement des diagonales augmente le multiplicateur de charge global, la nécessité de renforcer les étages en dessous de ceux qui ont été trouvés faibles dans la version EC8 des tableaux pourrait se poser. En fait, les exemples montrent qu'avec la méthode RSBD, la situation où le renforcement d'un étage faible risque de provoquer le transfert de la faiblesse d'étage à un autre étage, est évitée avec succès. Les ossatures triangulées renforcées selon cette méthode, ne répondent pas rigoureusement à la condition d'uniformité des déplacements relatifs inélastiques. Néanmoins, les réponses de chaque bâtiment montrent des familles de courbes formant un faisceau beaucoup plus étroit que celui des courbes initiales avec l'EC8. Un comportement dissipatif bien plus favorable, mieux distribué sur la hauteur de l'ossature est donc réalisé avec le renforcement. Ces dimensionnements corrigés avec la méthode RSBD ont même tendance à être beaucoup plus performants que nécessaire, la ruine se produisant pour des facteurs d'échelle d'accélération sismique supérieurs à 1(par exemple de l'ordre de 1,5). Cette ruine se produit généralement sur les premier et deuxième étages, avec une augmentation rapide des déplacements qui traduit un effondrement par l'instabilité dynamique.

Tableau 2; *CBF62-EC8*

Etage	*Poteau intérieur.*	*Poteau extérieur.*	*diagonale*	Ω	λ_{loc}	λ_{glob}	$\frac{\lambda_{loc}}{\lambda_{glob}}$	*BPR*
6	HEA 180	HEA 180	90×5	1.00	**436.9**	**513.9**	**0.85**	**0.62**
5	HEB 180	HEB 180	100×6	0.98	343.1	280.3	1.22	0.72
4	HEB 240	HEB 200	100×8	1.01	316.2	205.5	1.54	0.80
3	HEB 260	HEB 240	100×10	1.04	300.6	171.3	1.75	**0.84**
2	HEB 280	HEB 260	100×10	0.99	272.6	154.2	1.77	0.78
1	HEB 320	HEB 320	120×10	1.00	186.0	146.8	1.27	0.78

$\Omega_{max}/\Omega_{min}$=1,06

Tableau 3 *CBF62-RSBD*

étage	*Poteau intérieur.*	*Poteau extérieur.*	*diagonale*	Ω	λ_{loc}	λ_{glob}	$\frac{\lambda_{loc}}{\lambda_{glob}}$	*BPR*
6	HEA 180	**HEB 180**	**100×5**	**1.15**	524.5	528.1	0.99	**0.70**
5	HEB 180	HEB 180	**100×6.3**	1.00	385.2	288.1	1.34	0.76
4	HEB 240	HEB 200	100×8	1.00	320.6	211.3	1.52	0.78
3	HEB 260	HEB 240	100×10	1.03	300.6	176.0	1.71	**0.81**
2	HEB 280	HEB 260	100×10	0.97	272.6	158.4	1.72	0.76
1	HEB 320	HEB 320	120×10	0.98	186.0	150.9	1.23	0.76

$\Omega_{max}/\Omega_{min}$=1,19

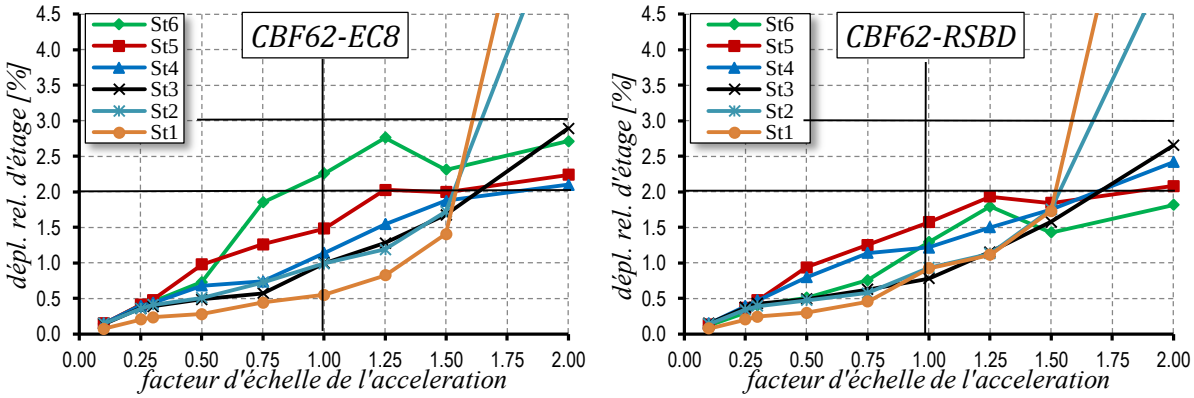

Figure 13; *Réponses en déplacements relatifs selon l'ADI*

Tableau 4; *CBF81-EC8*

étage	*Poteau intérieur.*	*Poteau extérieur.*	*diagonale*	Ω	λ_{loc}	λ_{glob}	$\frac{\lambda_{loc}}{\lambda_{glob}}$	*BPR*
8	HEA 160	HEA 160	90×5	0.99	**402.0**	**609.5**	**0.66**	**0.53**
7	HEB 180	HEA 180	100×6.3	1.05	**296.3**	**325.1**	**0.91**	0.67
6	HEB 220	HEB 200	100×8	1.01	245.0	232.2	1.05	0.71
5	HEB 240	HEB 220	100×10	1.10	229.0	187.5	1.22	0.77
4	HEB 280	HEB 240	120×10	1.01	217.5	162.5	1.34	**0.88**
3	HEB 300	HEB 280	120×10	0.98	192.3	147.8	1.30	0.78
2	HEM 240	HEB 320	140×10	0.98	210.8	139.3	1.51	0.85
1	HEM 240	HEM 240	140×10	1.00	147.2	135.5	1.09	0.74

$\Omega_{max}/\Omega_{min}$=1,07

Tableau 5; *CBF81-RSBD*

étage	*Poteau intérieur.*	*Poteau extérieur.*	*diagonale*	Ω	λ_{loc}	λ_{glob}	$\frac{\lambda_{loc}}{\lambda_{glob}}$	*BPR*
8	HEA 160	**HEA 240**	**100×6.3**	**1.40**	689.3	662.2	1.04	0.70
7	HEB 180	**HEA 240**	**100×8**	1.21	471.3	353.2	1.33	0.78
6	HEB 220	HEB 200	**100×10**	1.22	309.2	252.3	1.23	0.80
5	HEB 240	HEB 220	100×10	1.11	242.6	203.8	1.19	0.77
4	HEB 280	HEB 240	120×10	1.17	217.5	176.6	1.23	**0.80**
3	HEB 300	HEB 280	120×10	1.07	192.3	160.5	1.20	0.72
2	HEM 240	HEB 320	140×10	1.08	210.8	151.4	1.39	0.79
1	HEM 240	HEM 240	140×10	0.98	147.4	147.2	1.00	**0.69**

$\Omega_{max}/\Omega_{min}$=1,43

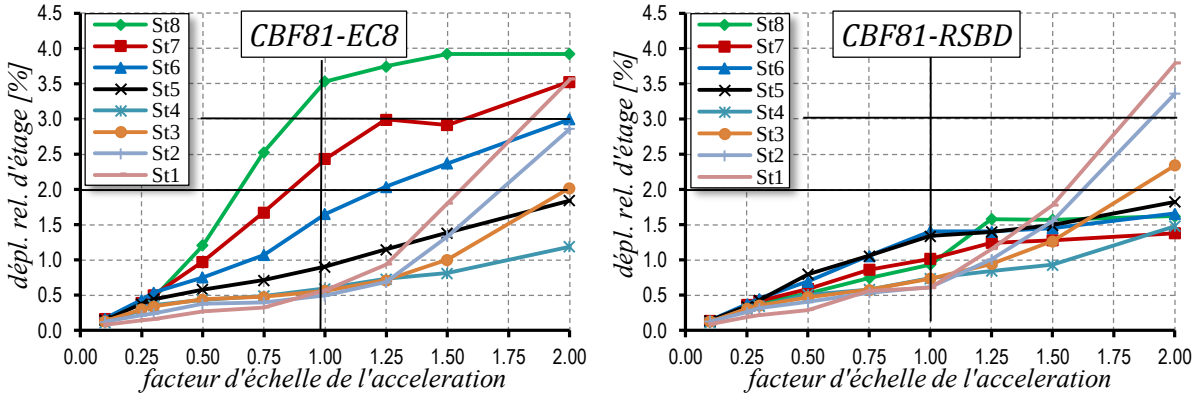

Figure 14; *Réponses en déplacements relatifs selon l'ADI*

Afin de pouvoir quantifier la largeur des faisceaux de courbes, les résultats IDR des étages pour un facteur d'échelle donné peuvent être considérés comme des valeurs d'une variable probabiliste discrète dont la dispersion peut être décrite par l'écart-type σ. Pour chaque enregistrement d'accélération et chaque facteur d'échelle, la valeur σ des déplacements relatifs entre étages peut être calculée comme suit:

$$\sigma_{IDR} = \sqrt{\frac{1}{n}\left[\left(IDR_1 - IDR_\mu\right)^2 + \left(IDR_2 - IDR_\mu\right)^2 + \ldots + \left(IDR_n - IDR_\mu\right)^2\right]} \qquad (12)$$

où la moyenne est donnée par:

$$IDR_\mu = \frac{1}{n}\left(IDR_1 + \ldots + IDR_n\right) \qquad (13)$$

Comme pour les faibles valeurs du facteur d'échelle, l'épaisseur du faisceau ne peut être développée et comme pour les fortes valeurs de ce facteur les résultats peuvent être faussés par le comportement asymptotique des courbes correspondant à l'atteinte de l'effondrement, il apparaît opportun de limiter ce type de calcul de σ dans l'intervalle de facteur d'échelle 0,75 à 1,25. En calculant la moyenne de tous les écart-types dans cet intervalle, on obtient de la sorte un écart-type moyen des déplacements relatifs, exprimé par un chiffre unique ci-après dénommé le « coefficient d'épaisseur du faisceau de courbes».

Pour décrire la robustesse des résultats obtenus par la méthode RSBD à un facteur d'échelle donné, l'écart-type pour chaque accélérogramme est calculé. Pour savoir si la dispersion entre les écart-types des divers accélérogrammes est faible et donc si la réponse de l'ossature examinée est sensible ou non aux variations aléatoires de l'excitation sismique, on calcule à nouveau l'écart-type de ces écart-types, d'où une valeur σ pour chaque facteur d'échelle considéré. La moyenne des σ sur l'intervalle de facteur d'échelle 0,75 à 1,25 décrit alors la robustesse de la réponse sismique (en unité IRD), il est désigné « coefficient de robustesse ».

Sur la Figure 15, les coefficients d'épaisseur et de robustesse obtenus avec le dimensionnement EC8 et celui corrigé par la méthode RSBD sont présentés dans deux histogrammes. Comme on peut le voir, le coefficient d'épaisseur des bâtiments selon l'Eurocode 8 croît avec la hauteur des bâtiments, alors qu'avec la méthode RSBD ce coefficient est maintenu dans un intervalle de 0,3 à 0,5% IDR pour chaque ossature, y compris celles avec une forte irrégularité de la distribution des masses. En outre, le dimensionnement selon l'Eurocode 8 peut difficilement montrer une telle performance; le coefficient d'épaisseur de la plupart des bâtiments conçus selon l'EC8 dépasse 0,6% et peut aller même au-delà de 1,2%. L'histogramme de robustesse montre de plus que les ossatures conçues selon l'EC8 sont

nettement plus sensibles aux aléas de l'excitation sismique. Le coefficient de robustesse est d'au moins 0,20% avec l'EC8, mais il est beaucoup plus élevé dans certains cas, alors que tous les renforcements avec la méthode RSBD restent remarquablement dans la plage 0,10 - 0,16% IDR. Cela permet d'affirmer que la correction par la méthode RSBD conduit à des ossatures contreventées fiables en résistance au regard des variations aléatoires de l'action sismique.

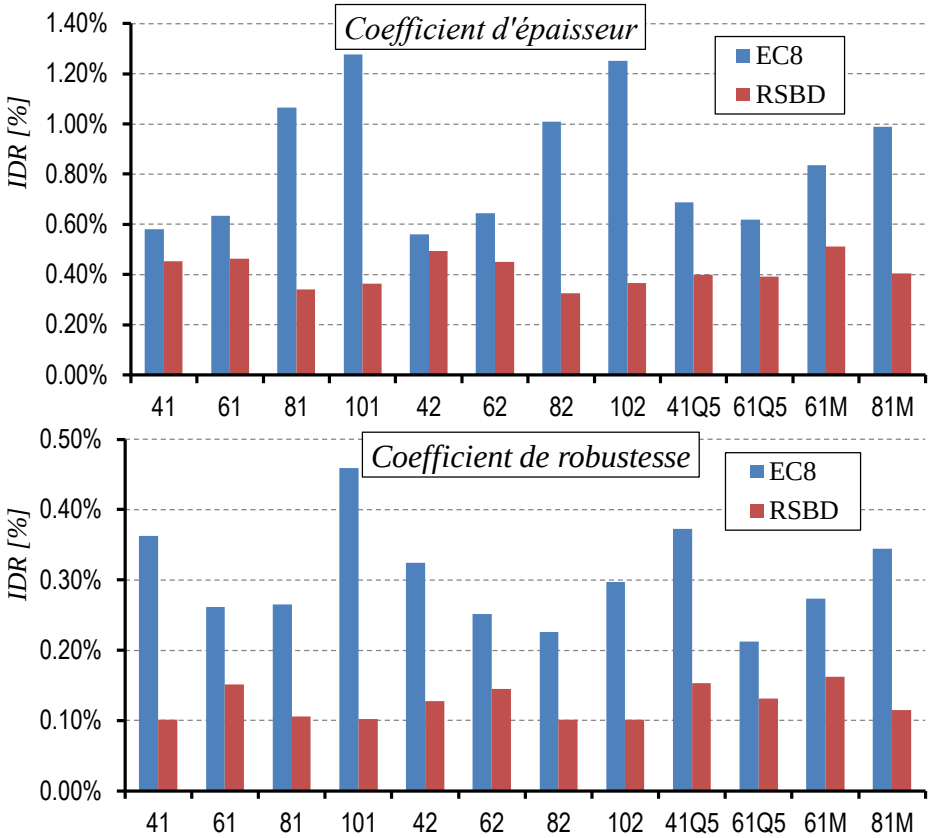

Figure 15; *Histogrammes de l'efficacité de l'Eurocode 8 et de la méthode RSBD*

Összefoglalás és Tézisek

készült a:

WEAK STOREY BEHAVIOUR OF CONCENTRICALLY BRACED STEEL FRAMES SUBJECTED TO SEISMIC ACTIONS

című disszertációhoz

Merczel Dániel Balázs

szerző, doktorjelölt által

Készült a:

Budapesti Műszaki és Gazdaságtudományi Egyetemen

témavezető:

Dr Lógó János

és a

Institut Nationale des Sciences Appliquées Rennes egyetemen

témavezető:

Dr Mohammed Hjiaj

2015 Január

Tartalom

1. A disszertáció rövid összefoglalása 2

2. A disszertációban vizsgált probléma bemutatása 4

3. Az Eurocode 8 szerint tervezett épületek hatékonysága 7

4. A gyengeszinti viselkedés kialakulásának okai 9

5. A Robust Seismic Brace Design módszer 12

6. Az RSBD módszerrel megerősített épületek viselkedése 15

7. A disszertáció tézisei 19

8. Theses of the dissertation in English 21

9. A disszertációhoz kapcsolódó publikációk 23

1. A DISSZERTÁCIÓ RÖVID ÖSSZEFOGLALÁSA

A „Weak storey behaviour of concentrically braced steel frames subjected to seismic actions” című doktori disszertáció a Budapesti Műszaki és Gazdaságtudományi Egyetem Építőmérnöki Karán és az INSA de Rennes egyetemen folytatott közös felügyeletű doktori képzés és a hozzá kapcsolódó kutatás eredménye. A disszertáció és a teljes eljárás nyelve az érintett felek által kötött szerződésnek megfelelően angol. Az alábbiakban egy rövid, magyar nyelvű tartalmi összefoglaló, illetve a magyar doktori eljárás követelményeinek eleget téve a disszertáció tézisei kerülnek bemutatásra.

A disszertáció első fejezetében azok az ismeretek kerülnek bemutatásra, amelyek szükségesek ahhoz, hogy rácsos merevítő szerkezetek szeizmikus viselkedéséről és méretezéséről beszélni lehessen. Definíciók és elvek kerülnek ismertetésre és betekintés nyerhető az Eurocode 8 idevonatkozó részébe is.

A második fejezet lényegében a vonatkozó irodalomból kiemelt darabok bemutatásának szentelt. A fejezet első része a szerkezeti elemek, úgymint acél zártszelvényű rácsok, csomólemezek illetve acél oszlopok várható ciklikus tönkremenetelével foglalkozik. A második rész a területen tevékenykedő legjelentősebb szerzők kutatási eredményeinek rövid bemutatása

A harmadik fejezet az Eurocode 8 szerint tervezett központos rácsozással merevített keretek földrengés válaszát vizsgálja. Először bemutatásra kerülnek azok a 4 és 10 szint közötti 24×24 méter alapterületű épületek, melyeken növekményes dinamikai analízissel kerül megvizsgálásra azok viselkedése. A fejezet részletes leírást ad továbbá a valós dinamikai analízishez használt modellek felépítéséről, a használt végeselemekről, anyagmodellről és egyéb vonatkozó paraméterekről. Az elvégzett nagyszámú modellkísérletek lehetőséget adnak a merevített keretek viselkedésének átfogó jellemzésére és az eredményekben ismétlődő szabályszerűségek is megállapításra kerülnek.

A negyedik fejezet első felében bemutatásra kerül a központos rácsozással merevített keretek sajátságos viselkedése földrengés esetén. Megállapítást nyer, hogy hogyan függ össze a gyengeszinti viselkedés, a halmozódó képlékeny alakváltozás, a merevítő rudak állagromlása és az épület modális viselkedésének ebből származó minőségi változása. A gyengeszinti viselkedéssel összefüggésbe hozható tényezők azonosítása lehetővé teszi a fejezet második felében az Eurocode 8 vonatkozó részeinek kritikai vizsgálatát, hiányosságainak felismerését.

Az ötödik fejezetben felhasználásra kerülnek a korábban, a gyengeszinti viselkedésről tett megállapítások egy új tervezési eljárás kialakításában. A Robust Seismic Brace Design (röviden RSBD) névre keresztelt módszer alapvetően két új feltételt fogalmaz meg, amelyeket az Eurocode 8 eljárásával párhuzamosan, illetve annak egyes részei helyett kell alkalmazni. A módszer elvét tekintve képlékeny analízis alapú és a szerkezet nem rugalmas viselkedésére épített. A módszer célja egyfelől a gyengeszinti tönkremeneteli mechanizmus kialakulásának megakadályozása, illetve a képlékeny alakváltozások arányos elosztása a szintek között. A fejezet egy jelentős részét a képlékeny analízishez szükséges belső és külső munkák meghatározásának bemutatása teszi ki. Ugyan a képlékenység anyagi nemlinearitást feltételez, a merev képlékeny anyagmodell használatának köszönhetően a módszer viszonylag egyszerű, kézi számítással is kiértékelhető képletek alkalmazására vezet. A fejezet végén a módszer alkalmasságának vizsgálatára a korábbival azonos növekményes dinamikai vizsgálat eredményei találhatók. A korábban már felhasznált épületek

újratervezésre kerülnek az RSBD módszerrel, és nagyszámú diagram bemutatásával nyer igazolást, hogy a módszer egyenletes megbízhatósággal, a vizsgált modellek mindegyikénél jelentősen javítja a földrengéssel szembeni ellenállást és megszünteti a gyengeszinti viselkedést.

2. A DISSZERTÁCIÓBAN VIZSGÁLT PROBLÉMA BEMUTATÁSA

Többszintes acél, öszvér vagy akár vasbeton szerkezetű épületek vízszintes merevítésére gyakran használt megoldás az egyes oszlopközök ferde rácsozása acél szelvényekkel, lásd *1. ábra*. Ez a szerkezettípus meglévő épületek földrengéssel szembeni megerősítésére is elterjedten alkalmazott. A rácsozás viselkedését földrengés hatására az elmúlt évtizedekben számos szerző vizsgálta. Kutatásaik során több problémát is azonosítottak, melyek a feltételezett és a valós viselkedés közötti jelentős különbségekkel, vagy a szabványos tervezési eljárásokkal kapcsolatosak. A vizsgált témák közül a legfontosabbak a rácsrudak képlékeny ciklikus viselkedésének leírása, újszerű rácselrendezési formák, ellentmondó követelmények a hatályos szabványokban illetve a képlékeny alakváltozások lokalizációjával kapcsolatos, un. gyengeszinti tönkremenetel. A korábbi kutatások összefoglaló tanulsága, hogy a rácsozással merevített keretek szeizmikus viselkedése jelentősen eltér attól az egyszerűsített modellétől, amelyet a vonatkozó szabványok, így az Eurocode 8 is feltételez. Így tehát nyilvánvaló, hogy az EC8 vonatkozó követelményei módosításra szorulnak.

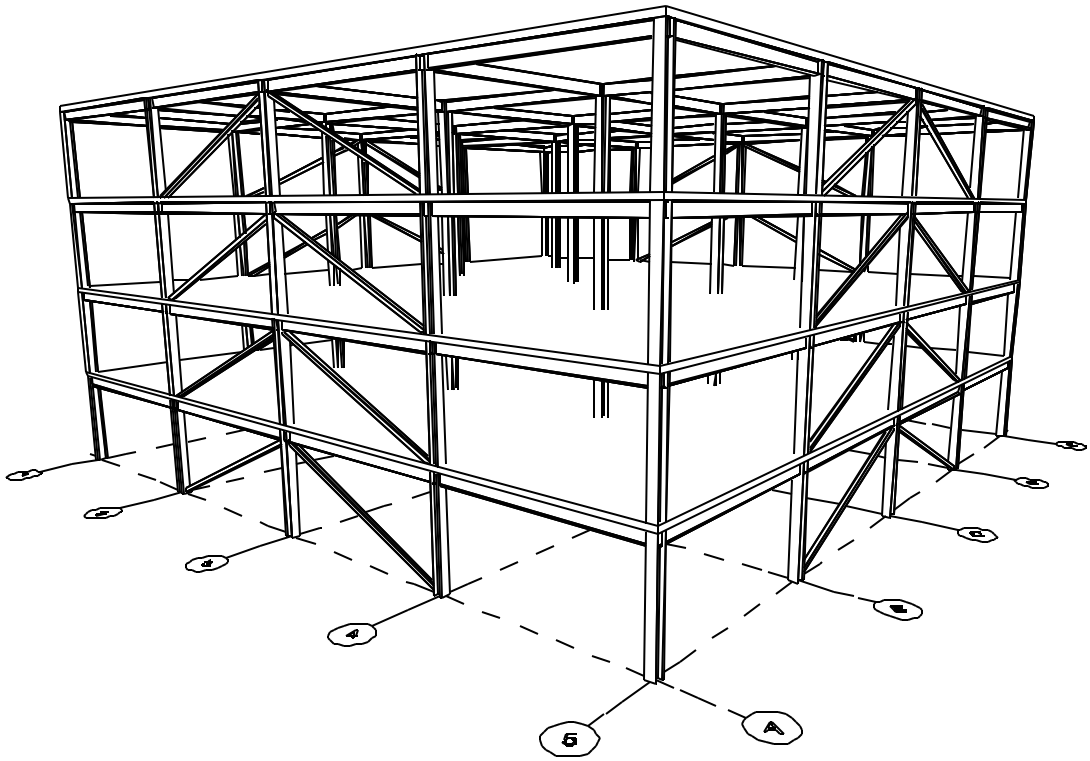

1. ábra; *Központos rácsozással merevített épület*

Az vonatkozó kérdések összessége túlmutat egy doktori disszertáció keretein, ezért a dolgozatban bemutatott vizsgálatok tárgyát a lokálisan, egy szinten, földrengés hatására kialakuló gyengeszinti tönkremenetel képzi. A disszertáció az alábbi kérdésekre kíván választ adni:

- Mik a gyengeszinti viselkedés okai, illetve az azt befolyásoló szerkezeti tényezők?
- Mi a gyengeszinti viselkedés kialakulásának módja és menete?
- Milyen hatással van a gyengeszint a teljes épület ellenállásának szintjére és mennyiben segíti elő a tönkremenetelt?

- Általában milyen viselkedés várható egy Eurocode 8 szerint tervezett rácsos merevítéstől? Hajlamos-e a szerkezet gyengeszinti viselkedést mutatni?
- Mely Eurocode 8 követelmények támasztanak megkérdőjelezhető elvárásokat a szerkezettel szemben?
- Milyen hatásokat és hogyan szükséges még figyelembe venni a méretezési eljárásban?

A kutatás végső célkitűzése olyan méretezési eljárás kidolgozása, amely az Eurocode 8 kereteibe illeszthető, és amellyel kiküszöbölhető a rácsos merevítések gyengeszinti viselkedése és tönkremenetele. További elvárás az új eljárással szemben, hogy nagyméretű egyenletrendszerek, illetve összetett nem lineáris számítások nélkül, kézi eljárással is alkalmazható legyen, ez által gyors és hatékony alternatívát biztosítva a tervezéshez.

Tervezés során a központos rácsozással merevített keretekről hagyományosan azt feltételezzük, hogy erős földrengés hatására a *2/a. ábrán* látható globális képlékeny mechanizmus alakul ki. Ebben a mechanizmusban az elmozdulás irányának függvényében az egyik oldali átlók képlékenyen megnyúlnak, még a nyomott rudak kihajlanak. Ez a szeizmikus válasz kedvező, mert ez teszi lehetővé a legnagyobb tetőponti elmozdulást és ez nyeli el a leghatékonyabban a földrengés energiáját lévén, hogy az összes rácsrúd azonosan részt vesz a disszipációban. Az energia elnyelésével kialakuló csillapítás lehetővé teszi a méretezésben figyelembe vett egyenértékű szeizmikus terhek jelentős redukcióját. Azért, hogy ez a kedvező viselkedés kialakulhasson, biztosítani kell, hogy csak az energia elnyelő rácsrudak szenvednek képlékeny deformációkat, a gerendák és főként az oszlopok nem. Ezt a kapacitás tervezési filozófiának megfelelően az oszlopok és gerendák előírt mértékű túlméretezésével lehet elérni.

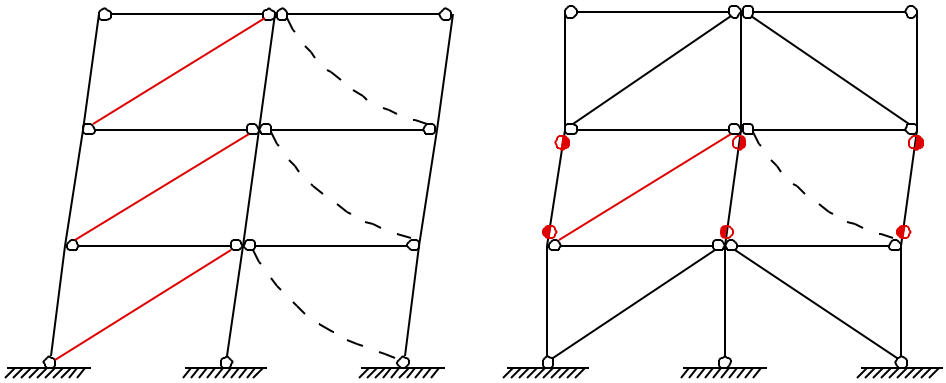

2/a; Globális mechanizmus *2/b; Gyengeszinti mechanizmus*

2. ábra; *Globális és gyengeszinti képlékeny mechanizmus*

A szabványos tervezésben a szeizmikus terhek az un. viselkedési tényezővel redukáltak. Ennek megengedett értéke központos rácsozással merevített keretek esetén viszonylag magas q=4, ami a gyakorlatban annyit jelent, hogy az egyenértékű vízszintes terhek a földrengés intenzitás 25%-ából származtatottak. Az e fölötti rész a képlékeny elnyelésre illetve kisebb részben a szerkezeti csillapításra bízott. A redukált terhekből a belső erőket egyszerű rugalmas analízissel kell meghatározni, így a szerkezeti tulajdonságok megváltozása a képlékeny deformációk hatására elhanyagolt.

Az Eurocode 8 a rácsrudak egyidejű képlékeny alakváltozását és ezzel a globális mechanizmus elősegítését azzal próbálja biztosítani, hogy megköveteli, hogy szeizmikus tervezési helyzetben a legnagyobb és a legkisebb rácsrúd kihasználtság nem térhet el többel, mint 25%. Ez a követelmény az alábbi képletekben kerül megfogalmazásra.

$$\Omega_i = \frac{N_{pl,Rd,i}}{N_{br,Ed,i}} \tag{1}$$

$$\frac{\Omega_{\max}}{\Omega_{\min}} \leq 1.25 \tag{2}$$

Annak biztosítására, hogy az oszlopok és gerendák nem szenvednek képlékeny alakváltozásokat, az Eurocode 8 a bennük fellépő, a földrengésből származó normálerőket, $N_{Ed,E}$, különböző túlméretezési tényezőkkel növeli. (γ_{ov}=1.25 Ω= Ω_{min})

$$N_{Rd}\left(M_{Ed}\right) \geq N_{Ed,G} + 1.1 \cdot \gamma_{ov} \cdot \Omega \cdot N_{Ed,E} \tag{3}$$

A tartószerkezet geometriájából fakadó rácsos tartó hatás miatt és a rugalmas analízis miatt a tartószerkezeti elemekben kis elhanyagolással kizárólag tengelyirányú erők ébrednek lásd *3. ábra*, nyomaték nem. Éppen ezért a fenti (3) követelmény kizárólag a normál teherbírással szemben támasztott.

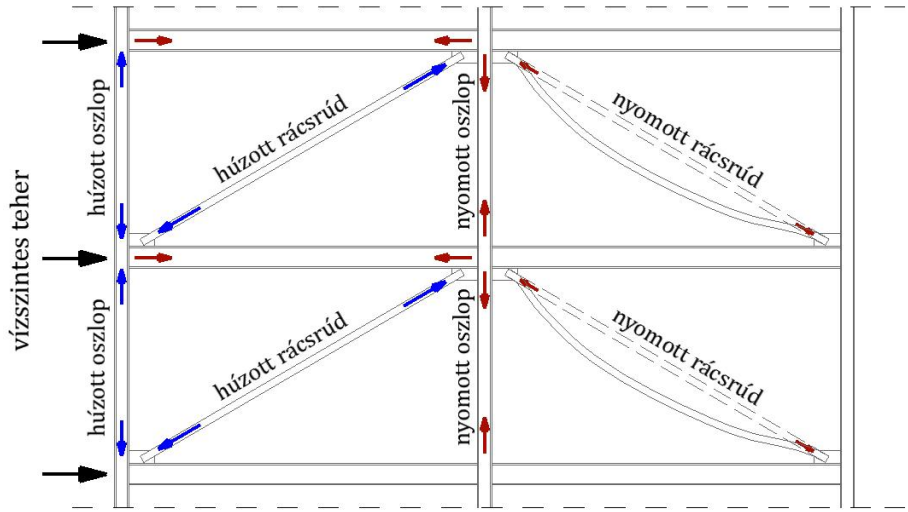

3. ábra; *Rácsos tartó erőjátéka*

Annak ellenére, hogy a tervezés során a globális mechanizmus feltételezett (és látszólag biztosított), ismert tény, hogy a merevített keretek igen hajlamosak egy másik mechanizmus, a korábban már említett gyengeszinti mechanizmus kialakítására, lásd *2/b ábra*. A gyengeszinti mechanizmus során képlékeny deformációk csak egy, vagy igen limitált számú szinten jelentkeznek. Ebben az esetben a rácsrudak többségének képlékeny energiaelnyelő képessége kiaknázatlan marad és az oldalirányú alakváltozások is leginkább csak a gyenge szintről származnak. a gyengeszinti mechanizmus kapacitása tehát messze elmarad a globális mechanizmusétól. További hátrányt jelent, hogy a szintmechanizmusban a folytonos (nem csuklósan toldott) oszlopok is érintettek, azok végein képlékeny csuklók alakulnak ki. Más szóval a szintmechanizmusban az oszlopoknak olyan jelentős nyomatékokat kell elviselniük, amelyre a tervezés során nem is lettek méretezve. Ez magában hordozza az igen korai tönkremenetel lehetőségét ezért, valamint a kedvezőtlen disszipációs tulajdonságok miatt a gyengeszinti mechanizmus kialakulásának megakadályozása feltétlenül szükséges.

A disszertáció az Eurocode 8 szerint tervezett központos rácsozással merevített acélvázak gyengeszinti viselkedésével foglalkozik. Egy átfogó numerikus szimulációs program keretében feltárásra kerül a szabványnak megfelelő épületek kedvezőtlen viselkedésre mutatott hajlama. Az analízis eredményeinek mélyebb kiértékelésével

azonosításra kerülnek a gyengeszinti viselkedést elősegítő tényezők mely egy új, az un. Robust Seismic Brace Design (RSBD) módszer kifejlesztéséhez vezet. A módszer hatékonyan megakadályozza a gyengeszinti mechanizmus kialakulását, amit a numerikus szimulációs program ismételt futtatása igazol.

3. AZ EUROCODE 8 SZERINT TERVEZETT ÉPÜLETEK HATÉKONYSÁGA

Az Eurocode 8 eljárás hatékonyságának vizsgálatára számos különböző, központos rácsozással merevített keretszerkezetű épületet terveztem. Az egyes épületek alapvetően a szintek számában és a tartószerkezeti rendszerben térnek el egymástól. A 4, 6, 8 és 10 szintes épületek azonosító kódja CBF4, CBF6, CBF8 illetve CBF10 rövidítéssel kezdődik (Concentrically Braced Frame angol rövidítésből). Az épületek alaprajza megegyező, a két merőleges irányban 4-4 6 méter tengelytávú raszterre szerkesztett. A szintmagasság minden esetben 3 méter, lásd *4 ábra*.

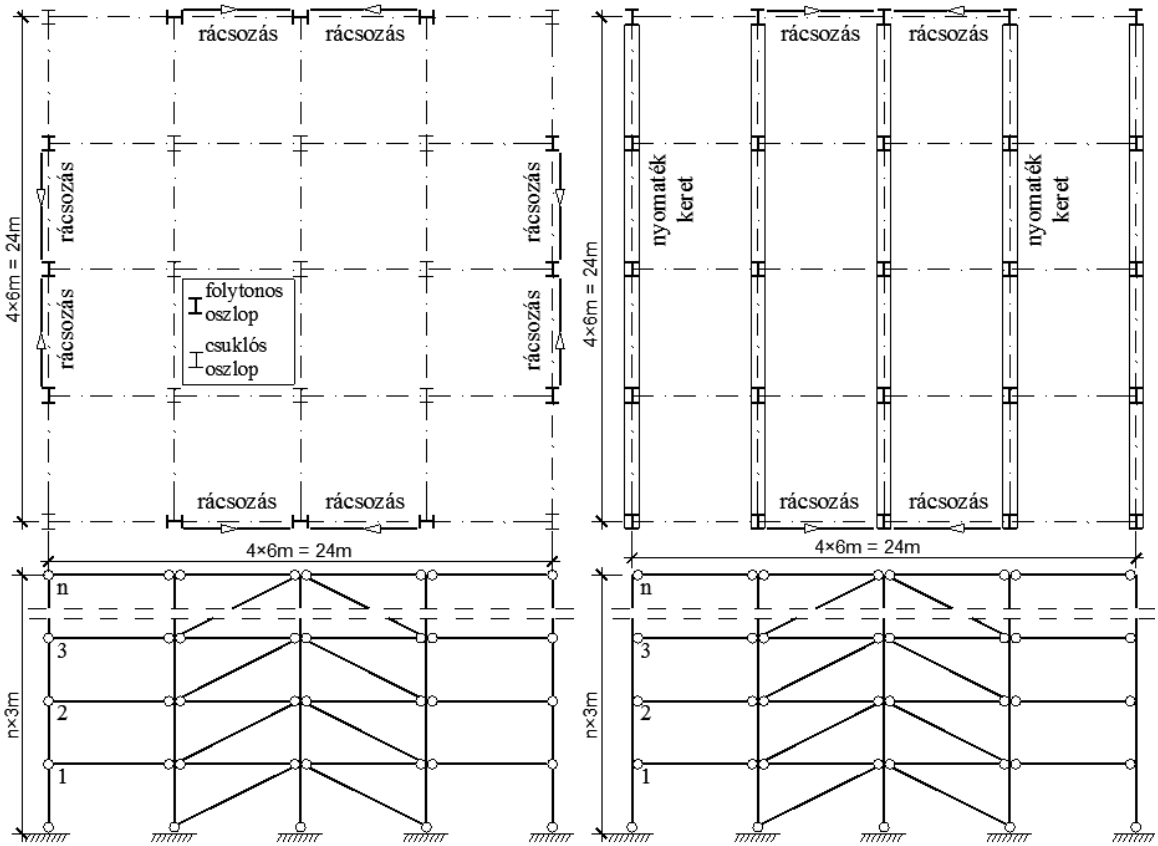

4. ábra; *Vizsgált épületek alaprajza és nézete*

A szintszámot követő 1 azonosítóval rendelkező épületek mindkét irányban rácsozottak, lásd bal oldali alaprajz. A 2 típusú épületek nyomatékbíró keretek az egyik és rácsozottak a másik irányban. Az alábbi táblázatban a vizsgálatok során felhasznált épületek kódja, specifikációja és első sajátrezgés alakjának periódus ideje van feltüntetve. Az azonosító kódban az EC8 rövidítés a tervezési eljárásra utal.

1. Táblázat; *A tervezett épületek listája*

Épület	*Sajátosság*	*Periódus (T_1)*
CBF41-EC8	4 szintes, mindkét alaprajzi irányban merevített	1.13
CBF42-EC8	4 szintes, nyomatékbíró keret az egyik irányban	1.19
CBF61-EC8	6 szintes, mindkét alaprajzi irányban merevített	1.65
CBF62-EC8	6 szintes, nyomatékbíró keret az egyik irányban	1.61
CBF81-EC8	8 szintes, mindkét alaprajzi irányban merevített	2.10
CBF82-EC8	8 szintes, nyomatékbíró keret az egyik irányban	2.04
CBF101-EC8	10 szintes, mindkét alaprajzi irányban merevített	2.54
CBF102-EC8	10 szintes, nyomatékbíró keret az egyik irányban	2.41
CBF41Q5-EC8	4 szintes, q=5 viselkedési tényezővel tervezett	1.21
CBF61Q5-EC8	6 szintes, q=5 viselkedési tényezővel tervezett	1.68
CBF61M-EC8	6 szintes, 50%-kal megnövelt födém tömeg a felül	1.78
CBF81M-EC8	8 szintes, 2%-kal megnövelt födém tömeg felül	2.17

Az épületek viselkedésének meghatározása egy növekményes dinamikai analízis program (NDA) végrehajtásával történt. A nemlineáris dinamikai számításokhoz a FinelG végeselemes analízis program került felhasználásra. A földrengés terhelés hét mesterséges gyorsulás adatsor által meghatározott. Minden adatsor hossza 20 másodperc és az egyes rengések spektruma a tervezés során felhasznált Eurocode 8 spektrumhoz igazított, lásd *5 ábra*. A növekményes dinamikai analízis miatt a rengések változó intenzitással lettek az épületeken működtetve. Az intenzitás változtatásához az adatsorok egy növekményi tényezővel szorzottak, melynek értéke 0.1 és 2.0 között változik.

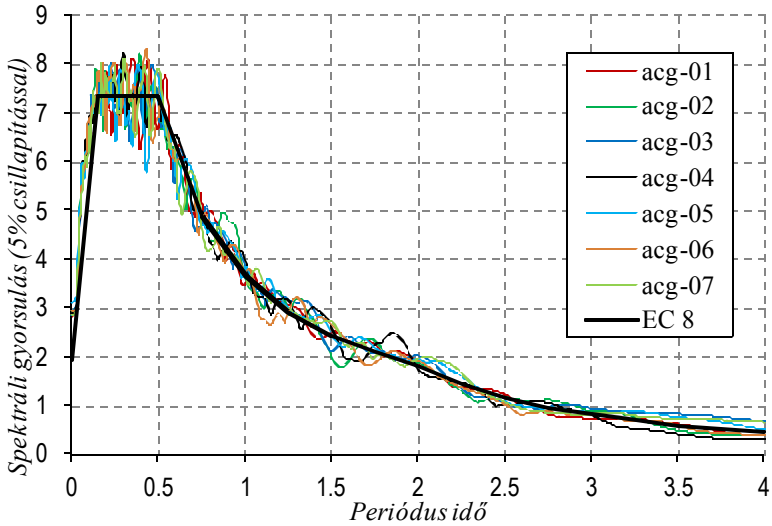

5. ábra; *Mesterséges accelerogrammok spektrumai és a tervezési spektrum*

A végeselemes kísérleti program elsődleges célja, hogy meghatározzuk, hogy a vizsgált épületek hajlamosak-e gyengeszint kialakulására és, hogy ez eredményez-e korai tönkremenetelt. Ennek meghatározására NDA görbék készültek a számítások eredményeiből, melyek az egyes szinteken tapasztalt legnagyobb relatív eltolódást ábrázolják (IDR) a növekményi tényező függvényében. A relatív eltolódások a szintmagassággal osztottak, így az eredmények a szintmagasság százalékában adottak. A diagramokon minden szintnek külön görbéje van, így a különbségek az egyes válaszok között szemléletesek. Az *6 ábrán*

bemutatott néhány diagramon látható, hogy a görbék igen széles intervallumban vesznek fel értékeket. Az egyes szinteken tapasztalt válaszok különbsége jelentős a tervezési intenzitásnál alacsonyabb tartományban is (növekményi tényező<1.0). Megfigyelhető, hogy a maximum értékek többszörösen meghaladják a minimumokat. Megállapítható tehát, hogy a vizsgált épületekben a disszipáció és a képlékeny deformációk eloszlása nem egyenletes, egyes szinteken a deformációk koncentrálódnak más szintekhez viszonyítva. Fontos észrevenni továbbá, hogy az alacsonyabb szinteken tapasztalható kiugrások, magasabb intenzitásoknál mérséklődnek. A bemutatott diagramokon a tönkremeneteli határnak tekintett 2% relatív eltolódást a gyenge szintek az 1.0 növekményi tényezőnél kisebb szinten elérik. Elmondható tehát, hogy a vizsgált épületek nem csupán hajlamosak a gyengeszinti viselkedésre, de ennek okán a másodlagos szerkezeti elemek károsodása vagy az elsődlegesek törése az épületek tönkremeneteléhez is vezethet a tervezési szeizmikus intenzitásnál alacsonyabb szinten is. Az Eurocode 8 követelményei így nem megfelelőek, mert nem akadályozzák meg a korai tönkremenetelt és nem eredményezik az elvárt globális képlékeny viselkedés kialakulását.

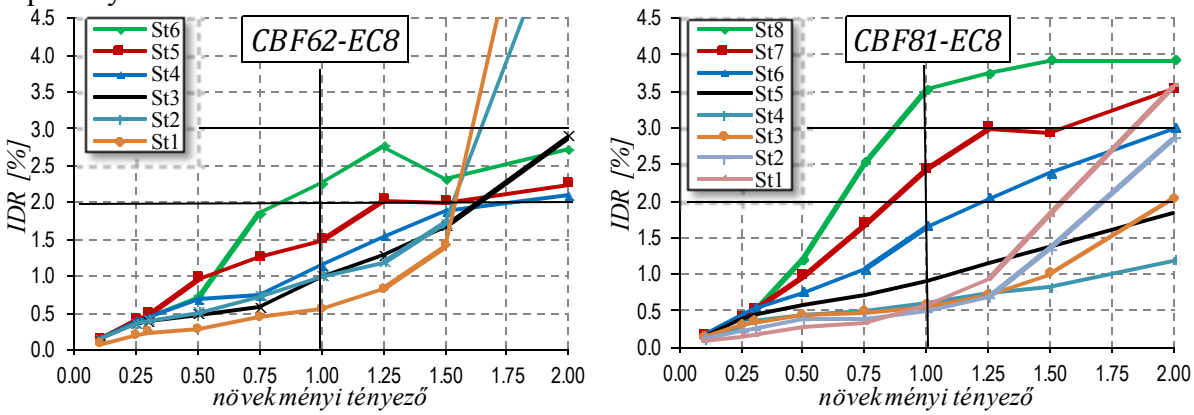

6. ábra; *NDA görbék*

4. A GYENGESZINTI VISELKEDÉS KIALAKULÁSÁNAK OKAI

Az eddig bemutatott kedvezőtlen eredmények szükségessé teszik a gyengeszinti viselkedést mutató rácsozott keretek válaszának behatóbb vizsgálatát. Ha megvizsgáljuk a *7 ábrán* bemutatott deformálódott szerkezet alakját a gerjesztés után, látható, hogy a merevítő rudak szögletesen kihajlanak. A szögletesség oka, hogy a rudak közepén a gerjesztés során képlékeny csukló alakul ki, melynek ellenállása a halmozódó képlékeny alakváltozások miatt csökken, és ez megkönnyíti a kihajlást. Húzás során a rudak képlékeny megnyúlásai megnövelik a terheletlen hosszat, minek következtében a rudak akkor is nyomottak, ha az épület oldalirányban terheletlen és függőlegesen nyugalmi helyzetben van. A képlékeny megnyúlások tehát tovább növelik a rudak szögletes kihajlásának mértékét.

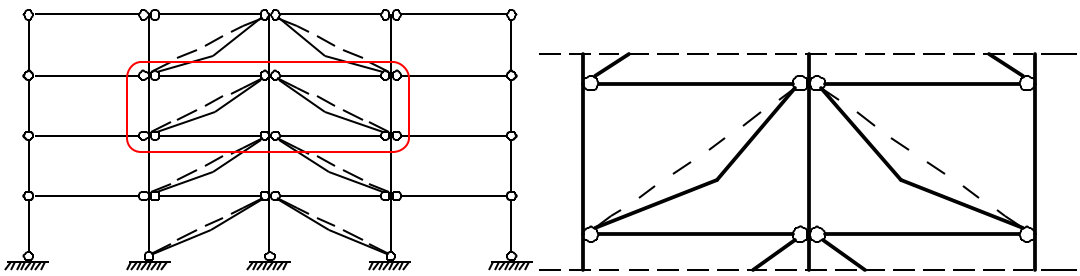

7. ábra; *A rácsrudak képlékeny deformációja*

A 8 ábrán egy rúd tengelyirányú erő – elmodulás diagramja látható, mely egy 20 másodperces gerjesztésből származik. Megfigyelhető, hogy a számos ciklus közül háromban jelenős képlékeny megnyúlás alakul ki. A megnyúlás halmozódása a kihajlási pont eltolódásához vezet, amit az ábrán a piros ív jelöl. A kihajláshoz tartozó erő lecsökken és a kihajlás már a pozitív, tehát a húzás tartományában kialakul. Az is megfigyelhető továbbá, hogy a megnyúlás miatt jelentős húzóerőkhöz lényegesen nagyobb elmozdulások szükségesek, mint kezdetben. Ez úgy is értelmezhető, hogy a rúd tengelyirányú merevsége lecsökken, melyet a piros egyenesek jelölnek.

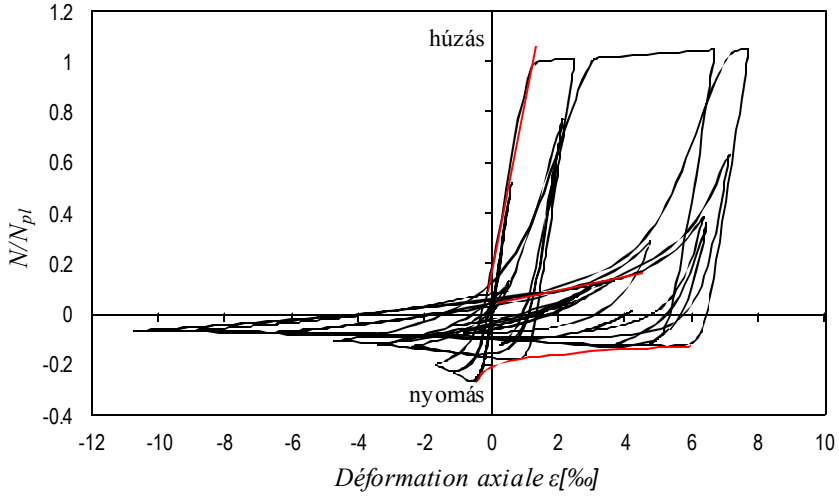

8. ábra; *Egy rácsrúd fajlagos normál igénybevétel – deformáció diagramja*

A rácsrudak növekvő deformációja miatt a normálerő lecsökken a rudakban és a vízszintes terhelés fokozatosan az oszlopokra hárul. Az oszlopok hajlítómerevsége többnyire lényegesen kisebb vízszintes eltolódással szembeni merevséget biztosít az érintett szinten, mint a merevítő rudak normálmerevége. Ezért a gyenge szinteken, ahol a rudak deformációja kiemelkedő, a vízszintes merevség lényegesen lecsökken a többi szinthez képest. A merevségi viszonyok ilyen jellegű változása jelentősen megváltoztatja az épület sajátrezgés alakjait és periódusait. A 9 ábrán egy a harmadik emeleten gyenge szint viselkedést mutató 4 szintes épület első két sajátrezgés alakja és az eltolódások várató maximumai láthatók. A rezgésalakok elkülönülnek olyan esetekre, melyek a gyenge szint feletti, illetve alatti épületrészek rezgését mutatják. Az első rezgésalak periódusa lényegesen magasabb, mint a másodiké, továbbá az egyéb magasabb módok elhanyagolhatók, ezért a maximális elmozdulások elsősorban az első rezgés alak által meghatározottak. Így az épület várható válasza a gerjesztésre olyan módon alakul, hogy az elősegíti az elmozdulások és a halmozódó képlékeny alakváltozások koncentrációját a már eleve gyenge szinten, ami a merevség további csökkenéséhez vezet.

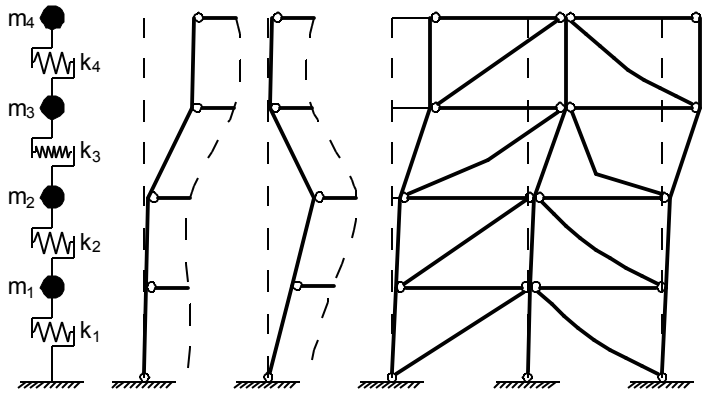

9. ábra; *Gyengeszint hatása a modális viselkedésre*

A fent leírt folyamat egy ismétlődő ciklus kialakulásához vezet, amely fokozatosan növeli a képlékeny deformációt és alakítja ki a gyengeszinti viselkedést. Következés képpen a gyengeszinti mechanizmus egy öngerjesztő, földrengés során kialakuló folyamatként jellemezhető. A ciklus ismétlődését a gyenge szint tönkremenetele töri meg. Ez egyrészről bekövetkezhet az oszlopok teherbírásának kimerülése miatt, vagy a merevítő rudaknak a képlékeny alakváltozások halmozódásából származó törése miatt. A ciklus kellően nagyszámú ismétlés esetén szükségszerűen tönkremenetelhez vezet. Lévén, hogy egy rengés során a ciklus ismétlődésének száma véges, kellően duktilis rácsrudak valamint kellő merevségű és képlékeny nyomatéki többlet-teherbírású oszlopok választásával a tönkremenetel megakadályozató.

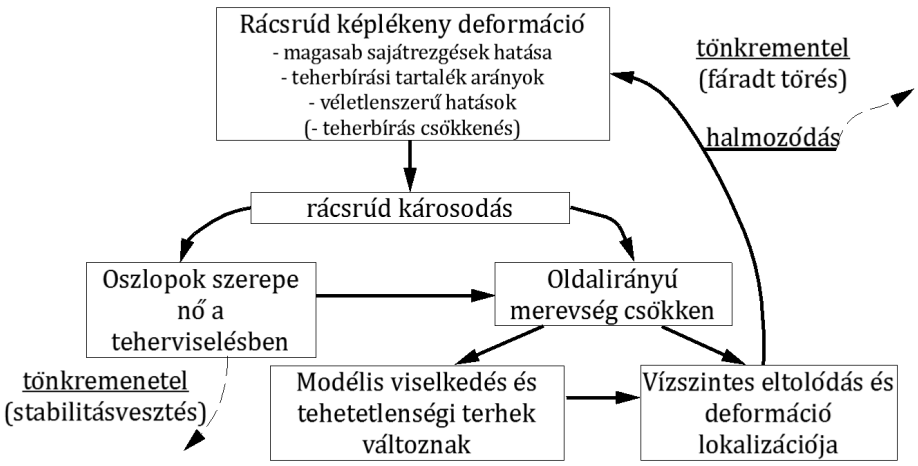

10. ábra; *A gyengeszinti viselkedés kialakulásának organigramja*

Egy merevített keret lineáris statikai analízise a rácsos tartó viselkedés miatt csaknem kizárólag normál igénybevételeket eredményez a szerkezeti elemekben. Ezzel szemben, mint ahogy azt korábban már említettük, a rácsok deformációja bevonja a folytonos oszlopokat a vízszintes teherviselésbe, ezért azok hajlítottak lesznek. Tekintettel arra, hogy hajlító nyomaték a lineáris analízisből valós nagyságrendben nem nyerhető, a méretezés során az oszlopok normál teherbírása túlbecsült, ami alulméretezéshez vezet. Továbbá az oszlopokban a gyengeszinti viselkedés során képlékeny alakváltozások is előfordulhatnak, ezért azoknak kellő duktilitással is rendelkezniük kell. Ez még szigorúbb követelmények használatát teszi szükségessé az oszlopméretezésben.

Az eddig leírtak alapján a disszertációban az alábbi konklúziók találhatók az Eurocode 8 tervezési követelményeire vonatkozóan:

- Az épületek többnyire hajlamosak a gyengeszinti viselkedés kialakítására
- A képlékeny deformációk lokalizációja a gyenge szinten számos esetben korai tönkremenetelhez vezet.
- A rácsrudak képlékeny deformációja a modális viselkedés és ezzel együtt a vízszintes teherelrendezés megváltozásához vezet, ami az Eurocode 8-ban semmilyen módon sem jelenik meg.
- Az Eurocode 8-ban alkalmazott rugalmas méretezés és a kapcsolódó feltevések lényegesen eltérnek a valós rugalmatlan viselkedéstől
- A rácsrudak kihasználtságát egységesítő követelmény, *(2) egyenlet*, nem érvényes bármilyen véletlenszerűen kialakuló rugalmatlan viselkedés tartományában a teherelrendezés és a belső erők megváltozása miatt, ezért a követelmény nem alkalmas a gyengeszinti viselkedés kialakulásának megakadályozására.
- Az Eurocode 8 szerinti analízis alulbecsüli az oszlopokban várható nyomaték nagyságát, ezért a méretezési eljárás nem biztosít kellő teherbírási tartalékot az oszlopokban.
- Az Eurocode 8 még csak folytonos oszlopok használatát sem követeli meg. A követelményeket folytonos és csuklósan toldott oszlopok is kielégítik.

5. A ROBUST SEISMIC BRACE DESIGN MÓDSZER

Az RSBD módszer első alapvető tulajdonsága, hogy a tökéletes, rugalmas modell helyett valószerűbb, a rugalmatlan viselkedésre jellemző modellt vizsgál. Ez gyenge szinttel rendelkező épületben a vízszintes eltolódások közelítőleg merevtest-szerűek a kérdéses szint fölött és elhanyagolhatók az alatt. Az ebből származó vízszintes tehetetlenségi erő eloszlás konstans a gyengeszinttől felfelé az épület tetejéig (azonos födémtömegeket feltételezve), lásd 11. ábra. A képlékenységtan kinematikai elve alapján ez a teherelrendezés akkor eredményezheti a globális mechanizmust a lokális helyett, ha a globális mechanizmus teher paramétere, λ_{glob}, kisebb, mint a szint mechanizmus teher paramétere, λ_{loc}. Egy n szintes merevített keretben n különböző teherelrendezés lehetséges (fentről az n-edik szintig), ezért az alábbi feltételt n különböző paraméter párnak kell kielégíteni.

$$\frac{\lambda_{loc,i}}{\lambda_{glob,i}} \geq 1.0 \text{ ahol } i=1..n \tag{4}$$

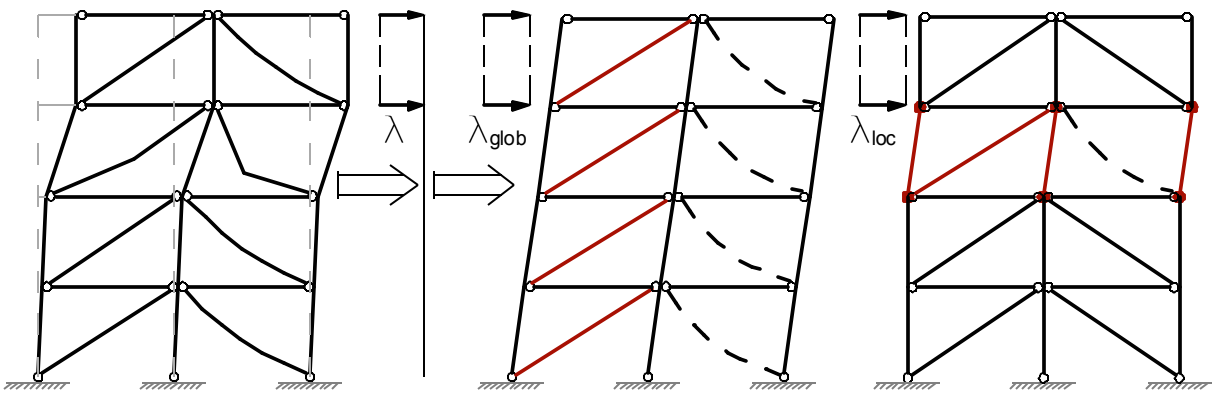

11. ábra; *Rugalmatlan számítási modell*

A fenti feltétel a rácsok és az oszlopok keresztmetszetének növelésével egyaránt kielégíthető, mert ezek egyaránt érintettek a szintmechanizmusban. Ha egy szélsőséges esetet tekintve a teljes képlékeny teherbírás egy szinten kizárólag a rácsrúdból származik, akkor az eső folyáshoz és a képlékeny szintmechanizmus kialakulásához tartozó teherszint azonos. Lévén, hogy a módszer megakadályozni szándékozik a szintmechanizmus kialakulását, a vizsgált esetben a rácsrúd megfolyását is megakadályozza. Így a szint rugalmas marad, és nem vesz részt a képlékeny disszipációban. Ezzel szemben, ha egy szint képlékeny teherbírása főként az oszlopokból származik, akkor ezen a szinten lényegesen nagyobb elmozdulásokra lehet számítani, mint más szinteken. Ennek oka, hogy a hajlított oszlopok lényegesen nagyobb elmozdulásokat engednek meg a teherbírási határ eléréséig, mint a rácsos merevítés. Egy ilyen szinten tehát gyengeszinti viselkedés várható. Az imént bemutatott két alternatíva a 12. ábrán fel van tüntetve az ideális szeizmikus intenzitás – elmozdulás viselkedéssel együtt.

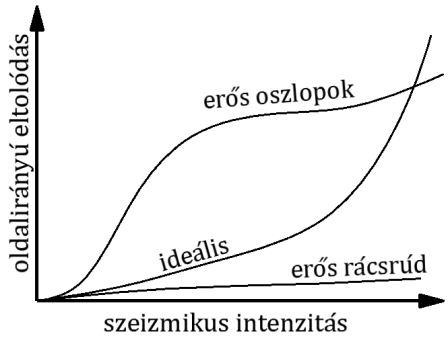

12. ábra; *Egy szint lehetséges válaszainak alternatívái*

Az RSBD módszer második feltételének célja, hogy megakadályozza azokat az eseteket, melyek túl nagy vagy túl kicsi rugalmatlan alakváltozásokat eredményeznek egyes szinteken. Egy ilyen feltétel definiálásához a várható rugalmas – képlékeny viselkedések vizsgálata szükséges. A 13. ábrán a két szélsőséges viselkedést bemutató teher paraméter – vízszintes eltolódás diagramok láthatók. A fekete vonal egy károsodás mentes szint idealizált Pushover görbéje. A piros vonalak különböző mértékű rácsrúd deformációval zavart szintek viselkedését írják le. Ha a rácsrúd folyásához tartozó teherparaméter, λ_{br}, közel van a globális mechanizmus paraméteréhez, λ_{glob}, nagy rugalmatlan alakváltozások nem alakulnak ki és az első folyáshoz és a globális mechanizmus kialakulásához tartozó elmozdulások közel esnek egymáshoz (bal diagram). Ellenben, ha a lobális paraméter lényegesen meghaladja az első folyás paraméterét, az oszlopok jelentős eltolódásokat engednek meg a globális mechanizmus teherszintjének eléréséig (jobb diagram). Láthatóan, a várható rugalmatlan elmozdulások nagysága összefüggésben van a globális és az első folyás teherparaméterének arányával. A részletek elhanyagolásával az RSBD módszer második feltétele szerint ez az arány, mely a BPR (Brace Performance Ratio) neve kapta, az egyes szinteke nem térhet el jobban, mint 0.1. Ez a feltétel tehát azt kívánja biztosítani, hogy a rugalmatlan elmozdulások aránya se térjen el jelentősen.

$$BPR_i = \frac{\lambda_{br,i}}{\lambda_{glob,i}} \text{ és } BPR_{\min} + 0.1 \geq BPR_{\max} \tag{5}$$

Nyilvánvaló, hogy ha a BPR 1.0 közeli, akkor a rácsrúd részesedése túl magas, az oszlopok teherbírása nem szükséges és így ez a szint nem szenved rugalmatlan alakváltozásokat. Ezért javasolt, hogy a BPR értéke ne haladja meg a 0.9-et.

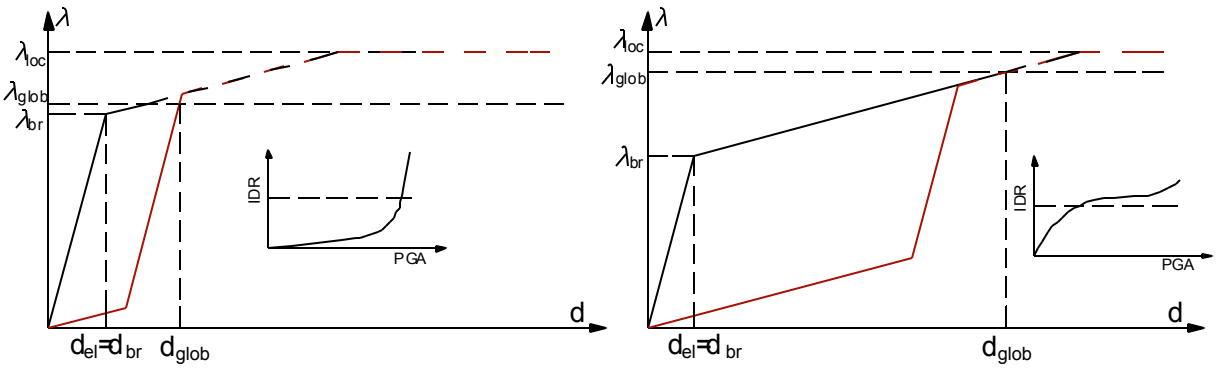

13. ábra; *Túl és alulméretezett rácsok hatása a rugalmatlan alakváltozásokra*

Az RSBD módszer feltételeihez szükséges teker paramétereket a képlékeny mechanizmusokon végzett külső és belső munkák ekvivalenciájával határozhatjuk meg. A globális mechanizmus esetén ez az alábbi:

$$W_{\lambda,glob,i} + W_{G,glob} = \sum_i W_{t,br,i} \tag{6}$$

A fenti képletben $W_{\lambda,glob,i}$ a külső horizontális erők munkája, $W_{G,glob}$ a gravitációs terhek másodrendű munkája és $W_{t,br,i}$ egy rácsrúd belső munkája az i-edik szinten. A részleteket mellőzve a fenti összefüggés az alábbi bővített alakban írható:

$$\lambda_{glob,i} \cdot \sum_{k=i}^{n} \left(mp_k \cdot \sum_{l=1}^{k} \Delta B_l \right) + \sum_{k=1}^{n} \left[\sum_{l=1}^{m} G_{k,l} \cdot \frac{\left(\sum_{k=1}^{i} \Delta B_k \right)^2}{2 \sum_{k=1}^{i} H_k} \right] = \sum_i N_{pl,br,i} \cdot \Delta B_i \cdot \cos \alpha_i \tag{7}$$

ahol mp a szintek tömegarányait jelölő vektor (nem állandó födémtömegek esetén), ΔB az előírt vízszintes szinteltolódás (javasolt értéke 2%), $G_{i,j}$ az i-edik szinten és j-edik oszlop - gerenda csomópontba redukált egyidejű gravitációs teher, H a szintmagasság, N_{pl} a képlékeny normál teherbírás és α a rácsrúd és a vízszintes által bezárt szög. A szintmechanizmus esetén az energia egyenértékűség az alábbi formában írható:

$$W_{\lambda,loc,i} + W_{G,loc,i} = W_{t,br,i} + W_{col,i} \tag{8}$$

A részleteket ismét elhanyagolva, bővített formában:

$$\begin{aligned} \Delta B_i \cdot \lambda_{loc,i} \cdot \sum_{k=i}^{n} mp_k + \sum_{k=i}^{n} \sum_{l=1}^{m} \left[G_{k,l} \cdot \left(\frac{\Delta B_i^2}{2H_i} + e_{col,l} \cdot \frac{\Delta B_i}{H_i} \right) \right] = \\ = N_{pl,br,i} \cdot \Delta B_i \cdot \cos \alpha_i + \sum_{j=1}^{m} M_{col,i,j} \cdot \frac{\Delta B_i}{H_i} \end{aligned} \tag{9}$$

A (7) és (9) egyenletekből a teherparaméterek explicit módon kifejezhetők.

$$\lambda_{glob,i} = \frac{\sum_i N_{pl,br,i} \cdot \Delta B_i \cdot \cos \alpha_i - \sum_{k=1}^{n} \left[\sum_{l=1}^{m} G_{k,l} \cdot \frac{\left(\sum_{k=1}^{i} \Delta B_k \right)^2}{2 \sum_{k=1}^{i} H_k} \right]}{\sum_{k=i}^{n} \left(mp_k \cdot \sum_{l=1}^{k} \Delta B_l \right)} \tag{10}$$

$$\lambda_{loc,i} = \frac{N_{pl,br,i} \cdot \Delta B_i \cdot \cos\alpha_i + \sum_{j=1}^{m} M_{red,i,j} \cdot \frac{\Delta B_i}{H_i} - \sum_{k=i}^{n}\sum_{l=1}^{m} G_{k,l} \cdot \frac{\Delta B_i^2}{2H_i}}{\Delta B_i \cdot \sum_{k=i}^{n} mp_k} \tag{11}$$

A λ_{br} meghatározásához szükséges képlet azonos a (11) egyenlettel az oszlopok nyomatéki tartalékából (M_{red}) származó munkavégzés nélkül.

$$\lambda_{br,i} = \frac{N_{pl,br,i} \cdot \Delta B_i \cdot \cos\alpha_i - \sum_{k=i}^{n}\sum_{l=1}^{m} G_{k,l} \cdot \frac{\Delta B_i^2}{2H_i}}{\Delta B_i \cdot \sum_{k=i}^{n} mp_k} \tag{12}$$

6. AZ RSBD MÓDSZERREL MEGERŐSÍTETT ÉPÜLETEK VISELKEDÉSE

Az alábbiakban két kiválasztott épület esetén az eredeti Eurocode 8 szerinti és az RSBD módszerrel nyert szerkezetek kerülnek bemutatásra táblázatosan illetve azok szeizmikus viselkedése a korábban már használt NDA görbékkel. A táblázatokban a lényeges keresztmetszetek, a túltervezési tényezők (Ω_i) illetve az RSBD teherparaméterek adottak. Az első táblázatban az első RSBD feltételt nem kielégítő paraméter arányok illetve a legnagyobb és legkisebb BPR (második feltétel) vastagon szedett. A második táblázatban a módosított keresztmetszetek és a két BPR kiemelt. A táblázatok alatt a legnagyobb és legkisebb túltervezési tényező aránya látható, melynek a (2) feltételt kell(ene) kielégítenie.

Az egyes épületekre adott első táblázatot és a vonatkozó NDA görbét vizsgálva megfigyelhető, hogy az RSBD módszer igen pontosan azonosítja a gyenge szinteket az EC8 épületekben. Látható továbbá az is, hogy a feltételtől való eltérés mértéke arányos a gyengeszint jelentőségével. Mivel a gyengeszintek megerősítése módosítja a globális teherparamétereket is, egyes épületek esetén szükséges a gyenge szinttel szomszédos szintek megerősítése is. Ez azt igazolja, hogy az RSBD módszer nem csak a gyengeszintek azonosítására és megerősítésére jó, hanem egyszersmind azt is megakadályozza, hogy a megerősítés után a gyenge szint máshol továbbra is jelen legyen. Ez utóbbi jelenségre a kutatás során számos példa adódott. A megerősített épületek legtöbbször megsértik a (2) egyenletben definiált EC8 követelményt. Ennek ellenére a megerősített épületek viselkedése kivétel nélkül igen kedvező, karcsú görbesereget mutat az NDA diagramon. Ez igazolja, hogy az RSBD módszer az épületben jól elosztott disszipációt eredményez. E mellett az RSBD épületek mind megfelelnek a tervezési, sőt sok esetben lényegesen erősebb szeizmikus intenzitás esetén is. A bemutatott példákban a tönkremenetel a tervezési intenzitás 150%-a után várható és nem gyengeszinti viselkedés következtében.

2. táblázat; *CBF62-EC8*

szint	*belső oszlop*	*homlokzati oszlop*	*rácsrúd*	Ω	λ_{loc}	λ_{glob}	$\frac{\lambda_{loc}}{\lambda_{glob}}$	*BPR*
6	HEA 180	HEA 180	90×5	1.00	**436.9**	**513.9**	**0.85**	**0.62**
5	HEB 180	HEB 180	100×6	0.98	343.1	280.3	1.22	0.72
4	HEB 240	HEB 200	100×8	1.01	316.2	205.5	1.54	0.80
3	HEB 260	HEB 240	100×10	1.04	300.6	171.3	1.75	**0.84**
2	HEB 280	HEB 260	100×10	0.99	272.6	154.2	1.77	0.78
1	HEB 320	HEB 320	120×10	1.00	186.0	146.8	1.27	0.78

$\Omega_{max}/\Omega_{min}$=1.06

3. táblázat; *CBF62-RSBD*

szint	*belső oszlop*	*homlokzati oszlop*	*rácsrúd*	Ω	λ_{loc}	λ_{glob}	$\frac{\lambda_{loc}}{\lambda_{glob}}$	*BPR*
6	HEA 180	**HEB 180**	**100×5**	**1.15**	524.5	528.1	0.99	**0.70**
5	HEB 180	HEB 180	**100×6.3**	1.00	385.2	288.1	1.34	0.76
4	HEB 240	HEB 200	100×8	1.00	320.6	211.3	1.52	0.78
3	HEB 260	HEB 240	100×10	1.03	300.6	176.0	1.71	**0.81**
2	HEB 280	HEB 260	100×10	0.97	272.6	158.4	1.72	0.76
1	HEB 320	HEB 320	120×10	0.98	186.0	150.9	1.23	0.76

$\Omega_{max}/\Omega_{min}$=1.19

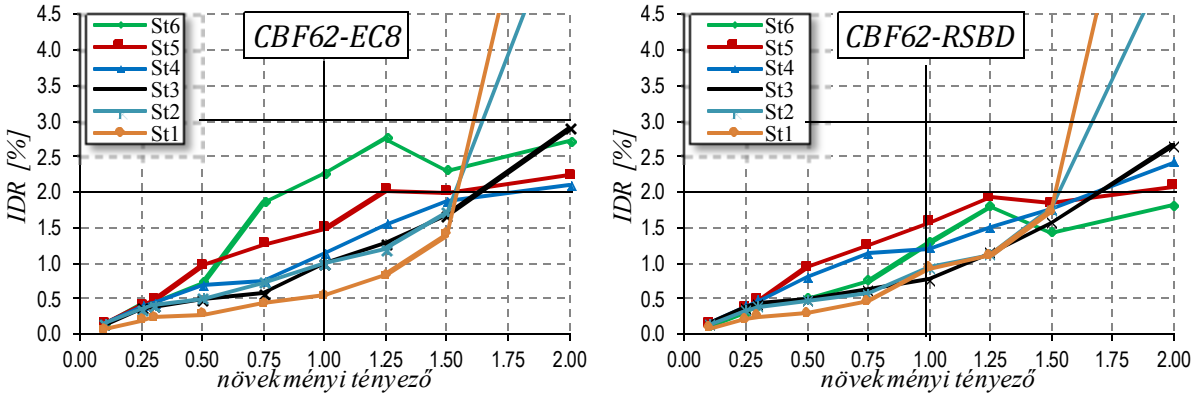

14. ábra; *NDA görbék, hatszintes épület*

4. táblázat; *CBF81-EC8*

szint	*belső oszlop*	*homlokzati oszlop*	*rácsrúd*	Ω	λ_{loc}	λ_{glob}	$\frac{\lambda_{loc}}{\lambda_{glob}}$	*BPR*
8	HEA 160	HEA 160	90×5	0.99	**402.0**	**609.5**	**0.66**	**0.53**
7	HEB 180	HEA 180	100×6.3	1.05	**296.3**	**325.1**	**0.91**	0.67
6	HEB 220	HEB 200	100×8	1.01	245.0	232.2	1.05	0.71
5	HEB 240	HEB 220	100×10	1.10	229.0	187.5	1.22	0.77
4	HEB 280	HEB 240	120×10	1.01	217.5	162.5	1.34	**0.88**
3	HEB 300	HEB 280	120×10	0.98	192.3	147.8	1.30	0.78
2	HEM 240	HEB 320	140×10	0.98	210.8	139.3	1.51	0.85
1	HEM 240	HEM 240	140×10	1.00	147.2	135.5	1.09	0.74

$\Omega_{max}/\Omega_{min}$=1.07

5. táblázat; *CBF81-RSBD*

szint	*belső oszlop*	*homlokzati oszlop*	*rácsrúd*	Ω	λ_{loc}	λ_{glob}	$\frac{\lambda_{loc}}{\lambda_{glob}}$	*BPR*
8	HEA 160	**HEA 240**	**100×6.3**	**1.40**	689.3	662.2	1.04	0.70
7	HEB 180	**HEA 240**	**100×8**	1.21	471.3	353.2	1.33	0.78
6	HEB 220	HEB 200	**100×10**	1.22	309.2	252.3	1.23	0.80
5	HEB 240	HEB 220	100×10	1.11	242.6	203.8	1.19	0.77
4	HEB 280	HEB 240	120×10	1.17	217.5	176.6	1.23	**0.80**
3	HEB 300	HEB 280	120×10	1.07	192.3	160.5	1.20	0.72
2	HEM 240	HEB 320	140×10	1.08	210.8	151.4	1.39	0.79
1	HEM 240	HEM 240	140×10	0.98	147.4	147.2	1.00	**0.69**

$\Omega_{max}/\Omega_{min}$=1.43

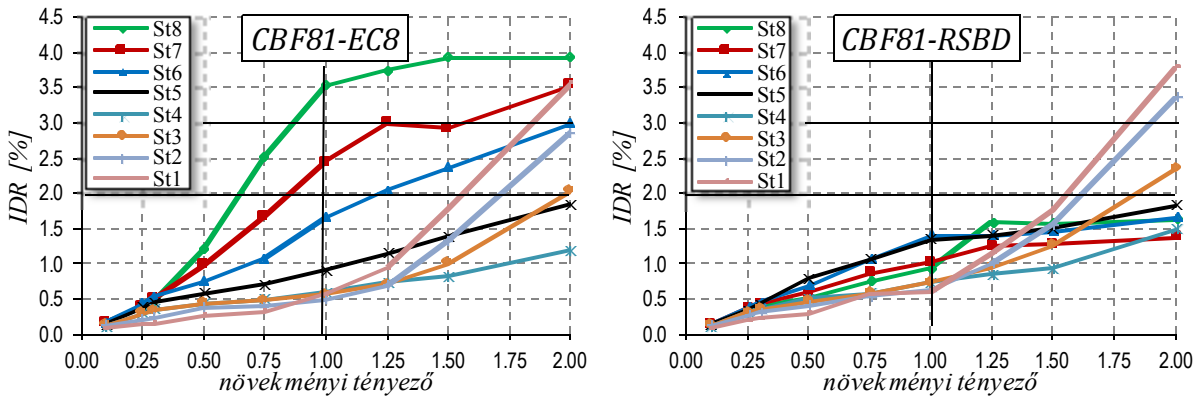

15. ábra; *NDA görbék, nyolcszintes épület*

Az egyes NDA görbeseregeknél a gyengeszinti hajlam jellemzésére használható a legnagyobb és legkisebb relatív eltoldás közötti különbség. Ahhoz azonban, hogy megkülönböztethetők legyenek azok az esetek, melyeknél csupán egy szint tér el jelentősen a többitől és azok, amelyekben több és ezért a gyengeszinti viselkedés fokozottabb, célszerű az eltolódás eredmények szórását (σ) meghatározni minden gyorsulás adatsornál.

$$\sigma_{IDR} = \sqrt{\frac{1}{n}\left[\left(IDR_1 - IDR_\mu\right)^2 + \left(IDR_2 - IDR_\mu\right)^2 + \ldots + \left(IDR_n - IDR_\mu\right)^2\right]} \qquad (13)$$

ahol:

$$IDR_\mu = \frac{1}{n}\left(IDR_1 + \ldots + IDR_n\right) \qquad (14)$$

Alacsony intenzitásnál a szórás semelyik épületnél sem nagy, a tervezésit jóval meghaladó intenzitásnál pedig a szórás a tönkremenetel miatt szükségszerűen nagy. Ezért a szórást csak a 0,75 – 1,25 növekményi tényező tartományban határozzuk meg. Egy-egy épület viselkedésének jellemzésére az megjelölt intervallumban és az összes gyorsulás adatsorhoz tartozó szórások átlagát vesszük. Az így kapott eredményt gyengeszint tényezőnek nevezzük.

Azért, hogy megvizsgálhassuk az épületek megbízhatóságát, vagy más szóval érzékenységét az azonos intenzitású gyorsulás adatsorok különbözőségeire, bevezetjük a megbízhatósági tényezőt is. Megvizsgáljuk, hogy mennyire térnek el az egyes gyorsulás adatsorokból kapott eredmények úgy, hogy a meglévő szórások szórását számoljuk minden növekmény tényezőnél külön, majd a már említett intervallumban ezek átlagát vesszük. Az így kapott eredmény egy számmal (relatív eltolódással) jellemzi az érzékenységet. Nagyobb megbízhatósági tényező nagyobb érzékenységet, más szóval kisebb megbízhatóságot jelent.

A 16 ábrán minden a kutatás során vizsgált épület gyengeszinti és megbízhatósági tényezője egy-egy oszlopdiagramon ábrázolt. Látható, hogy az EC8 épületek gyengeszinti hajlama a szintszámmal arányosan nő. Ezzel szemben az RSBD módszer ezt a tényezőt egy alacsony és nagyjából konstans értéken tartja még az utolsó négy speciális épület esetén is. Az EC8 épületekben a gyengeszinti tényező minden esetben magasabb, akár többszöröse az RSBD épületeknél számítottnak.

A megbízhatósági tényező grafikonja azt mutatja, hogy az EC8 épületek nem csak hajlamosabbak gyengeszinti viselkedésre, hanem jóval érzékenyebbek az adott gyorsulás adatsor jellegzetességeire, mint az RSBD épületek. Az RSBD módszer épületei ezen a grafikonon is alacsony és jobbára konstans érzékenységet mutatnak.

A két grafikon alapján megállapítható, hogy az RSBD módszer amely:

- képletszerűen, kézi módszerrel is kiértékelhető (excel)
- az Eurocode 8 keretbe illeszthető

alkalmas a gyengeszinti viselkedés és tönkremenetel megakadályozására és olyan épületeket szolgáltat, melyek megbízhatóan ellenállnak a tervezési intenzitású földrengéseknek.

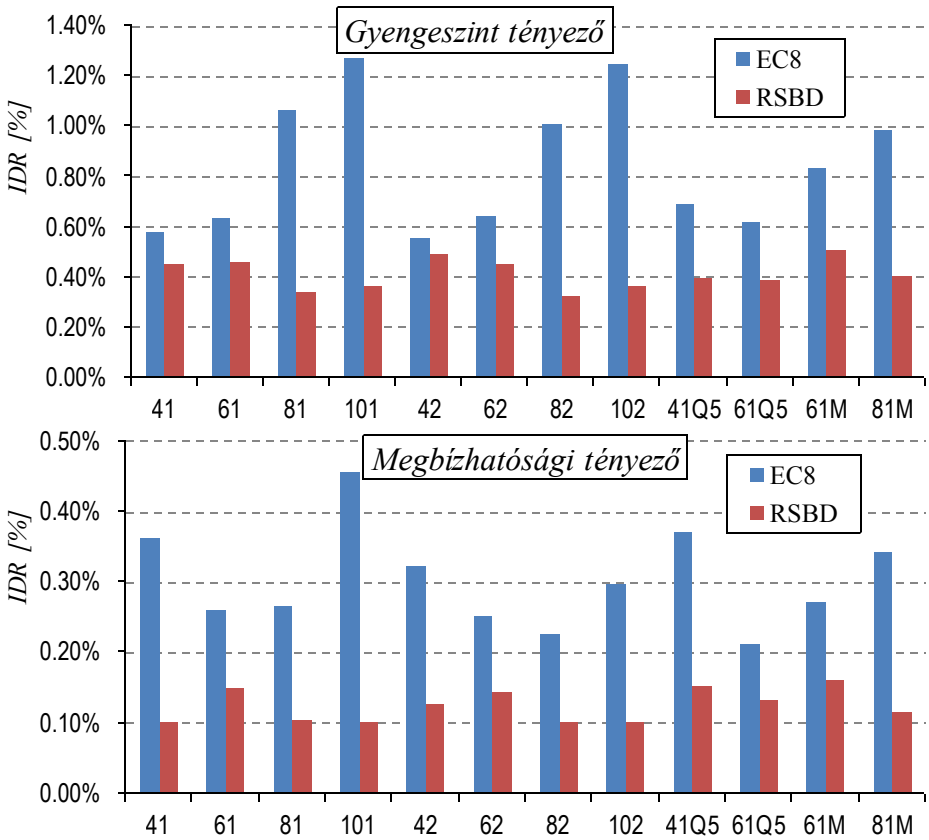

16. ábra; *Az RSBD módszer hatékonyságát mutató diagramok*

7. A DISSZERTÁCIÓ TÉZISEI

I. tézis [1, 2, 5, 7, 8, 9, 10]

Számos eltérő, az EN 1998-1 (a továbbiakban Eurocode 8) előírásainak megfelelő központos rácsozással merevített acélszerkezetű épületen végeztem növekményes dinamikai szeizmikus analízist és megvizsgáltam azok gyengeszinti viselkedését; valamint általánosítottam a gyengeszinti viselkedés jellegét a tapasztalatok alapján.

I/a A parametrikus vizsgálatok alapján megállapítottam, hogy az Eurocode 8 szerint tervezett rácsozott keretek hajlamosak gyengeszinti viselkedést mutatni többnyire az épület felső harmadában; a szintszám növekedése felerősíti ezt a viselkedést és több épületben tönkremenetel is várható a tervezési földrengés intenzitás elérése előtt.

I/b A tapasztalt válaszok alapján általánosságban különbséget tettem a gyengeszinti viselkedés és a gyengeszinti tönkremenetel között, ami a későbbiekben megalapozta a kifejlesztett tervezési eljárás követelményeinek számát és elvét.

I/c Megmutattam, hogy egy épület gyengeszinti viselkedési hajlama a tervezési szeizmikus intenzitástól függetlenül, pusztán a szerkezet teherbírási arányainak vizsgálatával is lehetséges.

I/d Példával illusztráltam, hogy a heurisztikus alapon végzett megerősítés nem szükségszerűen vezet jobb teljesítményű épülethez és, hogy a helyes megerősítést összehangoltan az oszlopok és a rácsok együttes változtatásával kell végrehajtani.

II. tézis [1, 2, 5, 7, 8, 9, 10]

A megvizsgált épületek szeizmikus viselkedésének részletes vizsgálatával leírást készítettem a maradó rácsrúd deformációk következtében fokozatosan kialakuló gyengeszinti viselkedéséről, az azt elősegítő tényezőkről és mindezek reprezentációjáról, illetve annak hiányáról az Eurocode 8 szabványban.

II/a Megmutattam, hogy a rácsrudak képlékeny deformációja az épület dinamikai viselkedésének jelentős megváltozásához vezet. Igazoltam, hogy a deformálódott alak geometriájának felvételével a lineáris modál analízissel jól közelíthetők az inelasztikusan viselkedő épületek válaszainak pillanatnyi állapotai.

II/b Megmutattam, hogy a rácsrudak deformációjából származó oldalirányú szintmerevség csökkenés jelentős minőségi változást eredményez az épület modális viselkedésében és így a várható szeizmikus válaszban is. Ez a változás a belső erők olyan jellegű átrendeződésével jár, ami szükségszerűen megsérti és így érvényteleníti az Eurocode 8-nak a túltervezési tényezőkre vonatkozó homogenitási követelményét.

II/c Megmutattam, hogy már kismértékű képlékeny rácsrúd megnyúlások is áthárítják jelentősen a vízszintes teherviselést az oszlopokra. Ennek következtében jelentős nyomatékok ébrednek a nem csuklós oszlopokban, mely hatás a szabványos analízisből nem származtatható, így az Eurocode 8 oszlopokkal szemben támasztott követelménye nem kielégítő.

II/d A központos rácsozással merevített keretek gyengeszinti viselkedésének kialakulását egy öngerjesztő folyamatként jellemeztem, amelyről folyamatábrát is készítettem és hitelességét az épületek elmozdulás – idő adatsorainak analízisével bizonyítottam.

III. tézis [3, 4, 6, 11]

Megalkottam a Robust Seismic Brace Design (RSBD) tervezési feltételeket, melyek célja az Eurocode 8 nem elégséges feltételeinek helyettesítése és a gyengeszinti viselkedés kialakulásának megakadályozása. A feltételek definiálásánál figyelembe vettem a deformációk által befolyásolt szerkezet lehetséges modális viselkedési módjait és az oszlopok nyomatéki teherbírásának szerepét.

III/a A képlékenységtan szélsőérték tételeinek felhasználásával definiáltam az RSBD módszer első követelményét, amely a gyengeszinti tönkremeneteli mechanizmus létrejöttét gátolja meg.

III/b Definiáltam az RSBD módszer második követelményét az egyes szinteken tapasztalható disszipáció és elmozdulások homogenizálására. A feltétel elvét a várható rugalmatlan elmozdulások arányaiból származtattam.

III/c Definiáltam az RSBD módszerben használt teher paraméterek meghatározására használható képleteket. A képleteket másodrendű és elsőrendű analízishez is megadtam, valamint egy harmadik egyszerűsített formát is levezettem.

IV. tézis [3, 6, 11]

Növekményes dinamikai analízis használatával megvizsgáltam az RSBD módszer szerint megerősített épületek viselkedését és ez alapján jellemeztem az új módszer hatékonyságát.

IV/a Megmutattam, hogy a megerősített épületek egyikében sem tapasztalható a gyengeszinti viselkedés és tönkremenetelük is lényegesen a tervezési szeizmikus intenzitás felett várható csupán. Bemutattam, hogy az épületek magas teljesítménye a szerkezeti méretek további csökkentését, a szerkezet gazdaságosabbá tételét teszi lehetővé.

IV/b Egy az egyes szinteken tapasztalható maximális eltolódások különbségéhez rendelt mérőszámmal igazoltam, hogy az RSBD módszer minden vizsgált épületben azonos mértékben egységesíti az egyes szintek szerepét az épület teljes oldalirányú eltolódásában.

IV/c Az egyes földrengés adatsorokra adott válaszok közötti különbséghez rendelt mérőszámmal igazoltam, hogy az RSBD módszerrel megerősített épületek kis érzékenységet mutatnak az adott rengés specifikációra szemben az Eurocode 8-nak megfelelő épületekkel.

8. THESES OF THE DISSERTATION IN ENGLISH

Thesis I [1, 2, 5, 7, 8, 9, 10]

I have conducted incremental dynamic analysis (IDA) on various multi-storey concentrically braced frames (CBF) designed according to EN 1998-1 (EC8). I have observed their susceptibility to exhibit weak storey behaviour and I have given a general description of the weak storey phenomenon in CBF-s upon the experiences.

- I/a Based upon the parametric studies I have determined that the EC8 CBF designs are prone to weak storey behaviour mostly in the upper third of the building. The increase of the storey number indirectly amplifies the behaviour. Due to the unfavourable behaviour collapse below the design seismic intensity is also likely.
- I/b I have introduced a distinction between the weak storey behaviour and the weak storey-induced early collapse, which later provided a basis for the development of the concept and criteria of a redesign method.
- I/c I have shown that the susceptibility of a CBF to exhibit the weak storey behaviour can be identified without the exact definition of the design seismic intensity, merely by the analysis of resistance relations between the storeys.
- I/d I have proven by examples that the heuristic reinforcing of the weak storey may not necessarily yield a better design and higher seismic resistance, and that the reinforcement has to be carried out by a properly synchronised reinforcement of both the braces and the continuous columns.

Thesis II [1, 2, 5, 7, 8, 9, 10]

Via the detailed analysis of the response of the CBF-s I have provided a detailed description on how the brace deterioration results in a gradual development of the weak storey behaviour, what are the contributing factors to this development and how these are not referred to EC8 provisions.

- II/a I have shown that the deterioration of the braces results in the change of the modal behaviour of a CBF. I have verified that he introduction of the triangular deformation of the braces in an elastic modal analysis model yields reliable snapshots of the inelastic behaviour.
- II/b I have shown that the change of the modal behaviour results in the change of the expected seismic response and seismic loading. This change rearranges the internal forces in a way that the uniformity condition of EC8 imposed on the storey overstrength factors gets violated and void.
- II/c I have shown that even moderate brace deteriorations devolve the lateral loading on the columns. Consequently the continuous columns become bent, which otherwise is not resulted by regular linear analysis. Therefore, the requirement imposed upon columns in EC8 is not satisfactory.
- II/d I have characterised the development of the weak storey behaviour as a self-amplifying phenomenon in CBF-s. I have provided an organigram of the process and I have proved its viability by the analysis of various responses.

Thesis III [3, 4, 6, 11]

I have created the two criteria of the Robust Seismic Brace Design (RSBD) method that aim to replace the insufficient requirements of EC8 and to prevent the development of weak storeys. I have taken into consideration in the criteria the probable changes of the modal behaviour and importance of the moment resistance of the columns.

- III/a With the application of the kinematic principle of the theory of plasticity I have defined the first criterion, which intends to prevent he occurrence of the weak storey failure.
- III/b I have defined the second criterion in order to distribute the dissipation and to equalize the lateral drift of the storeys. The concept of the criterion is based on the expected inelastic drift proportions of the storeys.
- III/c I have elaborated linear formulae for the calculation of the load multipliers needed for the evaluation of the RSBD method. I have given the formulae in first and second order form and also a third, simplified version has been derived.

Thesis IV [3, 6, 11]

I have examined the performance of CBF-s reinforced by the RSBD method by means of incremental dynamic analysis and I have determined the efficiency of the method.

- IV/a I have shown that none of the reinforced buildings were susceptible to exhibit weak storey behaviour and failure is also expected above the design seismic intensity. The high performance allows further reduction of the cross sections and a more economic design.
- IV/b With an appropriately chosen measure of the broadness of the IDA curves I have illustrated that the RSBD method unifies the involvement of the storeys in the lateral drift similarly in every considered example.
- IV/c With an appropriately chosen measure of the differences between the responses given to different acceleration records I have shown that the buildings reinforced by the RSBD method are not sensitive to accelerogram particularities, the design are robust unlike the ones designed according to EC8.

9. A DISSZERTÁCIÓHOZ KAPCSOLÓDÓ PUBLIKÁCIÓK

Folyóirat cikkek

[1] D. B. Merczel, H. Somja, J.-M. Aribert, J. Lógó: On the behaviour of concentrically braced frames subjected to seismic loading. *PERIODICA POLYTECHNICA-CIVIL ENGINEERING* 57:(2) pp. 113-122 (2013) doi.:10.3311/pp.ci.2013-2.02

[2] D.B. Merczel, H. Somja, J.-M. Aribert, M. Hjiaj: Investigation into the weak storey behaviour occurring in concentrically braced frames designed according to Eurocode 8. *Bulletin of Earthquake Engineering,* megjelenés alatt. (2015)

[3] D.B. Merczel, H. Somja, J.-M. Aribert, J. Lógó: Plastic analysis-based seismic design method of concentrically braced steel frames. *Bulletin of Earthquake Engineering,* megjelenés alatt. (2015)

[4] Kaliszky S, Lógó J, Merczel B D: Softening and hardening constitutive models and their application to the analysis of bar structures. *MECHANICS BASED DESIGN OF STRUCTURES AND MACHINES* 39:(3) pp. 334-345. (2011) doi: 10.1080/15397734.2011555733

Konferencia cikkek

[5] D. B. Merczel, H. Somja, J.-M. Aribert, M. Hjiaj, J. Lógó: On the weak storey behaviour of concentrically braced frames. Eurodyn 2014 Porto, Portugal, 2014.06.30-2014.07.02. Paper 1629.

[6] D. B. Merczel, H. Somja, J.-M. Aribert, M. Hjiaj, J. Lógó: Plasticity-based method to avoid weak storey behaviour of concentrically braced frames. Eurosteel 2014 Naples, Italy, 2014.09.10-2014.09.12. Paper 683.

[7] D. B. Merczel, H. Somja, J.-M. Aribert, M. Hjiaj, J. Lógó: On the plasticity based seismic design of concentrically braced steel frames. In: C Adam, R Heuer, W Lenhardt, C Schranz (szerk.) *Vienna Congress on Recent Advances in Earthquake Engineering and Structural Dynamics 2013* (VEESD 2013). Wien, Ausztria, 2013.08.28-2013.08.30. pp. 1-10. Paper 179.

[8] Merczel Dániel Balázs: On the behaviour of concentrically braced frames subjected to seismic loading. In: Józsa János, Lovas Tamás, Németh Róbert (szerk.) *Proceedings of the Conference of Junior Researchers in Civil Engineering* 2012. Budapest, Magyarország, 2012.06.19-2012.06.20. Budapesti Műszaki és Gazdaságtudományi Egyetem, pp. 116-125. ISBN: 978-963-313-061-2

[9] Merczel Dániel Balázs: The development of the soft-storey mechanism in concentrically braced steel frames subjected to seismic action. In: Józsa János, Lovas Tamás, Németh Róbert (szerk.) *Proceedings of the Second Conference of Junior Researchers in Civil Engineering*. Budapest, Magyarország, 2013.06.17-2013.06.18. Budapest: Budapesti Műszaki és Gazdaságtudományi Egyetem

[10] Daniel B. Merczel, Jean-Marie Aribert, Hugues Somja, Mohammed Hjiaj, János Lógó: On the weak storey behaviour of concentrically braced frames. *8th International Conference on Behavior of Steel Structures in Seismic Areas* STESSA 2015, Shanghai, China, July 1-3, 2015. Elfogadva.

[11] Daniel B. Merczel, Jean-Marie Aribert, Hugues Somja, Mohammed Hjiaj, János Lógó: A method to avoid weak storey mechanisms in concentrically braced frames. *8th International Conference on Behavior of Steel Structures in Seismic Areas* STESSA 2015, Shanghai, China, July 1-3, 2015. Elfogadva.

INSA de RENNES
Service des Formations

AVIS DU JURY SUR LA REPRODUCTION DE LA THESE SOUTENUE

Titre de la thèse:
Comportement étage faible des portiques contreventés en acier soumises aux efforts sismiques

Nom Prénom de l'auteur : MERCZEL DANIEL BALAZS

Membres du jury :
- Monsieur HJIAJ Mohammed
- Monsieur SOMJA Hugues
- Monsieur ARIBERT JEAN-MARIE
- Monsieur ELGHAZOULI Ahmed
- Monsieur DEGÉE Hervé
- Monsieur CASTIGLIONI Carlo
- Monsieur DUNAI László
- Monsieur LÓGÓ János

Président du jury : LASZLO DUNAI

Date de la soutenance : 23 Janvier 2015

Reproduction de la these soutenue

~~Thèse pouvant être reproduite en l'état.~~
Thèse pouvant être reproduite après corrections suggérées

Fait à Rennes, le 23 Janvier 2015

Signature du président de jury

Le Directeur

M'hamed DRISSI

Résumé

Les contreventements en acier sont des moyens couramment utilisés pour assurer une rigidité latérale et une résistance aux bâtiments en acier, mais aussi aux bâtiments mixtes acier-béton et aux bâtiments en béton armé. La performance sismique des ossatures contreventées a été étudiée par de nombreux auteurs, la plupart concluent que la réponse réelle de ces ossatures peut différer beaucoup de celle des modèles simplifiés préconisés dans les codes dont l'Eurocode 8. En conséquence, pour obtenir un comportement sismique satisfaisant, ces codes peuvent d'être amendés ou même fondamentalement modifiés.

Notre travail de thèse se concentre sur l'éventualité d'un comportement dissipatif localisé sur un étage de l'ossature. Les objectifs de la recherche sont les suivants:

- Donner une description plus réaliste de la réponse sismique des ossatures contreventées;
- Identifier les facteurs contribuant au développement d'un comportement dissipatif localisé sur un étage;
- Examiner la performance des ossatures contreventées dimensionnées conformément à l'Eurocode 8;
- Identifier les points faibles des règles de l'Eurocode 8 à l'origine de ce comportement insuffisant;
- Proposer une méthode de redimensionnement complémentaire à la procédure actuelle de l'Eurocode 8 faisant appel à d'autres critères et vérifier la validité de cette méthode de redimensionnement sur plusieurs exemples d'ossatures démontrant la disparition complète de mécanismes dissipatifs localisés à un ou quelques étages;

Afin de pouvoir apprécier l'insuffisance de l'Eurocode 8 à ce sujet, plusieurs bâtiments ont été dimensionnés selon cet Eurocode et ont été testés par des simulations numériques de type analyse dynamique incrémentale. L'évolution du déplacement relatif maximal entre étages (IDR) en fonction de l'augmentation du facteur d'échelle de l'accélération maximale du sol a été calculée à partir des résultats du calcul numérique.
Il est constaté que l'apparition d'étages faibles dans les ossatures contreventées a une nature, progressive et auto-amplifiante. La description précise du comportement fournit la possibilité d'une analyse critique des parties correspondantes de l'Eurocode 8 et de proposer une méthode de redimensionnement que nous avons appelé Robust Seismic Brace Design (RSBD). L'idée centrale de la méthode repose sur la nécessité d'utiliser un modèle inélastique d'analyse de la structure à la place du modèle élastique initial. Deux critères essentiels sont introduits dont l'objectif premier est de mieux répartir la dissipation en empêchant la réalisation d'un mécanisme local. Les performances des bâtiments renforcés sont sans exception meilleures que celles des bâtiments originaux; donc la méthode Robust Seismic Brace Design est une bon complément à la procédure de l'Eurocode 8 pour la conception parasismique des ossatures contreventées.

Abstract

The concentric steel bracing is a commonly used way of providing lateral stiffness and resistance in both steel, composite and even concrete multi-storey framed buildings. Also it is an alternative for seismic retrofitting. The seismic performance of concentrically braced frames has been investigated by numerous authors during the past decades as several issues have been identified either related to the actual response, or the seismic design procedure implemented by standards such as the Eurocode 8. The topics are various, e.g. the cyclic dissipative behaviour of axially loaded braces, innovative bracing arrangements and members, controversial requirements imposed on the same members, localization of inelastic deformations related to the so called weak storey behaviour. The conclusion of most of the prior research conducted on the seismic performance of braced steel frames is that the actual response of a braced building differs from that of a simplified model applied by corresponding codes. Consequently, to safeguard satisfactory seismic behaviour, the Eurocode 8 standard in particular needs to be modified or amended.

In order to confine the addressed topic to a size that may be discussed sufficiently in the frame of a PhD research, in the present thesis primarily the weak storey behaviour is looked into. The objectives of the research are:

- Provide a better description of the seismic response of concentrically braced frames;
- Identify the factors contributing to the development of weak storeys;
- Investigate the performance of braced buildings designed according to Eurocode 8;
- Identify the reasons why the Eurocode 8 designs are found usually inadequate;
- Propose a new design method or additional criteria to the existing Eurocode 8 procedure and verify their viability by providing designs that successfully counteract seismic actions without the development of weak storeys;

In the dissertation it is demonstrated by the incremental dynamic analysis of several braced frames that the Eurocode 8 provisions do not provide satisfactory designs. The examination of the responses of the designs is used to characterize the behaviour. It is found that the occurrence of weak storeys in braced frames has a specific, gradual, self-amplifying nature. By further analysis of the seismic responses, proof is given to the existence of this specific behaviour.

The better description of the behaviour provides the possibility of a critical analysis of the corresponding parts of Eurocode 8 and the basis of the Robust Seismic Brace Design method criteria. These criteria are related to the anticipated inelastic seismic response of braced frames, and with their application in design weak storeys can be easily recognized and reinforced. The performances of the reinforced buildings are without exception better than that of the original Eurocode 8 designs; therefore the Robust Seismic Brace Design method is found to be a good alternative of the Eurocode 8 procedure for the seismic design of concentrically braced frames.

N° d'ordre : 15ISAR 01 / D15 - 01

Institut National des Sciences Appliquées de Rennes
20, Avenue des Buttes de Coëmes • CS 70839 • F-35708 Rennes Cedex
Tel : 02 23 23 82 00 - Fax : 02 23 23 83 96